POLYPUBLIE
Polytechnique Montréal

POLYTECHNIQUE MONTRÉAL
UNIVERSITÉ D'INGÉNIERIE

Titre: Title:	Thermodynamic Model for Coal Tar Pitch and Carbonaceous Mesophase Present during Primary Carbonization: Thermal Treatment of Carbon Pastes in the Aluminum Industry
Auteur: Author:	Mahnaz Soltani Hosseini
Date:	2021
Type:	Mémoire ou thèse / Dissertation or Thesis
Référence: Citation:	Soltani Hosseini, M. (2021). Thermodynamic Model for Coal Tar Pitch and Carbonaceous Mesophase Present during Primary Carbonization: Thermal Treatment of Carbon Pastes in the Aluminum Industry [Thèse de doctorat, Polytechnique Montréal]. PolyPublie. https://publications.polymtl.ca/6286/

Document en libre accès dans PolyPublie
Open Access document in PolyPublie

URL de PolyPublie: PolyPublie URL:	https://publications.polymtl.ca/6286/
Directeurs de recherche: Advisors:	Patrice Chartrand
Programme: Program:	Génie chimique

Ce fichier a été téléchargé à partir de PolyPublie, le dépôt institutionnel de Polytechnique Montréal
This file has been downloaded from PolyPublie, the institutional repository of Polytechnique Montréal

https://publications.polymtl.ca

POLYTECHNIQUE MONTRÉAL

affiliée à l'Université de Montréal

Thermodynamic Model for Coal Tar Pitch and Carbonaceous Mesophase Present during Primary Carbonization: Thermal Treatment of Carbon Pastes in the Aluminum Industry

MAHNAZ SOLTANI HOSSEINI

Département de génie chimique

Thèse présentée en vue de l'obtention du diplôme de *Philosophiæ Doctor*

Génie chimique

Février 2021

© Mahnaz Soltani Hosseini, 2021.

POLYTECHNIQUE MONTRÉAL

affiliée à l'Université de Montréal

Cette thèse intitulée :

Thermodynamic Model for Coal Tar Pitch and Carbonaceous Mesophase Present during Primary Carbonization: Thermal Treatment of Carbon Pastes in the Aluminum Industry

présentée par **Mahnaz SOLTANI HOSSEINI**

en vue de l'obtention du diplôme de *Philosophiæ Doctor*

a été dûment acceptée par le jury d'examen constitué de :

Jamal CHAOUKI, président

Patrice CHARTRAND, membre et directeur de recherche

Jean-Philippe HARVEY, membre

Duygu KOCAEFE, membre externe

DEDICATION

Dedicated to

My husband, who is the best life-long companion,

My son, who is the greatest motivation,

My father, who has always been a symbol of effort and success,

My mother, my siblings, and my parents-in-law for their endless love and support.

ACKNOWLEDGEMENTS

I would like to give my sincere gratitude to all those who helped me during my PhD to complete the present thesis. Undoubtedly, the first and the most important is nobody but my supervisor, Professor Patrice Chartrand, who gave me the chance of promoting myself by working in his research group. Thank you Patrice for your supports, encouragement, care and patience. Your vast knowledge and way of critical thinking helped me throughout my research work. It was a pleasure to work with a person so formidable, both scientifically and morally, whose lessons will help me through all aspects of my life.

I would like to acknowledge the members of my committee, Prof. Jamal Chaouki, Prof. Duygu Kocaefe, and Prof. Jaen-Philippe Harvey for taking interest in my work, examining my thesis, and providing insightful comments.

I wish to acknowledge the Natural Sciences and Engineering Research Council of Canada, Alcoa, Hydro Aluminium, Rio Tinto and Constellium for their financial support.

I wish to gratefully acknowledge Professor Arthur D. Pelton, as an outstanding person in thermochemistry science. What he taught me was helpful in all stages of my research project.

I would also like to thank Dr. Aïmen E. Gheribi and Dr. Christophe Tribes, for their advice on mathematical issues related to this research project.

I would like to extend my thanks to my friends and colleagues at Center for Research in Computational Thermochemistry (CRCT). My special thanks to Ève Belisle for Software support, translation of thesis abstract into French and English review of some part of my thesis and Evguenia Sokolenko who helped me at various points during my PhD studies.

I would like to express my endless gratitude to my husband and son, my mother, my sisters and sisters-in-law, my brothers, my beloved nephew and my parents-in-law, whose constant support, love, and encouragement gave me the strength to get through many difficulties.

I would like to give sincere thanks to my father who was the first and the best teacher in my life. I always have a great time with his memories.

RÉSUMÉ

Il est bien établi que le procédé de carbonisation des matériaux joue un rôle critique dans la production de matériaux à base de carbone. La carbonisation est définie par la transformation thermique d'une substance carbonée en charbon (« carbon material », CM). Les CMs ont plusieurs usages, par exemple : les électrodes en graphite pour les fours à arc électriques, les brosses de charbon pour moteurs électriques, les scellants, les roulements à bille en acier et carbone, les accumulateurs électriques, les anodes et cathodes des alumineries.

Le brai provenant du goudron (« coal tar pitch », CTP) est par ailleurs très utilisé comme liant dans les procédés industriels mentionnés ci-dessus. Par exemple, le CTP est le principal matériau utilisé dans la fabrication du liant de la pâte de Söderberg, utilisée dans les anodes précuites du procédé Hall-Héroult des alumineries. Le CTP constitue entre 14 et 17% du poids total des blocs anodiques de coke vert. Les CTPs industriels ont une composition chimique extrêmement complexe, contenant des centaines, voire des milliers de composés, y compris des monomères, des oligomères et des polymères d'hydrocarbures aromatiques polycycliques (PAH) avec une large gamme de poids moléculaires. Une meilleure compréhension des propriétés thermodynamiques et du comportement des phases des constituants des CTPs lors de la carbonisation, et ce à plusieurs températures, améliore les procédés de production de CMs et, par conséquent, les propriétés des CMs résultants. L'acquisition de connaissances sur la description thermodynamique et la configuration d'équilibre de la mésophase, qui apparait lors de la cuisson des blocs anodiques verts et des pâtes à enfoncer entre les blocs cathodiques, se traduira par une amélioration de l'efficacité du processus de production d'aluminium Hall-Héroult.

Les propriétés thermodynamiques des PAHs prédites par Richard et Helgeson, basées sur des algorithmes d'additivité de groupe, souffrent d'un manque de cohérence dans la conciliation des données de transition de phase (enthalpie de fusion et vaporisation) et le calcul des pressions de vapeur à l'aide des fonctions énergétiques de Gibbs pour les phases condensées et gazeuses d'un composé PAH donné. L'une des principales contributions de la présente thèse (sous la forme d'un premier article) est une évaluation critique des propriétés thermodynamiques des PAH considérés importants dans les CTPs, et ce pour les plages de températures typiques des procédés de carbonisation (de la température ambiante à 1200 K). Cette évaluation est faite en appliquant l'approche CALPHAD, où toutes les données sont examinées de manière cohérente avec les données de transition de phase et de pression de vapeur. Un bon accord a été obtenu entre les propriétés thermodynamiques des PAH prédites et les données expérimentales disponibles. De plus, l'approche proposée offre une amélioration de la capacité prédictive par rapport aux méthodes précédentes. Compte tenu de la grande complexité des PAHs et leurs constituants dérivés inclus dans les CTPs (oligomères avec un poids moléculaire élevé (MW)), des améliorations ont été apportées à la méthode d'Richard et Helgeson pour prédire les propriétés thermodynamiques de ces PAHs à poids moléculaire élevé. De plus, le formalisme de l'énergie composée (CEF) a été appliqué pour estimer la chaleur spécifique de certains PAHs, tels que le phénanthrène et le pyrène, qui présentent un comportement anormal à l'état solide, associé à des pics de dépendance à la température des courbes de capacité thermique.

Au cours de la carbonisation, le brai subit des changements physiques et chimiques et est converti en coke infusible (qui ne fond pas). Les principaux changements physiques pertinents se produisant lors de la carbonisation du brai sont la volatilisation des composants condensables à bas point d'ébullition et le dégagement de gaz. Ces matières volatiles sont en grande partie constituées de

composants de faible poids moléculaire, qui se distillent hors du brai avant de pouvoir réagir. Étant donné que la température de traitement thermique du CTP atteint, avec le temps, environ 350-450°C, la polymérisation thermique des composés PAH réactifs se produit, se traduisant par une large distribution d'oligomères moléculaires qui apparaissent sous la forme d'une mésophase cristalline liquide. Le traitement thermique supplémentaire du brai entraîne une polymérisation irréversible supplémentaire et produit du coke infusible. Le processus de déshydrogénation lors de la carbonisation du brai s'accompagne d'une croissance continue de la taille des molécules aromatiques. L'hydrogène est éliminé en grande partie sous forme de H_2 et de CH_4 et le rapport H/C du CTP diminue régulièrement avec la température du traitement thermique. Cependant, le défi industriel consiste à obtenir des CMs de bonne qualité et des procédés efficaces pour la production de matériaux à base de carbone, tout en minimisant la consommation d'énergie, les émissions environnementales et les coûts.

Les connaissances actuelles sur les procédés de carbonisation sont qualitatives dans la plupart des aspects. Cependant, l'étude du comportement des phases de la mésophase du brai, sur des plages de températures de carbonisation typiques, est importante pour optimiser les procédés de production industriels des CMs. En tant que tel, sur la base des tentatives précédentes pour décrire quantitativement le comportement de transition de phase des brais contenant une mésophase, la deuxième contribution de la présente thèse est ainsi présentée (sous la forme d'un deuxième article). Il s’agit d’une extension du modèle thermodynamique et de l'approche développée par Hu et Hurt pour le calcul de l'énergie libre de Gibbs et l'estimation de la configuration d'équilibre des brais contenant une mésophase. Le modèle de Hu et al. est basé sur les comportements de solution non idéale et de cristaux liquides de la mésophase, comprenant des termes à la fois pour l'énergie libre d’excès de mélange et l'énergie libre d'orientation pour décrire quantitativement le comportement

de la mésophase dans le brai. Dans leur travail, le comportement de la mésophase a été estimé en résolvant une série d'équations dérivées de l'équation des potentiels chimiques de chaque composant dans les phases en équilibre. Une technique stochastique a été utilisée pour minimiser la différence absolue entre les deux côtés de ces équations. Pour pallier les limites associées à l'application de l'approche de Hu et al. et les difficultés de calcul du potentiel chimique à l'aide de la fonction d'énergie de Gibbs, une nouvelle approche est proposée ici, utilisant une technique numérique précise et robuste pour minimiser le total de la fonction d'énergie de Gibbs de la mésophase directement (i.e. en utilisant l'algorithme « Mesh Adaptive Direct Search », MADS). La fiabilité de l'algorithme MADS pour déterminer les minima globaux et locaux d'un ensemble de fonctions avec différents degrés de complexité a été présentée précédemment. Le comportement des phases des systèmes binaires, ternaires et d'ordre supérieur peut être estimé en utilisant l'approche proposée ici. Cette nouvelle approche permet également d'utiliser le modèle thermodynamique pour prédire, avec une grande précision, le comportement thermodynamique des brais contenant une mésophase présentant des lacunes de miscibilité.

En combinant des concepts provenant à la fois de l'évaluation critique des propriétés thermodynamiques des composés PAH purs, et de la thermodynamique et des relations de phase de la mésophase carbonée, une troisième contribution de la présente thèse a été développée (sous la forme d'un troisième article). Cette contribution visait à décrire les changements physiques et chimiques qui se produisent pendant le processus de carbonisation primaire, ce qui est utile pour l'optimisation des procédés dans les applications industrielles mentionnées précédemment. On présente donc une nouvelle approche simplifiée pour la modélisation thermodynamique-cinétique du procédé de carbonisation primaire pour fournir des connaissances semi-quantitatives sur ce procédé. L'approche proposée définit des équations thermodynamiques et cinétiques pour les

procédés de vaporisation et de condensation, représentant les nombreux phénomènes complexes se produisant pendant la carbonisation primaire. Les variables cibles importantes étudiées dans le troisième et dernier article sont la masse du brai résiduel et la composition et le pouvoir calorifique des espèces volatiles. Le modèle permet d'estimer la pression partielle des composés volatiles PAHs émis ainsi que les variations de masse et d'enthalpie du CTP au cours de la carbonisation primaire. Le modèle a été appliqué pour évaluer l'effet de paramètres importants dans la carbonisation du brai, tels que la vitesse de chauffage et le débit de gaz porteur sur le taux d'émission de matières volatiles.

ABSTRACT

The critical technological role played by the carbonization process in the production of carbon-based materials is well established. Carbonization is formally defined as the thermal transformation of carbonaceous materials into carbon materials (CM). CMs are widely used to produce various materials ranging from needle coke for graphite electrodes used in electric-arc furnaces, electrical and mechanical carbon materials widely applied to electric motors brushes, sealing materials, carbon bearings, current collectors, pitch-based fibers to aluminum-smelting prebaked electrodes.

Coal tar pitches (CTP) are of great interest as precursors (binders) in the above-mentioned industrial production processes. As a specific example, the major constituent of the binder of Soderberg paste used in carbon prebaked anodes in the Hall-Héroult process used for commercial plants of aluminum production is coal tar pitch, constituting between 14% and 17% (by mass) of the green anode blocks. Commercial CTPs are exceedingly complex materials containing hundreds to thousands of different constituents, including monomers, oligomers and polymers of polycyclic aromatic hydrocarbon (PAH) and heterocyclic compounds with a wide range of molecular weights. A better understanding of the thermodynamic properties and phase behavior of the constituents of CTPs during carbonization over a wide range of temperatures will improve CM production processes and, consequently, the properties of the resultant CMs. Obtaining the knowledge about thermodynamic description and equilibrium configuration of mesophase-containing pitches, which appear during baking of green anode blocks and ramming paste between cathode blocks, will result in efficient Hall-Héroult aluminum production process.

The thermodynamic properties of PAHs predicted by Richard and Helgeson based on group additivity algorithms suffer from a lack of consistency in reconciling phase transition data

(enthalpy of fusion and vaporization) and the computation of vapor pressures using the Gibbs energy functions of the condensed and gaseous phases of a given PAH compound. One of the key contributions of the present thesis (in the form of a first paper) is a critical assessment of the thermodynamic properties of the important PAHs in CTP in typical carbonization process temperature ranges (from room temperature to 1200 K) by applying the CALPHAD approach, where all data are rendered consistently with phase transition and vapor pressure data. Good agreement was obtained between the predicted thermodynamic properties of PAHs and available experimental data. The proposed approach also offers an improvement in predictive capacity compared to previous methods. In the view of the high complexity of the PAH and PAH-derived constituents of CTP (high molecular weight (MW) oligomers), improvements in Richard and Helgeson method for predicting the thermodynamic properties of such high-MW PAHs were developed. Moreover, Compound Energy Formalism (CEF) was applied to estimate the specific heat of some PAHs, such as phenanthrene and pyrene, which exhibit an anomalous solid state behavior associated with peaks in the temperature dependence of the heat capacity curves.

During carbonization, pitch undergoes physical and chemical changes and is converted into infusible coke. The major relevant physical changes that occur during heat treatments of pitches (carbonization) are the volatilization of low boiling condensable components and the evolution of gases. These volatiles consist largely of low molecular weight components, which distil out of the pitch before they can react. As the heat treatment temperature of CTP reaches approximately 350-450°C over a certain period of time, thermal polymerization of reactive PAH compounds take place, which results in a broad distribution of molecular oligomers that appear as a bulk liquid-crystalline, mesophase. Additional heat treatments of pitch result in further irreversible polymerization and produce infusible coke. The dehydrogenation process during pitch

carbonization is accompanied by continuous growth in the size of aromatic molecules. Hydrogen is removed largely in the form of H_2 and CH_4 and the H/C ratio of CTP decreases regularly with the temperature of the heat treatment. However, the industrial challenge resides in obtaining good CM quality and efficient carbon-based materials production processes while minimizing energy consumption, environmental emissions, and costs.

Current knowledge of the carbonization process is qualitative in most aspects. However, the study of the phase behavior of the mesophase in pitch over typical carbonization temperature ranges is important for optimizing industrial CM production processes. As such, based on previous attempts to quantitatively describe the phase transition behavior of mesophase-containing pitches, the second contribution of the present thesis is presented (in the form of a second paper). It consists in an extension of the thermodynamic model and the approach developed by Hu and Hurt for the calculation of the Gibbs free energy and the estimation of equilibrium configuration of mesophase-containing pitches. Hu et al.'s model is based on the non-ideal solution and liquid crystal behaviors of the mesophase that includes terms for both excess free energy of mixing and orientational free energy to quantitatively describe the behavior of the mesophase in the pitch. In their work, the phase behavior of mesophase pitches was estimated by solving a series of equations derived from equating the chemical potentials of each components in the phases in equilibrium. A stochastic technique was used to minimize the absolute difference between both sides of these equations. With respect to the limitations associated with the application of Hu's approach and the difficulties in calculating the chemical potential using the Gibbs energy function, a new approach is proposed here that uses a precise and robust numerical technique for minimization of the total Gibbs free energy function of the mesophase directly (i.e. mesh adaptive direct search or MADS algorithms). The reliability of MADS algorithms to determine the global and local minima of a set of functions

with different degree of complexity has been presented previously. The phase behavior of binary, ternary and higher order systems can be estimated using the proposed approach. The new approach also makes it possible to use the thermodynamic model to predict the thermodynamic behavior of mesophase-containing pitches exhibiting miscibility gaps with high accuracy.

By combining selected concepts from both the critical assessment of the thermodynamic properties of pure PAH compounds and the thermodynamics and phase relationships of carbonaceous mesophase, the third contribution of the present thesis is developed (which takes the form of a third paper). This contribution was aimed at describing the physical and chemical changes occurring during the primary carbonization process, which would be useful for process optimization in the above- mentioned industries. A new simplified approach for thermodynamic-kinetic modeling of the primary carbonization process to provide semi-quantitative knowledge about the process is presented. The proposed approach is based on defining thermodynamic and kinetic equations for the vaporization and condensation processes simply representing the numerous complicated phenomena happening during the primary carbonization process. The important target variables studied in last paper are the mass of the residue pitch and the composition and heating value of volatile species. The model enables estimating the partial pressure of the volatile PAH compounds emitted as well as variations in the mass and enthalpy of CTP during the primary carbonization process. The model was applied to evaluate the effect of important parameters in the carbonization of pitch such as the heating rate of the pitch and the carrier gas flow rate on the emission rate of volatiles.

TABLE OF CONTENTS

DEDICATION III

ACKNOWLEDGEMENTS IV

RÉSUMÉ V

ABSTRACT X

TABLE OF CONTENTS XIV

LIST OF TABLES XVIII

LIST OF FIGURES XX

LIST OF SYMBOLS AND ABBREVIATIONS XXVII

LIST OF APPENDICES XXX

CHAPTER 1 INTRODUCTION 1

CHAPTER 2 LITRATURE REVIEW 7

2.1 Coal Tar Pitch 7

2.1.1 Source and industrial applications of coal tar pitch 8

2.1.2 Content, properties and characteristic values of coal tar pitch 12

2.2 Evolution of coal tar pitch during carbonization 15

2.2.1 Physical and chemical changes during carbonization of pitches 17

2.2.2 Carbonaceous mesophase formation 23

2.2.3 Semi-coke (and coke) formation 30

2.3 Thermodynamics of carbonaceous materials (coal tar pitch) in different phase states: solid, mesophase, liquid and gas 31

2.3.1 Thermodynamics of pure PAHs 32

2.3.2 Phase transition of single-component PAH 39

2.3.3 Phase transitions in binary PAH mixtures 40

2.3.4 Thermodynamics of carbonaceous mesophase 41

CHAPTER 3 CRITICAL ANALYSIS AND ORGANIZATION OF THE THESIS 50

3.1 Critical analysis of the literature review 50

3.2 Research objectives 54

3.3 Organization of the thesis 55

CHAPTER 4 ARTICLE 1: CRITICAL ASSESSMENT OF THERMODYNAMIC PROPERTIES OF IMPORTANT POLYCYCLIC AROMATIC HYDROCARBON COMPOUNDS (PAHS) IN COAL TAR PITCH AT TYPICAL TEMPERATURE RANGES OF THE CARBONIZATION PROCESS 57

4.1 Introduction 58

4.2 Thermodynamic model for Gibbs energy of PAH compounds in coal tar pitch 60

4.2.1 Basis of the group contribution algorithms 61

4.2.2 Thermodynamic model parameters 69

4.3 Application of Compound Energy Formalism (CEF) to predict heat capacity functions of PAHs with anomaly behavior 78

4.4 Results and discussion 82

4.4.1 Prediction of heat capacity function coefficients of PAHs 82

4.4.2 Prediction of standard thermodynamic properties of PAHs 92

4.4.3 Application to prediction of thermodynamic properties of high molecular weight PAHs 100

4.4.4 Prediction of heat capacity function of PAHs with anomalous behavior 100

4.5 Conclusion and outlook 106

4.6 Acknowledgements 107

CHAPTER 5 ARTICLE 2: THERMODYNAMICS AND PHASE RELATIONSHIP OF CARBONACEOUS MESOPHASE APPEARING DURING COAL TAR PITCH CARBONIZATION 108

5.1 Introduction 109

5.2 Thermodynamic model of carbonaceous mesophase 111

5.2.1 Overview of the general thermodynamic theory 112

5.2.2 New approach for phase behavior prediction by Gibbs energy minimization using MADS 114

5.3 Results and discussion 118

5.3.1 Prediction of binary phase diagram describing the behavior observed in the hot stage experiments by Lewis 119

5.3.2 Prediction of mesophase content with varying thermal soaking time 123

5.3.3 Application to ternary phase diagram prediction 123

5.3.4 Application of ternary phase diagram to phase behavior observation of Lewis 129

5.3.5 Application to petroleum pitch data of Greinke and Singer 130

5.4 Conclusion and outlook 131

5.5 Acknowledgements 132

CHAPTER 6 ARTICLE 3: MODELING THE COAL TAR PITCH PRIMARY CARBONIZATION PROCESS 133

6.1 Introduction 134

6.2 Thermodynamic-kinetic modeling of coal tar pitch heat treatment process during primary carbonization 136

6.2.1 Overview of general steps of primary carbonization process 137

6.2.2 Simplified approach for modeling of internal phenomena occurring in coal tar pitch primary carbonization 139

6.2.3 Mass and energy balance through the process 152

6.2.4 Integrating equations for estimation of mass and enthalpy changes through the primary carbonization process 157

6.3 Results and discussion 159

6.3.1 General prediction of gas emission rate during heat treatment of coal tar pitch (below 350°C) 160

6.3.2 Application to Bouchard's experiments 164

6.4 Conclusion and outlook 176

6.5 Acknowledgements 179

CHAPTER 7 GENERAL DISCUSSION 180

CHAPTER 8 CONCLUSION 184

8.1 Summary of the work 185

8.2 Limitations of the work 187

8.3 Recommendations for future research 189

REFERENCES 191

APPENDICES 208

LIST OF TABLES

Table 2.1 Some polycyclic aromatic hydrocarbon monomers in coal tar pitch and their relative potency factor (RPF) [3, 30, 39]. 9

Table 2.2 Typical properties of coal tar pitch [35, 40]. 14

Table 2.3 Different groups of reference polycyclic aromatic compounds. 34

Table 2.4 Anomalous behavior information of some PAH compounds [96, 109, 113, 114, 116-123]. 36

Table 4.1 Selected reference compounds and group stoichiometries [111]. 63

Table 4.2 Selected reference compounds and group stoichiometries [111]. 64

Table 4.3 Group stoichiometries of perylene and coronene. 69

Table 4.4 Heat capacity coefficients of the constituent groups in the solid PAH compounds derived by group contribution calculation. 72

Table 4.5 Heat capacity coefficients of the constituent groups in the liquid and gas PAH compounds derived by group contribution calculation. 73

Table 4.6 Entropy and enthalpy of formation at 298.15 K and 1 bar of the constituent groups in the solid, liquid and gaseous PAH compounds from group contribution calculation. 76

Table 4.7 Enthalpy of formation at 298.15 K and 1 bar of some PAHs in solid and gas states. ...94

Table 4.8 Entropy of some PAHs in solid and gas states at 298.15 K and 1 bar. 94

Table 4.9 Phase transition properties of some PAHs. 94

Table 4.10 Entropy and enthalpy of formation at 298.15 K and 1 bar of some PAHs in solid and gas states. 98

Table 4.11 Optimized CEF formalism parameters corresponding to Eqs. (4.8-4.10). 102

Table 5.1 Calculated composition of the phases in equilibrium of the binary system shown in Figure 5.3. 122

Table 6.1 Selected set of representative PAH compounds in the present work. 145

Table 6.2 Proposed prototype oligomerization reactions in mesophase formation step of carbonization process. 149

Table 6.3 Proposed prototype polymerization reactions in semi-coke / coke formation step of carbonization process. 150

Table 6.4 Definition of different terms in Eqs. (6.15-a) and (6.15-b). 155

Table 6.5 Definition of different terms in Eq. (6.17). 156

Table 6.6 Mass distribution of an arbitrary 50 grams pitch sample at room temperature subjected to the calculations in the present work. 165

Table A.1 Summary of coefficients for Eq. (4.5) of solid reference compounds. 208

Table A.2 Summary of coefficients for Eq. (4.6) of liquid and gas reference compounds..... 209

Table A.3 Prediction of heat capacity coefficients for Eq. (4.5) of solid PAHs. 210

Table A.4 Prediction of heat capacity coefficients for Eq. (4.6) of liquid and gas PAHs. 210

Table A.5 Experimental data and optimized values of entropy and enthalpy of formation at 298.15K and 1 bar of solid, liquid and gas reference PAH compounds. 217

Table A.6 Experimental data and optimized values of phase transition thermodynamic data of reference PAH compounds..... 218

LIST OF FIGURES

Figure 1.1 Pre-baked anode manufacturing process flow sheet [22]. 2

Figure 1.2 Typical baking program for anode production (in open top furnace) [22]. 3

Figure 2.1 Mass spectra (MS) of a sample of coal tar pitch [21]. 8

Figure 2.2 Products in coal carbonization [38]. 11

Figure 2.3 constituents of coal tar pitch [22]. 13

Figure 2.4 Fragments of XRD patterns for pitch (1, "graphite-like" carbon fraction;2, γ_1-carbon fraction, 3,γ_2-carbon fraction) [47]. 15

Figure 2.5 Raman spectra evolution of a carbonaceous material to graphite [53, 54, 60]. 17

Figure 2.6 Thermogravimetric analysis and gas evolution data of coal tar pitch at 10°C min^{-1} in argon [3]. 18

Figure 2.7 General reaction scheme for carbonization [50]. 19

Figure 2.8 Initial reactions in the pyrolysis of naphthalene and anthracene [4, 50]. 20

Figure 2.9 Thermal polymerization of naphthalene [50]. 20

Figure 2.10 H/C ratio changes with heat treatment temperature [56]. 21

Figure 2.11 Thermal rearrangement reactions in pyrolysis [50]. 21

Figure 2.12 Polymerization-condensation process in carbonization [50]. 22

Figure 2.13 Two-dimensional polymerization for zethrene [50]. 23

Figure 2.14 Two-dimensional polymerization for tetrabenzonaphthalene [50]. 23

Figure 2.15 Model of a planar aromatic of the type that forms lamellar nematic liquid crystals [83]. 25

Figure 2.16 (a) Schematic diagram of a discotic nematic liquid crystal spheres in a liquid pyrolysate; and (b) an optical micrograph of mesophase spheres [80]. 25

Figure 2.17 Structure of a mesophase spherule [23, 85]. 26

Figure 2.18 (a) Rearrangement of molecules when two spheres coalesce; (b) optical micrographs of mesophase spheres from carbonization of petroleum feedstock at 713 K. [Y] spheres with Brooks and Taylor morphology during the coalescence process and [X] spheres with more complex structure [26, 80]. 27

Figure 2.19 Schematic of formation and development of bulk liquid crystalline mesophase. 28

Figure 2.20 Molecular weight distribution from GPC curves of pitch as a function of time at 400°C [87]. 29

Figure 2.21 Number average molecular weight of the coexisting isotropic liquid (line a) and mesophase (line b) fractions in the pitch during the transformation [89]. 30

Figure 2.22 Molecular weight distribution of pitch at different times during semi-coke formation [87]. 31

Figure 2.23 Heat capacity and phase transition of phenanthrene [116]. 36

Figure 2.24 Position of the phenanthrene molecule in the unit cell [124]. 38

Figure 2.25 Melting points of various single-component PAH [125]. PAH reaction temperatures in right panel from Lewis [50]. 39

Figure 2.26 Binary phase diagram for generic PAH of low and high molecular weight [125]. 41

Figure 2.27 Discotic nematic liquid crystalline phase [125]..... 41

Figure 2.28 Comparison of experimental binary phase diagram with model calculation by Shishido et al. [126, 128, 131]. 44

Figure 2.29 Comparison of experimental binary phase diagram with model calculation by Hu and Hurt without any consideration of non-ideal solution behavior [127, 128, 131]. 44

Figure 2.30 Configuration of mesogen molecule [137]. 48

Figure 2.31 Comparison of experimental binary phase diagram with model calculation by Hu et al. [127, 128, 131]. 49

Figure 4.1 Perylene, coronene, and their oligomers [25]. 67

Figure 4.2 Coronene “star” heptamer and its possible transformation to a graphene plate having a diameter of 26.4 Å [25]. 67

Figure 4.3 Definition of three different aromatic groups at the junction of three aromatic rings. . 68

Figure 4.4 Heat capacity and phase transition of highly purified phenanthrene: a, liquid; b, crystal I; c, crystal II; d, crystal III (mole fraction of impurity: 0.00013) [116]..... 79

Figure 4.5 Representation of the composition in an quaternary system where the components mix each other, two and two [207]. 80

Figure 4.6 Comparison of the predicted heat capacity of naphthacene (solid, liquid and gas state) with experimental data and Richard and Helgeson’s predicted values [111, 156, 166, 209]. 85

Figure 4.7 Zoom view of a portion of Fig. 4.6. 86

Figure 4.8 Comparison of the predicted heat capacity of pentacene (solid, liquid and gas state) with experimental data and Richard and Helgeson’s predicted values [111, 156, 209]. 87

Figure 4.9 Zoom view of a portion of Fig. 4.8. 88

Figure 4.10 Comparison of the predicted heat capacity of perylene (solid, liquid and gas state) with experimental data and Richard and Helgeson’s predicted values [111, 156, 166] (for anomaly, see Section 4.4.4). 89

Figure 4.11 Zoom view of a portion of Fig. 4.10. 90

Figure 4.12 Comparison of the predicted heat capacity of coronene (solid, liquid and gas state) with experimental data and Richard and Helgeson’s predicted values [111, 156, 166]. 91

Figure 4.13 Zoom view of a portion of Fig. 4.12. 92

Figure 4.14 Calculated vapor pressure of naphthacene as a function of temperature [111, 187]. 96

Figure 4.15 Calculated vapor pressure of pentacene as a function of temperature [111, 187]. 96

Figure 4.16 Calculated vapor pressure of perylene as a function of temperature [111, 178, 187]. 97

Figure 4.17 Calculated vapor pressure of benzo[a]anthracene as a function of temperature [111, 212]..... 99

Figure 4.18 Calculated vapor pressure of benzo[e]pyrene as a function of temperature [111, 212]. 99

Figure 4.19 Predicted heat capacity of phenanthrene [116, 171]. 103

Figure 4.20 Zoom view of solid phase transition region of Fig. 4.19. 103

Figure 4.21 Predicted heat capacity of pyrene [96, 109]. 104

Figure 4.22 Predicted heat capacity of perylene [166]. 104

Figure 4.23 Heat capacity of phenanthrene-pyrene solid solution (67 mol%: pyrene). 106

Figure 5.1 Formation and development of bulk liquid crystalline mesophase under a suitable condition (scale bar in PLM micrographs is 100 μm)-permitted from ref. [86]. 109

Figure 5.2 Calculated binary phase diagram of naphthalene pitch observed in hot stage microscope experiments of Lewis [28]. 120

Figure 5.3 Zoom view of the high MW compound-rich region of Figure 5.2. 122

Figure 5.4 Calculated ternary phase diagram at 600 K. 125

Figure 5.5 Calculated ternary phase diagram at 700 K. 126

Figure 5.6 Calculated ternary phase diagram at 800 K. 127

Figure 5.7 Calculated Gibbs energy of binary system (MW_1 = 500 g mol^{-1}, MW_2 = 1600 g mol^{-1}) at 800 K. 128

Figure 5.8 Calculated ternary phase diagram at 870 K. 129

Figure 5.9 Partition ratios of molecules in the coexisting phases in a heat treated petroleum pitch. Points: experimental data obtained by Greinke and Singer [89]; dotted line: predicted by Hu [127]; solid line: predictions in this work. $Tcli = 373 + 685 - 373(\ MWi\ - 400)(1000 - 400)$ (K) and α = 0.00183 (cal.cc^{-1})$^{1/2}$/(g mol^{-1}). 131

Figure 6.1 Mass spectra (MS) of a sample of coal tar pitch [21]. 141

Figure 6.2 Molecular weight distribution of pitch during volatilization and mesophase formation steps [87]. 143

Figure 6.3 Molecular weight distribution of pitch during semi-coke formation [87]. 143

Figure 6.4 Idealized crystallite representation used in the coke model developped by Ouzileau et al. [257] : (a) idealized ‘‘hexagonal’’ plane with n = 4; (b) crystallite size L_a, D_{aa} and n parameters; (c) crystallite height L_c and d_{002} from the stacking of m planes. 144

Figure 6.5 Hypothetical reactor design used to compute the mass and energy balances at every iteration in our model; dashed line: border of the system, blue lines: mass flows, and red lines: heat flows. 153

Figure 6.6 Binary phase diagram of anthracene and a mixture of representative PAHs, which do not contain anthracene indicating partial pressure of low MW compound; Dashed lines: iso-partial-pressure (bar) of anthracene and dash-dotted lines: metastable iso-partial-pressure (bar) of anthracene. 162

Figure 6.7 Zoom view of the anthracene-lean region of Fig. 6.6; Red solid line: evaporation path of anthracene during heat treatment of a 50 g pitch sample (heating rate: 50°C/h and carrier gas flow rate: 560 cm^3/min) 163

Figure 6.8 Effect of heating rate on total mass loss during heat treatment of a 50 g pitch in temperature range below 350°C, Solid line: experimental data obtained by Bouchard et al. [246] at 50°C/h; Points: predictions in this work (using ϕis = 1 and carrier gas flow rate : 2300cm^3/min). 165

Figure 6.9 Estimated mass loss of a)antheracene, b)pyrene and c)chrysene versus temperature for different carrier gas flow rates. Solid circle: 2300 cm^3/min, solid triangle: 560 cm^3/min and empty circle: 230 cm^3/min (heating rate: 50°C/h and ϕis: 1).....168

Figure 6.10 Effect of carrier gas flow rate on anthracene evaporation path during heat treatment of a 50 g pitch sample (assumed as one-phase glassy isotropic liquid); Solid circle: 2300 cm^3/min, solid triangle: 560 cm^3/min, and empty circle: 230 cm^3/min (heating rate: 50°C/h and ϕis: 1).....169

Figure 6.11 Estimated mass loss of anthracene, pyrene and chrysene versus temperature for: different heating rates at carrier gas flow rate of 2300cm^3/min and ϕis = 1 (a – c) and different

values of ϕis parameters (0.7 and 1) at heating rate 50°C/h, carrier gas flow rate 2300 cm^3/min (d – f). 170

Figure 6.12 Calculated released volatile matter from a 50 g coal tar pitch heat treated from T_{amb} to 450°C with heating rate of 50°C/h. 171

Figure 6.13 Calculated molecular weight distribution of the residue of a 50 g mass coal tar pitch at the end of mesophase formation step of carbonization process with heating rate of 50°C/h. 172

Figure 6.14 Calculated released volatile matter from a 50 g coal tar pitch in temperature range of Tamb - 550°C during carbonization process with heating rate of 50°C/h. 173

Figure 6.15 Calculated molecular weight distribution of the residue of a 50 g coal tar pitch at the end of semi-coke formation step of carbonization process with heating rate of 50°C/h. 173

Figure 6.16 Calculated molecular weight distribution of the residue of a 50 g coal tar pitch during coke formation step (where the temperature is about 550°C) of carbonization process with heating rate of 50°C/h. 174

Figure 6.17 Total required energy in first step of carbonization (25-350°C) of a 50 g CTP sample (using ϕis = 1, heating rate: 50°C/h and carrier gas flow rate : 2300 cm^3/min). 175

Figure A.1 Vapor pressure of naphthalene as a function of temperature [179-181, 183, 188]....211

Figure A.2 Heat capacity of naphthalene (solid, liquid and gas) as a function of temperature [92, 97, 98, 101, 105, 111, 154]....211

Figure A.3 Vapor pressure of anthracene as a function of temperature [178, 179, 184, 186, 187, 190]....212

Figure A.4 Heat capacity of anthracene (solid, liquid and gas) as a function of temperature [92, 95, 101, 103, 104, 111, 156]....212

Figure A.5 Vapor pressure of phenantrene as a function of temperature [179, 182, 186, 187]...213

Figure A.6 Heat capacity of phenanthrene (solid, liquid and gas) as a function of temperature [111, 116, 156, 171] (for anomaly, see Section 4.4.4). 213

Figure A.7 Vapor pressure of pyrene as a function of temperature [147, 161, 185, 187, 189, 190]. 214

Figure A.8 Heat capacity of pyrene (solid, liquid and gas state) as a function of temperature [96, 109, 111, 156] (for anomaly, see Section 4.4.4). 214

Figure A.9 Vapor pressure of triphenylene as a function of temperature [178]. 215

Figure A.10 Heat capacity of triphenylene (solid, liquid and gas state) as a function of temperature [111, 156, 166]. 215

Figure A.11 Position of the phenanthrene molecule in the unit cell [124] 216

LIST OF SYMBOLS AND ABBREVIATIONS

Abbreviations

BaP	Benzo[a]pyren
BI	Benzene insoluble
BS	Benzene soluble
CALPHAD	CALculation of PHAse Diagram
CEF	Compound energy formalism
CM	Carbon materials
CTP	Coal tar pitch
DSC	Differential scanning calorimetry
GC	Gas chromatography
GPC	Gel permission chromatography
MADS	Mesh adaptive direct search
MS	Mass spectrometry
MW	Molecular weight
MWD	Molecular weight distribution
NOMAD	Nonlinear optimization with MADS algorithm
PAH	Polycyclic aromatic compound
QI	Quinoline insoluble
RPF	Relative potency factor
TI	Toluene insoluble
TGA	Thermogravimetric analysis
TMA	Thermomechanical analysis
TS	Toluene insoluble

XRD	X-ray powder diffraction

Symbols

C_p	specific heat, $Jmol^{-1}K^{-1}$
g_i	molar Gibbs free energy of compound *i*, $Jmol^{-1}$
G_i	total Gibbs free energy of compound *i*, J
G	total Gibbs free energy of the system, J
G^{iso}	total Gibbs free energy of the isotropic phase, J
G^{meso}	total Gibbs free energy of the mesophase, J
ΔG_{mix}^{ideal}	total ideal Gibbs free energy of mixing, J
ΔG_{mix}^{excess}	Total excess Gibbs energy of mixing, J
G_{orient}	total orientational free energy, J
h_i	molar enthalpy of compound *i*, $Jmol^{-1}$
H_i^{pitch}	total enthalpy of compound *i in pitch*, J
H_i^{gas}	total enthalpy of compound *i in gas phase*, J
H_i	total enthalpy of compound *i*, J
K	Boltzman constant, $m^2kg\ \ s^{-2}K^{-1}$
n_i	number of mole of compound *i*, *mol*
n_i^{iso}	number of mole of compound *i* in isotropic phase, *mol*
n_i^{meso}	number of mole of compound *i* in mesophase, *mol*
n_i^{gas}	number of mole of compound *i* in gas phase, *mol*
N_A	Avogadro number, mol^{-1}
P_i	partial pressure of component *i*, atm
P_{tot}	total pressure, atm

$\bar{P}_i$	mean order parameter for component *i*
R	gas constant, $Jmol^{-1}K^{-1}$
T	temperature, K
T_{cl_i}	clearing temperature of compound *i*, K
V_i	molar volume of compound *i*, cm^3mol^{-1}
V	molar volume of phase, cm^3mol^{-1}
x_i	mole fraction of compound *i*
Z_i	orientational partition function for compound *i*

Greek symbols

α_i	chemical activity of compounds *i*
δ_i	solubility parameter of compound *i*, $(cal\ cm^{-3})^{1/2}$
ε_{ij}	orientational pair potential
θ_i	angle between director and directional unit vector for molecules of class *i*
μ_i	chemical potentials of compound *i*, $Jmol^{-1}$
Φ_i	volume fraction of species *i*

LIST OF APPENDICES

Appendix A Heat capacity function coefficients and thermodynamic properties of PAHs.....208

Appendix B Convergence tests for min G and variables in Eq. (5.6).....219

Appendix C Chemical potential formulation of the species in isotropic liquid and nematic phases 220

CHAPTER 1 INTRODUCTION

Pitch was described by Webster in 1956 [1, 2] as a black or dark viscous substance obtained as a residue following the distillation of coal tar, wood, and petroleum, etc. A more suitable technical description of pitch would be that it is a complex mixture of hundreds or thousands of organic aromatic compounds (mostly polycyclic aromatic hydrocarbons) with an average molecular weight of several hundred of g/mol [2-4]. These compounds are formed by an array of thermal decomposition, hydrogen transfer, and oligomerization reactions. Although the compounds in pitch may melt individually at a fairly high temperature (several hundreds of °C), the pitch mixture softens at much lower temperatures (approximately 100-150°C). In fact, the low softening point of pitch is key to its useful rheological properties and flow behavior [1].

The capacity of thermal transformation of coal tar pitches (CTP) into carbon materials (CM) as well as their specific binding properties make CTPs an important source of a wide range of different CMs. CTPs are used in the production of various carbon-based materials ranging from needle coke for graphite electrodes used in electric-arc furnaces [5-8], electrical and mechanical carbon materials widely applied to electric motor brushes, sealing materials, carbon bearings, current collectors [9-15], pitch-based fibers [16-19] to aluminum-smelting prebaked electrodes [20, 21].

In this last example, it is used as binder to join calcined petroleum coke and crushed recycled green and baked anodes to prepare green anode blocks that will later be baked to obtain the desired electrical and mechanical properties suitable for the Hall-Héroult aluminum production process. Fig. 1.1 presents the typical steps for the production of pre-baked anodes. The anode raw materials consist of calcined petroleum coke, recycled green and baked anodes, and coal tar pitch. The coke and butts (after cleaning and crushing) are ground and classified and to the desired particle size distribution. This is the dry aggregate preparation step. The dry aggregate is then pre-heated. It is

followed by the mixing of the dry aggregate with the softened pitch. The softening point (the temperature at which a material softens beyond some arbitrary softness) is one of the main properties of coal tar pitch which determines its flow behavior. Maintaining an appropriate pre-heating temperature (50°C to 60°C above the pitch softening point) is important during adding pitch to the dry aggregate blend. This can assure proper pitch penetration into the filler matrix. The green anode blocks formed either using a press or a vibro-compactor are placed in an open ring baking furnace and undergo thermal transformation process [22].

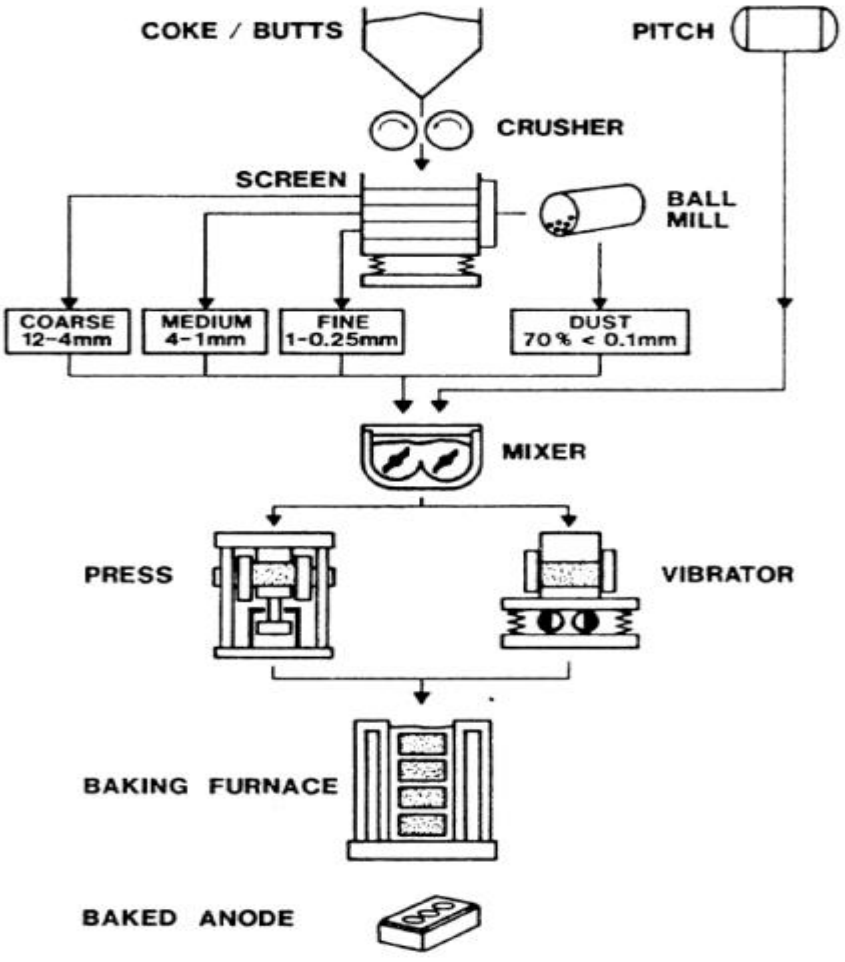

Figure 1.1 Pre-baked anode manufacturing process flow sheet [22].

Fig.1.2 shows a typical baking program for anode production. The quality of the anodes with respect to the properties affected by the baking process is mainly determined by the following factors of the baking cycle: controlled heating rate and final baking temperature.

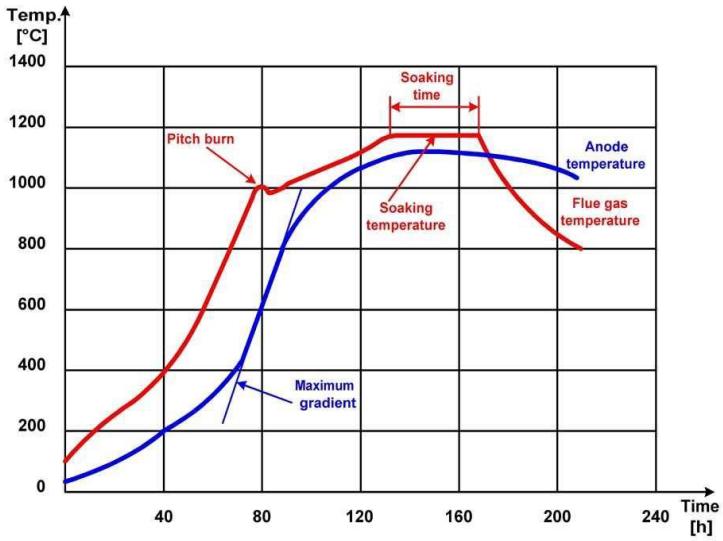

Figure 1.2 Typical baking program for anode production (in open top furnace) [22].

During transformation of CTP part of green anode blocks to CM, CTP undergoes a carbonization process that enriches it in carbon constituents. In the early steps of the carbonization process, the smaller, more volatile PAHs in CTP distill, raising the average molecular weight and viscosity of the remaining pitch. Continuing the heat treatment of CTP results in the thermal oligomerization and polymerization of the more reactive residual species, the cracking of substituent side chains from aromatic rings, and the release of volatiles. As first demonstrated by Brooks and Taylor [23], as the heat treatment temperature reaches approximately 350°C, a mesophase in the form of anisotropic spherules is observed during the thermal transformation (polymerization) of pitches (aromatic compounds) to coke [24, 25]. Mesophase is the intermediate discotic nematic liquid crystals whose molecular ordering lies between that of a solid and that of an isotropic liquid [26-28]. The spherules are composed of mostly fully condensed high molecular weight polycyclic

aromatic hydrocarbon (PAH) molecules. The formation of the mesophase allows the spatial rearrangement of the molecules favoring the oligomerization and polymerization needed for semi-coke formation. Additional heat treatments of the pitch up to 400-600°C (as the penultimate stage of primary carbonization) result in continuous growth in the molecular size of aromatics due to further irreversible polymerization which leads to a brittle solid state materials (semi-coke) formation.

Actually, any changes in heating rate in baking program affects the carbonization process and consequently the prebaked anode quality as well as emission of gaseous product through the baking process.

The constituents of the gas released throughout the process are mostly composed of light PAH monomers, hydrogen and methane. The designs of some specific processes currently provide suitable conditions for burning released volatiles, which can supply about half of the energy required for the carbonization process. For example, the gaseous mixture which is emitted during the baking of the green anode blocks and penetrated to the flue wall of the baking furnace, is burnt and provides some portion of required heat for the baking process. In this way, the fuel consumption of system decreases while some PAHs are consumed as fuel. On the other hand, the volatiles emitted during the ramming the carbon pastes between cathode blocks in aluminum electrolysis cells, are released into the work place. Based on a 4-year analysis of aluminium smelters [29-31], PAH monomers have been classified as non-genotoxic, genotoxic, or highly genotoxic with respect to the toxicity of benzo(a)pyrene (BaP) as an indicator. Acute or short-term exposure to these volatiles has been associated with several health effects.

The industrial challenge resides in obtaining a good quality final product and an efficient CM production process while minimizing energy consumption, environmental emissions, and cost [32]. A better understanding of the factors controlling carbonization and consequently volatilization will contribute to developing green and efficient CM production processes. Information about thermodynamic properties of CTP constituents such as vapor pressure and phase transition data (which is difficult to get experimentally) enables evaluating the emission rate of volatile matters during carbonization. Thermodynamics and relationship of the phases (solid, mesophase, isotropic liquid, and gas) appearing during carbonization process, which allows the mass loss and heat requirement estimation during the process, will help contribute to improve the CM production processes.

This doctoral project focuses on development of a thermodynamic model to estimate the thermodynamic properties and phase behavior of CTP in the gas, liquid, solid phases as well as in the mesophase in order to provide the industry with scientific tools for their simulations aimed at optimizing the carbon- based material production processes.

The present thesis is structured as follows. A literature review is presented first. The specific objectives are then described. The scientific papers either published or submitted are then presented as three chapters of the thesis. Chapter 4 presents “Critical assessment of thermodynamic properties of important polycyclic aromatic hydrocarbon compounds (PAHs) in coal tar pitch at typical temperature ranges of the carbonization process”, Chapter 5 discusses “Thermodynamics and phase relationship of carbonaceous mesophase appearing during coal tar pitch carbonization”, and Chapter 6 presents “Modeling the coal tar pitch primary carbonization”. Finally, the strengths and

limitations of the present thesis as well as future scientific contributions that may be based on the work accomplished to date are discussed.

CHAPTER 2 LITRATURE REVIEW

To propose a new approach in this thesis for thermodynamic modelling of coal tar pitch and carbonaceous mesophase present during primary carbonization leading to optimization of carbon-based material production process, literature review must include a combination of several practical and theoretical knowledge in different fields. These fields can be divided into thermodynamics, chemical reactions, material characterization techniques, numerical modelling and process optimization.

Firstly, source of coal tar pitch production, contents, properties and characteristic values of coal tar pitch are reviewed in Section 2.1

A comprehensive literature review of existing studies for qualitative understanding of evolution of coal tar pitch during carbonization as well as investigation of carbonaceous mesophase nature appearing during carbonization is then presented in Section 2.2.

Subsequently, in Section 2.3, existing thermodynamic models to predict the properties of coal tar pitch in different phase states and phase behavior of mesophase-containing pitches are reviewed. Strengths and limitations concerning these models revealed in the literatures are discussed in detail in this section.

2.1 Coal Tar Pitch

Coal tar pitch (CTP) can be defined as a solid, fusible product of the pyrolysis of coal [33, 34]. The characterization of commercial pitches shows them to be exceedingly complex materials containing hundreds to thousands of different components: monomers, oligomers and polymers of polycyclic aromatic hydrocarbon (PAH) and heterocyclic compounds with a variety range of molecular weight (MW) [3, 4].

Fig. 2.1 presents a mass spectrum of a coal tar pitch [21], species are observed at every molecular weight interval over the mass range covered [35]. In fact, the pitches prepared from different sources exhibit essentially the same degree of diversity in molecular weight [1].

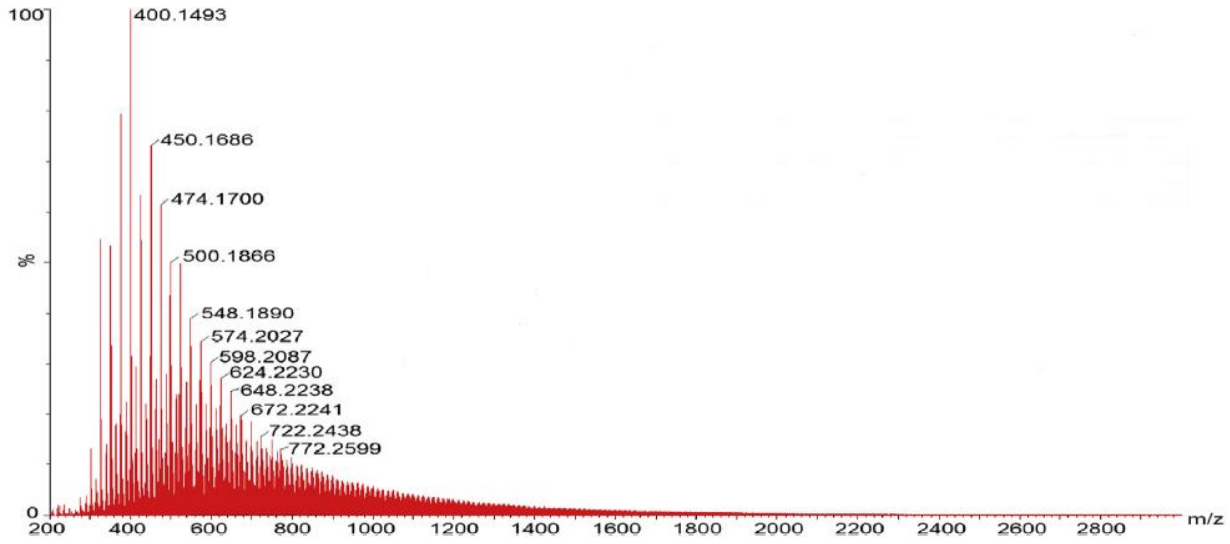

Figure 2.1 Mass spectra (MS) of a sample of coal tar pitch [21].

A typical set of some polycyclic aromatic monomers of coal tar pitch is summarized in Table 2.1 [4, 30, 31]. From an analysis performed over a 4-year period in aluminum smelters [29],[36], it has been confirmed that one of these PAHs, benzo(a)pyrene (BaP), is an excellent indicator to evaluate the toxicity of a coal tar pitch product. So, the PAH compounds have been classified based on the toxicity using BaP as a reference. Table 2.1 shows the classification of PAHs according to their genotoxic level and to their relative potency factor [30, 31].

2.1.1 Source and industrial applications of coal tar pitch

Coal tars are produced during the production of metallurgical coke which then used in blast furnace to producing iron for steel production [37]. A coking coal is placed in a coke oven (Fig. 2.2) and undergoes carbonization at high temperature (1100-1200°C) in reducing atmosphere. The process

removes volatile matters of coal and concentrates the carbon to make coke feed. Released volatiles are condensed and form tars. Coal tar pitches are produced by tar direct distillation [37, 38].

Table 2.1 Some polycyclic aromatic hydrocarbon monomers in coal tar pitch and their relative potency factor (RPF) [3, 30, 39].

PAH	**Chemical Formula**	**Molecule representation**	**Molecular weight**	**RPF**
Non-genotoxic				
Naphthalene	$C_{10}H_8$		128.17	N/A
Fluorene	$C_{13}H_{10}$	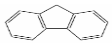	166.22	nil
Phenanthrene	$C_{14}H_{10}$	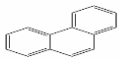	178.22	nil
Anthracene	$C_{14}H_{10}$	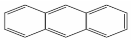	178.22	nil
Pyrene	$C_{16}H_{10}$	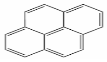	202.25	nil
Naphthacene	$C_{18}H_{12}$	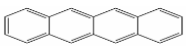	228.29	N/A
Perylene	$C_{20}H_{12}$	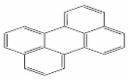	252.31	N/A
Benzo(b)chrysene	$C_{22}H_{14}$	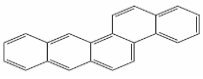	278.35	N/A
Coronene	$C_{24}H_{12}$	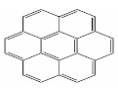	300.35	N/A

PAH	Chemical Formula	Molecule representation	Molecular weight	RPF
Ovalene	$C_{32}H_{14}$		398.45	N/A
Genotoxic				
Benzo(k)Fluoranthene	$C_{20}H_{12}$	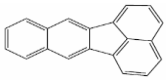	252.31	0.01
Benzo(a)Anthracene	$C_{18}H_{12}$	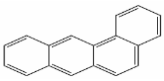	228.29	0.033
Fluoranthene	$C_{16}H_{10}$	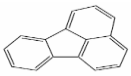	202.25	0.034
Benzo(e)Pyrene	$C_{20}H_{12}$	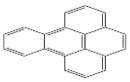	252.31	0.050
Benzo(b)Fluoranthene	$C_{20}H_{12}$	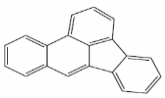	252.31	0.100
Indeno(1,2,3-c,d)pyrene	$C_{22}H_{12}$	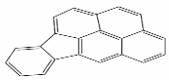	276.33	0.100
Highly Genotoxic				
Chrysene	$C_{18}H_{12}$	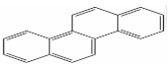	228.29	0.260
Benzo(a)pyrene	$C_{20}H_{12}$	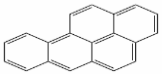	252.31	1.000
Benzo(g,h,i)perylene	$C_{22}H_{12}$	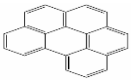	276.33	1.000

PAH	Chemical Formula	Molecule representation	Molecular weight	RPF
Dibenzo(a,h)anthraceen	$C_{22}H_{14}$	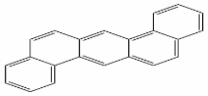	278.35	1.400

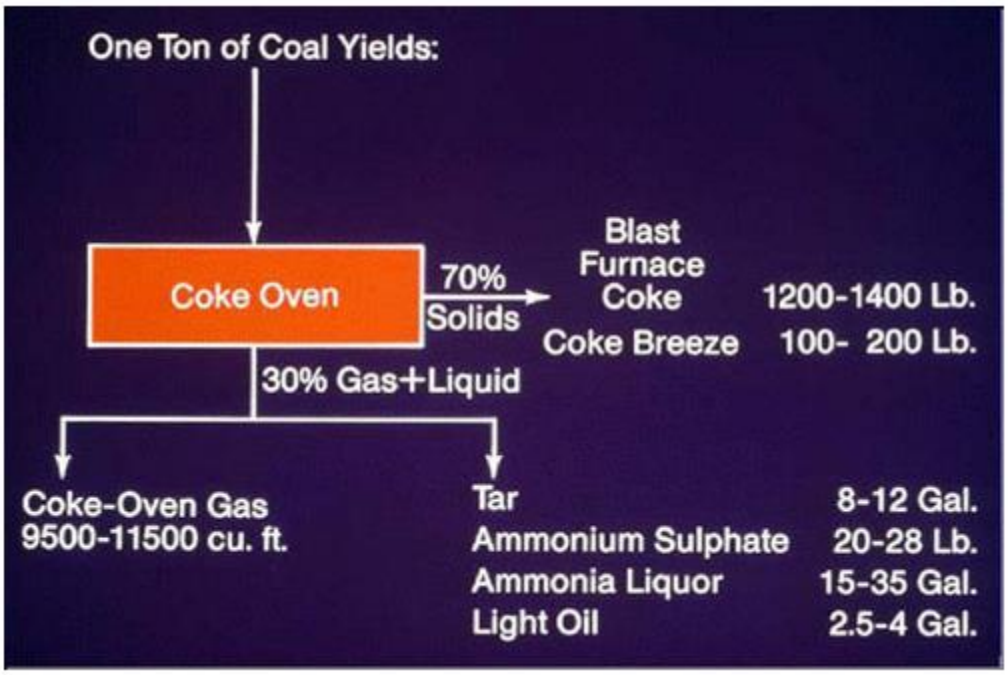

Figure 2.2 Products in coal carbonization [38].

Coal tar pitch is used in the production of various materials ranging from needle coke for graphite electrodes used in electric-arc furnaces [5-8], electrical and mechanical carbon materials widely applied to electric motors brushes, sealing materials, carbon bearings, current collectors [9-15], pitch-based fibers [16-19] to aluminum-smelting prebaked electrodes [20, 21].

2.1.2 Content, properties and characteristic values of coal tar pitch

A. Radenovic [40] reported an average value for properties of coal tar pitch (Table 2.2). This report is based on available experimental data in the literature [41, 42].

Although the separate compounds in the pitch may melt in individually at a fairly high temperature (several hundred °C), the pitch mixture softens in low temperature ranges, e.g. at 100-150°C, because of its unique rheological properties and glass-like behaviors [1, 35]. The "softening point" which is determined using a Mettler softening point apparatus is associated with the flow behavior of pitch at a particular temperature. The glass transition of pitches can be determined using differential scanning calorimetry (DSC) or thermomechanical analysis (TMA) techniques [43, 44]. Coking value as another typical property of the pitch represents the amount of remaining carbon after releasing hydrocarbons volatile constituents of pitch, which happens during heat treatment of pitch in carbon-based material production process. A higher coke value is desired as more carbon remains in the residual pitch. Indeed, the high coking value of coal tar pitch distinguishes it from other pitches (like petroleum pitch) for use in carbon-based material production processes. [45].

Liquid chromatographic technique according to ASTM 2007-75 can be used to determine the content of aromatic and asphaltene compounds in coal tar pitch. The most frequent coal tar pitch characterization method is analysis of group composition of coal tar pitch fractions, based on partition of pitches according to solubility of their compounds in organic solvents. On this basis, one can distinguish between [40]:

- α-fraction of resin or quinoline – insolubles (QI) known in two main forms:
  - α1-fraction or primary fraction, formed by cracking of volatile components and their separation at high temperatures in the process of coal distillation;

- α2-fraction or secondary fraction, formed by polymerization of initially present α1-fractions at increased temperatures.

- β-fraction of resin is the difference between toluene – insolubles (TI) and quinoline – insolubles (QI) matter (Fig. 2.3).

The content of α-fraction in coal tar pitch is determined using the H. March method [42] based on dissolution of coal tar pitch in warm quinoline (75^0C). The obtained mixture is filtered and undissolved part washed with toluene and acetone i.e. benzene and acetone. The amount of β-fraction is calculated from the toluene insolubles (TI) and the quinoline insolubles (QI) fractions according to the expression: β-fraction = TI -QI. Toluene insolubles are determined by dissolution of coal tar pitch sample in warm toluene and following the technique described in reference [46] . A summary of the properties of coal tar pitch is shown in Table 2.2.

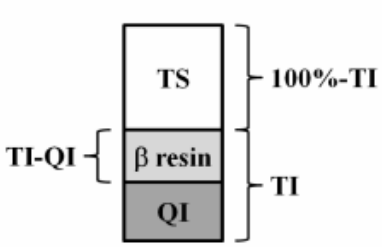

Figure 2.3 constituents of coal tar pitch [22].

Table 2.2 Typical properties of coal tar pitch [35, 40].

Coal Tar Pitch	
Content	
Softening point, °C	116
T_g, °C	34
Coking value (%)	58
Ash, Wt.%	0.14
Metal, mgkg^{-1}	
Ca	140.1
Na	160.2
V	18.2
Sulphur, wt.%	0.43
Aromatics, wt.%	91.2
Asphaltenes, wt.%	1.3
Quinoline insoluble, wt%	7.5
Toluene insoluble, wt%	29.6
β-fraction β-fraction	22.1

One of the main criteria that determine the use of coal tar pitch as binder in carbon based material production is the α-fraction content. This fraction has an effect on carbonization processes and product structure. Higher ratio of α1-fraction indicates increased aromatic compound content and relatively low pitch softening temperature, necessary for its binding properties. However, higher content of that fraction reduces the wetting ability of the pitch. With that in mind, the α1-fraction content is limited to 16%. Increase of temperature results in secondary, α2-fraction, which acts as a centre of nucleation in the carbonization process, ensuring the creation of well-graphitized secondary carbon, which is a result of binder carbonization [40, 42].

The XRD patterns of the pitch is shown in Fig. 2.4. This figure shows the convolution of the (002) peaks for the pitch. They are assigned to three carbon structures represented by a rather ordered

"graphite-like" component (at 2θ about 25.0°) and by two poorly ordered γ-components (at 2θ of 19.0° and 10.0°). As seen in Fig. 2.4, a dominant proportion of carbon in the pitch occurred in the disordered γ_1-matter (65%) and much less proportion did for the least ordered γ_2-matter (10%). The most ordered graphite-like matter accounted for 25 % [47].

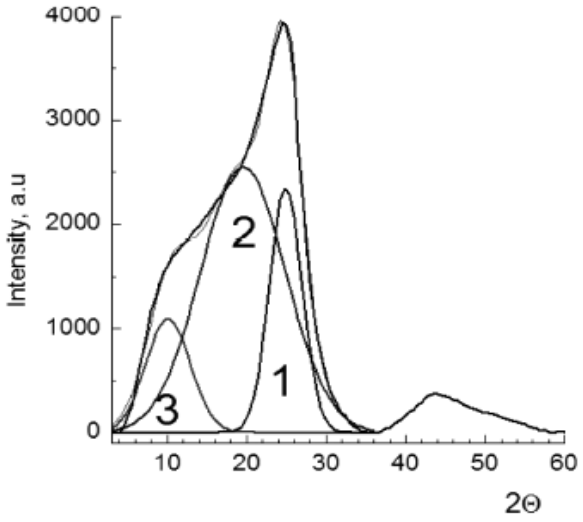

Figure 2.4 Fragments of XRD patterns for pitch (1, "graphite-like" carbon fraction;2, γ_1-carbon fraction, 3,γ_2-carbon fraction) [47].

Some other investigations [48] indicate that the raw coal tar pitch is an amorphous material with no structural ordering in it.

2.2 Evolution of coal tar pitch during carbonization

Carbonization is formally defined as the thermal transformation of carbonaceous materials to carbon materials (CM). CMs are widely applied to produce graphite electrodes used in electric-arc furnaces [5-8], electrode motors brushes, sealing materials, carbon bearing, current collectors [9-15], pitch based fibers [16-19], and aluminum-smelting carbon electrodes [21, 49]. In reviewing the carbon literature, one would have to conclude that there is no area of carbon technology in which more progress has been made than in the fundamentals of carbonization [3, 35, 37, 50-52].

This increased understanding is the result of the efforts of a large number of investigators representing laboratories and institutes throughout the world and development of improved characterizations techniques such as chromatographic methods, thermal analysis, mass spectroscopy, Raman spectroscopy, and electron and nuclear magnetic resonance [37, 50-56]. Franklin is credited as one of the first investigators in this research field [54, 55]. Later, Oberlin and Bonnamy continued the work of Franklin. They have extensively reviewed the carbonization process [37, 51, 52, 56].

Fig. 2.5 shows the structural evolution of carbonaceous materials during progressive heat treatment [53, 57, 58]. Primary carbonization, as the research interest in this thesis, proceeds up to 750-785K; the temperature at which all aliphatic and light compounds are removed and a brittle solid material is obtained (semi-coke stage). This solid carbon material composed of relatively large polycyclic aromatic molecules mutually cross-linked by a solid medium composed of carbon functions containing heteroatoms [59]. This structural description can be represented as a turbostratic crystallite structure. The turbostratic order is defined as the absence of graphenic stacks of carbon, i.e. two-dimensional crystallographic order. However, continuing the heat treatment up to 2300-3000 K results in transforming the turbostratic structure into a three-dimensional graphitic structure (rigorous definition of graphitization) [51, 52, 56, 59].

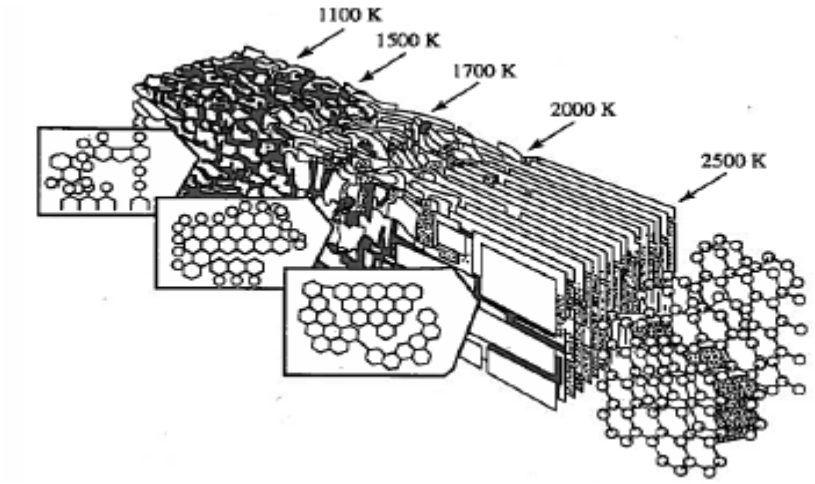

Figure 2.5 Raman spectra evolution of a carbonaceous material to graphite [53, 54, 60].

2.2.1 Physical and chemical changes during carbonization of pitches

As pitches go under carbonization, low molecular weight compounds evaporate. Physical distillation is accompanied by several chemical reactions including oligomerization and polymerization of the more reactive species and cracking of substituent side chains from aromatic rings [61]. Low molecular weight by-products, generated through thermal reactions, are also included in the volatiles from pitch carbonization. Fig. 2.6 presents thermogravimetric analysis (TGA) and gas evolution data for a coal tar binder pitch. The weight loss is attributed largely to physical removal of low molecular weight volatiles in the original pitch [3].

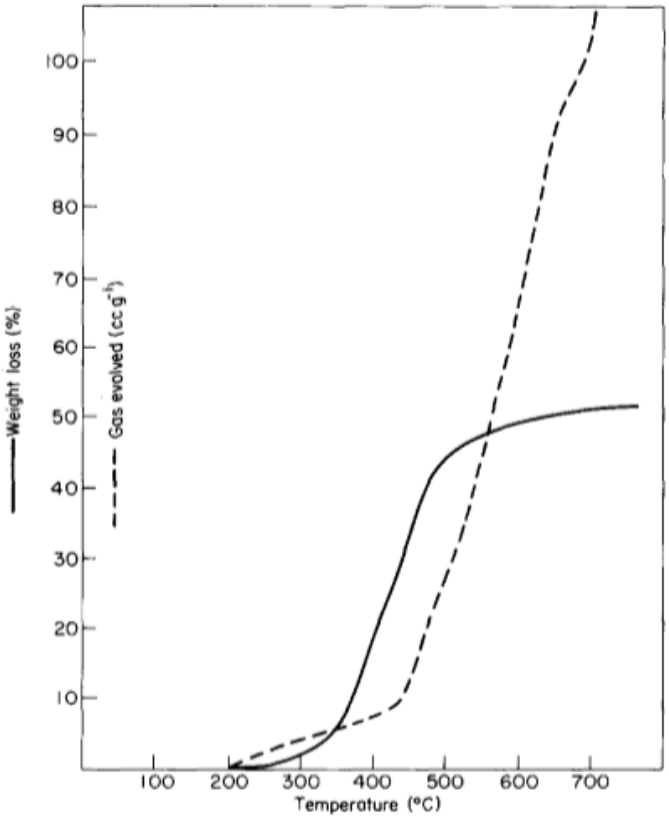

Figure 2.6 Thermogravimetric analysis and gas evolution data of coal tar pitch at 10°C min^{-1} in argon [3].

From chemistry point of view, carbonization can be envisioned by the scheme shown in Fig. 2.7. A small aromatic structure is polymerized to an aromatic polymer, which achieves the turbostratic crystalline structure of coke in temperature range of 500-1000°C. Additional heat treatment of coke which accompanied by dehydrogenation process results in carbon and ultimately the three-dimensional order of graphite [50, 62].

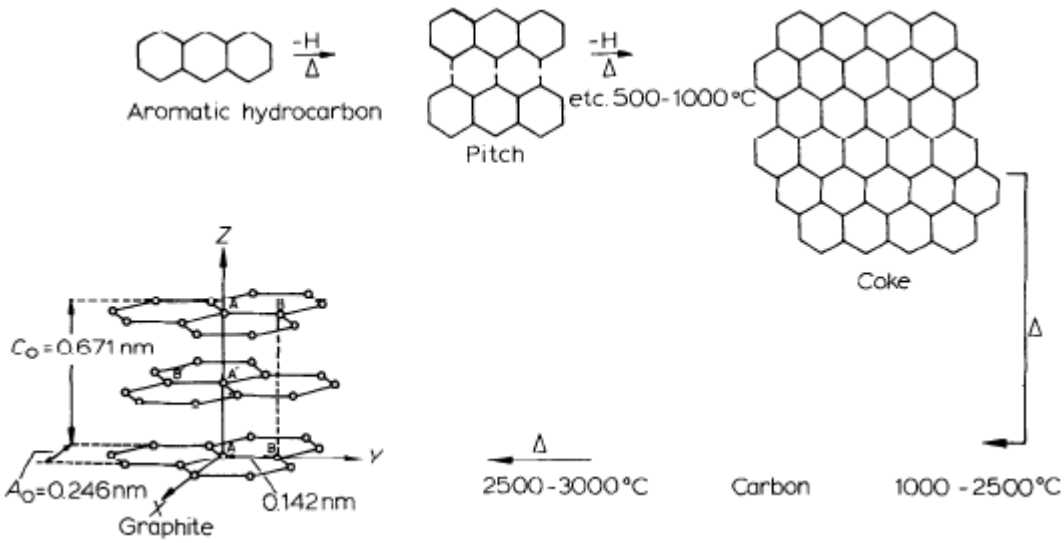

Figure 2.7 General reaction scheme for carbonization [50].

The overall process of carbonization is exceedingly complex. However, we can consider individually the following processes, which represent some of the major reactions involved in the pyrolysis of aromatic hydrocarbons:

1. C-H, C-C bond cleavage to form reactive free radicals;

2. Molecular rearrangement;

3. Thermal polymerization;

4. Aromatic condensation.

The initial thermal reaction in the carbonization of an aromatic hydrocarbon is poorly understood. It is believed to involve the formation of a free radical intermediate (Fig. 2.8) [4, 50, 63, 64].

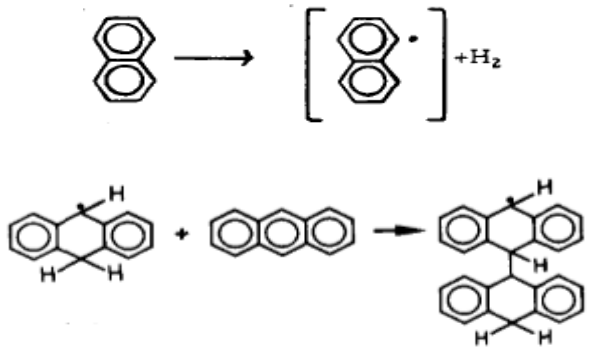

Figure 2.8 Initial reactions in the pyrolysis of naphthalene and anthracene [4, 50].

The reacting intermediate once formed, can undergo direct polymerization as in the formation of naphthalene polymer (Fig. 2.9). These initial polymerization reactions involve the loss of hydrogen. Decreasing of the H/C ratio with heat treatment temperature (up to 1000°C) indicates the removal of hydrogen in different forms (hydrogen or methane) during the carbonization of pitches (with different characteristics) to coke (Fig. 2.10) [3, 56].

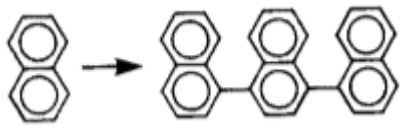

Figure 2.9 Thermal polymerization of naphthalene [50].

Another step in early stages of carbonization is that of thermal rearrangement. This reaction often makes it difficult to relate the starting structure to the subsequent course of graphitization. Fig. 2.11 presents several instances of thermal rearrangement which have been studied by Lewis [28, 50]. As shown in the examples for acenaphthalene and bifluorene, this reaction can transform unstable five-membered rings into more stable six-membered ring system without the loss of carbon atoms. The last example, methyl-phenanthrene illustrates a similar type rearrangement which involves the loss of carbon atoms.

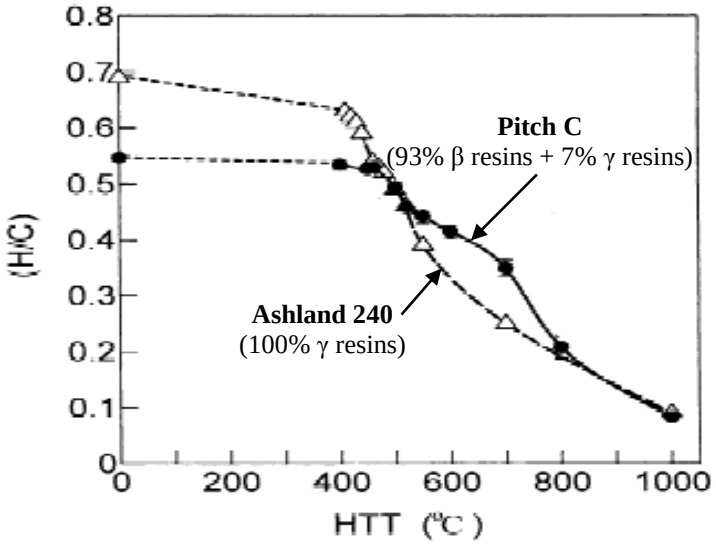

Figure 2.10 H/C ratio changes with heat treatment temperature [56].

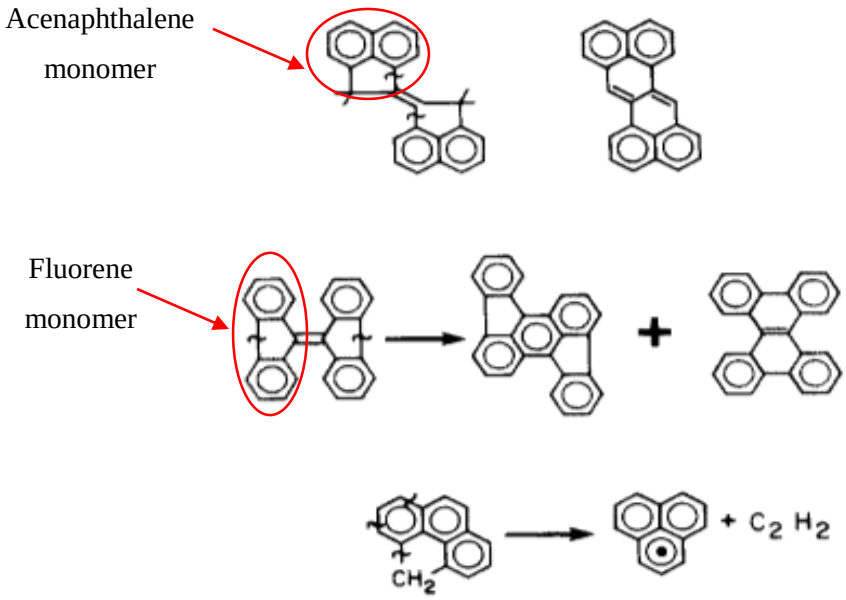

Figure 2.11 Thermal rearrangement reactions in pyrolysis [50].

Either the starting molecule or a rearranged entity serves as the building block in carbonization. One of the factors that makes carbonization so complex is the presence of many polymerization sites in an aromatic molecule. Various reactivity parameters including localization energies [65, 66], activation energies and pre-exponential factors [67, 68] as well as steric effects [69-71] can be

used to predict the site in aromatic ring at which polymerization should predominantly occur [50]. As shown in Fig. 2.12, polymerization process can occur in two stages resulting in either noncondensed or condensed polymers [50, 72].

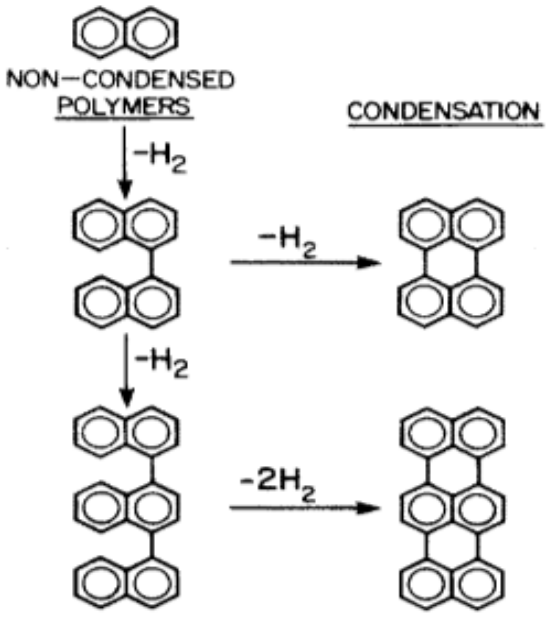

Figure 2.12 Polymerization-condensation process in carbonization [50].

The loss of two hydrogen atoms between two naphthalene molecules leads to polymers in which the units are linked by single bonds. Additional loss of two hydrogen atoms creates fully condensed polymer.

Eventual polymerization to carbon occurs in two dimensions. Figs. 2.13 and 2.14 show how the molecule zethrene has the perfect shape and reactivity to polymerize in two dimensions to a planar graphitic-like structure without vacancies but poorly graphitizing compound tetrabenzonaphthalene cannot polymerize without creating vacancies.

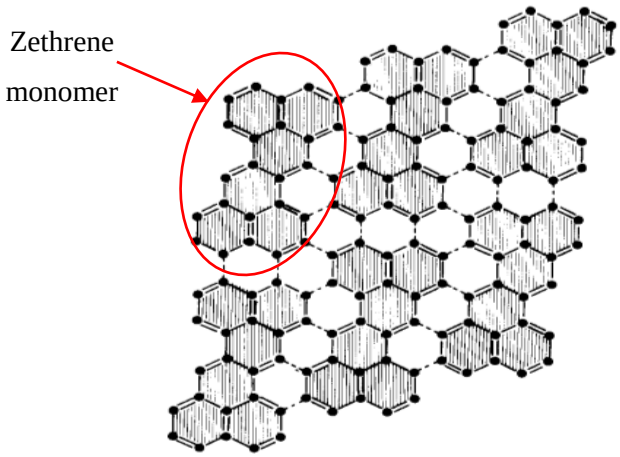

Figure 2.13 Two-dimensional polymerization for zethrene [50].

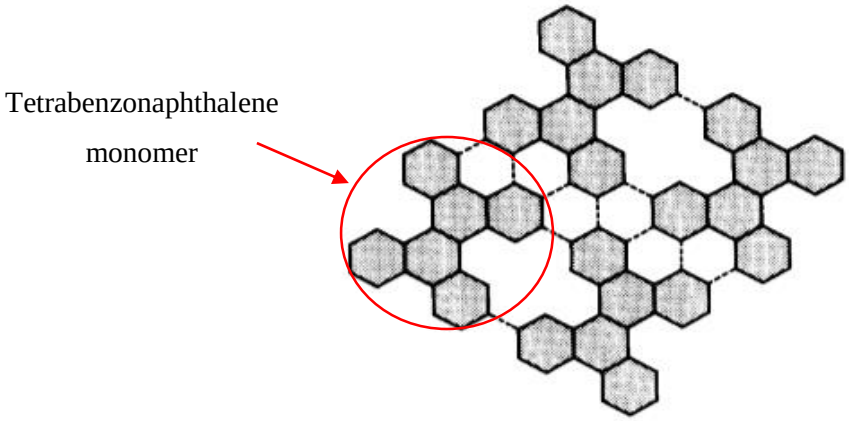

Figure 2.14 Two-dimensional polymerization for tetrabenzonaphthalene [50].

2.2.2 Carbonaceous mesophase formation

History and Prospects

Ramdohr [73] in 1928 for the first time described the optical anisotropy of cokes. Then, Marshall [74], Stach [75] and Abramski and Mackowsky [76] and others have described the optical anisotropy of various cokes and coke-like carbons [23, 77]. None of them has recognized intermediate stages in the development of the characteristic anisotropic mosaic structure. In 1961,

Taylor made initial observations in the Wongawillie coal seam in New South Wales, Australia [78]. An igneous dyke passed vertically through a coal seam, which resulted in the slow carbonization of the coal over long distances. Taylor examined the coal samples approaching the dyke using polarized-light microscopy and discovered small anisotropic spheres. On approaching the dyke, the spheres were larger due to coalescence to form anisotropic coke [79, 80]. Then, in 1965, Brooks and Taylor [23, 26] concluded that these spheres are result of formation of nematic liquid crystals during the thermal transformation of aromatic compounds (specifically as the constituents of pitches) to coke and named them as "carbonaceous mesophase". Mesophase means "intermediate phase" and was suggested to discriminate these materials from conventional "liquid crystals". Brooks and Tylor suggested the name "carbonaceous materials" to emphasize on the liquid crystal nature of these carbon-rich materials [23, 26, 79, 81].

Microscopic view of mesophase formation - Nucleation of mesophase, growth and coalescence

When pitches and aromatic hydrocarbons are heat treated at temperatures around 350-450°C and polymerization reactions are taken place, the size of the constituent polyaromatics is large enough to be considered as "discs" [80, 82]. Fig. 2.15 shows the model of constituent molecules in the mesophase-containing pitch as proposed by Zimmer and White [83]. When the association of the constituent molecules becomes energetically favorable, molecules of this type become bound to each other, surface to surface, by van der Waals forces.

Due to the mobility of the molecules in early stages of polymerization, the association times are short but with continuing the polymerization, the time of association of the mesogen molecules (molecules with tendency to form mesophase) of similar size and shape increases and, consequently, growth units of molecules are formed as reflecting spheres as seen in the optical

microscope [80, 84]. Fig. 2.16 shows a model diagram representing mesogen molecules and optical micrograph of mesophase spheres when the heat treatment temperature is 450°C [80].

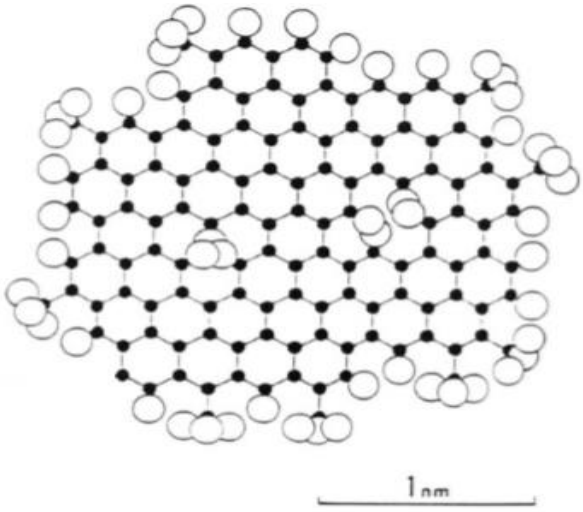

Figure 2.15 Model of a planar aromatic of the type that forms lamellar nematic liquid crystals [83].

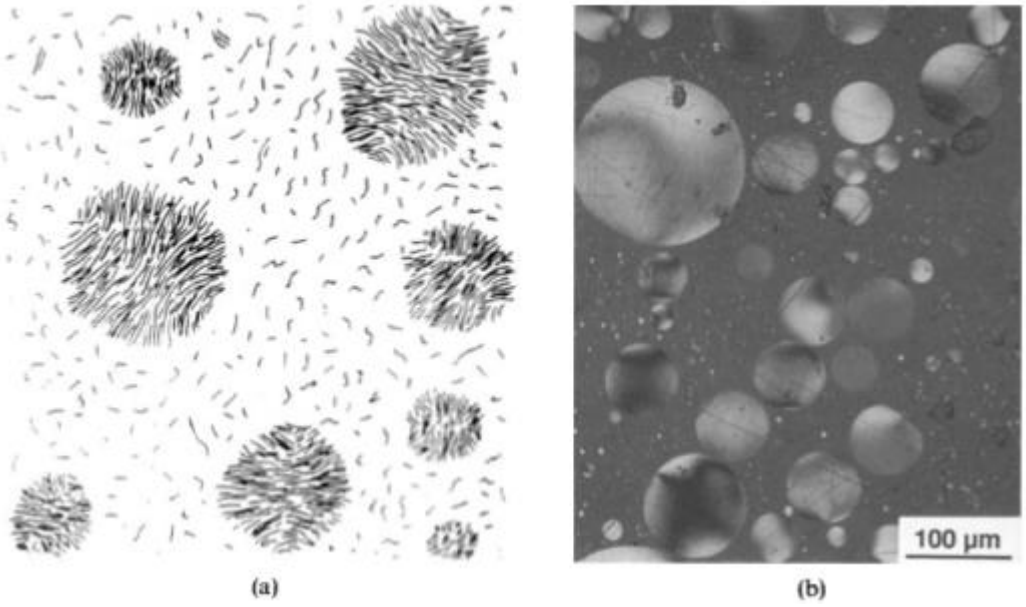

Figure 2.16 (a) Schematic diagram of a discotic nematic liquid crystal spheres in a liquid pyrolysate; and (b) an optical micrograph of mesophase spheres [80].

Observation of Oberlin indicates that during the very initial stages of mesophase formation, the discotic mesogen stacks in columns [33, 51]. Then, as a requirement of minimum surface energy, a spherical shape of growing mesophase becomes established [80]. As indicated by electron diffraction study carried out by Brooks and Taylor [26], the constituent lamellar molecules of the sphere are parallel to each other and parallel to an equatorial plane. Optical microscopy shown in Fig. 2.17 indicates that the layers become orientated toward the poles of the spheres and they are perpendicular to the interface with the isotropic matrix.

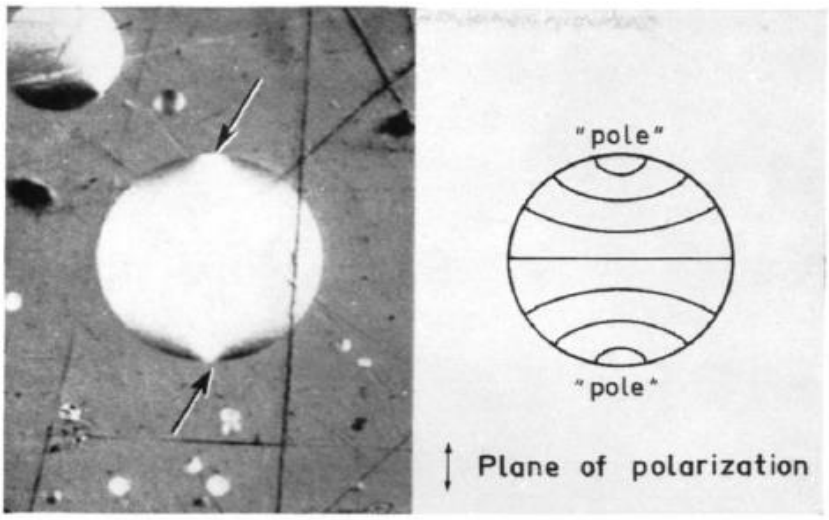

Figure 2.17 Structure of a mesophase spherule [23, 85].

The size of mesophase spheres increase with increasing time and /or temperature of carbonization. The growth of these spheres continues until contact is made with others and instantaneously a larger sphere is formed. This phenomenon is known as “coalescence” (Fig. 2.18) [26, 80]. Coalescence is a function of viscosity of the polymeric mesophase which must remain sufficiently deformable (low viscosity/high plasticity) to respond to the requirement of minimum surface energy. When spheres of low viscosity mesophase coalesce, the structure within the resultant unit is rapidly reorganized [80]. The new mesophase units adopt the spherical shape with larger size but do not

retain the detail of the Brook and Taylor morphology [26]. Fig 2.18 shows how small spheres in position Y with the Brook and Taylor morphology are coalescing to form larger spheres losing initial structure and becoming more complicated coalesced spheres (position X).

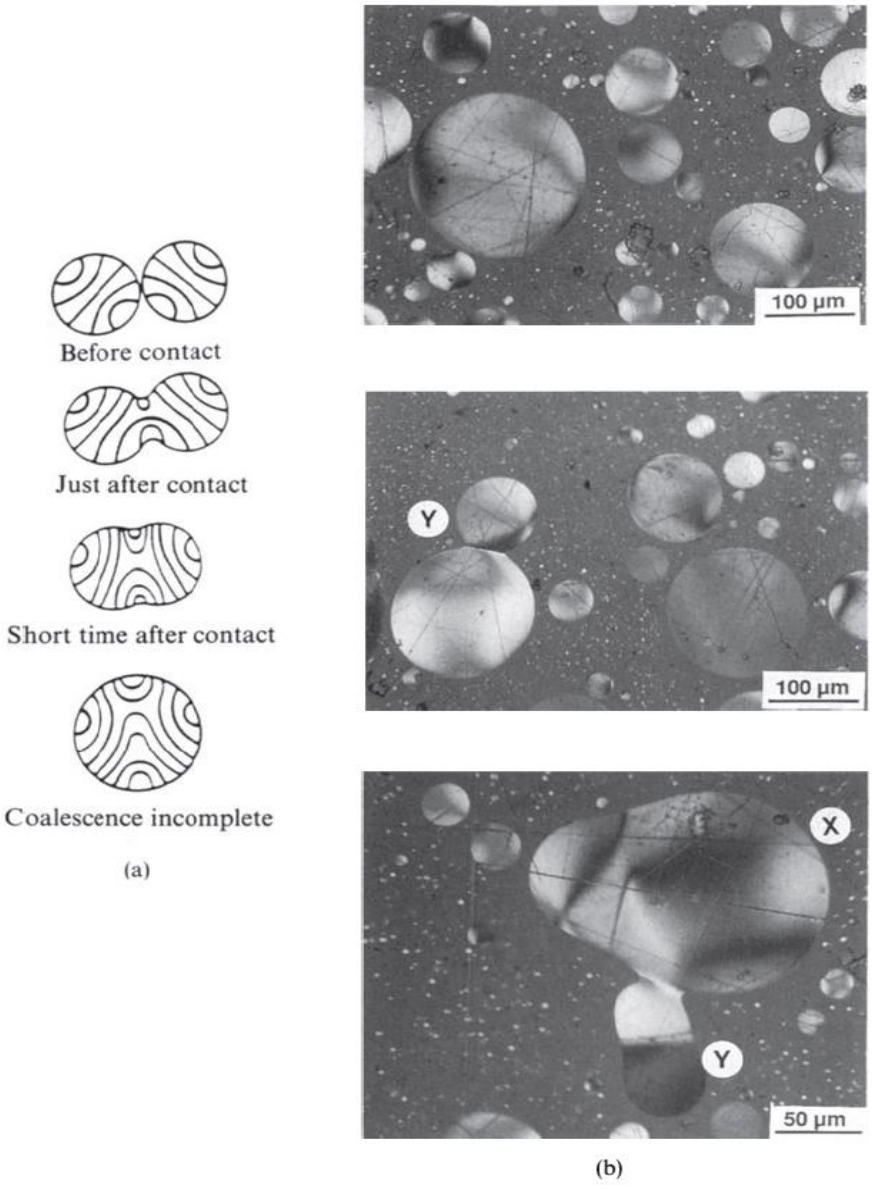

Figure 2.18 (a) Rearrangement of molecules when two spheres coalesce; (b) optical micrographs of mesophase spheres from carbonization of petroleum feedstock at 713 K. [Y] spheres with Brooks and Taylor morphology during the coalescence process and [X] spheres with more complex structure [26, 80].

When the coalescence of spheres takes place toward the end of the heat treatment process of pitch, they are transformed into bulk of mesophase [35, 86]. Fig. 2.19 shows the schematic of transformation of small Brook and Taylor spheres to bulk of mesophase in early stages of carbonization [86].

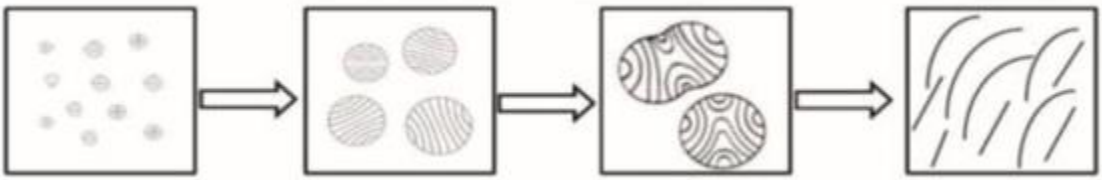

Figure 2.19 Schematic of formation and development of bulk liquid crystalline mesophase.

Macroscopic view of mesophase formation

Molecular weight distribution (MWD) changes of pitch during mesophase formation has been studied using gel permission chromatography (GPC) by Greinke [87, 88]. MWD obtained for some of polymerized pitches heated at 400°C for reaction time between zero and 16 hours are shown in Fig. 2.20. After 2 hours, when most of the pitch volatiles are distilled and the pitch becomes rich in mesogen molecules, average molecular weight of the pitch increases with time due to progressing polymerization reactions and subsequent mesophase formation. The pitch contains 100% mesophase after 16 hours of heat treatment. This increase in average MW is entirely attributed to polymerization reactions of 400-700 MW PAH molecules present in the pitch. The most interesting observation of these studies is that significant amounts of pitch components with MW greater than 1000 are present in two-hour pitch sample, but molecules with molecular weights near 2000 are not observed after 16 hours. This result indicates that the reaction of 1000 MW molecules and larger with each other must be extremely slow. In fact, polymerization reactivity of molecules with molecular weights between 700 and 1000 rapidly decrease and ultimately

molecules larger than 1000 MW react negligibly during mesophase formation. This lack of reactivity of the larger molecules ensures that the mesophase remains highly fluid during a wide range of reaction conditions. This prolonged fluidity is critical for many industrial processes utilizing mesophase pitch.

Later, Greinke and Singer [89] studied the separated coexisting phases (isotropic liquid and mesophase) during transformation of pitch to mesophase by GPC (Fig. 2.21). They established that the molecular weight distribution of the mesophase did not change during mesophase formation but the average MW of the isotropic liquid increased significantly.

The results indicates that both coexisting phases contain similarly sized molecules in different proportions (Fig. 2.21). This phenomenon can be explained by the polymerization of smaller molecules (400-1100 amu) within the isotropic phase, the selective transfer of these molecules into the mesophase and also by the stability within the isotropic phase of larger size molecules (>1100 amu).

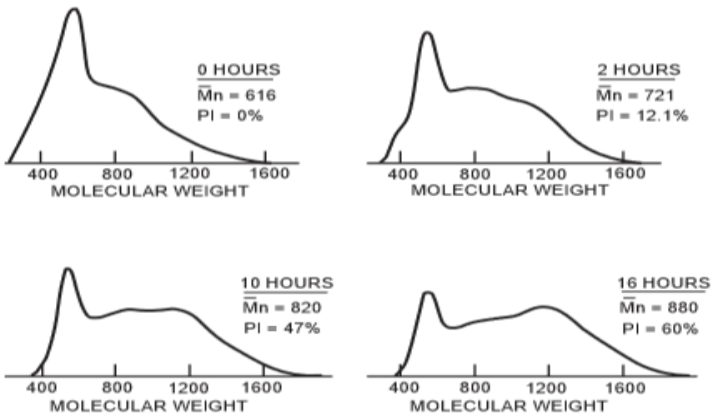

Figure 2.20 Molecular weight distribution from GPC curves of pitch as a function of time at 400°C [87].

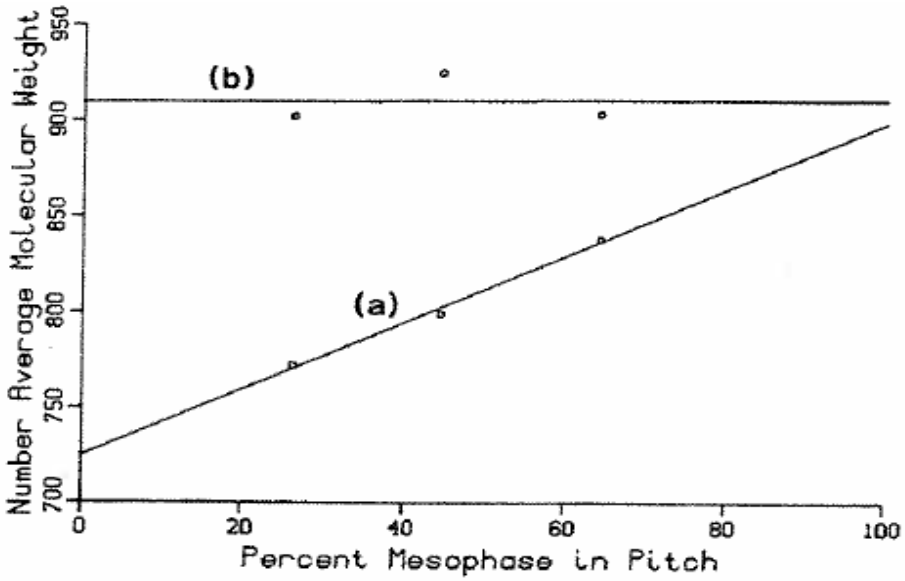

Figure 2.21 Number average molecular weight of the coexisting isotropic liquid (line a) and mesophase (line b) fractions in the pitch during the transformation [89].

2.2.3 Semi-coke (and coke) formation

As the temperature increases to around 450°C, higher MW PAHs become more reactive because of increasing reaction rate constants and activation energies with increasing temperature [87]. Further irreversible polymerization accompanied by dehydrogenation process results in a continual growth in the aromatic molecular size and semi-coke formation. Greinke's investigation suggests equal molecular reactivity of the 700-1200 MW molecules in semi-coke formation step. However, a number of experiments in his studies illustrates that the kinetics of carbonization changes significantly after mesophase has formed and when the system is transformed into a semi-coke. It is due to a physical phenomenon in which solid state reactions occur in the polymerized pitch [87]. Fig. 2.22 shows the MWD changes during semi-coke formation. The polymerization of pitch molecules with MW greater than 1000 results in the buildup of the greater than 2000 MW peak in this figure [87].

Continuing the heat treatment of semi-coke beyond 500°C leads to the formation of carbon materials. However, primary carbonization (as the research interest in this thesis) refers to heat treatment of pitches up to around 550°C corresponding to early stages of coke formation [37, 51, 52, 56].

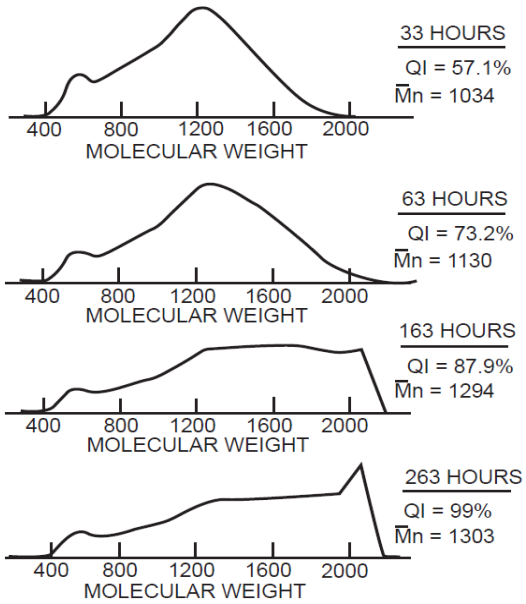

Figure 2.22 Molecular weight distribution of pitch at different times during semi-coke formation [87].

2.3 Thermodynamics of carbonaceous materials (coal tar pitch) in different phase states: solid, mesophase, liquid and gas

Coal tar pitch as one of the important carbonaceous material, which is used as binder in carbon-based materials production, appears in different states when it goes under carbonization process. Description of phase behavior of pitch in different steps of carbonization requires prediction of thermodynamic properties of pitch constituents including different monomers, oligomers and polymers of polycyclic aromatic hydrocarbon compounds. Specifically, thermodynamic of

mesophase as an intermediate state appearing during the carbonization process is discussed in this section.

2.3.1 Thermodynamics of pure PAHs

Thermodynamic properties of pure PAHs in different states (solid, liquid or gas) at different temperatures can be calculated using standard thermodynamic properties at 298.15 K and 1 bar and heat capacity as a function of temperature.

$$H_T^\circ = H_{298.15\,K}^\circ + \int_{298.15}^{T} Cp\, dT \qquad \text{Eq. (2.1)}$$

$$S_T^\circ = S_{298.15\,K}^\circ + \int_{298.15}^{T} \frac{Cp}{T} dT \qquad \text{Eq. (2.2)}$$

$$G_T^\circ = H_T^\circ - T.S_T^\circ \qquad \text{Eq. (2.3)}$$

One issue in these equations is to find the temperature dependent function of heat capacity. Consideration of heat capacity experimental data of PAHs in a wide range of temperature (50-1200 K) indicates that the molar heat capacities of PAHs in solid, liquid, and gaseous states can be represented as a polynomial function of temperature.

$$C_p(solid) = a + bT + cT^2 + dT^{-2} \qquad \text{Eq. (2.4)}$$

$$C_p(liquid, gas) = a + bT + cT^2 + dT^3 + eT^4 \qquad \text{Eq. (2.5)}$$

a, *b*, *c*, *d*, and *e* in these empirical functions stand for temperature-independent coefficients for the species of interest. Different terms in Eq. (2.4) enables fitting accurately the experimental data of solid PAHs in temperature range of interest for the carbonization process (up to 1200 K). Meanwhile, flat form of heat capacity function of solid PAHs at high temperature ranges can be

correlated using Eq. (2.4). Two last terms in Eq. (2.5) permit correlating the experimental data of liquid and gaseous PAHs, which is mostly available in temperature ranges above 300 K.

Standard thermodynamic properties and correlation for heat capacity of a limited number of PAHs in different states can be found using available experimental data in the literatures [90-110].

Richard and Helgeson [111] have shown that standard thermodynamic properties as well as heat capacity coefficients of other pure PAHs (with lack of experimental data reported in the literature) can be predicted using group contribution method. In this method, some PAHs (with enough experimental data and containing required groups to generate a new high molecular weight compound) were selected as reference compounds. These groups for polycyclic aromatic compounds studied in Richard and Helgeson's work are listed in Table 2.3 [111].

Standard thermodynamic properties (or heat capacity coefficients) for groups are calculated from corresponding standard thermodynamic properties (or heat capacity power function coefficients) of the reference compounds using following expression:

$$\Xi_j^\circ = \sum_i n_{ij}\ \Xi_i^\circ \qquad \text{Eq. (2.6)}$$

where n_{ij} represents the number of moles of the i^{th} group in one mole of j^{th} reference compound, $\Xi^{o}{}_{i}$ and $\Xi^{o}{}_{j}$ denote any thermodynamic property (or heat capacity function coefficient) of the subscripted group and that of j^{th} reference compound, respectively [111].

Table 2.3 Different groups of reference polycyclic aromatic compounds.

Groups	Description
	Carbon atom in a bridge (B) between two benzene rings in a polycyclic aromatic hydrocarbon
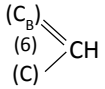	Group adjoining a bridge (B) between two benzene rings in a polycyclic aromatic hydrocarbon
	Group not adjacent to a bridge (B) between two benzene rings in a polycyclic aromatic hydrocarbon
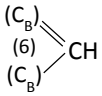	Group adjacent to two bridges
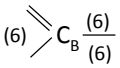	Group at the junction of three aromatic rings
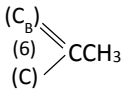	Methyl group adjacent to a bridge

Finally, standard thermodynamic properties (or heat capacity coefficients) of high molecular weight PAH compounds (oligomers or polymers of PAH) can be derived using standard thermodynamic properties (or heat capacity coefficients) of the groups present in the compounds [111].

In Richard and Helgeson's approach, standard thermodynamic properties and heat capacity coefficients of the PAH compounds in different states (liquid and solid) are estimated separately without any consideration for consistency between them. Hence, it is expected that these data do not have enough accuracy to be utilized for the estimation of other thermodynamic properties (such as vapor pressure) which requires the information on different phases.

The philosophy of the CALPHAD approach is to obtain the thermodynamic data rendered consistently with phase transition data and computation of vapor pressure using the Gibbs energy

function of condensed and gaseous phases of a given compound [112]. This approach can be applied to optimize thermodynamic properties obtained based on group contribution method.

Moreover, thermodynamic model developed by Richard and Helgeson [111] does not take into account PAH compounds exhibiting anomalous behavior due to specific molecular structure which is discussed in the next section. Meanwhile, this model has not been extended for thermodynamic propertyestimation of PAHs in gas state.

Anomalous Behavior in PAH Compounds

Literature review was carried out to determine PAH compounds exhibiting heat capacity anomaly in solid state. An anomalous absorption of energy is found in the vicinity of the temperature at which the anomalous behavior appears and results in a big jump in temperature dependent heat capacity function of these PAH compounds in crystalline phase (see heat capacity function of phenanthrene in Fig. 2.23). It has been found that this anomalous behavior which previously suggested by the anomalies in thermal expansion is associated with a second-order phase transition in solid state [113]. Regarding Eqs. (2.1) and (2.2), changing the heat capacity function of these compounds in temperature range of the phase transition affects their temperature dependent enthalpy and entropy functions.

Table 2.4 shows a summary of this study for PAHs with 3 and 4 benzene rings in their molecular structure. According to obtained data, some PAH compounds such as phenanthrene, pyrene, and chrysene show a phase transition in solid state. X-ray and Neutron diffraction of crystal structure of these compounds showed that the overcrowded hydrogen atoms in the molecular structure are responsible for the anomalous behavior [114-116].

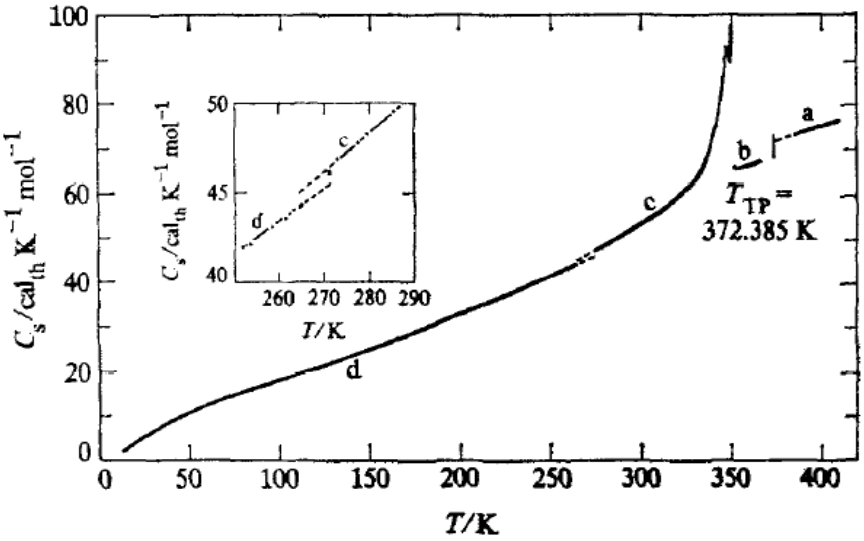

Figure 2.23 Heat capacity and phase transition of phenanthrene [116].

Table 2.4 Anomalous behavior information of some PAH compounds [96, 109, 113, 114, 116-123].

Number of rings	3	4	4
Compound	Phenanthrene ($C_{14}H_{10}$)	Pyrene (C16H10)	Chrysene (C18H12)
geometry	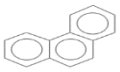		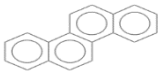
Anomaly in heat capacity	■[116, 118, 121]	■ [109, 121]	■ [118, 121]
Peak temp.(°C)	72 [121],74 [116],72 [114],70 [123],71 [113],72 [96]	-152.35 [109],-157 [124]	230 [121]
Temp. range for thermal anomaly (°C)	58-71 [118] ,45-70 [113],60-80 [117]		234-244 [118]
ΔH of crystal transition(cal/mol)	300 [118] ,260 [113],380 [117]	69±1 [109]	860±40 [121],770±50
Origin of anomaly	Over-crowded hydrogen [121], hydrogen overcrowding, molecular distortion caused by overcrowded H atom [123],[96]	Over-crowded hydrogen [121]	Over-crowded hydrogen [121]

Number of rings	3	4	4
Crystallography method	x-ray [121] neutron scattering [114] x-ray and neutron diffraction [123] infrared and Raman spectra [96]	x-ray [119] neutron diffraction [120] Ramen Scattering [122]	x-ray [121]
Transition effect	Neither order-disorder nor displactive change, rearrangement of hydrogen atoms, slight change on lattice constants, [96], [118], [114], [113]	No change either crystal structure or space group, only small rotation of molecule around c-axis, [119]	Small change on lattice constants, no change on crystal system or space group [118]

Heat Capacity Anomaly in Phenanthrene

Phenantherene with chemical formula $C_{14}H_{10}$ is the isomer of anthracene. The solid properties of two isomers differ significantly. The most important difference is that phenanthrene has an crystal transition at ambient pressure while anthracene does not [124]. The phase transition in phenanthrene has been the object of much study since its behavior is unusual. Heat capacity studies show a thermal anomaly with a maximum at 347.15 K (Fig. 2.23) [116].

Structural evidence given by x-ray and neutron diffraction studies shows that the observed phase transition may be related to increased vibration of hydrogen atom on the 4^{th} and 5^{th} sites of the phenanthrene molecule (Fig. 2.24). On passing through the phase transition temperature, both the crystal system (which is monoclinic) and the space group remain unaltered. Only slight changes in lattice constants are observed during this phase transition [124].

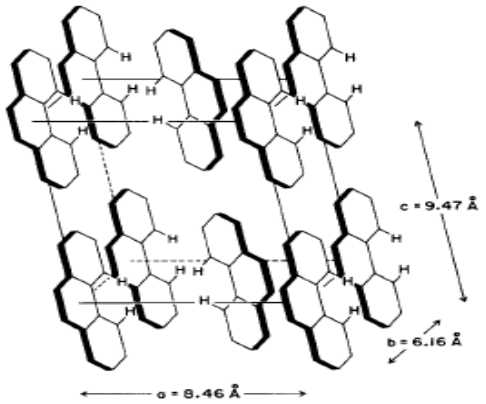

Figure 2.24 Position of the phenanthrene molecule in the unit cell [124].

2.3.2 Phase transition of single-component PAH

Fig.2.25 presents melting points for a selection of single-component, fully condensed PAHs. Also, as shown in the Fig. 2.25, there is a shaded region identifying the temperature and molecular weight range in which carbonaceous mesophase typically appears. The temperature upon heating at which mesophase (with a liquid crystal nature) reverts to an isotropic liquid is defined as the clearing temperature. Indeed, it can be considered as a "second melting" which is an orientational order/disorder transition within the liquid state.

Some PAHs with melting temperature higher than clearing temperature range cannot form liquid crystal. In this case, freezing and appearance of the crystalline solid phase is the first phase transition encountered during cooling of isotropic liquid phase [125].

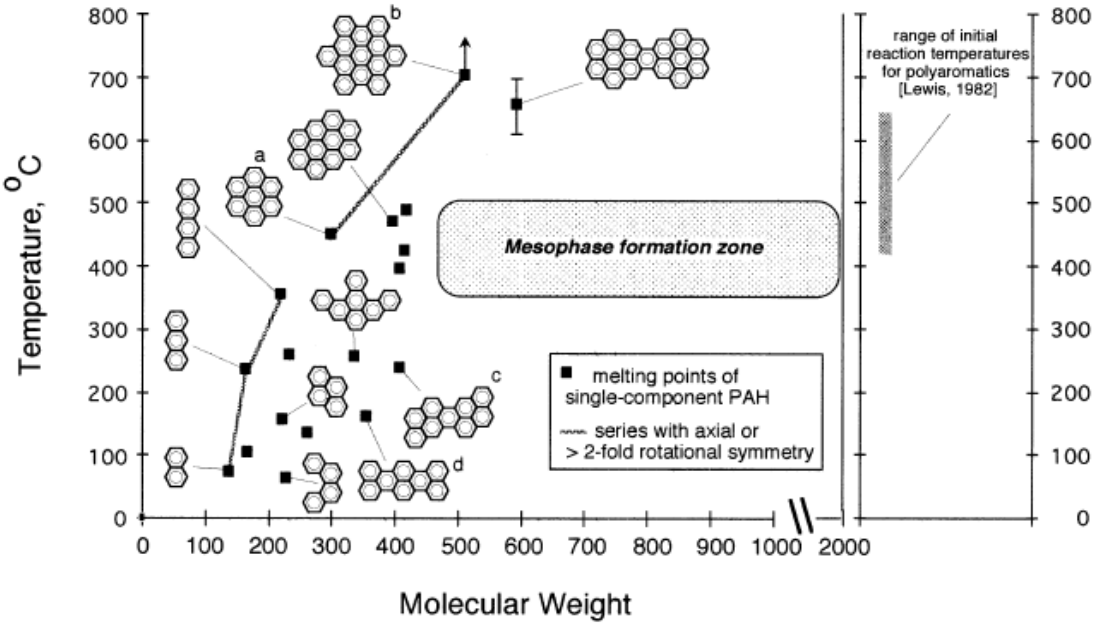

Figure 2.25 Melting points of various single-component PAH [125]. PAH reaction temperatures in right panel from Lewis [50].

2.3.3 Phase transitions in binary PAH mixtures

Hu and Hurt [125] showed that the phase behavior of binary PAH mixture, which has been treated by Cummings and Diefendorf [27], can be understood by consideration liquid / nematic equilibrium relations. Fig. 2.26 presents a hypothetical phase diagram of the binary mixture consisting of a low molecular weight, non mesogenic PAH, component A, and a higher molecular weight mesogenic PAH, component B. Note that the melting temperature of pure A lies above the clearing temperature . Therefore, as the isotropic liquid A is cooled from high temperature, the first phase transition observed is the formation of the crystalline solid. While, cooling the isotropic liquid B results in the formation of liquid crystal (mesophase) regarding the clearing temperature of pure B, which lies below the melting point. In certain region on the phase diagram (Fig. 2.26) where the temperature is above eutectic temperature as well as the melting temperature of component B and the composition of A/B mixtures is rich enough in component B (with tendency to form liquid crystal), calculations of Gibbs energy are needed to describe the phase behavior of mesophase-containing mixtures. Equality of the chemical potential for each component *i* in different phases at equilibrium (i.e. mesophase and isotropic liquid) leads to phase diagram determination of the mixture. These regions on the phase diagram do include mesophase, including a pure mesophase region, and a two-phase region with coexisting isotropic liquid.

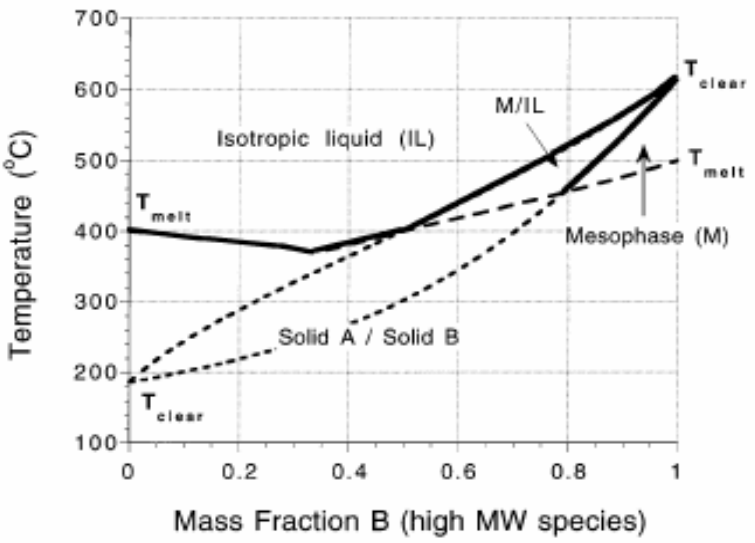

Figure 2.26 Binary phase diagram for generic PAH of low and high molecular weight [125].

2.3.4 Thermodynamics of carbonaceous mesophase

It is now well known that carbonaceous mesophase is a discotic nematic liquid crystal phase composed of mostly fully condensed high molecular weight PAH molecules. Discotic nematic liquid crystal phase represents a liquid crystalline phase including nearly planar disc-shape species with their basal planes preferentially aligned perpendicular to a common vector (see Fig. 2.27). In fact, the species in this phase oriented in parallel but not arranged in planes.

Figure 2.27 Discotic nematic liquid crystalline phase [125]

It has been suggested that two driving forces are important for the formation of mesophase: liquid crystal nature of mesophase [125, 126] and non-ideal solution behavior of pitches [127, 128].

The first approach is based on the theory that mesophase is a liquid crystal phase and the orientational potential effect is the main subject for mesophase formation. Shishido et al. [126] applied the molecular field treatment of mesogen-nonmesogen mixtures to describe a phase diagram for a mesophase pitch [129, 130]. Mesogen species in this mixtures refers to low molecular weight PAHs whose the melting temperature lies above the clearing temperature and nonmesogen molecules are high molecular weight PAHs with the melting point higher than the clearing temperature. Their model does not consider the effect of non-ideal mixing of pitch fractions of differing molecular weights or chemical compositions and thus can be classified as an ideal solution approach. They applied the model to an experimental phase diagram reported previously by Mochida and Korari [131]. In the original experiments, Mochida and Korai [131] separated a petroleum pitch into benzene soluble (BS) and benzene insoluble (BI) fractions and recombined them in various weight ratios and at various temperatures to obtain the partial phase diagram. Shishido et al. [126] treated both fractions as pseudo single components in order to reduce the complexity of the problem. They assumed the benzene soluble fraction to be non-mesogenic (having no liquid crystal forming tendency), and the benzene insoluble fraction to be mesogenic (having liquid crystal forming tendency). Fig. 2.28 compares binary phase diagram predicted by Shishido et al. and experimental data of Mochido et al. [128]. Later, Hu et al. [125] continue the work of Shishido et al. by applying the theory which is based on virtual clearing temperatures assigned to individual molecular weight fractions taken as pseudo components. The virtual clearing temperatures are determined using an empirical formula. Hu and Hurt [125] offer no technique for determining activity coefficients in the mesophase or isotropic phases, thus forcing a potential user

to adopt the additional assumption of ideal solution behavior for practical application of the model. Fig. 2.29 shows the result (binary phase diagram)obtained by Hu and Hurt [125] in comparison with experimental data of Mochida [131].

All these attempts were based on ideal solution behavior. Since, there is strong experimental evidence for non-ideal solution behavior in pitch [127, 128], Hu et al. [127] utilized a treatment of non-ideal solution for an accurate description of mesophase-isotropic liquid equilibrium. In fact, they proposed a new theory that integrates two distinct conceptual approaches: liquid crystal and non-ideal behavior of mesophase.

General thermodynamic theory of Hu et al. for mesophase-containing pitch

In order to develop a comprehensive thermodynamic model, Gibbs free energy model must be formulated. Hu and Hurt [127] proposed the Gibbs free energy function of a mesophase-containing pitch system (which appears as an intermediate mixture during heat treatment of coal tar pitch) as follows:

$$G = \sum n_i \, g_i^0 + \Delta G_{mix} + G_{orient} + G_{surface} + G_{elastic} \qquad \text{Eq. (2.7)}$$

$$\Delta G_{mix} = \Delta G_{mix}^{ideal} + \Delta G_{mix}^{excess} \qquad \text{Eq. (2.8)}$$

where, G is the Gibbs free energy of the system, g_i^0 are reference molar free energy functions for the pure components as isotropic liquids, ΔG_{mix}^{ideal} is the ideal Gibbs free energy of mixing, ΔG_{mix}^{excess} is the excess Gibbs energy of mixing, G_{orient} is the orientational free energy and n_i are the number of moles of each components in the system[127, 132] . Interfacial and elastic strain energies in Gibbs free energy function can be neglected when one focuses only on macroscopic samples [133, 134].

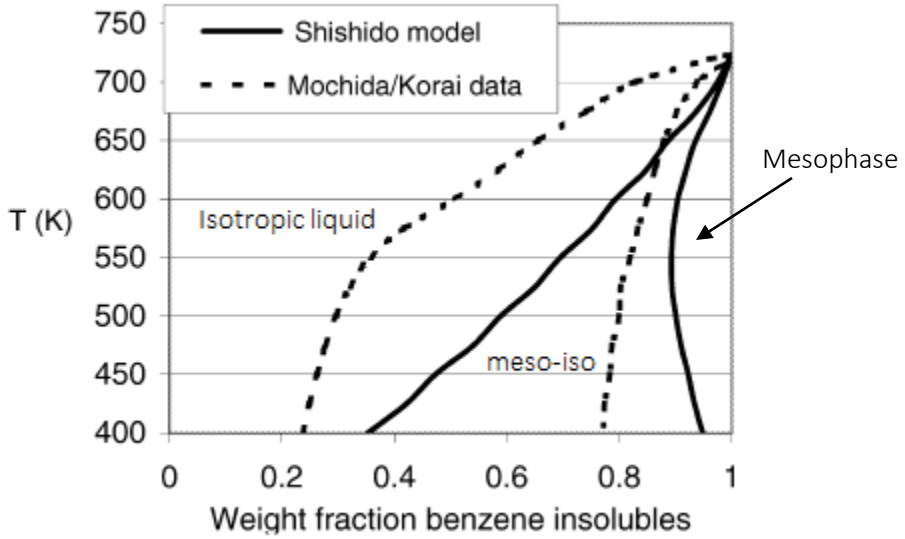

Figure 2.28 Comparison of experimental binary phase diagram with model calculation by Shishido et al. [126, 128, 131].

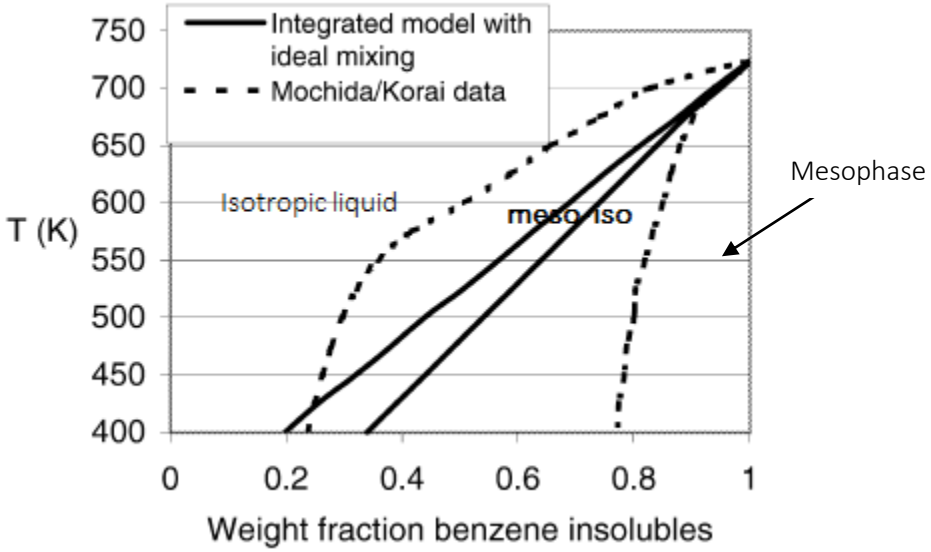

Figure 2.29 Comparison of experimental binary phase diagram with model calculation by Hu and Hurt without any consideration of non-ideal solution behavior [127, 128, 131].

However, total Gibbs free energy of co-existing phases during the carbonization process, the isotropic liquid and the mesophase, can be estimated using Eq. (2.7) and the submodels described by Hu and Hurt [127] for the excess Gibbs energy of mixing and the orientational free energy determination of the system:

$$G^{iso} = \left[\sum_i n_i\, g_i^0 \;+\; RT\sum_i n_i \ln x_i \;+\; \sum_i n_i\, V_i\, \left(\delta_i - \bar{\delta}\right)^2 \;+\; RT\sum_i n_i \ln\left(\frac{\Phi_i}{x_i}\right)\right]^{iso} \qquad \text{Eq. (2.9)}$$

$$G^{meso} = \left[\sum_i n_i\, g_i^0 \;+\; RT\sum_i n_i \ln x_i \;+\; \sum_i n_i\, V_i\, \left(\delta_i - \bar{\delta}\right)^2 \;+\; RT\sum_i n_i \ln\left(\frac{\Phi_i}{x_i}\right)\right]^{meso}$$

$$-\left[\frac{N_A}{2}\sum_{i,j} n_i x_j \mathcal{E}_{ij} \bar{P}_{2(i)} \bar{P}_{2(j)} \;+\; RT\sum_i n_i \ln Z_i\right]^{meso} \qquad \text{Eq. (2.10)}$$

where, N_A is Avogadro number, the sums are over all species in the mixture (isotropic liquid or mesophase), i=1, 2, …, N, V_i is the molar volume and Φ_i is the volume fraction of species i in either isotropic liquid phase or nematic phase:

$$\Phi_i = \frac{x_i V_i}{\sum_j x_j V_j} \qquad \text{Eq. (2.11)}$$

For application to pitch, the molar volumes in Eqs. (2.7) - (2.9) are set proportional to molecular weight as estimated by Hu and Hurt [127].

Solubility parameters are known for many low molecular weight compounds in pitch. Hu and Hurt [127] proposed an empirical relation to predict solubility parameters as follows:

$$\delta_i = \delta_0 + \alpha\,(MW - MW_0) \qquad \text{Eq. (2.12)}$$

where δ_0 and MW_0 are reference values ($\delta_0 = 10\ (cal\ cm^{-3})^{1/2}$, $MW_0 = 250\ g\ mol^{-1}$) chosen from experimental solubility parameters for low MW PAHs (with MW around 250 g/mol) which

lies in a narrow range near 10 $(cal\ cm^{-3})^{1/2}$. The factor α becomes a model parameter that describes the effect of increasing molecular weight.

In Eq. (2.10), Z_i is the orientational partition function given by:

$$Z_i = \int_0^{\pi/2} exp\left\{-\frac{1}{kT}\sum_j \varepsilon_{ij} x_j \bar{P}_{2(j)} P_{2(i)}(\cos\theta)\right\} \sin(\theta)\ d\theta \qquad \text{Eq. (2.13)}$$

where *k* is Boltzman constant, θ is the angle between the long axis of the molecule and the optic axis of the mesophase (Fig. 2.30), x_j is the mole fraction of the mesogen and $\bar{P}_{2(i)}$ is the single component order parameter which is given by:

$$\bar{P}_{2(i)} = \int_0^{\pi/2} P_{2(i)}(\cos\theta)\ .\ exp\left\{-\frac{1}{kT}\sum_j \varepsilon_{ij} x_j \bar{P}_{2(j)} P_{2(i)}(\cos\theta)\right\} \sin(\theta)\ d\theta \quad /Z_i \qquad \text{Eq. (2.14)}$$

where $\bar{P}_{2(i)} = \frac{3}{2} <\cos^2\theta_i> - \frac{1}{2}$ (defined as the second Legendre function for each species) and < > means the statistical average [18, 35].

The ε_{ij} terms represent the strengths of the pairwise orientation potentials, which are given as shown below for molecules of different size:

$$\varepsilon_{ij} = \tilde{\varepsilon}_{ij}\ \sqrt{V_i V_j}\ /\ \sum x_k V_k \qquad \text{Eq. (2.15)}$$

where the $\tilde{\varepsilon}_{ij}$terms are the geometric means of the single component values:

$$\tilde{\varepsilon}_{ij} = -\sqrt{\tilde{\varepsilon}_{ii}\ \tilde{\varepsilon}_{jj}} \qquad \text{Eq. (2.16)}$$

The $\tilde{\varepsilon}_{ii}$ terms are related to the single component clearing temperatures, T_{cl_i}, by the Maier-Saupe solution [135, 136]

$$\tilde{\varepsilon}_{ii} = -4.54.k.T_{cl_i} \quad \text{Eq. (2.17)}$$

The clearing temperature is the temperature upon heating at which liquid crystal reverts to an isotropic liquid. Following empirical relation has been proposed by Hu and Hurt [127] to estimate clearing temperatures of each compounds:

$$T_{cl_i} = a + b\,MW_i \quad \text{Eq. (2.18)}$$

where a and b are constants which can be derived using two known clearance temperatures related to two compounds with different molecular weights [127, 128].

The chemical potential of each species in either isotropic phase or nematic phase is determined as derivation of total Gibbs energy. Hu and Hurt [127] estimated the phase diagram by solving a series of equations derived from equating the chemical potentials of each species in each phases in equilibrium and considering the mass balance and the constraints defined as follows:

$$\left[\ln x_i + \ln\left(\frac{V_i}{V}\right) - \frac{V_i}{V} + \frac{V_i}{RT}\left(\delta_i - \bar{\delta}\right)^2\right]^{iso} = \left[\ln x_i + \ln\left(\frac{V_i}{V}\right) - \frac{V_i}{V} + \frac{V_i}{RT}\left(\delta_i - \bar{\delta}\right)^2\right]^{meso}$$
$$- \left[\ln(Z_i) + \frac{1}{2kT}\left(\sum_{k,j} x_k x_j \varepsilon_{kj} \bar{P}_k \bar{P}_j \frac{V_i}{V}\right)\right]^{meso} \quad \text{Eq. (2.19)}$$

$$N^{iso} x_i^{iso} + N^{meso} x_i^{meso} = N_i \quad \text{Eq. (2.20)}$$

$$\sum_i n_i^{iso} = N^{iso};\ \sum_i n_i^{meso} = N^{meso} \quad \text{Eq. (2.21)}$$

Here, i is the number of components in the system and N^{iso} and N^{meso} are total number of moles in isotropic liquid and mesophase, respectively.

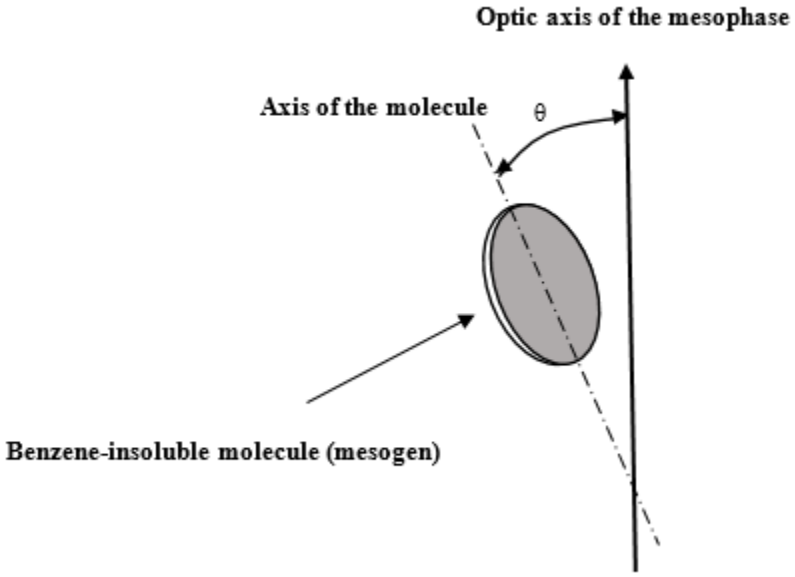

Figure 2.30 Configuration of mesogen molecule [137].

Using this approach, improvement was found in phase behavior prediction of Mochida et al. as shown in Fig. 2.31. Indeed, the model equations were solved numerically. Efforts were focused on solution techniques for the general multicomponent case, since these are needed in carbonizing systems due to the broad molecular weight distributions. A stochastic solution technique was used, in which each of the individual component mole numbers in the mesophase was perturbed in sequence by a random increment, and the mole number in the isotropic phase adjusted to maintain the species balance. These trial perturbations were kept if they reduced the absolute difference between the right and left hand sides of Eq. 2.19. However, this stochastic technique was found to converge for most but not all sets of input parameters.

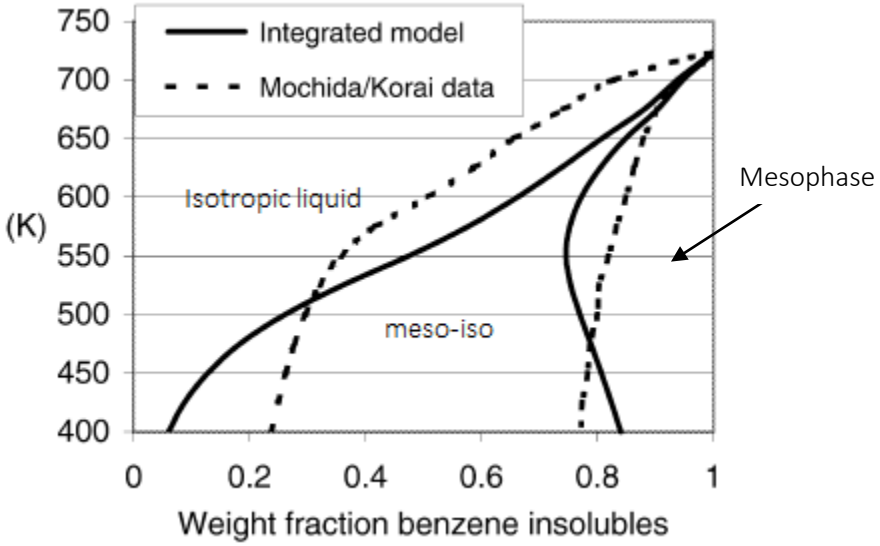

Figure 2.31 Comparison of experimental binary phase diagram with model calculation by Hu et al. [127, 128, 131].

CHAPTER 3 CRITICAL ANALYSIS AND ORGANIZATION OF THE THESIS

In Chapter 1 and Chapter 2, the work undertaken to understand the fundamentals of the primary carbonization of carbonaceous materials, with a focus on mesophase formation as an intermediate phase appearing during carbonization, was reviewed in detail. A comprehensive review of existing thermodynamic models for estimating the thermodynamic properties and phase behavior of coal tar pitch (CTP) in the solid, liquid and mesophase states was then performed.

As the evolutions happening during the primary carbonization process and thermodynamics and phase relationship of coal tar pitch and carbonaceous mesophase are the main underpinning of the present thesis, a brief critical analysis of the scientific concept that led to the results of this research project is given. The objectives of the present thesis are then described. Finally, the structure and organization of the present thesis is presented to give a view of the research strategy used to achieve the objectives.

3.1 Critical analysis of the literature review

Primary carbonization has been extensively reviewed, starting with Franklin [54, 55] as the pioneer in these studies, and following up with the review works of Oberlin and Bonnamy [37, 51, 52, 56]. Primary carbonization refers to the transformation of an initial precursor carbon into a mesophase state and, ultimately, semi-coke, a brittle solid state materials. It reaches its penultimate stage at approximately 400 - 600°C (the exact temperature of completion depending on the precursor composition and other factors) [59]. The primary carbonization of CTP, with an emphasis on the generation of the mesophase as an intermediate step, is the focus of the present thesis. The goal of this critical analysis is to present the proposals of certain important authors within the framework

of this doctoral work. The holes of knowledge related to the process and the thermodynamic aspects of pitch carbonization are consequently presented.

Process aspects of pitch carbonization

The discovery by Brooks and Taylor [23] in 1965 of a mesophase state in pitch that undergoes carbonization had a major impact on the future of carbon technology. The mesophase concept explained for the first time how isotropic pitches are transformed into anisotropic materials. In addition, the mesophase concept provided the impetus for extensive research and development that led to new and significant applications for carbon materials (CM). In the ensuing two decades, an extensive number of publications related to mesophase pitch appeared in the literature. Although these investigations encompassed a wide variety of practical and fundamental objectives, one of the major concerns was to understand the chemistry and development of the mesophase. At this time, Lewis [3, 28, 35, 50] revealed his findings related to these aspects. He described the conversion of pitch to carbon as a complex process encompassing a multitude of physical and chemical transformations of the numerous components of pitch. His studies on pitches as a complex mixture PAHs show that polymerization through loss of side chains and hydrogen is the main chemical reaction occurring during the transformation of pitch. The continuous increase in molecular weight via polymerization and the loss of low molecular weight volatiles results in the transformation of pitch into mesophase, semi-coke, coke, and, ultimately, graphite. These various aspects, which were reviewed by Lewis [3, 28, 35, 50], led to the development of a general mechanistic sequence for pitch carbonization. Greinke [87, 88] continued the work of Lewis using gel permission chromatography (GPC). The main objective of his studies was to quantify the molecular weight distributions of coexisting phases during pitch carbonization as a function of heat

treatment time in order to gain fundamental insights into the changing phase relationships and the mechanism of mesophase and semi-coke development during the transformation process. By the way, knowledge about primary carbonization is qualitative in most aspects and only some efforts was performed by Greinke to quantify it.

Indeed the general mechanism above-discussed can be used as the key concepts in the context of the present thesis to build the pitch carbonization process formalism in order to quantify the thermal, physical and chemical evolutions occurring throughout the process.

Thermodynamic aspects of pitch carbonization

A better understanding of the primary carbonization process will be gained through a quantitative treatment of the equilibrium phase transformations of PAH compounds and pitches with known molecular weight distributions. Group additivity algorithms were developed by Richard and Helgeson [111] to estimate the heat capacity function coefficients and standard thermodynamic properties of high molecular weight PAHs in solid and liquid states at 25°C and 1 bar. The group contributions for each coefficient and property were generated from the thermodynamic properties of lower molecular weight reference species for which calorimetric data are available in the literature. However Richard and Helgeson's approach suffers from a lack of consistency in reconciling phase transition data (enthalpy of fusion, vaporization) and the computation of vapor pressures using the Gibbs energy functions of the condensed and gaseous phases of a given PAH compound. As such, conducting a critical assessment of the thermodynamic properties (heat capacity functions, enthalpy of formation and absolute entropy) of pure PAH compounds in the gas, liquid, and solid states such that all data are rendered consistent is one of the objectives of this doctoral work. Meanwhile, there is no consideration for prediction of the heat capacity of PAHs

exhibiting an anomalous behavior in solid state in Richard and Helgeson's model. Specific studies is needed on heat capacity function of these specific type of PAHs.

Due to the complex nature of the mesophase in pitches, the quantitative treatment of the phase equilibrium of mesophase-containing pitch is a major challenge. Given this, some considerations have to be taken into account to reduce it to a simplified system with respect to the characterization of the real system. To date there have been two attempts to develop quantitative descriptions of the phase transition behavior of mesophase-containing pitches: one by Shishido et al. [126] and one by Hu and Hurt [125, 127, 128]. Shishido et al. [126] applied the molecular field treatment of mesogen-nonmesogen mixtures to describe a phase diagram for a mesophase pitch. This model does not consider the effect of non-ideal mixing of pitch fractions of differing molecular weights or chemical compositions. Deviations of the estimated phase diagram by Shishido et al. from the experimental data (reported by Mochida and Korai [131]) stimulated the search for a treatment of non-ideal mixing for accurate description of mesophase/isotropic equilibrium. So, Hu and Hurt [125, 127, 128] developed the Gibbs free energy model for mesophase-containing pitches based on non-ideal solution and liquid crystal behaviors of mesophase that includes terms for both excess free energy of mixing and orientational free energy to quantitatively describe the phase behavior of mesophase in pitch. In Hu and Hurt's work, the phase behavior of mesophase pitches was estimated by solving a series of equations derived from equating the chemical potentials of each component in the phases in equilibrium. Due to the complexity of the problem, a stochastic technique was used to minimize the absolute difference between both sides of these equations. Implementing Hu et al.'s approach presents difficulties from a technical point of view as the orientation Gibbs energy of the mesophase is defined through the second Legendre function. It has been only applied to three data sets reported in the carbon science literature. Utilizing a precise and

robust numerical technique for minimization of total Gibbs free energy function of mesophase, directly, enables us the estimation of phase behavior of binary, ternary and higher order systems. The reliability of MADS algorithm to determine the global and local minima of set of functions with different degree of complexity was demonstrated in references [49-51]. The improvement of Hu and Hurt's approach to estimate the thermodynamic behavior of different carbonaceous mesophase-containing pitches is another objective of this thesis.

3.2 Research objectives

The heart of this doctoral research is the following:

Research subject: Thermodynamics of carbon materials

Research question: What are the relationships between the coal tar pitch specifications as the raw material used in the carbon-based material production process and the properties of the product, the emission of volatile and hazardous materials, and the energy consumption of the process?

Main objective:

Development of a thermodynamic model to estimate the behavior and thermodynamic properties of CTP in the gas, liquid, solid phases as well as in the mesophase (as an intermediate phase appearing through heat treatment of carbon-based materials) in order to provide industry with a better mathematical solid-mesophase-liquid-gas relation for their simulations aimed at the optimizing the carbon-based material production processes.

Specific objectives:

1. Development of a thermodynamic model to predict the thermodynamic properties of pure polycyclic aromatic hydrocarbon compounds, in gas, liquid, and solid states;

2. Development of a new thermodynamic approach to predict the thermodynamic behavior of carbonaceous mesophase with liquid crystal nature that appears as an intermediate phase during carbonization of coal tar pitch;
3. Development of a generic prototype model of the thermal, physical and chemical evolutions of coal tar pitch undergoing carbonization process.

3.3 Organization of the thesis

This thesis is built in the format of a thesis by article. Each of the specific three objectives defined in the previous section constitutes the chapters of the thesis (Chapter 4, 5, and 6) that have compatibility with the articles.

Chapter 4 presents a critical assessment of the thermodynamic properties of important PAHs in CTP over typical temperature ranges of carbonization produced in the framework of this doctoral work. The CALPHAD approach is used to modify the group additivity algorithm proposed by Richard and Helgeson [111] for estimating the heat capacity function coefficients and the standard thermodynamic properties of high molecular weight PAHs at 25°C and 1 bar. The philosophy of the CALPHAD approach is to obtain the thermodynamic data rendered consistently with phase transition data and computation of vapor pressure using the Gibbs energy function of condensed and gaseous phases of a given compound.

The heat capacity function of PAHs exhibiting thermal anomaly behavior, which is associated with a second order phase transition, is modeled as a specific case. The modeling is performed using Compound Energy Formalism (CEF).

Chapter 5 presents a new thermodynamic approach for predicting the phase behavior of mesophase-containing pitches, which appears as an intermediate phase during the heat treatment of CTP. The proposed approach in this chapter is based on the Gibbs free energy formalism for isotropic liquid and mesophase pitches developed by Hu and Hurt [125, 127, 128]. Equilibrium configuration of a mesophase-containing pitch system is estimated by minimization of Gibbs free energy function, directly, utilizing a precise and robust numerical technique. The application of the new thermodynamic approach allows phase behavior prediction of the binary, ternary and higher order systems specifically the systems exhibiting miscibility gaps.

Chapter 6 presents the thermodynamic-kinetic model of the physical and chemical changes occurring during heat treatments of CTP developed in the framework of the present thesis. This model is based on a general mechanism of pitch carbonization inspired by the work of Lewis and Greinke and developed models for estimating the thermodynamic properties of pitch constituents (Chapter 4) and phase relationships of mesophase-containing pitches (Chapter 5). The model makes it possible to estimate the quantity of gas emitted as well as the mass and enthalpy changes of pitch over time during CTP primary carbonization.

CHAPTER 4 ARTICLE 1: CRITICAL ASSESSMENT OF THERMODYNAMIC PROPERTIES OF IMPORTANT POLYCYCLIC AROMATIC HYDROCARBON COMPOUNDS (PAHS) IN COAL TAR PITCH AT TYPICAL TEMPERATURE RANGES OF THE CARBONIZATION PROCESS

Mahnaz Soltani Hosseini, Patrice Chartrand

Submitted to Calphad, December 15, 2020

Abstract: Because of the importance of thermodynamic behavior of Polycyclic Aromatic Hydrocarbon (PAH) compounds in coal tar pitch carbonization process, a thermodynamic model for the prediction of thermodynamic properties of PAH compounds is developed. Heat capacity functions as well as standard thermodynamic properties of PAHs in solid, liquid, and gas states are estimated using modified group additivity algorithms first proposed by Richard and Helgeson and thermal physical data of those PAHs for which enough experimental data exists in the literature. For the first time, thermodynamic properties of PAHs are optimized by applying the CALPHAD (CaLculation of PHAse Diagrams) approach where all thermodynamic data are rendered consistently to reconcile phase transitions and vapor pressure data. The heat capacity function of PAHs exhibiting thermal anomaly behavior is modeled as a specific case. This modeling is performed using an order-disorder approach with the Compound Energy Formalism (CEF). Good agreement has been obtained between the predicted thermodynamic properties of PAHs and available experimental data. The proposed model has improved the predictive capacity compared to that of the previous models predicting thermodynamic properties of PAHs at typical temperature ranges of the carbonization process. The application of the model to predict the thermodynamic properties of major and high molecular weight PAHs available in coal tar pitch has been discussed.

4.1 Introduction

The binder pitch, which is one of the major constituents of prebaked carbon anodes used in the Hall-Héroult process for commercial plants of aluminum production constitutes between 14% and 17% (by mass) of the green anode blocks [40]. Similar binders, as the major constituents of Soderberg paste, are also used in some parts of cathode processing and in ramming pastes of aluminum electrolysis cells. Characterization of commercial pitches shows them to be exceedingly complex materials, containing from hundreds to thousands of different compounds, mostly monomers, oligomers and polymers of Polycyclic Aromatic Hydrocarbon (PAH) compounds with a variety range of molecular weights [3, 4]. During heat treatment (carbonization) of coal tar pitch as a part of the anode baking process, PAH compounds are converted to infusible coke via distillation of smaller compounds and polymerization reactions of more reactive residual species [138]. Volatile low molecular weight PAHs as well as hydrogen and methane produced by chemical reactions, are emitted throughout the process [23, 28, 35, 87, 139]. Burning gaseous products inside the anode baking furnace, coming from the anodes placed in pits between two flue walls, provides an important part of the energy needed to reach the baking temperature (1100 – 1250°C) of the system and decreases the fuel consumption of the process. Emission of some volatile and toxic PAH compounds during the heat treatment of green anode blocks and ramming paste between the cathode blocks pose the health and environment risks, which has to be considered as a serious inconvenience of coal tar pitch applications [140].

However, obtaining a good anode quality and efficient aluminum production process while keeping the energy consumption, environmental emissions and cost minimum (industrial challenge) stimulates the search for a better understanding of the thermodynamic behavior of coal tar pitch constituents during carbonization over a wide range of temperatures. Current knowledge of the

thermodynamic properties of PAHs (present in coal tar pitch) such as specific heat and standard entropy and enthalpy of formation is not well defined in a consistent manner. It suffers from a lack of consistency to reconcile phase transition data (enthalpy of fusion and vaporization) and computation of vapor pressures using the Gibbs energy functions of the condensed and gaseous phases of a given PAH compound. Moreover, structural anomalies in some solid PAH compounds (like phenanthrene and pyrene) are associated with peaks in the temperature dependence of the heat capacity curves. In the view of high complexity of the PAH and PAH-derived constituents of coal tar pitch (high molecular weight (MW) oligomers), improvements to Richard and Helgeson's method [111] for predicting thermodynamic properties of such high-MW PAHs should be developed.

The aim of present work is to develop a thermodynamic model predicting the thermodynamic properties (heat capacity functions, enthalpy of formation and absolute entropy) of pure PAH compounds, in gas, liquid, and solid states, with consistency in the prediction of their phase transition data and their vapor pressure, as an improvement of Richard and Helgeson's approach. For the first time, the CALPHAD approach is applied to optimize the model parameters, where all data are rendered consistent. The philosophy of the CALPHAD approach is to obtain the thermodynamic data rendered consistently with phase transition data and computation of vapor pressure using the Gibbs energy function of condensed and gaseous phases of a given compound. Indeed, experimental data for heat capacity, standard entropy and enthalpy of formation at 25°C and 1 bar as well as phase transition data (enthalpy of fusion and vaporization) of PAH compounds reported in the literature [39, 90, 92-98, 100, 102, 103, 105, 106, 109, 110, 116, 118, 141-171] are utilized to develop the proposed thermodynamic model. Moreover, a thermodynamic model is

developed to estimate the specific heat of some PAHs exhibiting an anomalous behavior in solid state.

The paper is organized as follows. Sections 4.2 and 4.3 present the development of the model to predict the thermodynamic properties of pure PAH compounds and the heat capacity function of PAHs with anomalous behavior, respectively. Section 4.4 presents the main results obtained using the proposed thermodynamic model, with comparison of model predictions with reported experimental data, and results obtained by other methods for prediction of thermodynamic properties of PAHs (mainly the results derived from first principal calculations for thermodynamic properties prediction of PAHs in gaseous state [172] and thermodynamic properties predicted by Richard and Helgeson's method [111]). The future perspectives of the present model is discussed in Section 4.5.

4.2 Thermodynamic model for Gibbs energy of PAH compounds in coal tar pitch

There is a very large number of different components, monomers, oligomers and polymers of PAHs with a variety range of molecular weights in coal tar pitch. In the present work, a thermodynamic model is developed to predict the thermodynamic properties of unsaturated PAHs that do not contain impurity elements such as sulfur and nitrogen.

Regarding the following basic thermodynamic expressions:

$$\Delta H_T^\circ = \Delta H_{298.15\,K}^\circ + \int_{298.15}^{T} Cp\, dT \qquad \text{Eq. (4.1)}$$

$$S_T^\circ = S_{298.15\,K}^\circ + \int_{298.15}^{T} \frac{Cp}{T} dT \qquad \text{Eq. (4.2)}$$

$$\Delta G_T^\circ = \Delta H_T^\circ - T.S_T^\circ \quad \text{Eq. (4.3)}$$

Thermodynamic properties of pure PAH compounds at any given temperature can be calculated using the standard thermodynamic properties at 298.15 K and 1 bar and the heat capacity. In these equations, heat capacity of pure compounds is a temperature dependent function derived based on either theoretical models or experimental calorimetric data.

The group additivity approach, pioneered by Benson and Buss [173] and continued by Dolmaski and Hearing [146] for predicting the thermodynamic properties of organic gases, solids and liquids, which was specifically applied by Richard and Helgeson. [111] to predict the thermodynamic properties of solid and liquid hydrocarbons, is modified and used in the present work to estimate the heat capacity function and standard thermodynamic properties of PAH compounds. The basis of group contribution calculations is explained in detail in Section 4.2.1. Subsequently, obtained standard thermodynamic properties are optimized by applying the CALPHAD approach, where all data are rendered consistent to reconcile phase transition data (enthalpy of fusion, vaporization) and computation of vapor pressures using the Gibbs energy functions of the condensed and gaseous phases of a given PAH compound. Optimization strategies are presented in Section 4.2.2.

4.2.1 Basis of the group contribution algorithms

Very few experimental data sets are available in the literature for heat capacity function coefficients and standard thermodynamic properties of high molecular weight PAH compounds. Close estimates of these properties can be generated from group additivity algorithms using group properties derived from calorimetric data of lower molecular weight reference compounds.

4.2.1.1 **Reference compounds and constituent aromatic groups**

The first step in group contribution algorithms is to determine some reference compounds to define the necessary groups to generate the species subjected to thermodynamic properties estimations. There should be enough experimental thermodynamic data for them in the literature that make it possible to estimate the thermodynamic properties of group constituents. Another criterion to select the reference compounds is that they can provide all required groups to create any new high MW PAH compound. The total number of reference compounds required to calculate the thermodynamic properties of the constituent groups is equal to the total number of these groups.

The reference compounds and group stoichiometries of the reference compounds are listed in Table 4.1. A zoom view of the aromatic groups together with a description is shown in Table 4.2. These aromatic groups were defined by following and respecting Richard and Helgeson's work, as the main reference used in the present work. As shown in Tables 4.1 and 4.2, each group includes *C*, *CH*, or CCH_3 and the bonds that attach it to other carbon atoms. The distinguishing feature of these groups is the location of the carbon atom.

Aromatic groups defined in these tables enable the generation of the polycyclic aromatic hydrocarbon compounds including the compounds with a methyl substituent (assumed to be present in very low concentration in coal tar pitch), adopted in the present work.

Table 4.1 Selected reference compounds and group stoichiometries [111].

Reference compounds	**Formula**	**Molecule representation**	**Group stoichiometries of the reference compounds**
Naphthalene	$C_{10}H_8$	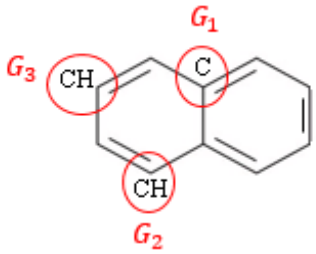	$2G_1 + 4G_2 + 4G_3$
Phenanthrene	$C_{14}H_{10}$	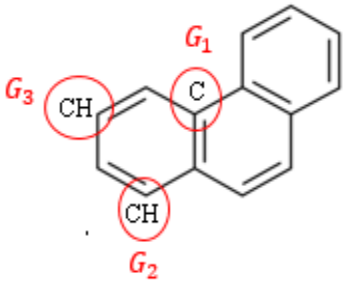	$4G_1 + 6G_2 + 4G_3$
Anthracene	$C_{14}H_{10}$	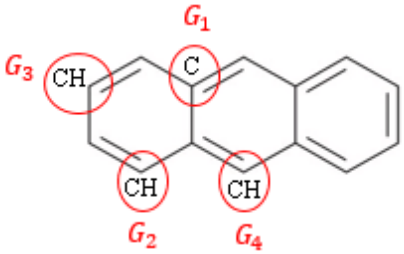	$4G_1 + 4G_2 + 4G_3 + 2G_4$
Pyrene	$C_{16}H_{10}$	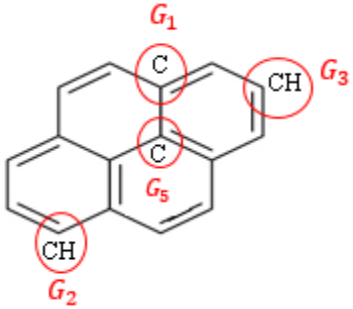	$4G_1 + 8G_2 + 2G_3 + 2G_5$

Reference compounds	**Formula**	**Molecule representation**	**Group stoichiometries of the reference compounds**
Triphenylene	$C_{18}H_{12}$	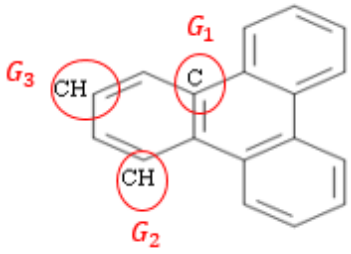	$6G_1 + 6G_2 + 6G_3$
1-Methylnaphthalene	$C_{11}H_{10}$	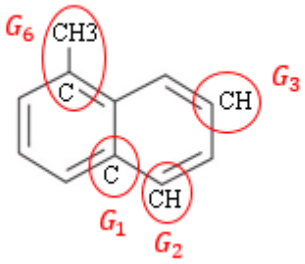	$2G_1 + 3G_2 + 4G_3 + G_6$

Table 4.2 Selected reference compounds and group stoichiometries [111].

Groups	**Abbreviation**	**Description**
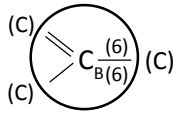	G_1	Group on a bridge (B) between two benzene rings in a polycyclic aromatic hydrocarbon.
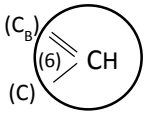	G_2	Group adjoining a bridge (B) between two benzene rings in a polycyclic aromatic hydrocarbon.

Groups	Abbreviation	Description
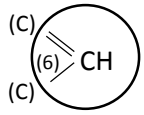	G_3	Group that is not adjacent to a bridge (B) between two benzene rings in a polycyclic aromatic hydrocarbon.
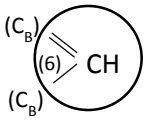	G_4	Group that is adjacent to two bridges (B) between two benzene rings in a polycyclic aromatic hydrocarbon.
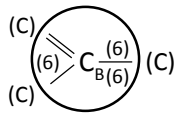	G_5	Group at the junction of three aromatic rings in a polycyclic aromatic hydrocarbon. .
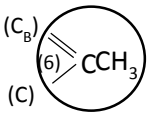	G_6	Group including a methyl chain and adjoining a bridge (B) between two benzene rings in a polycyclic aromatic hydrocarbon.

4.2.1.2 Calculation of group contribution to the thermodynamic properties of high molecular weight PAH compounds

Regarding the group additivity hypothesis, any standard thermodynamic property or heat capacity function coefficient of the j^{th} reference compound (Ξ_j°) can be expressed as:

$$\Xi_j^\circ = \sum_i n_{ij}\ \Xi_i^\circ \qquad \text{Eq. (4.4)}$$

Where n_{ij} represents the number of moles of the i^{th} group in one mole of j^{th} reference compound and Ξ_i° denotes any heat capacity power function coefficient or standard thermodynamic property at 298.15 K and 1 bar of the subscripted group.

The heat capacity function and standard thermodynamic properties of the aromatic G_1, G_2 and G_3 groups can be calculated from those of naphthalene, phenanthrene and triphenylene using Eq. (4.4) and the group stoichiometries for these reference compounds as are shown in Table 4.1. Combining the heat capacity coefficients and the standard thermodynamic properties of these aromatic groups with those of anthracene, pyrene and 1-methylnaphthalene according to the strategy and group stoichiometry shown in Table 4.1 allows the calculation from Eq.(4.4) of the corresponding coefficient and properties of G_4 , G_5 and G_6 groups. The heat capacity function coefficients and standard thermodynamic properties of any high molecular weight PAH compounds can be derived using heat capacity coefficients and standard thermodynamic properties of the groups having contributed to the compounds.

In the present work, some modifications are proposed to apply group contribution algorithms to predict the thermodynamic properties of PAH-derived constituents, high MW oligomers, and polymers, of coal tar pitch which are considered as constituents of graphene sheet [25, 174]. Very large polycyclic aromatic hydrocarbons (VLPAHs) such as quaterrylene and dicoronylene (Fig. 4.1) can be considered subsections of a graphene sheet (Fig. 4.2) since the length of both quaterrylene and dicoronylene is about 17.9 Å [25].

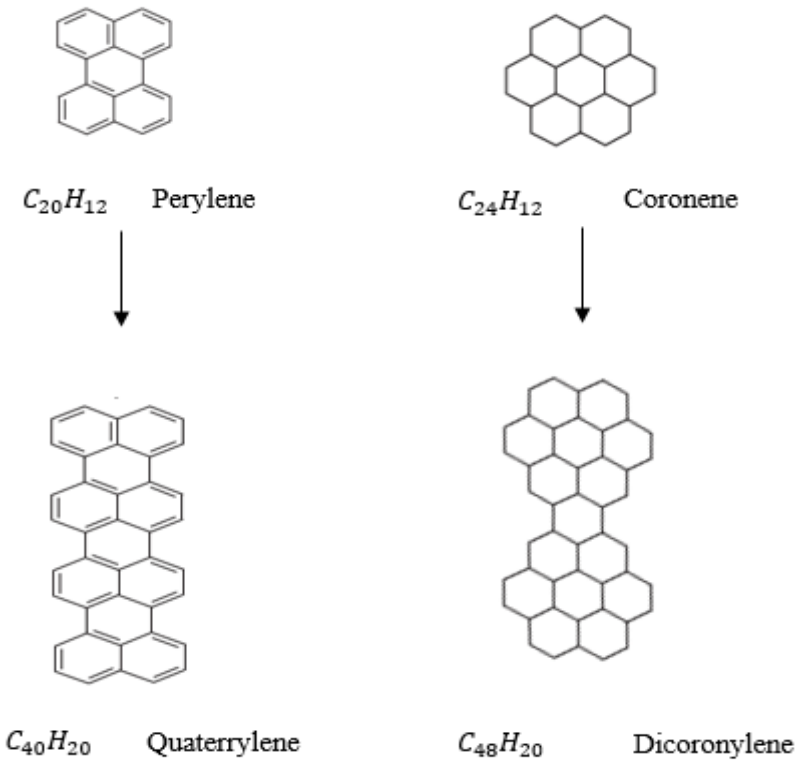

Figure 4.1 Perylene, coronene, and their oligomers [25].

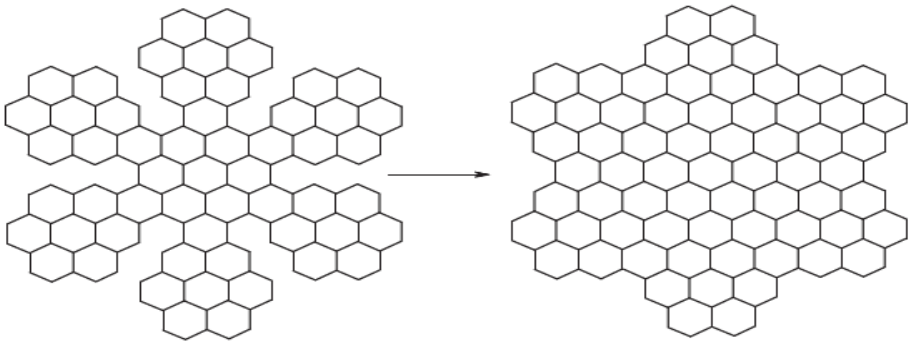

Figure 4.2 Coronene "star" heptamer and its possible transformation to a graphene plate having a diameter of 26.4 Å [25].

The modifications are based on consideration of different types of aromatic rings available in the monomers of these VLPAHs (Fig. 4.3): 1) Internal ring, which is surrounded by other aromatic

rings on all sides, 2) External ring, which is surrounded by other rings on two sides and 3) Semi-internal ring, which is surrounded by other rings on more than two sides, shown as IN-R, EX-R, and SIN-R, respectively. Subsequently, three aromatic groups are defined and introduced to the model with respect to which aromatic rings are placed around them. These aromatic groups named G_5 as the aromatic group at the junction of two SIN-R and one EX-R, G_7 as the aromatic group at the junction of one SIN-R and two EX-R, and G_8 as the aromatic group at the junction of two SIN-R and one IN-R (shown in Fig. 4.3).

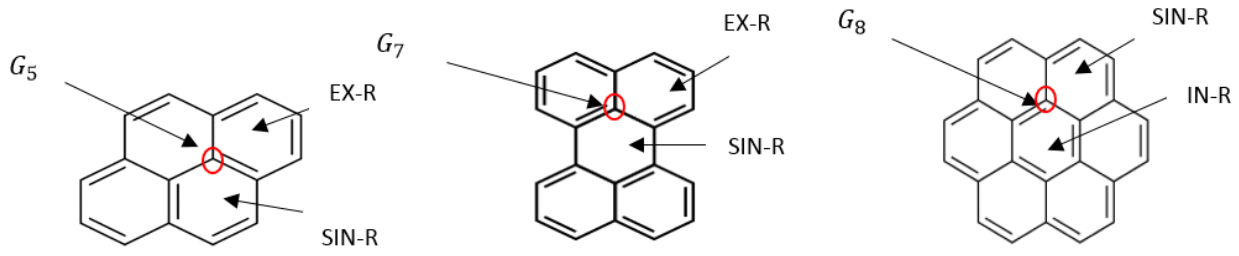

Figure 4.3 Definition of three different aromatic groups at the junction of three aromatic rings.

Group stoichiometries of coronene and perylene are listed in Table 4.3. Combining the thermodynamic properties of aromatic G_1 , G_2 and G_3 groups with those of perylene and coronene (as new reference compounds) in accord with the group stoichiometry seen in Table 4.3 enables the calculation from Eq. (4.4) of correspondence heat capacity coefficients and standard thermodynamic properties of the aromatic G_7 and G_8 groups.

Table 4.3 Group stoichiometries of perylene and coronene.

Reference compounds	**Formula**	**Molecule representation**	**Group stoichiometries of new reference compounds**
Perylene	$C_{20}H_{12}$	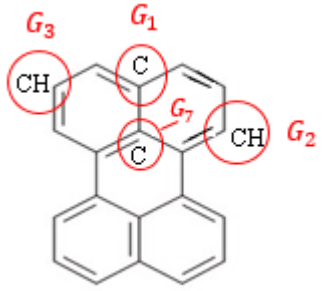	$6G_1 + 8G_2 + 4G_3 + 2G_7$
Coronene	$C_{24}H_{12}$	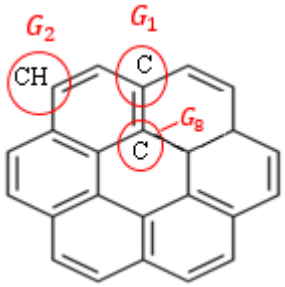	$6G_1 + 12G_2 + 6G_8$

* Groups at the junction of three aromatic rings in perylene and coronene (shown in Fig. 4.3)

4.2.2 Thermodynamic model parameters

The heat capacity function coefficients and standard thermodynamic properties of constituent groups in solid, liquid and gas PAHs are defined as the thermodynamic model parameters which are used to predict the heat capacity function coefficients and standard thermodynamic properties of PAHs in different states by applying group additivity algorithms followed by the CALPHAD approach to optimize them. Then, Gibbs energy, enthalpy, and entropy of any solid, liquid and gas PAHs at any given temperature can be generated using derived thermodynamic model parameters utilizing Eqs. (4.1-4.4).

4.2.2.1 **Coefficients for Heat capacity function of PAHs**

Solid polycyclic aromatic hydrocarbon compounds

Following semi-empirical expression is used to fit the heat capacity function of solid PAH compounds:

$$C_p(solid) = a + bT + cT^2 + dT^{-2} \quad \text{Eq. (4.5)}$$

In some cases, getting a unique correlation for the entire range of temperature of coal tar pitch carbonization process is not possible. In this case, correlations should be obtained in different ranges of temperature using the proposed method by Voronin and Kutsenok (see ref. [175] for detail). Heat capacity experimental data, reported in the literature [92, 95, 96, 101, 104, 109, 116, 154, 166, 171], are used to obtain the heat capacity correlations of all the solid reference compounds. The heat capacity coefficients of the reference PAHs, together with those of perylene and coronene corresponding to Eq. (4.5) are summarized in Table A.1.

Liquid and gas phases

The reported experimental data [95, 97, 98, 105, 109, 116, 156] for the heat capacity of liquid and gaseous PAH compounds can be represented as a function of temperature as follows:

$$C_p(liquid, gas) = a + bT + cT^2 + dT^3 + eT^4 \quad \text{Eq. (4.6)}$$

Two last terms in Eq. (4.6) enable us to fit accurately the experimental data of liquid and gaseous PAHs which is mostly available in temperature ranges above 300 K.

Fitting the experimental data with Eq. (4.6) results in the heat capacity coefficients of reference compound in liquid and gas states as summarized in Table A.2.

Constituent groups in Solid, liquid and gaseous PAHs

The values of the a, b, c, d and e coefficients of the constituent groups of the solid, liquid and gaseous PAH compounds (listed in Table 4.2 and 4.3) are calculated using the above obtained values (the heat capacity coefficients of reference PAH compounds) and applying group contributions calculations as described in Section 4.2.1.2. Tables 4.4 and 4.5 show the heat capacity coefficients of constituent groups in solid, liquid and gaseous states.

It should be noted that the heat capacity coefficients of aromatic G_7 and G_8 groups are only calculated in solid state and not in liquid and gaseous states with respect to the following explanation. Two new reference compounds, i.e. perylene and coronene, which introduced to the model at the end of Section 4.2.1.2 for modification purpose, suffer from lack of heat capacity experimental data in liquid state and consequently calculation of the heat capacity of the constituent groups (i.e. G_7 and G_8) in liquid state is not possible. Meanwhile, using group contribution algorithm and experimental data for gaseous perylene and coronene result in the same values for heat capacity of G_5, G_7, and G_8 groups. So, the heat capacity coefficients of aromatic G_7 and G_8 groups in liquid and gaseous states are considered as those of G_5 group in Table 4.5.

Table 4.4 Heat capacity coefficients of the constituent groups in the solid PAH compounds derived by group contribution calculation.

Temp. (K)		G_1	G_2	G_3	G_4	G_5	G_6	G_7	G_8
50-200	a^1	-1.821699E+01	2.548127E+01	-4.398821E+00	1.123238E+01	-4.257999E+01	-3.872917E+01	-2.066392E+01	-2.595578E+01
	b^2	2.249041E-01	-2.517710E-01	1.524696E-01	-6.972700E-02	5.559900E-01	5.808348E-01	2.404551E-01	3.132502E-01
	c^3	1.817778E+04	-2.601914E+04	5.061565E+03	-1.323691E+04	4.375278E+04	7.254518E+04	2.720787E+04	3.004537E+04
	d^4	-6.232282E-04	9.674492E-04	-3.490982E-04	3.909837E-04	-1.665518E-03	-1.102035E-03	-5.558542E-04	-7.866004E-04
200-250	a^1	-8.223261E+01	2.320357E+00	5.076990E+01	7.524800E+01	1.229262E+02	-6.189008E+01	4.740651E+01	8.129820E+01
	b^2	5.550962E-01	1.168413E-01	-3.812388E-01	-3.999191E-01	-1.045135E+00	9.494471E-01	-5.028459E-01	-6.002603E-01
	c^3	5.517376E+05	-2.382733E+05	-4.946421E+04	-5.467967E+05	-1.198246E+05	-1.397090E+05	3.943104E+05	-2.675771E+05
	d^4	-9.983697E-04	-1.730677E-04	9.789895E-04	7.661253E-04	2.318745E-03	-2.242552E-03	1.230230E-03	1.284893E-03
250-400	a^1	-3.482306E+01	2.320357E+00	3.360354E+00	-1.820664E+01	-9.860012E+00	3.292902E+01	-3.038400E-03	3.388865E+01
	b^2	1.251865E-01	1.168413E-01	4.867085E-02	1.480288E-01	-1.560062E-03	8.962781E-02	-7.293630E-02	-1.703507E-01
	c^3	7.234051E+05	-2.382733E+05	-2.211318E+05	1.163791E+05	-8.032725E+04	2.036261E+05	2.226429E+05	-4.392446E+05
	d^4	-7.574924E-05	-1.730677E-04	5.636907E-05	-9.326909E-05	2.535996E-04	-3.973112E-04	3.076100E-04	3.622730E-04
400-500	a^1	-3.482306E+01	1.109152E+02	-1.052345E+02	-1.820664E+01	-3.356445E+02	8.040067E+01	-2.171927E+02	-1.833010E+02
	b^2	1.251865E-01	-3.130736E-01	4.785858E-01	1.480288E-01	1.288185E+00	-3.498420E-01	7.868936E-01	6.894792E-01
	c^3	7.234051E+05	-2.141188E+06	1.681783E+06	1.163791E+05	5.628416E+06	6.730097E+05	4.028472E+06	3.366584E+06
	d^4	-7.574924E-05	2.986745E-04	-4.153731E-04	-9.326909E-05	-1.161627E-03	5.075130E-04	-6.358740E-04	-5.812120E-04
500-600	a^1	-2.954114E+00	-1.847988E+01	5.698917E+01	3.428821E+01	1.531550E+02	-5.809399E+01	-1.196666E+02	3.896191E+01
	b^2	5.394388E-02	6.361851E-02	-1.520978E-02	2.156371E-02	-1.610025E-01	2.503491E-01	4.814441E-01	2.926871E-02
	c^3	-1.256345E+06	2.719857E+06	-3.630035E+06	-2.495145E+06	-1.154049E+07	-4.828033E+05	1.147177E+06	-4.183370E+06
	d^4	-2.914640E-05	-1.544830E-05	9.208300E-06	-8.993400E-06	5.836240E-05	-1.240003E-04	-3.683544E-04	-2.694680E-05
600-1000	a^1	-2.954114E+00	-1.847988E+01	5.698917E+01	3.428821E+01	1.531550E+02	-5.809399E+01	1.692918E+02	3.896191E+01
	b^2	5.394388E-02	6.361851E-02	-1.520978E-02	2.156371E-02	-1.610025E-01	2.503491E-01	-1.702533E-01	2.926871E-02
	c^3	-1.256345E+06	2.719857E+06	-3.630035E+06	-2.495145E+06	-1.154049E+07	-4.828033E+05	-1.626103E+07	-4.183370E+06
	d^4	-2.914640E-05	-1.544830E-05	9.208300E-06	-8.993400E-06	5.836240E-05	-1.240003E-04	4.937270E-05	-2.694680E-05
1000-1200	a^1	9.909911E+00	5.816287E+00	2.021078E+01	2.654899E+01	3.954880E+01	1.474176E+02	5.758769E+01	1.990122E+01
	b^2	2.152741E-02	2.972395E-02	4.117534E-02	2.667964E-02	1.120957E-02	3.663063E-01	-1.708664E-02	3.827320E-02
	c^3	-1.285616E-03	-7.300083E-03	7.449057E-03	-5.324897E-04	2.275152E-02	-6.453756E-03	1.346386E-02	1.292846E-02
	d^4	-1.077160E-05	-3.090870E-	-1.410810E-	-8.838830E-	-1.199680E-	-1.177652E-	-8.494160E-	-2.089760E-05

[1] J mol^{-1} K^{-1}; [2] Jmol^{-1}K^{-2} [3] J mol^{-1} K^{-3}; [4] Jmol^{-1}K

By the way, as discussed in Section 4.2.1.2, heat capacity function coefficients of G_7 and G_8 groups are only needed in the estimation of heat capacity function coefficients of PAH-derived constituents, high MW oligomers, and polymers, of coal tar pitch and not in those of PAH monomers.

For the verification purposes, the heat capacity function coefficients of reference PAH compounds have been regenerated from group additivity algorithms using group properties (listed in Tables 4.4 and 4.5) and Eq. (4.4). The heat capacity of these compounds in solid, liquid and gas states as a function of temperature were estimated using Eqs.(4.5 and 4.6) and shown in Figs. A.2, A.4, A.6, A.8 and A.10 in Appendix A.

Table 4.5 Heat capacity coefficients of the constituent groups in the liquid and gas PAH compounds derived by group contribution calculation.

Group	**state**	**Heat capacity coefficients**				
		a[1]	**b**[2]	**c**[3]	**d**[4]	**e**[5]
G_1	liquid	-1.617360E+01	1.093380E-01	-1.119950E-04	3.827290E-08	0.000000E+00
	gas	-4.649600E+00	7.170500E-02	-6.146730E-05	1.999860E-08	-1.158070E-12
G_2	liquid	9.444750E-01	8.622750E-02	-5.865660E-05	1.486880E-08	0.000000E+00
	gas	-9.378990E+00	1.026970E-01	-9.358780E-05	4.409810E-08	-8.385950E-12
G_3	liquid	1.392490E+01	2.393380E-02	2.250530E-05	-1.619910E-08	0.000000E+00
	gas	-5.683710E+00	8.306620E-02	-7.088990E-05	3.650290E-08	-8.439500E-12
G_4	liquid	9.340290E+00	5.005510E-02	-7.306680E-06	-6.070890E-09	0.000000E+00
	gas	-8.776320E+00	9.450110E-02	-7.296430E-05	2.536960E-08	-2.722110E-12
G_5	liquid	1.416440E+01	-4.233970E-02	8.962710E-05	-4.037230E-08	0.000000E+00
	gas	-2.373540E+00	4.935830E-02	-4.544510E-05	2.511450E-08	-6.241770E-12
G_6	liquid	-1.411738E-01	2.689842E-01	-2.378692E-04	7.715645E-08	0.000000E+00
	gas	-1.101553E+01	2.128106E-01	-1.721755E-04	6.749102E-08	-9.503758E-12

[1] J mol^{-1} K^{-1}; [2] Jmol^{-1}K^{-2}; [3] J mol^{-1} K^{-3}; [4] Jmol^{-1}K^{-4}; [5] J mol^{-1} K^{-5}

4.2.2.2 Entropy and enthalpy of formation at 298.15 K and 1 bar ($\Delta H^{\circ}_{298\,K}$, $S^{\circ}_{298\,K}$) of PAHs and constituent groups

Experimental data for standard thermodynamic properties of reference PAH compounds in solid and gas states, which are available in the literature [39, 90, 92-98, 100-103, 105, 106, 109, 110, 116, 118, 141-146, 148-173, 175-178], together with those derived from first principle calculations in gaseous state [172], are summarized in Table A.5. Experimental values of enthalpy and entropy of fusion of PAH compounds as the required information for liquid phase thermodynamic property calculations are listed in Table A.6.

These data, which are obtained separately without any consideration of consistency between them, do not have enough accuracy for the estimation of thermodynamic properties such as vapor pressure and phase equilibria data. The philosophy of the CALPHAD approach [112] is to obtain the thermodynamic data rendered consistently with phase transitions and vapor pressure data. The CALPHAD approach is applied to optimize the enthalpy and entropy of formation of PAH compounds in solid, liquid and gas states while satisfying the available experimental data for vapor pressure and phase transitions thermodynamic data. Phase transition data and vapor pressures of reference compounds as a function of temperature calculated using both standard thermodynamic properties of PAHs obtained by group contribution algorithms and those optimized with the CALPHAD approach are shown in Figs. (A.1, A.3, A.5, A.7 and A.9) in Appendix A. Comparing the results presented in these figures (highlighted as before and after CALPHAD) shows how the CALPHAD approach can be applied to estimate the thermodynamic properties of PAH compounds in a consistent manner. Meanwhile, good agreement between experimental data [110, 147, 161, 179-190] and estimated values in these figures shows that the obtained optimized values of standard

thermodynamic properties can be utilized reliably to predict thermodynamic data of PAH compounds.

Optimized values of standard thermodynamic properties at 298.15 K and 1 bar and phase transition data of reference compounds are summarized in Tables A.5 and A.6, respectively. Subsequently, entropy and enthalpy of formation at 298.15 K and 1 bar of the constituent groups (listed in Tables 4.2 and 4.3) in solid, liquid and gaseous PAH compounds are calculated using optimized values of standard thermodynamic properties at 298.15 K and 1 bar of reference PAH compounds and applying group contribution calculations as described in Section 4.2.1.2. Table 4.6 shows standard thermodynamic properties at 298.15 K and 1 bar of constituent groups in solid, liquid and gaseous states. It is important to point out that with respect to the subject discussed in Section 4.2.1.2, this table includes the standard thermodynamic properties of G_7 and G_8 groups as the aromatic groups introduced to the model for modification purpose which is only utilized in the estimation of the standard thermodynamic properties of PAH-derived constituents, high MW oligomers and polymers, of coal tar pitch and not in those of PAH monomers.

The standard thermodynamic properties of PAHs adopted in the present work can be estimated using group contribution algorithms and the thermodynamic properties of constituent groups (listed in Table 4.6) as well as applying the CALPHAD approach to optimize them.

Table 4.6 Entropy and enthalpy of formation at 298.15 K and 1 bar of the constituent groups in the solid, liquid and gaseous PAH compounds from group contribution calculation.

Group	$\Delta H^{\circ}_{298\,K}$ (kJ mole^{-1})			$S^{\circ}_{298\,K}$ (J mole^{-1} K^{-1})		
	solid	liquid	gas	solid	liquid	gas
G_1	1.027907E+04	6.846422E+03	1.374594E+04	1.353433E+00	-1.366000E+01	-1.739543E+01
G_2	5.863926E+03	8.119181E+03	1.168583E+04	2.278917E+01	3.289500E+01	4.629013E+01
G_3	8.458483E+03	1.236173E+04	1.914076E+04	1.829907E+01	2.828250E+01	4.633158E+01
G_4	1.323923E+04	1.993953E+04	2.420519E+04	1.860457E+01	3.155530E+01	4.610353E+01
G_5	7.572321E+03	9.597051E+03	1.730251E+04	-2.093300E+00	-4.231000E+00	3.499750E+00
G_6	-1.698033E+01	-2.329556E+01	-1.111935E+01	7.392496E+01	6.928722E+01	9.700356E+01
G_7	2.398548E+01	3.042708E+01	3.492553E+01	-1.275236E+00	4.902884E+00	5.135100E+00
G_8	2.272483E+01	2.212005E+01	3.111083E+01	-9.441183E-02	-6.494944E+00	2.736787E+00

However, some modifications are needed to be made to the proposed model in the case of prediction of standard thermodynamic properties of the PAH compounds which suffer from a lack of experimental data. The following procedure is proposed for optimization purposes when there is not enough phase transition and vapor pressure data for the PAH compound subjected to standard thermodynamic properties calculations. Consequently, specific application of this modification appears for standard thermodynamic properties prediction of high molecular weight PAH oligomers.

Resonance stabilization energies and molecular rotational symmetry are significant factors to be considered in predicting standard thermodynamic properties of aromatic hydrocarbons.

The resonance energy of an aromatic compound is a measure of the extra stability of the conjugated system compared to the corresponding number of isolated double bonds [191-193]. Resonance energy as an important attribute of PAH compounds affects the enthalpy of formation of these compounds. Resonance energies of some conjugated hydrocarbons have been reported in the literature [193-196]. In these studies, it has been shown that the resonance energy of compounds

containing aromatic segments (like PAH oligomers) can be estimated as the sum of resonance energies of the various aromatic segments in it [194].

In the present work, the enthalpy of formation at 298 K and 1 bar of the PAH compounds with lack of experimental data (including PAH oligomers), which already predicted using the proposed approach at the beginning of Section 4.2.2.2, is modified by calculating the resonance energies of these compounds and using resonance energies of the constituents segments in the compound reported in the literature [193-196]. In fact, the effect of the resonance energy in this calculation appears as a subtracting factor in the initial estimated values of enthalpy of formation at 298 K and 1 bar.

The relationship between molecular symmetry and entropy of the compounds was first observed by Carnelley [197] and then thoroughly reviewed by Brown [198]. Yalkowsky and Martin et al. [199, 200] were the first to quantitate the role of molecular symmetry in determining the entropy of specific compounds. They observed that the melting points of a number of disubstituted benzene isomers are inversely related to the logarithms of their rotational symmetry numbers. In other words, a symmetrical molecule with a high-symmetry number σ has increased order and reduced rotational entropy by the amount of R ln(σ), which elevates the melting point [201, 202]. The rotational symmetry number, σ, is defined as the rotational degeneracy of the molecule. It is equal to the number of identical images that can be produced by rotation of the molecule within 360 in any direction. The rotational symmetry number of some simple molecules has been reported in references [202, 203].

Using these reported values and the fact that UPPER (United Physical Property Estimation Relationship) gives the radially symmetrical molecules a value of 20 to indicate that they are more

symmetrical than benzene, the symmetry number of the PAHs adopted in the present work can be evaluated. Subsequently, the entropy at 298 K and 1 bar, which has been already estimated using the defined approach at the beginning of Section of 4.2.2.2, will be revised with -R ln(σ) term, where R and σ represent the gas constant value and the symmetry number of the molecule, respectively.

4.3 Application of Compound Energy Formalism (CEF) to predict heat capacity functions of PAHs with anomaly behavior

As a summary of the literature review [113-116, 124, 204-206], some PAH compounds like phenanthrene, pyrene, and perylene exhibit heat capacity anomaly in the solid state. An anomalous absorption of energy is found in the vicinity of the temperature at which the anomalous behavior appears and results in a big jump in temperature-dependent heat capacity function of these PAHs in the crystalline phase (Fig. 4.4) [116].

Phenanthrene with chemical formula $C_{14}H_{10}$ is the isomer of anthracene. The solid properties of the two isomers differ significantly The most important difference is that phenanthrene has a crystal transition at ambient pressure while anthracene does not [124]. The phase transition in phenanthrene has been the object of much study since its behavior is unusual. Heat capacity studies show a thermal anomaly with a maximum of 347.15 K [116].

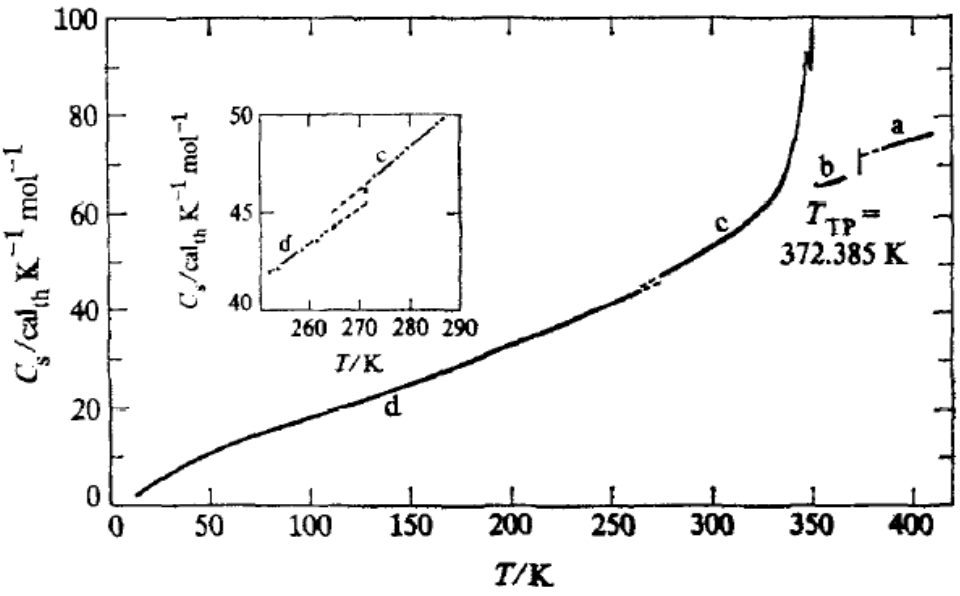

Figure 4.4 Heat capacity and phase transition of highly purified phenanthrene: a, liquid; b, crystal I; c, crystal II; d, crystal III (mole fraction of impurity: 0.00013) [116].

Structural evidence given by X-ray and neutron diffraction studies shows that the overcrowded hydrogen atoms in the molecular structure are responsible for the anomalous behavior [124]. In fact, the observed transition may be related to increased vibration and rearrangement of hydrogen atoms on the 4^{th} and 5^{th} sites of the phenanthrene molecule (Fig. A.11 in Appendix A) [114-116, 124]. On passing through the phase transition temperature, the lattice constants for the monoclinic cell increase conspicuously, while both the crystal system (which is monoclinic) and the space group remain unaltered [113, 124]. It has been found that this phase transition which previously suggested by the anomalies in thermal expansion is associated with a second-order phase transition [113].

The Compound Energy Formalism (CEF) is used to develop the thermodynamic model for the heat capacity function prediction of PAHs with anomalous behavior in solid state. The application of

CEF has been presented previously [207, 208] and will not be described in detail in the present article. It is common, in the CEF, to represent the list of species mixing on the respective sub-lattices using a description similar to $(A;B)_x(D;E)_y(F;G;H)_z$ representation, where A, B,…,H are chemical species and x, y and z are the sublattice stoichiometric factors. A simple case can be represented as (A;B)(C;D). In this case, in the system under consideration there are four elements and the composition is conveniently can be plotted on a square where the corners represent the four basic compounds AC, BC, AD, and BD and the parameters X_B and X_D used to represent the composition of any intermediate point, Fig. 4.5, where $X_B = \frac{n_B}{n_A + n_B}$ and $X_D = \frac{n_D}{n_C + n_D}$. Using the Gibbs free energies of pure components and minimization of Gibbs energy of the system as defined in references [207, 208] enables the calculation of the internal state of the system.

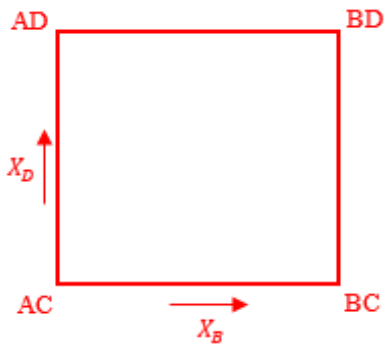

Figure 4.5 Representation of the composition in an quaternary system where the components mix each other, two and two [207].

Applied to our specific case, for any given PAH compound, sublattice species are: the compound before phase transition represented as (C_xH_y) and the compound after the phase transition, $(C_xH_y)_P$. In the CEF, for our choice of sublattice species, four end-members are defined: $(C_xH_y):(C_xH_y)$, $(C_xH_y):(C_xH_y)_P$, $(C_xH_y)_P:(C_xH_y)$ and $(C_xH_y)_P:(C_xH_y)_P$. It should be noted that $(C_xH_y):(C_xH_y)$ and $(C_xH_y)_P:(C_xH_y)_P$ end-members are present in temperature ranges

much below and much above the solid phase transition temperature, respectively, and 4 end-members in different proportions are available between these two temperature limits (including solid phase transition region).

The Gibbs energy functions of the four end-members, i.e, $G_{(C_xH_y):(C_xH_y)}$, $G_{(C_xH_y):(C_xH_y)_P}$, $G_{(C_xH_y)_P:(C_xH_y)}$, and $G_{(C_xH_y)_P:(C_xH_y)_P}$ are defined based on Gibbs energy function of sublattice species, as follows:

$$G_{(C_xH_y):(C_xH_y)} = 2\,G_{(C_xH_y)} \quad \text{Eq. (4.7)}$$

$$G_{(C_xH_y):(C_xH_y)_P} = G_{(C_xH_y)} + G_{(C_xH_y)_P} + DG_1 + DG_{ex} \quad \text{Eq. (4.8)}$$

$$G_{(C_xH_y)_P:(C_xH_y)} = G_{(C_xH_y)_P} + G_{(C_xH_y)} + DG_1 + DG_{ex} \quad \text{Eq. (4.9)}$$

$$G_{(C_xH_y)_P:(C_xH_y)_P} = 2\,G_{(C_xH_y)_P} + 2DG_1 \quad \text{Eq. (4.10)}$$

In these equations $G_{(C_xH_y)}$ and $G_{(C_xH_y)_P}$ are the Gibbs energies of sublattice species (i.e. chemical species) which are defined with Eqs. (4.1-4.3) at any given temperatures.

In Eqs. (4.1-4.3), $\Delta H^{\circ}_{298.15\,K}$ and $S^{\circ}_{298.15\,K}$ are entropy and enthalpy at 298.15 K and 1 bar of PAH compound, i.e. (C_xH_y), which are estimated by applying the method presented in Section 4.2.2.2. The heat capacity, Cp, in Eqs. (4.1-4.3) represents the heat capacity function of sublattice species. Heat capacity of the compound before phase transition represented, $C_{p_{(C_xH_y)}}$, can be calculated by following the approach defined in Section 4.2.2.1. The heat capacity of the compound after phase transition, $C_{p_{(C_xH_y)_P}}$ is described as follows:

$$C_{p_{(C_xH_y)_P}} = C_{p_{(C_xH_y)}} + a \qquad \text{Eq. (4.11)}$$

DG_1 , DG_{ex} and a in Eqs. (4.8-4.11) become model parameters which are determined in such a way satisfying heat capacity function of PAH compound in whole temperature ranges under study (including solid phase transition temperature). Subsequently, coded Gibbs energy equations (Eqs. 4.7-4.10) used in a Gibbs energy minimization routine permits the computation of the internal state of equilibrium of solid PAH compound.

4.4 Results and discussion

The present thermodynamic model was applied to estimate the thermodynamic properties, phase transition data as well as vapor pressures of pure PAHs. The estimation of the heat capacity function of PAHs with an anomalous behavior was performed using the concept defined in Section 4.3 and utilizing the SOLUTION and EQUILIB modules of the FactSage^{TM} thermochemical software.

4.4.1 Prediction of heat capacity function coefficients of PAHs

The group properties summarized in Tables 4.4 and 4.5 and Eqs. (4.4) have been used to calculate the heat capacity function coefficients of some PAH compounds. Naphthacene, pentacene, perylene, and coronene were selected to be studied in this section. These compounds are commonly found in coal tar pitch and there is enough reported experimental data in the literature to allow the comparison of their thermodynamic properties with predictive calculation results. It is important to be pointed out that to justify determined heat capacity function coefficients of G_5 group, perylene and coronene are considered as the compounds subjected to the prediction in this section. Regarding the subject presented in Sections 4.2.1.2 and 4.2.2.1, the heat capacity function coefficients of them are estimated by using those of G_1-G_6 groups without any intervention of

thermodynamic properties of G_7 and G_8 groups (application of the thermodynamic properties of G_7 and G_8 groups will be discussed in Section 4.4.3). The heat capacity function coefficients of these compounds in solid, liquid and gas states have been estimated and summarized in Table A.3 and Table A.4, respectively. The results for heat capacity function of naphthacene, pentacene, perylene and coronene as a function of temperature are shown in Figs. 4.6-4.13. The predictive calculations are compared with reported experimental data and those obtained according to Richard and Helgeson's prediction method [111, 156, 166, 171, 209]. Although there is some deviation between the results from this work and experimental data (seen in Figs. 4.7, 4.9, 4.11, and 4.13 as zoom view of a portion of Figs. 4.6, 4.8, 4.10, and 4.12), a major improvement was achieved when compared to Richard and Helgeson's prediction.

As seen in these figures, Richard and Helgeson's approach can predict the heat capacity of solid PAH compounds only in a specific range of temperature, neither at low ranges nor at high ranges of temperature. At low temperatures, heat capacity values of solid PAHs predicted by Richard and Helgeson have a dramatic difference from experimental data and those predicted in the present work. In fact, the type of heat capacity function chosen to model the heat capacity of PAHs affects the results. The heat capacity correlation proposed in this work (Eq. 4.5) is different from that used by Richard and Helgeson (Eq. 6 in ref. [111]) and improves the heat capacity prediction of solid PAH compounds. According to the dependence of the heat capacity of solid components on the temperature, reported as experimental data or predicted theoretically, the heat capacity will become plateau at relatively high temperatures [175]. The heat capacity values of solid PAHs predicted using the model presented in this work in the temperature range of interest for the carbonization process (25 – 1200°C) can satisfy the plateau function of heat capacity at relatively high temperatures while the Richard and Helgeson's method cannot.

The proposed model can predict a reasonable heat capacity function for PAH compounds in liquid and gaseous states. There is a good agreement between the heat capacity of gas PAHs predicted in the present work and experimental data. Predicted heat capacity function of liquid PAHs shows good agreement with experimental data in temperature ranges where the data is available (only one data set reported by Wong [166] for liquid perylene) and can satisfy the trend of heat capacity function at high temperature, which is expected to be plateau such as solid and gaseous states. A major improvement is achieved when compared to Richard and Helgeson's prediction for liquid PAHs which are so linear. Indeed, in Richard and Helgeson's method, the heat capacity of most of the reference compounds in liquid state (naphthalene, anthracene, pyrene, phenanthrene, and triphenylene) has been correlated linearly (Table 2 in ref. [111]) which results in so linear heat capacity function of liquid PAHs subjected to the prediction.

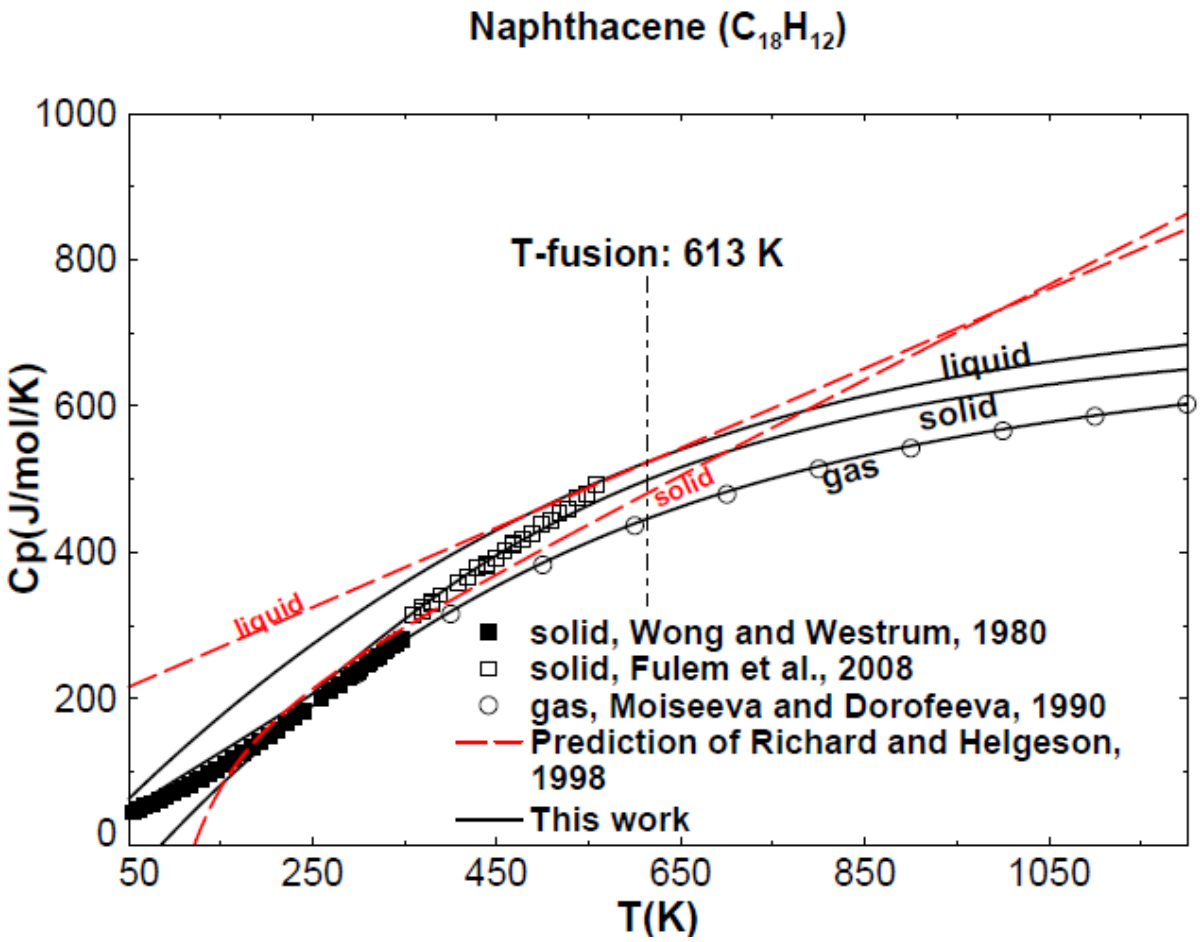

Figure 4.6 Comparison of the predicted heat capacity of naphthacene (solid, liquid and gas state) with experimental data and Richard and Helgeson's predicted values [111, 156, 166, 209].

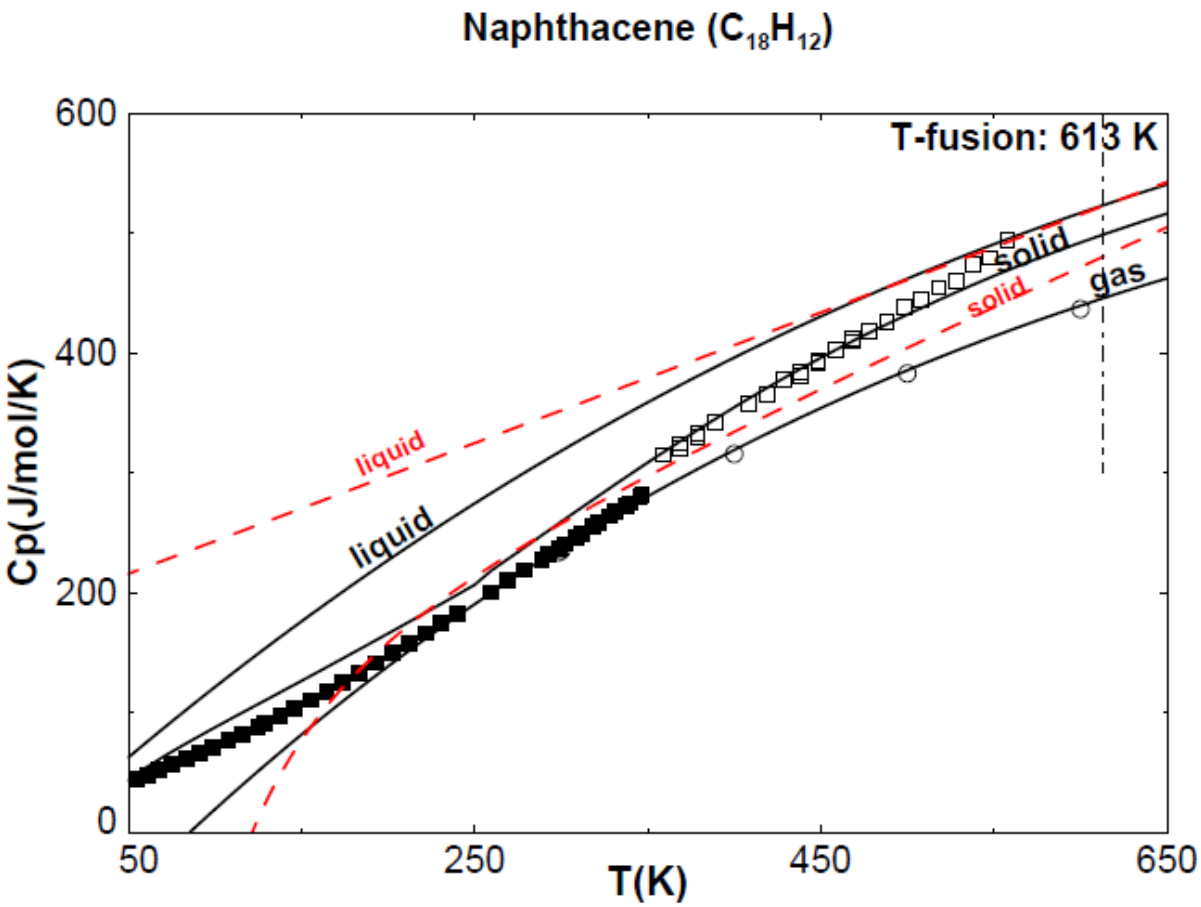

Figure 4.7 Zoom view of a portion of Fig. 4.6.

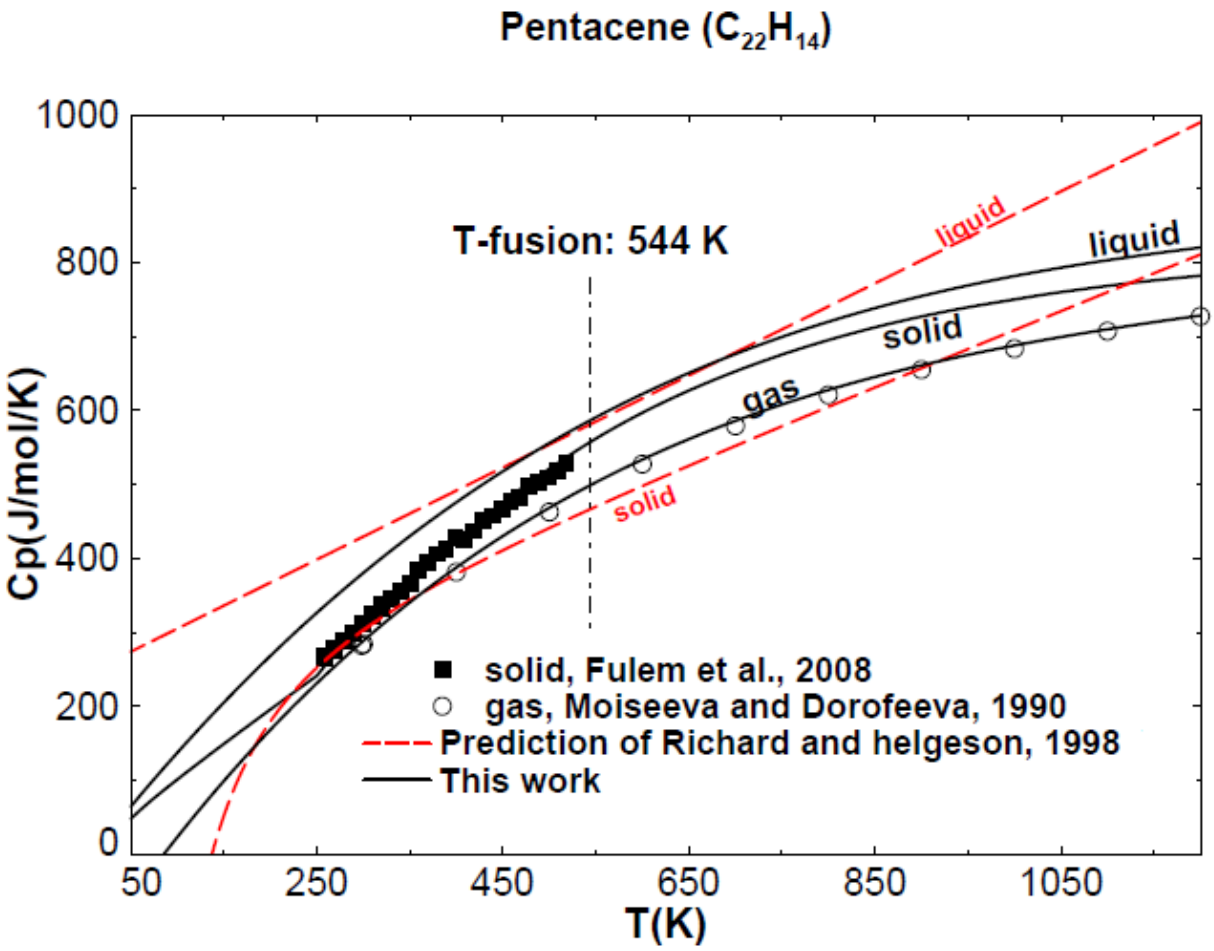

Figure 4.8 Comparison of the predicted heat capacity of pentacene (solid, liquid and gas state) with experimental data and Richard and Helgeson's predicted values [111, 156, 209].

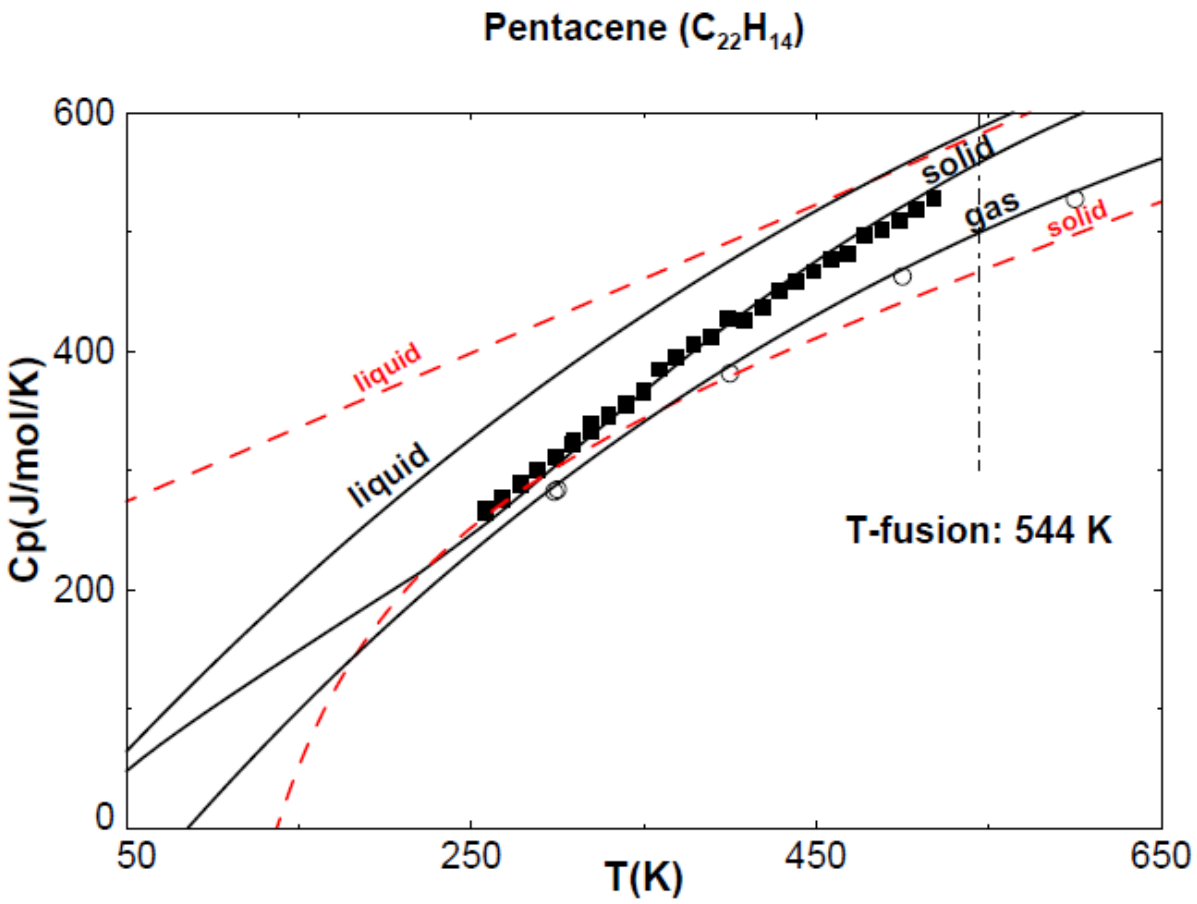

Figure 4.9 Zoom view of a portion of Fig. 4.8.

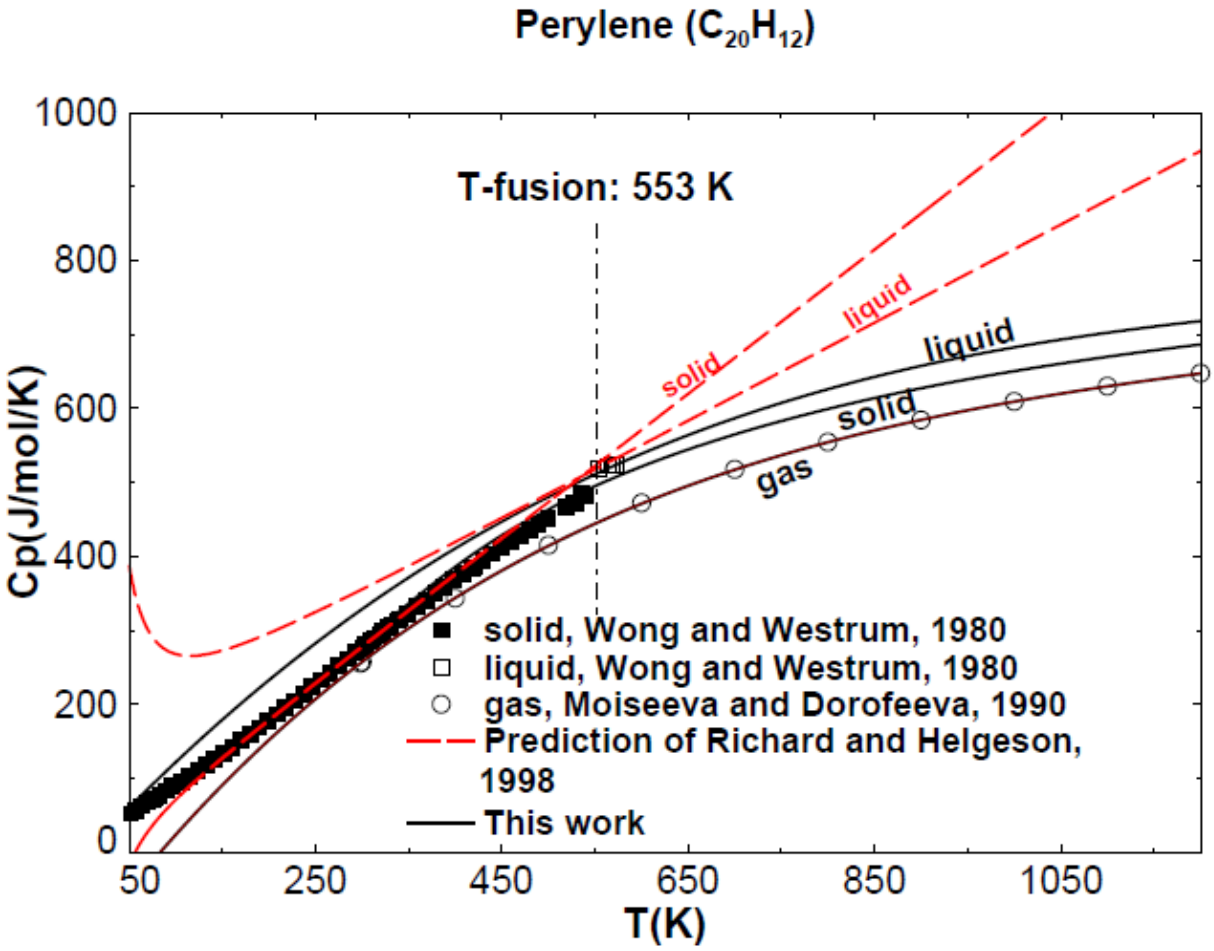

Figure 4.10 Comparison of the predicted heat capacity of perylene (solid, liquid and gas state) with experimental data and Richard and Helgeson's predicted values [111, 156, 166] (for anomaly, see Section 4.4.4).

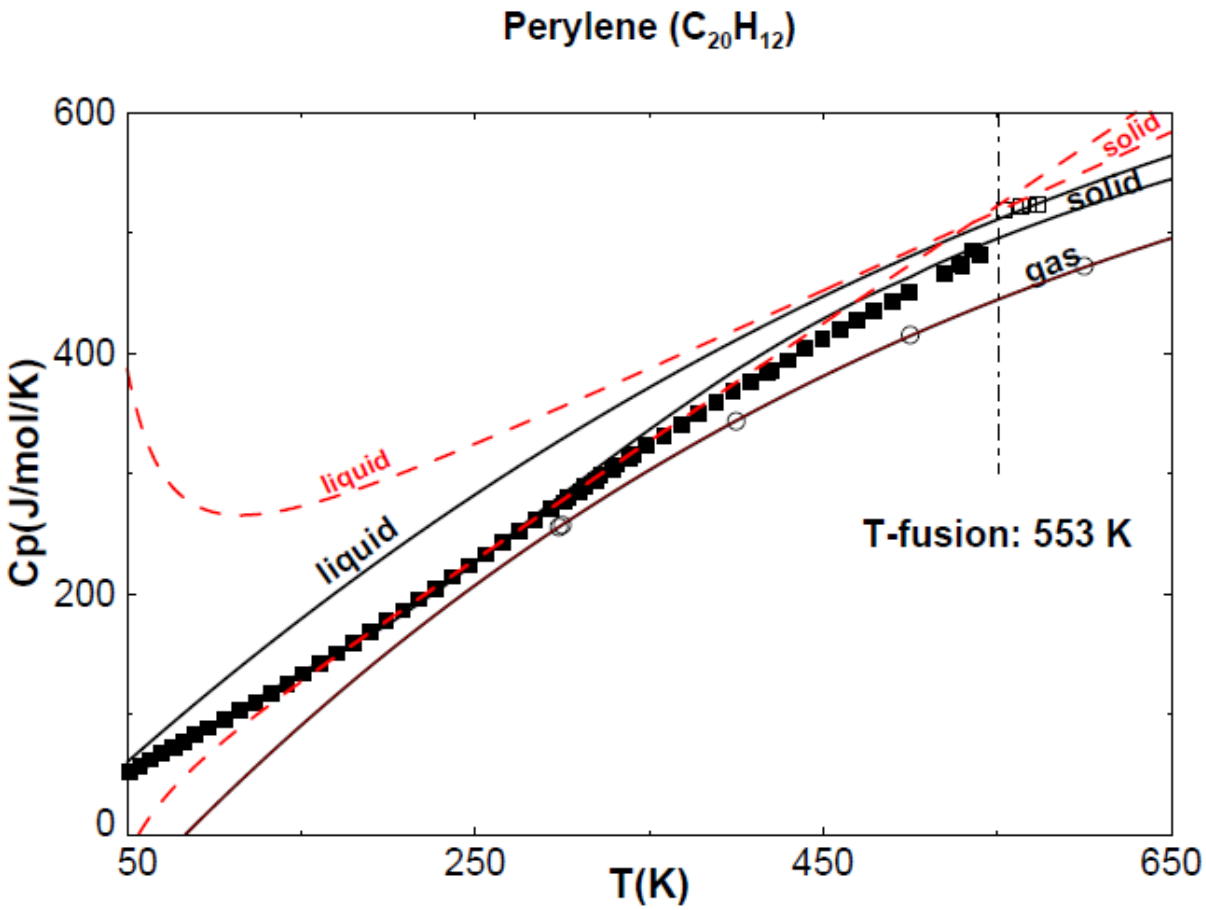

Figure 4.11 Zoom view of a portion of Fig. 4.10.

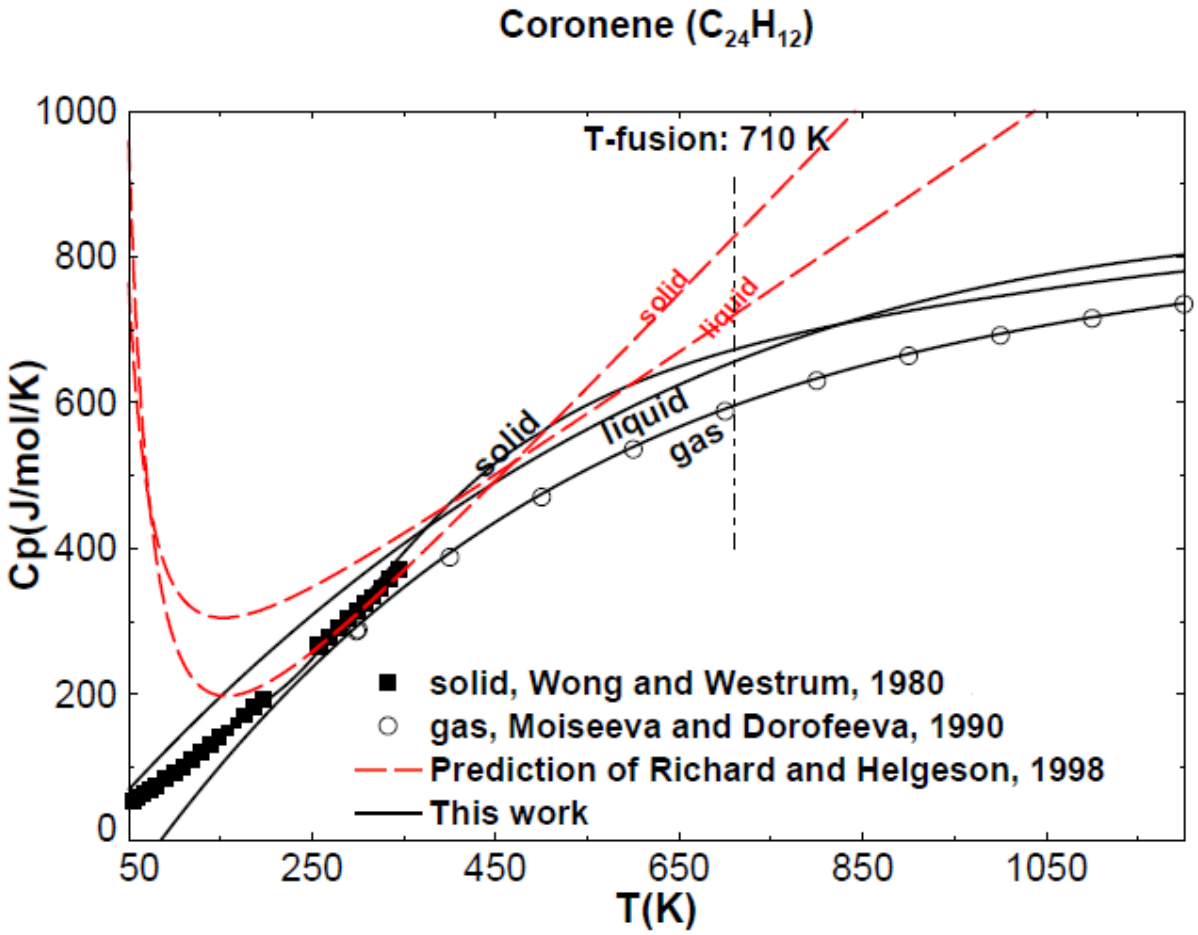

Figure 4.12 Comparison of the predicted heat capacity of coronene (solid, liquid and gas state) with experimental data and Richard and Helgeson's predicted values [111, 156, 166].

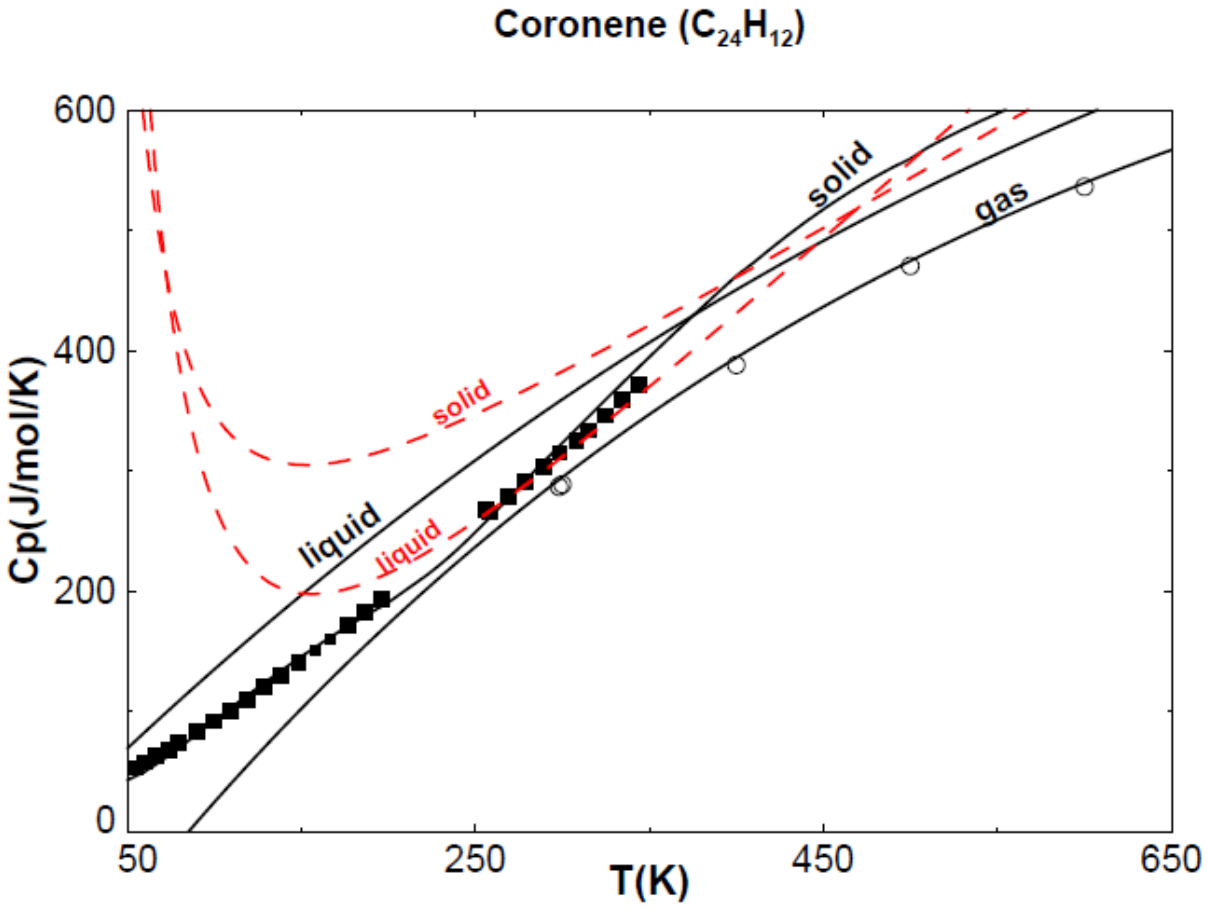

Figure 4.13 Zoom view of a portion of Fig. 4.12.

4.4.2 Prediction of standard thermodynamic properties of PAHs

Entropy and enthalpy of formation at 298 K and 1 bar of PAH compounds adopted in the present work can be generated from group additivity algorithms and the group properties presented in Table 4.6. The obtained values have been optimized by applying the CALPHAD approach for compounds with enough available experimental data. However another approach (as presented in Section 4.2.2.2) which considers the effect of resonance energy and molecular rotational symmetry, was used to modify the values obtained from group additivity algorithms for PAHs suffering from a lack of experimental data.

4.4.2.1 **Applying the CALPHAD approach for standard thermodynamic properties and vapor pressure predictions of PAHs**

Standard thermodynamic properties predicted using group additivity algorithms were optimized by applying the CALPHAD approach, as explained in Section 4.2.2.2. Firstly, standard thermodynamic properties of PAHs subjected to the calculations are calculated using standard thermodynamic properties of the constituents groups (listed in Table. 4.6) and applying group contribution method. Obtained Standard thermodynamic properties are then optimized by applying CALPHAD approach. Standard thermodynamic properties in solid and gas states and phase transition data of some PAHs such as naphthacene, pentacene, and perylene with enough experimental data [39, 93, 105, 112, 113, 115, 118, 167, 172, 177, 210, 211] are estimated and summarized in Tables 4.7-4.9. It is important to be pointed out that in order to justify determined standard thermodynamic properties of G_5 group, perylene is considered as a compound subjected to prediction in this section. Regarding the subject presented in Sections 4.2.1.2 and 4.2.2.2, standard thermodynamic properties of this compound are estimated by using those of G_1-G_6 groups without any intervention of thermodynamic properties of G_7 and G_8 groups (application of the thermodynamic properties of G_7 and G_8 groups will be discussed in Section 4.4.3).

Tables 4.7-4.9 compare the thermodynamic properties of naphthacene, pentacene and perylene obtained using group contribution calculations, optimized by applying the CALPHAD approach, the values reported in the literature (experimental data and data from first principle calculations) and those derived by Richard and Helgeson [111]. There is a good agreement between optimized values (obtained by applying the CALPHAD approach), experimental data and the data from first principle calculations. The deviation between the values predicted by Richard and Helgeson, group

Table 4.7 Enthalpy of formation at 298.15 K and 1 bar of some PAHs in solid and gas states.

Compound	Formula	$\Delta H°_f$ (kJ mole^{-1})							
		solid				gas			
		Exp. value	Group contr.	Opt. value	Predict. by Helgeson	Exp. value	FPC value	Group contr.	Opt. value
Naphthacene [39, 93, 115, 172]	$C_{18}H_{12}$	203-209.7	171.9	202.1	180.6	336.7-348.5	320.4	302.6	330.4
Pentacene [39, 93, 172]	$C_{22}H_{14}$	-	219	249.3	232.1	-	411.2	378.5	411.9
Perylene [39, 93, 167, 172, 211]	$C_{20}H_{12}$	180.4-186.0	157.6	183.1	162.8	315-321.3	319.4	287.1	315.1

Table 4.8 Entropy of some PAHs in solid and gas states at 298.15 K and 1 bar.

Compound	Formula	$S°_{298.15K}$ (J mole^{-1} K^{-1})							
		solid				gas			
		Exp. value	Group contr.	Opt. value	Predicted by Helgeson	Exp. value	FPC value	Group contr.	Opt. value
Naphthacene [39, 93, 172, 179]	$C_{18}H_{12}$	215.4	246.9	249.8	246.9	-	444.7	450.5	441.7
Pentacene [39, 93, 172]	$C_{22}H_{14}$	-	286.8	286.3	286.7	-	499.8	507.94	501.2
Perylene [39, 172, 179]	$C_{20}H_{12}$	264.6	259.4	261.1	270.8	-	461.5	458.27	501.2

Table 4.9 Phase transition properties of some PAHs.

Compound	$T°_{fusion}$ (K)			$\Delta H°_{fusion}$ (kJ mole^{-1})			$\Delta S°_{fusion}$ (J mole^{-1} K^{-1})		
	Exp. value	Pred. value	Pred. by Helg.	Exp. value	Pred. value	Pred. by Helg.	Exp. value	Pred. value	Pred. by Helg.
Naphthacene [113, 115, 210]	613.0-623.0	618.0	581.2	35.9	35.6	47.1	58.1	57.6	81.1
Pentacene [113, 167]	544.0	544.0	631.6	-	44.5	71.8	-	81.3	113.7
Perylene [105, 118, 172, 177]	533.0-553.0	543.0	472.0	31.9-32.6	31.4	18.1	58.8-60.0	57.8	38.4

contribution method and the experimental data shows that applying the CALPHAD approach is required to optimize the set of thermodynamic properties with full consistency.

The vapor pressures of naphthacene, pentacene, and perylene as a function of temperature have been calculated using the predicted heat capacity function in the present work (Section 4.1) and optimized values of entropy and enthalpy of formation at 298.15 K and 1 bar (Tables 4.7-4.9) utilizing the FactSage^{TM} thermochemical software. The results are shown in Figs. 4.14- 4.16 [111, 178, 187]. Although available experimental data for vapor pressure of PAH compounds is limited but it is enough to show that the present work significantly improves the estimation of vapor pressures of PAH compounds in comparison with that proposed by Richard and Helgeson [111]. As shown in Fig. 4.16, there is some uncertainty in the experimental vapor pressure data of perylene. The vapor pressure values of perylene presented by Goldfarb and Suuberg [178] are slightly higher than those obtained by Oja and Suuberg [187] in the same range of temperature. In their paper, Goldfarb and Suuberg explain that the high purity of the used perylene sample in his studies and good agreement obtained between several different experiments results in more reliable set of vapor pressure data compared to another set of vapor pressure data reported by Oja and Subberg. Thus, the set of vapor pressure data presented by Goldfarb and Suuberg has been utilized in the CALPHAD approach.

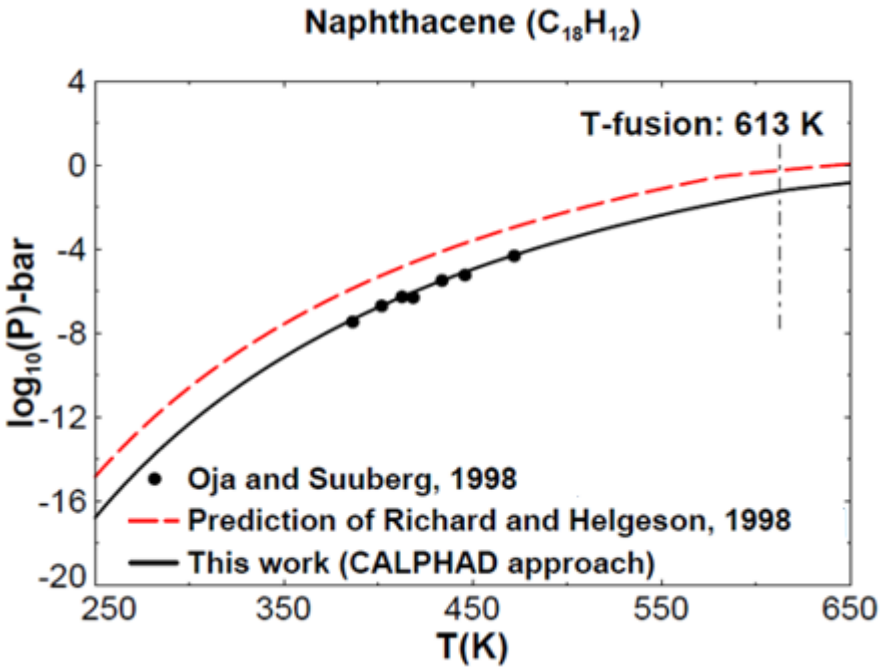

Figure 4.14 Calculated vapor pressure of naphthacene as a function of temperature [111, 187].

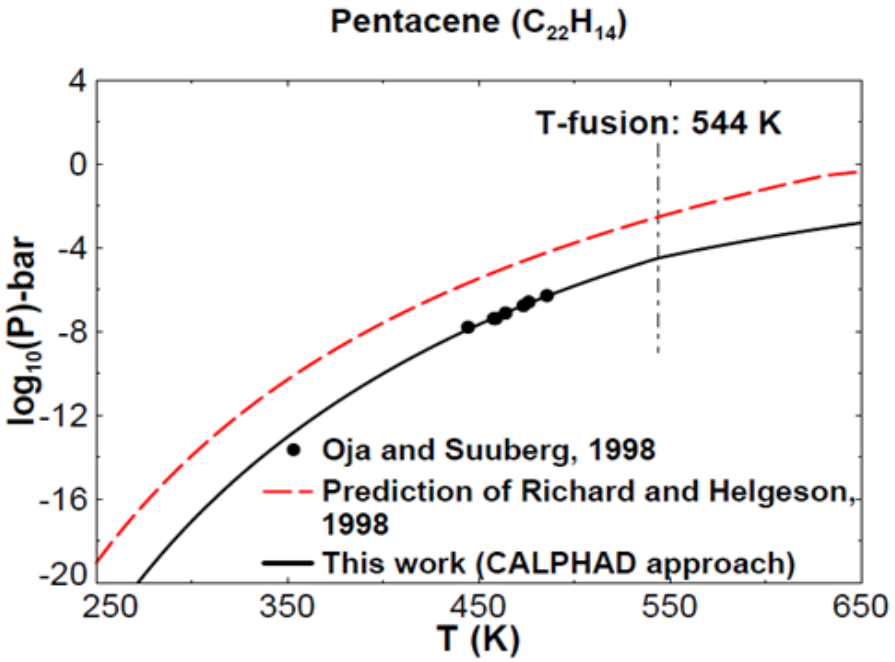

Figure 4.15 Calculated vapor pressure of pentacene as a function of temperature [111, 187].

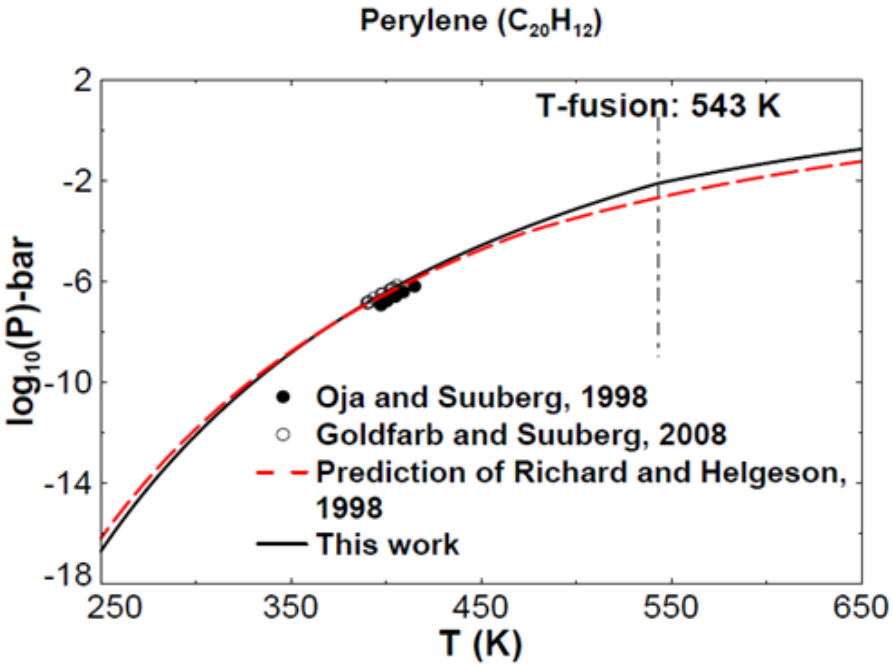

Figure 4.16 Calculated vapor pressure of perylene as a function of temperature [111, 178, 187].

4.4.2.2 **Standard thermodynamic properties prediction of PAHs with lack of experimental data**

It was pointed out in the second part of Section 4.2.2.2 that the predication of standard thermodynamic properties of PAH compounds which suffers from a lack of experimental data needs some considerations concerning resonance energy and molecular rotational symmetry of these molecules. Following the approach proposed in that section and the method defined for resonance energy and molecular rotational symmetry calculations [193-195, 202, 203], standard thermodynamic properties of some PAHs such as Benzo[a]anthracene, Benzo[e]pyrene, Dibenzo[a,c]anthracene, Dibenzo[a,j]anthracene and Dibenzo[a,j]naphthacene are estimated and shown in Table 4.10. Comparison of the estimated standard thermodynamic properties with experimental data and the data obtained by first principles calculation (FPC) [39, 93, 172, 212]

confirms the pertinence of applying the proposed approach for optimizing the standard thermodynamic properties estimation of PAHs in the case of a lack of experimental data.

Table 4.10 Entropy and enthalpy of formation at 298.15 K and 1 bar of some PAHs in solid and gas states.

Compound	**Formula**	**$\Delta H°_f$ (kJ mole^{-1})**				**$S°_{298.15\ K}$ (J mole^{-1} K^{-1})**			
		solid		**gas**		**solid**		**gas**	
		Exp. value	Pred. value	Exp., FPC value	Pred. value	Exp. value	Pred. value	Exp., FPC value	Pred. value
Benzo[a]anthracene [39, 93, 172]	**$C_{18}H_{12}$**	167.5 – 174.1	156.2	284.3-296.3	274.9	-	255.7	458.0	448.3
Benzo[e]pyrene [172]	**$C_{20}H_{12}$**	-	153.6	299.8	283.2	-	253.7	463.7	458.3
Dibenzo[a,c]anthracene [39, 172]	**$C_{22}H_{14}$**	176.1-193.5	190.8	331.0	337.8	-	298.2	511.8	506.2
Dibenzo[a,j]anthracene [172]	**$C_{22}H_{14}$**	-	185.9	346.2	323.2	-	298.2	507.4	506.1
Dibenzo[de,mn]naphthacene (Zethrene)[172]	**$C_{24}H_{14}$**	-	260.8	431.3	420.0	-	295.6	523.2	516.4

The vapor pressures of Benzo[a]anthracene and Benzo[e]pyrene as a function of temperature have been estimated using the predicted heat capacity of aromatic groups and optimized values of entropy and enthalpy of formation at 298.15 K and 1 bar listed in Tables 4.4, 4.5, and 4.10, respectively. Figs. 4.17 and 4.18 show a good agreement between predicted and experimental values of the vapor pressure of Benzo[a]anthracene and Benzo[e]pyren.

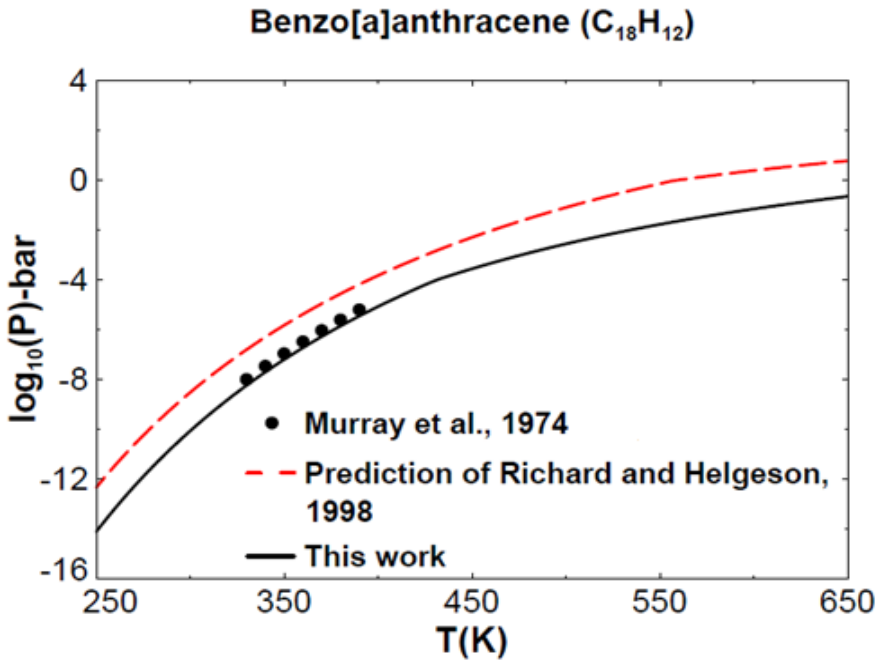

Figure 4.17 Calculated vapor pressure of benzo[a]anthracene as a function of temperature [111, 212].

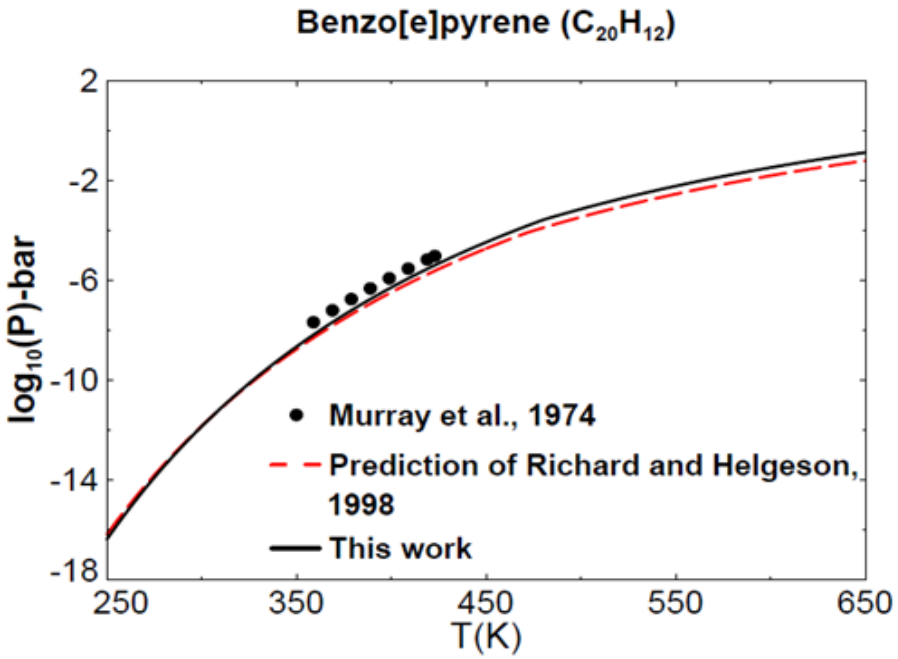

Figure 4.18 Calculated vapor pressure of benzo[e]pyrene as a function of temperature [111, 212].

4.4.3 Application to prediction of thermodynamic properties of high molecular weight PAHs

Heat capacity function coefficients, entropy and enthalpy of formation at 298 K and 1 bar of high MW PAH oligomers can be generated from group additivity algorithms, group properties presented in Tables 4.4-4.6 and the approach presented in Section 4.2.2.2 for estimating standard thermodynamic properties of PAHs suffering from a lack of experimental data. Regarding the paucity of experimental data for oligomers of PAHs, the application of the present model has only been verified for the predictions of the melting and boiling temperatures of quaterrylene (bi-perylene) and tri-phenylene. The melting point of quaterrylene is estimated as 759 K compared to the experimental value of 816 K [25]. The boiling points of quaterrylene and tri-perylene were estimated as 1046 K and 1237 K, respectively. While there is no data in the literature to compare with, the values seem reasonable with respect to the boiling point of monomer for this compound (i.e. $T_{b_{perylene}} = 740\ K$).

4.4.4 Prediction of heat capacity function of PAHs with anomalous behavior

To conclude the discussion from Section 3, about the unusual phase transition in solid state of some PAHs such as phenanthrene which has a special molecular structure (Fig. A.11 in Appendix A), this phase transition is a second-order phase transition with only slight changes in lattice constants. There are no changes in either crystal structure or the space group. Indeed, an anomalous absorption of energy is found in the vicinity of the temperature at which the anomalous behavior appears results in a big jump in temperature-dependent heat capacity function of these compounds in crystalline phase [124, 204, 206]. Model parameters defined in Section 4.3 , i.e. DG_1 , DG_{ex} in Eqs. (4.8-4.10), are optimized to match the experimental data of heat capacity of phenanthrene in

the transition region as listed in Table 4.11. The value of the model parameter "*a*" in Eq. 4.11 is also determined as 10 by fitting to heat capacity experimental data. Subsequently, the heat capacity function of phenanthrene has been estimated using the FactSage^{TM} thermochemical software (both the SOLUTION and EQUILB modules) and optimized model parameters and are shown in Fig. 4.19. Scientific heat capacity in this figure represents the anomalous heat capacity function of the compound predicted by applying the proposed approach in Section 3, a combination of group additivity algorithm and compound energy formalism (CEF). As seen in Fig. 4.20, as a zoom view of solid phase transition region of Fig. 4.19, the proposed approach in this work has the ability to model the heat capacity of PAH compounds with anomalous behavior in solid state.

Regarding the heat capacity experimental data for pyrene and perylene [96, 109, 166], [96, 109, 166], these compounds exhibit an unusual phase transition (above the room temperature) which can be modeled using the procedure mentioned for phenanthrene. Using CEF formalism parameters in Table 4.11 and *a* equal to zero in Eq. 4.11 predicted values of heat capacity for pyrene and perylene are shown in Figs. 4.21 and 4.22.

Table 4.11 Optimized CEF formalism parameters corresponding to Eqs. (4.8-4.10)

Phenanthrene	$G_{(C_{14}H_{10})_L:(C_{14}H_{10})_L} = 2\,G_{(C_{14}H_{10})_L}$ $G_{(C_{14}H_{10})_L:(C_{14}H_{10})_H} = G_{(C_{14}H_{10})_L} + G_{(C_{14}H_{10})_H} + 5150 + 1.3T$ $G_{(C_{14}H_{10})_H:(C_{14}H_{10})_H} = 2\,G_{(C_{14}H_{10})_H} + 7500 - 21.4T$
Pyrene	$G_{(C_{16}H_{10})_L:(C_{16}H_{10})_L} = 2\,G_{(C_{16}H_{10})_L}$ $G_{(C_{16}H_{10})_L:(C_{16}H_{10})_H} = G_{(C_{16}H_{10})_L} + G_{(C_{16}H_{10})_H} + 8400 - 3.6T$ $G_{(C_{16}H_{10})_H:(C_{16}H_{10})_H} = 2\,G_{(C_{16}H_{10})_H} + 8200 - 19.2T$
Perylene	$G_{(C_{20}H_{12})_L:(C_{20}H_{12})_L} = 2\,G_{(C_{20}H_{12})_L}$ $G_{(C_{20}H_{12})_L:(C_{20}H_{10})_H} = G_{(C_{20}H_{12})_L} + G_{(C_{20}H_{12})_H} + 4780 + 8.2T$ $G_{(C_{20}H_{12})_H:(C_{20}H_{12})_H} = 2\,G_{(C_{20}H_{12})_H} + 8600 - 15.6T$

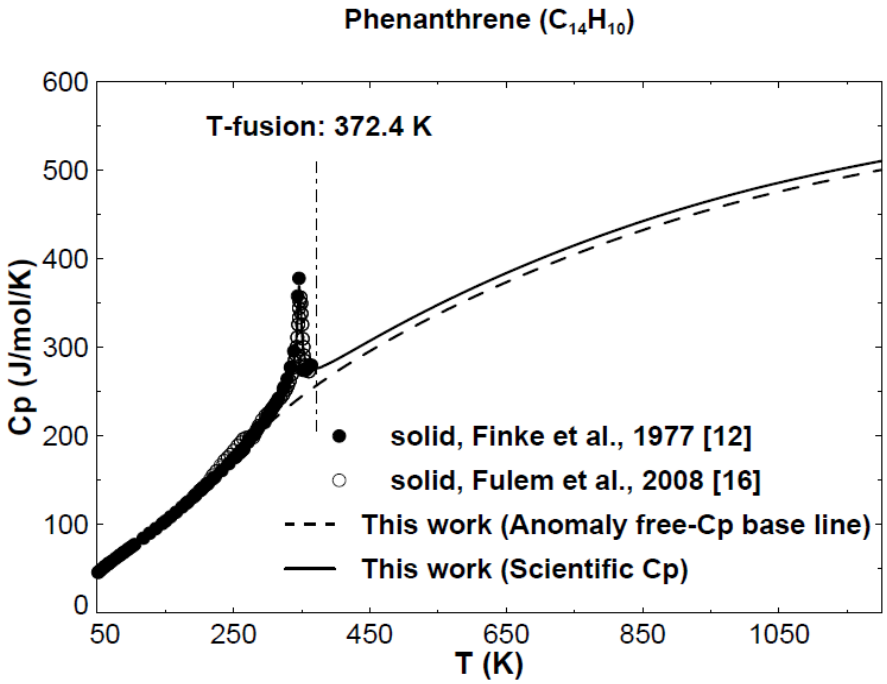

Figure 4.19 Predicted heat capacity of phenanthrene [116, 171].

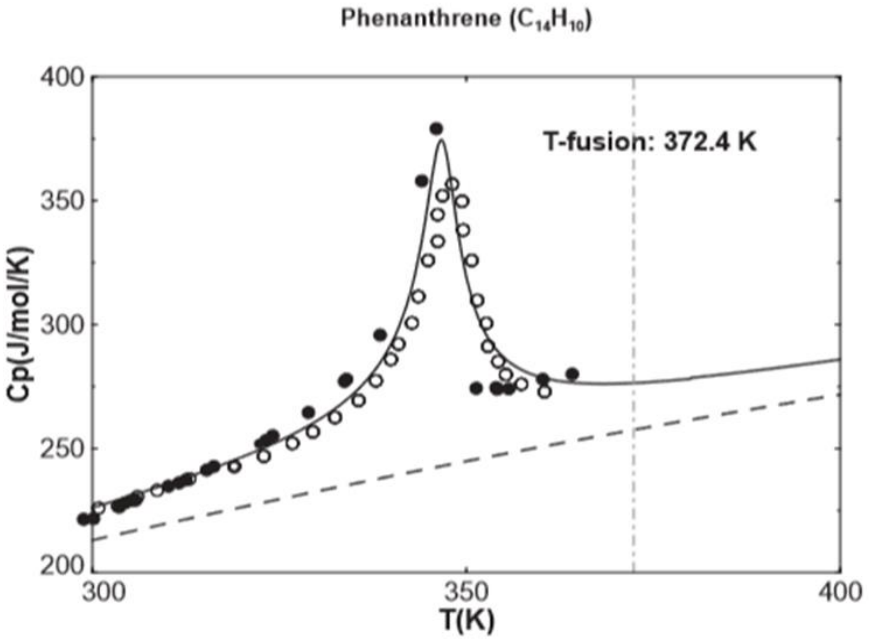

Figure 4.20 Zoom view of solid phase transition region of Fig. 4.19.

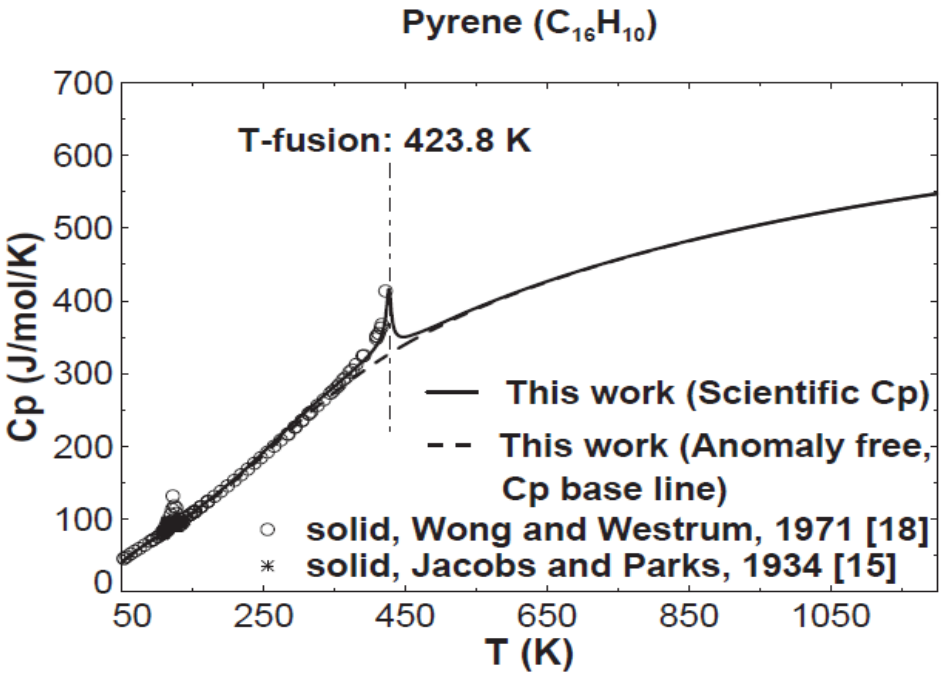

Figure 4.21 Predicted heat capacity of pyrene [96, 109].

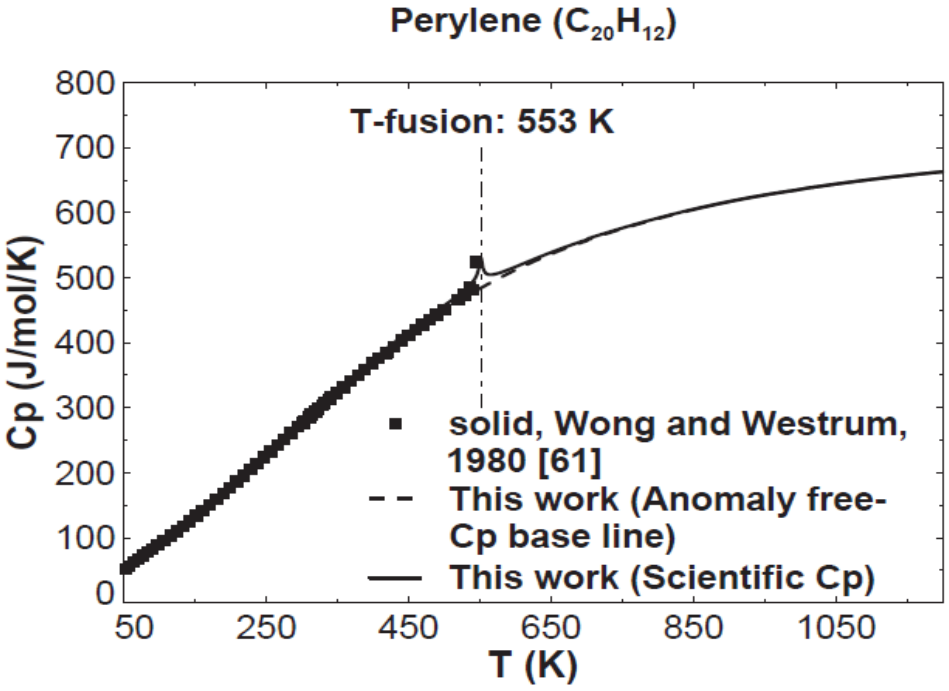

Figure 4.22 Predicted heat capacity of perylene [166].

Predicting the transition temperature of anomalous PAH compounds in solid solutions

According to the X-ray and neutron diffraction patterns reported in the literature [114, 120, 123, 213-215], the crystal structures of PAH compounds studied in this section are similar and are known to form solid solutions [216-219]. Applying the conventional method for fitting the experimental data at the anomalous region of these compounds in pure state cannot be extended to predict the heat capacity function of solid solutions containing anomalous PAH compounds. Nevertheless, the heat capacity function of anomalous PAHs solid solutions can be predicted following the approach proposed in the present work.

The heat capacity of phenanthrene-pyrene solid solution as a function of temperature is estimated by applying the CEF described in Section 4.3. Pyrene and phenanthren both exhibit anomaly behaviors. Therefore, defining two sublattice species for each compounds, before and after phase transition, results in 16 end-members as the basis for the Gibbs energy calculations in the CEF. Subsequently, following the procedure defined in Section 4.3, the heat capacity of the solid solution can be estimated. Fig. 4.23 shows the heat capacity function of a solid solution of 0.33 mole fraction of phenanthre. In fact, the transition temperature of the solid solution varies depending on the molar fraction of PAH compounds. This result is consistent with the investigation of Couvrat et al. [220] for the phenanthrene-Dibenzothiophene solid solution which contains at least one well known PAH compound with an anomalous behavior (i.e. phenanthrene).

Obviously, regarding Eqs. (2.1) and (2.2), changing the heat capacity function of the solid solutions containing PAHs with anomalous behavior in temperature range of the phase transition affects their temperature dependent enthalpy and entropy functions.

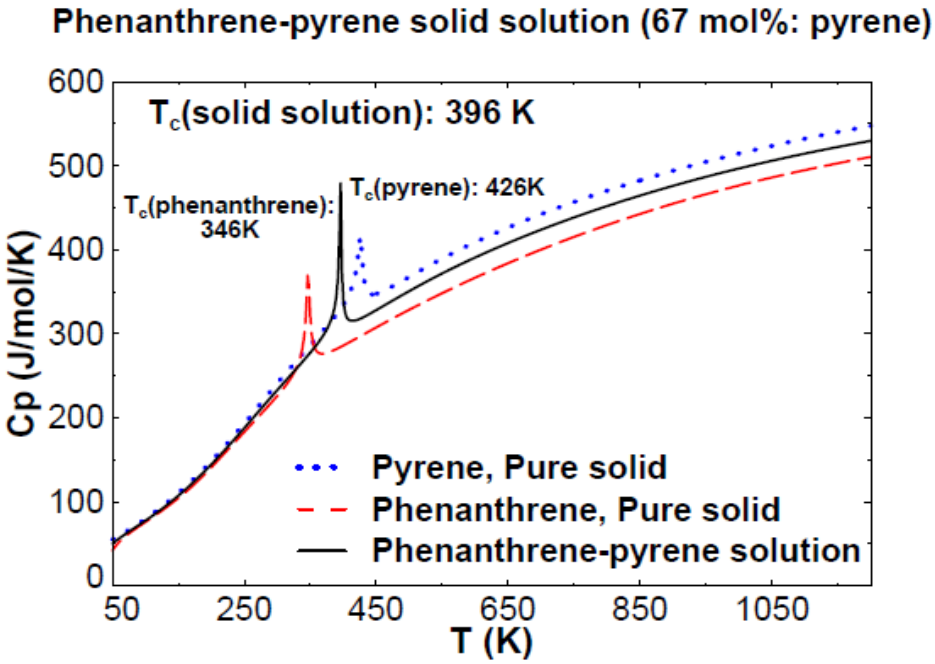

Figure 4.23 Heat capacity of phenanthrene-pyrene solid solution (67 mol%: pyrene).

4.5 Conclusion and outlook

The present thermodynamic approach enables the calculation of the heat capacity function and standard thermodynamic properties of PAH-derived constituents of coal tar pitch and consequently the estimation of their other thermodynamic properties (such as vapor pressure and the Gibbs free energy) which will be required for ongoing studies on coal tar pitch carbonization processes. In fact, in the present work, group contribution algorithms extended by Richard and Helgeson [111] to predict the thermodynamic properties of PAHs are modified by applying the CALPHAD approach to optimize the predicted values in a consistent manner to reconcile phase transition data and computation of vapor pressures. A good agreement was obtained for the model's prediction of PAHs thermodynamic properties, in comparison with experimental data reported in the literature and values derived by other prediction methods. One of the strengths of the proposed model is that

it predicts heat capacity, enthalpy of formation, absolute entropy and vapor pressure of PAHs in the entire temperature range of the carbonization process (25-1200°C) consistent with experimental data, while the previous prediction methods are able to predict these thermodynamic properties only in a specific and narrow range of temperature. A thermodynamic model was also developed for the prediction of anomalous changes of heat capacity for some PAHs exhibiting a phase transition in solid state.

The developed thermodynamic model in the present work will serve as the basis for future work to estimate thermodynamic properties of mixtures containing different PAH compounds and also to predict thermodynamic behavior of carbonaceous mesophase as an intermediate state appearing during coal tar pitch carbonization process. This models enables the extension of a new approach to obtain semi-quantitative knowledge for the thermal, physical and chemical evolutions of coal tar pitch occurring during the carbonization process which can be applied as a useful tool for improving the different aspects of this process such as energy consumption, environmental emissions and cost.

4.6 Acknowledgements

This project was supported by the Natural Sciences and Engineering Research Council of Canada, Alcoa, Hydro Aluminium, Rio Tinto and Constellium.

CHAPTER 5 ARTICLE 2: THERMODYNAMICS AND PHASE RELATIONSHIP OF CARBONACEOUS MESOPHASE APPEARING DURING COAL TAR PITCH CARBONIZATION

Mahnaz Soltani Hosseini, Patrice Chartrand

Published in Fuel volume 275, page 117899, September 1, 2020

Abstract: Carbonaceous mesophase appears as an intermediate product in production of electrical and mechanical carbon materials, needle coke for graphite electrodes used in electric-arc furnaces, pitch-based fibers and aluminum-smelting prebaked electrodes through carbonization process. A thermodynamic approach for phase behavior estimation of carbonaceous mesophase is presented to provide more insights and to lead to semi-quantitative modeling of this process. Phase behavior of binary, ternary and multi-component systems are described by minimization of the Gibbs free energy function proposed by Hu and Hurt for mesophase pitches which exhibits orientational energy contribution of molecules in mesophase. The model enables estimating the reversible phase transition of mesophase upon temperature cycling as suggested by Lewis. The capability of the model to estimate the molecular weight distribution of species in the phases in equilibrium and variation of mesophase content with thermal soaking time has been discussed. Estimated ternary isothermal sections showing isotropic-mesophase and iso- iso immiscibility are presented for the first time. The phase behavior of ternary systems with average molecular weight in the range of average molecular weight of coal tar pitches are described. The application of the model to phase diagram prediction of the specific systems, which exhibit the miscibility gap, has been studied.

5.1 Introduction

Some organic materials exhibit more than a single transition from solid to liquid, thereby necessitating the existence of one or more intermediate phases [24, 127]. Molecular ordering in these intermediate phases, known as “mesophase”, lies between that of a solid and that of an isotropic liquid [24]. As first demonstrated by Brooks and Taylor [23, 78], mesophase is observed during the thermal transformation of pitches and aromatic compounds to coke. When such materials (e.g. naphthalene) are heat treated at temperatures of about 350-450°C for a certain period of time, a bulk liquid-crystalline mesophase from an isotropic liquid phase is formed (Figure. 5.1). The general four-stage conversion of liquid crystals (obtained by polarized light microscopy) during whole process is diagramed as follows: (I) generation of optically anisotropic spheres in isotropic matrix, (II) growth of anisotropic spheres in isotropic matrix, (III) coalescence of anisotropic spheres in isotropic matrix, and (IV) deformation and disintegration of anisotropic coalesced spheres to form bulk liquid-crystalline mesophase [28, 35, 80, 86, 139, 221].

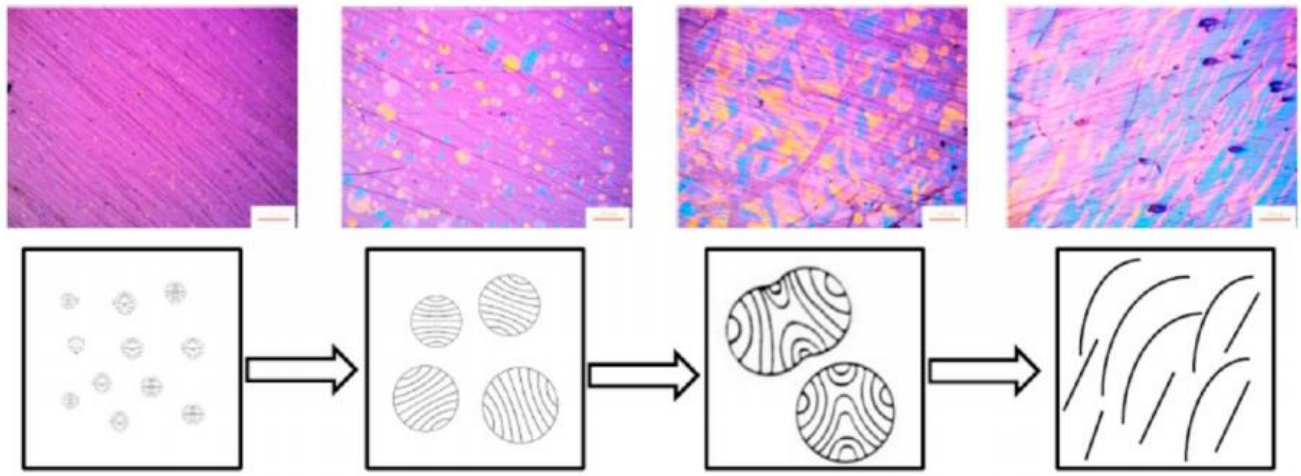

Figure 5.1 Formation and development of bulk liquid crystalline mesophase under a suitable condition (scale bar in PLM micrographs is 100 μm)-permitted from ref. [86].

The important technological role of carbonaceous mesophase in production of carbon-based materials through carbonization process has been well established. There has been a large number of studies on mesophase formation related to the production of various materials ranging from needle coke for graphite electrodes used in electric-arc furnaces [5-8], electrical and mechanical carbon materials widely applied to electric motors brushes, sealing materials, carbon bearing, current collectors [9-15], pitch-based fibers [16-19] to aluminum-smelting prebaked electrodes [20, 21]. However, the study of phase behavior of mesophase in pitch at typical temperature ranges of carbonization is an important step in optimization of the above-mentioned process. It has been studied that carbonaceous mesophase appears as an intermediate product in carbonization process via polymerization of basic compounds in coal tar pitch [28, 35]. The characterization of commercial pitches shows them to be exceedingly complex materials containing from hundreds to thousands of different components, monomers, oligomers and polymers of polycyclic aromatic hydrocarbon compounds (PAHs) with a variety range of molecular weight [3, 4]. So, due to the complex nature of mesophase in pitches, the quantitative treatment of phase equilibrium of the mesophase-containing pitch system is a major challenge and needs some consideration to simplify it into a simple multi-component system with respect to the characterization of the real system. To date there have been two attempts to the quantitative descriptions of the phase transition behavior of mesophase-containing pitches: one by Shishido et al. [126, 129, 130, 137] and one by Hu et al. [125, 127, 128].

Shishido et al. applied the molecular field treatment of mesogen-nonmesogen mixtures to describe a phase diagram for a mesophase pitch [126]. This model does not consider the effect of non-ideal mixing of pitch fractions of differing molecular weights or chemical compositions [222]. Deviations of the estimated phase diagram by Shishido et al. from the experimental result obtained

by Mochida and Korai [131] stimulated the search for a treatment of non-ideal mixing for accurate description of mesophase/isotropic equilibrium. So, Hu and Hurt developed the Gibbs free energy model for mesophase-containing pitches based on non-ideal solution and liquid crystal behaviors of mesophase that includes terms for both excess free energy of mixing and orientational free energy to quantitatively describe the phase behavior of mesophase in pitch [127]. In Hu and Hurt's work, the phase behavior of mesophase pitches was estimated by solving a series of the equations derived from equating the chemical potentials of each components in the phases in equilibrium. A stochastic technique was used to minimize the absolute difference between both sides of these equations. This integrated model has been only applied to three data sets reported in the literature related to carbon science.

The aim of the present work is to propose a new approach to describe the phase diagrams of mesophase-containing pitch. With respect to the difficulties in the chemical potential calculation from the Gibbs energy function, the proposed approach utilizes a robust numerical technique for minimization of total Gibbs free energy function of mesophase. Using the proposed approach, phase behavior of binary, ternary and higher order systems can be estimated which is applicable for optimization of carbonization process as an interest aspect of above mentioned industries. Meanwhile, the new approach enables us to apply the thermodynamic model to predict the thermodynamic behavior of the mesophase-containing pitch exhibiting miscibility gap, with high accuracy.

5.2 Thermodynamic model of carbonaceous mesophase

Carbonaceous mesophase is a discotic nematic liquid crystal phase composed of mostly fully condensed high molecular weight polycyclic aromatic hydrocarbon (PAH) molecules. It has been

suggested that two driving forces could be important for the formation of mesophase: The first is based on the theory that mesophase is a liquid crystal phase, and thus postulates that orientational potential effect is important for mesophase formation. The second is based on non-ideal solution behavior of pitches [125-128]. There is strong evidence for non-ideal solution behavior in pitches. Therefore, it is necessary to utilize the thermodynamic model integrating these two approaches, liquid crystal and non-ideal behavior of mesophase, to predict the thermodynamic behavior of mesophase. The thermodynamic model of Hu and Hurt [127] is used in this work. We will show that different results are obtained by our phase equilibrium calculation approach in section 5.3.

5.2.1 Overview of the general thermodynamic theory

In order to develop a comprehensive thermodynamic model, Gibbs free energy model for isotropic liquid and mesophase must be formulated. Equilibrium configuration of a mesophase-containing pitch system (which appears as an intermediate mixture during heat treatment of coal tar pitch) can be estimated by minimization of Gibbs free energy function proposed by Hu et al. [127] as follows:

$$G = \sum n_i \, g_i^0 + \Delta G_{mix} + G_{orient} \qquad \text{Eq. (5.1)}$$

$$\Delta G_{mix} = \Delta G_{mix}^{ideal} + \Delta G_{mix}^{excess} \qquad \text{Eq. (5.2)}$$

where, G is the Gibbs free energy of the system, g_i^0 are reference molar free energy functions for the pure components as isotropic liquids, ΔG_{mix}^{ideal} is the ideal Gibbs free energy of mixing, ΔG_{mix}^{excess} is the excess Gibbs energy of mixing, G_{orient} is the orientational free energy and n_i are the number of moles of each components in the system[127, 132] . Interfacial and elastic strain energies in Gibbs free energy function can be neglected when one focuses only on macroscopic samples [133, 134].

However, considering G_{chem} as the ideal and the excess energy of mixing terms and G_{orient} as orientational term in Eq. (5.1) as well as the submodels described by Hu and Hurt [127] for the excess Gibbs energy of mixing and the orientational free energy determination of the system, total Gibbs free energy of co-existing phases during the carbonization process can be estimated as follows:

$$G_{chem}= \left[\sum_i n_i\, g_i^0 \;+\; RT \sum_i n_i \ln x_i \;+\; \sum_i n_i\, V_i \;\left(\delta_i - \bar{\delta}\right)^2 \;+\; RT \sum_i n_i \ln\left(\frac{\Phi_i}{x_i}\right)\right] \qquad \text{Eq. (5.3)}$$

$$G_{orient} = -\left[\frac{N_A}{2} \sum_{i,j} n_i x_j \varepsilon_{ij} \bar{P}_{2(i)} \bar{P}_{2(j)} + \; RT \sum_i n_i \ln Z_i \right] \qquad \text{Eq. (5.4)}$$

The Gibbs energy of the isotropic phase is purely chemical as $G^{iso} = G^{iso}_{chem}$, while for mesophase, the orientational contribution term must be taken into account in the Gibbs energy formulation:

$$G^{meso} = G^{meso}_{chem} + G^{meso}_{orient.} \qquad \text{Eq. (5.5)}$$

Here, N_A is Avogadro number, the sums are over all species in the mixture (isotropic liquid or mesophase), i=1, 2… N, V_i is the molar volume and Φ_i is the volume fraction of species i in either isotropic liquid phase or nematic phase. Z_i is the orientational partition function and $\bar{P}_{2(i)}$ is average order parameter for component i in mesophase.

The solubility parameter (δ_i) can be estimated using empirical relation proposed by Hu and Hurt [127]: $\delta_i = \delta_0 + \alpha\,(MW - MW_0)$, where δ_0 and MW_0 are reference values ($\delta_0 = 10\ (cal\ cm^{-3})^{1/2}$, $MW_0 = 250\ g\ mol^{-1}$) chosen from experimental solubility parameters for low MW PAHs (with MW around 250 g/mol) which lies in a narrow range near 10 $(cal\ cm^{-3})^{1/2}$. The factor α becomes

a model parameter that describes the effect of increasing molecular weight. Average of solubility parameter ($\bar{\delta}$) in Eq. (5.3) is defined by Hu [128] as: $\bar{\delta} = \frac{\sum_i n_i \delta_i V_i}{\sum_i n_i V_i}$.

The ε_{ij} term in Eq. (5.4) is a parameter describes the strengths of the pairwise orientation potentials and defines as: $\varepsilon_{ij} = -\sqrt{\tilde{\varepsilon}_{ii}\,\tilde{\varepsilon}_{jj}} \cdot \sqrt{V_i V_j} \,/\, \sum x_k V_k$. Here, the $\tilde{\varepsilon}_{ii}$ term is related to the single component clearing temperatures, T_{cl_i} (in K), by the Maier-Saupe solution [135, 136] as $\tilde{\varepsilon}_{ii}$ = -4.54.k.T_{cl_i}.

The clearing temperature is the temperature upon heating at which liquid crystal reverts to an isotropic liquid. The empirical relation has been proposed by Hu and Hurt [127] to estimate clearing temperatures of each compounds: $T_{cl_i} = a + b\,MW_i$. a and b are constants which can be derived using two known clearance temperatures related to two compounds with different molecular weight [127, 128].

The chemical potential of each species in either isotropic phase or nematic phase is determined as derivation of total Gibbs energy. The difference between chemical potentials derived in this work and those described by Hu et al. [127] will be discussed in section 5.3. For more detail information on the Gibbs energy formulation see the ref. [127].

5.2.2 New approach for phase behavior prediction by Gibbs energy minimization using MADS

Hu et al. predicted the equilibrium configuration of pitch systems by equating the chemical potential of each compounds in the isotropic liquid and mesophase phases in equilibrium derived from the Gibbs free energy function. In this work, the Gibbs energy function is minimized (directly)

to find the composition of the phases in equilibrium. Considering g_i^0s in Eq. (5.3) are the constant values and with respect to the Gibbs energy definition of the isotropic phase and mesophase as above mentioned: G^{iso} and G^{meso}, the number of moles of each species in the co-existing phases are determined by minimization of total Gibbs energy defined in Eq. (5.6):

$$\min_{\underline{n}\in\mathbb{R}^N} \{ G^{iso}\left(\underline{n}^{iso}, T, P_0\right) + G^{meso}\left(\underline{n}^{meso}, T, P_0\right)\} \qquad \text{Eq. (5.6)}$$

where $\underline{n}^{iso} = (n_1^{iso}, n_2^{iso} \dots n_i^{iso} \dots, n_r^{iso})$ and $\underline{n}^{meso} = (n_1^{meso}, n_2^{meso} \dots n_i^{meso} \dots, n_p^{meso})$ represent the vector number of isotropic liquid and mesophase, respectively and r and p are the dimensions of $\underline{n}^{iso}$ and $\underline{n}^{meso}$. $P_0 = 1\ atm$ indicating the pressure of the system. n_i^{iso} and n_i^{meso} are subjected to the constraints: $\sum_{i=1}^{r} n_i^{iso}$=N^{iso} and $\sum_{i=1}^{p} n_i^{meso}$=$N^{meso}$ ($N^{iso}$and N^{meso} being the total number of moles in isotropic liquid and mesophase, respectively).

The minimization problem defined by Eq. (5.6) can, in principle, be solved with a mathematical optimization software exploiting first and second derivatives (Hessians) information or, if no Hessians are provided, using quasi-Newton methods. In the Hu and Hurt formalism, Hessians are difficult to implement from a technical point of view as the orientation Gibbs energy of the mesophase is defined through the second Legendre function (for detail see Section 2.3.4). Failing to provide 1st and 2nd derivatives of the Gibbs energy, in order to solve Eq. (5.6), one must consider utilizing free-derivatives minimization techniques. Instead of considering metaheuristic methods, like Hu and Hurt via the simulated annealing method [223], to approximate the global minimum, we have chosen a free-derivative optimization method, i.e. with a rigorous convergence method.

In particular, we considered the mesh adaptive direct search (MADS) [224]. This choice was motivated by considering several requirements for the solver. In particular, it had to provide default

values for all the algorithmic parameters and handle constraints via a built-in strategy. The MADS algorithm [224] is a direct search method generalizing the coordinate search [225] and the generalized pattern search [226] algorithms. The principle of MADS is basically that at each iteration trial points are generated on a spatial discretization and the functions defining the black-box are evaluated at these locations. Then, depending on the success of these evaluations, the coarseness of the discretization is updated and the new trial points are generated. The convergence analysis in MADS is based on Clarke's calculus for nonsmooth functions [227]. The reliability of MADS algorithm to determine the global and local minima of set of functions with different degree of complexity was demonstrated in references [228-230]. From practical point of view, Nonlinear Optimization with the MADS algorithm (NOMAD) software [231] has been utilized to solve Eq. (5.6) and the exactness of the solution has been approved employing both Latin hypercube sampling (LHS) search and variable neighborhood search (VNS) [228].

To ensure that the global minimum was reached, a rigorous convergence test has been performed and Eq. (5.6) has been solved via MADS for different total calculation times, which are not controlled by NOMAD, via convergence analysis, but imposed by the user. The convergence tests were based on square deviations of both Gibbs energy and mole fraction of phases in equilibrium versus time. The convergence tests are given in Appendix B for 2, 3 and 6 component systems as a function of CPU time (calculation time per one CPU). After a certain CPU time, the global minimum is reached and no improvement in solving of Eq. (5.6) can be found beyond this characteristic time, which indicates the unicity of the solution. The required CPU time (in second) to converge to the global minimum increases exponentially with the size of the system as: $\ln(t_{CPU}) = 0.75N + 4.2$ for N greater than 2.

5.2.2.1 Binary phase diagram calculation

The composition of each phase in equilibrium in a given binary mesophase-containing pitch can be computed by applying the following procedure. At a given temperature, Gibbs free energy of the binary systems with different compositions (from pure component 1 to pure component 2) is calculated using Eqs. defined in section 5.2.1 and built in MATLAB software [232]. Drawing of obtained Gibbs free energy values versus composition help us to have an idea of equilibrium configuration of the system at the given temperature. To find the composition of the phases in the equilibrium in the binary mesophase –containing pitch with a specified composition, the procedure defined in section 5.2.2 is applied. Temperature and the global composition of the pitch are the independent variables, which are considered as the entered values in MATLAB and NOMAD programs. The number of phases in equilibrium as well as the composition of each phase are estimated as the outcome of the programs. It distinguished that the entered global composition will be considered as the composition of either isotropic liquid phase or mesophase when it is in one-phase region of the Gibbs free energy vs composition curve. In the case of two-phase system, the composition of each phases in equilibrium are determined as the variables in Eq. (5.6).

5.2.2.2 Phase behavior prediction of ternary and multi-component pitch systems

The equilibrium configuration of a ternary mesophase-containing system can be determined as follows. At first, three binary systems are defined with two components from three components of a specified ternary system. In a given temperature, the composition of the phases in equilibrium for three binary systems is determined based on the procedure explained in section 5.2.2.1.

Finally, the procedure defined for binary phase diagram is applied to find the composition of the phases in equilibrium of different solutions in the ternary system in the given temperature.

This procedure is applicable to predict the partition ratios of molecules in the phases in equilibrium of heat- treated multi-component pitch systems.

5.3 Results and discussion

The general thermodynamic theory explained in section 5.2.1 and the Gibbs energy minimization approach defined in section 5.2.2 were applied to different mesophase-containing pitch systems. For binary system, visual observations of phase behavior in naphthalene pitch from hot stage microscope experiments of Lewis [28] was modeled and compared with calculated phase diagram by Hu et al. [127]. Predicted binary phase diagram was able to estimate the variation of mesophase content of pitch with thermal soaking time which was consistent with experimental data reported by Kumar et al. [12]. For ternary system, a three component system containing typical low, medium and high molecular weight compounds available in coal tar pitch analyzed by Zhang et al. [21] was studied. The molecular weight distribution (MWD) in the coexisting meso and isotropic phases in petroleum pitch data of Greinke and Singer (determined by GPC) [87] was modeled to investigate the application of the model for phase behavior prediction of multi-component pitch system. In all the systems studied, the equilibrium calculations using the model equations for mesophase-containing pitch systems were performed with the MATLAB and NOMAD software [231, 232]. The strength of the proposed approach in thermodynamic behavior prediction of two or three available phases in equilibrium will be presented in section 5.3.2.

5.3.1 Prediction of binary phase diagram describing the behavior observed in the hot stage experiments by Lewis

Lewis presents a series of photomicrographs for the mesophase-containing naphthalene pitch as it was being heated and then cooled on the hot-stage [28]. The results indicate that mesophase formation is reversible for a few cycle of heating and cooling. However, ongoing thermal reactions gradually eliminate its reversible behavior [233-235].

Figure 5.2 shows the binary phase diagram of naphthalene pitch (studied by Lewis) predicted in the present work using the defined thermodynamic model and numerical approach in section 5.2. The following parameters (as used by Hu et al. [127]) are used to generate the phase behavior observed by Lewis [28]: MW_1= 600 g mol^{-1} MW_2 = 1400 g mol^{-1}, T_{cl_1}= 300 K, T_{cl_2}= 890 K, α = 0.0024 (cal.cc^{-1})$^{1/2}$ / (g mol^{-1}). MW and T_{cl} are the molecular weight and the clearing temperature of the lowest and the highest compounds found in naphthalene pitch, respectively and α is solubility parameter.

Observation of Lewis [28] for phase transition of naphthalene pitch when heated from about 650-770 K is predictable in obtained phase diagram by following any dotted line in gray shaded region in Figure 5.2. The mesophase in pitch gradually is converted to isotropic phase during heating and reappeared upon cooling.

According to the phase diagram shown in Figure 5.2, reappearance of small isotropic spherules in mesophase occur at the temperature which is a much lower temperature than the isotropic conversion of the mesophase. This result has agreement with that has been previously noted by Lewis [236].

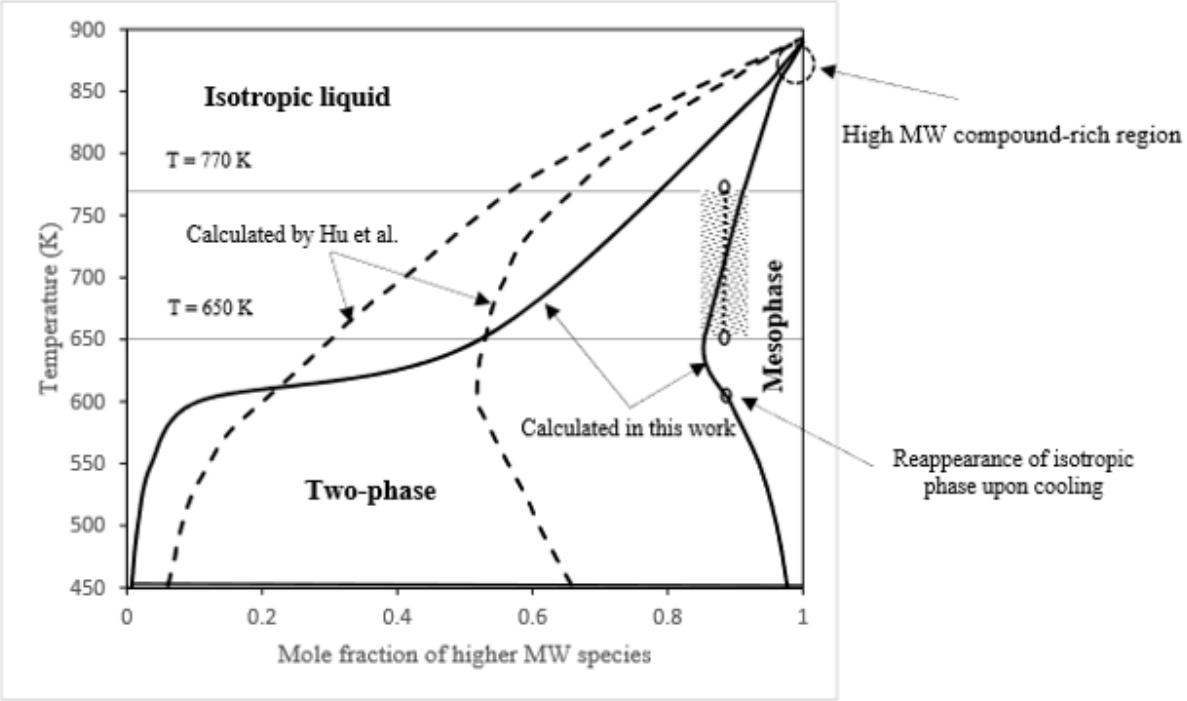

Figure 5.2 Calculated binary phase diagram of naphthalene pitch observed in hot stage microscope experiments of Lewis [28].

The big difference between the calculations in the present work and those by Hu et al., seen in Figure 5.2, can be explained as follows:

Hu and Hurt estimated the phase diagram by solving a series of equations derived from equating the chemical potentials of each species in each phases in equilibrium and considering the mass balance and the constraints defined in Eqs. (5.17) - (5.19) in ref. [127].

Derivation of Gibbs free energy of the system and equating the chemical potential of each species in the phases in equilibrium (Appendix C) results in a new equation (Eq. (5.7) replacing of Eq. (17) in ref. [127]) where $\frac{V_i}{V}$ in summation term appeared only when k ≠ j:

$$\left[\ln x_i + \ln\left(\frac{V_i}{V}\right) - \frac{V_i}{V} + \frac{V_i}{RT}\left(\delta_i - \bar{\delta}\right)^2\right]^{iso} = \left[\ln x_i + \ln\left(\frac{V_i}{V}\right) - \frac{V_i}{V} + \frac{V_i}{RT}\left(\delta_i - \bar{\delta}\right)^2\right]^{meso} -$$

$$\left[\ln(Z_i) + \frac{1}{2kT}\left(\sum_{k\neq j} x_k x_j \varepsilon_{kj} \bar{P}_k \bar{P}_j \frac{V_i}{V} + \sum_{k=j} x_k x_j \varepsilon_{kj} \bar{P}_k \bar{P}_j\right)\right]^{meso} \quad \text{Eq. (5.7)}$$

Obviously, applying Eq. (5.7) in phase equilibrium calculations instead of Eq. (17) in Hu's work results in different phase diagram. In this work, the Gibbs energy minimization approach (defined in section 5.2.2) was applied for phase behavior estimation instead of equating of chemical potential approach proposed by Hu et al. which is difficult to implement for phase diagram calculation of multi-component systems. Satisfying the Eq. (5.7) by the results obtained from the new approach indicates that one can be confident of the results. It should be noted that re-producing of the results presented in Figure 5.2 as Hu's results could not possible because of lack of data for orientational partition and second Legendre of the species in nematic phase in references [127, 128].

Figure 5.3 is a zoom view of the high MW compound-rich region of Figure 5.2. The calculated compositions of the phases in equilibrium for the binary system at temperature close to clearing temperature of the higher MW specie (shown in Figure 5.3) has been presented in Table 5.1. It is concluded (from the data of Table 5.1) that the applied method in this work has the ability to compute the equilibrium conditions without numerical failure for the binary system very close to pure state. In other words, Table 5.1 shows how the mole fraction of the higher MW specie in the phases in equilibrium at temperature very close to 890 K, gradually reaches to 1.

Table 5.1 Calculated composition of the phases in equilibrium of the binary system shown in Figure 5.3.

Temperature (K)	**Mole fraction higher MW species**	
	Mesophase	Isotropic liquid
889.000	0.999177392	0.998827466
889.500	0.999721547	0.999602823
889.600	0.999830244	0.999757873
889.700	0.999937281	0.999910628
889.756	0.999999905	0.999999864

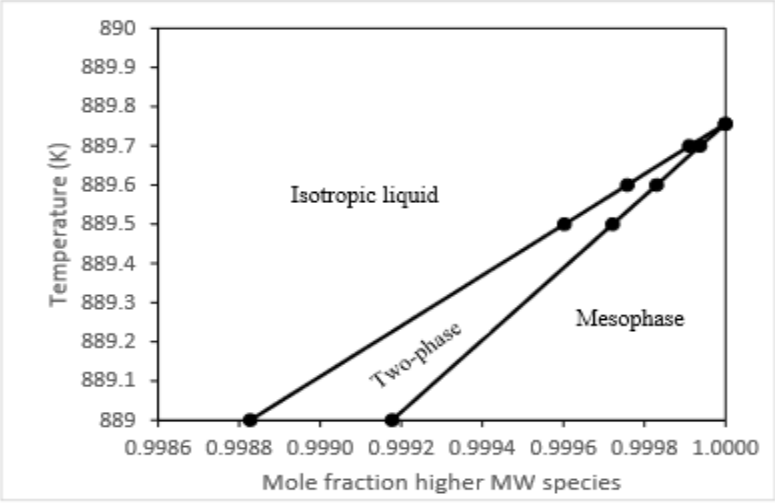

Figure 5.3 Zoom view of the high MW compound-rich region of Figure 5.2.

5.3.2 Prediction of mesophase content with varying thermal soaking time

Polarized light optical microscopy is the technique most commonly employed (ASTM D 4616 standard procedure) to measure the mesophase content of pitches [237]. Kumar et al. [12] utilized this technique to determine the mesophase content of different pitch samples heat treated at 380°C with different thermal soaking time. The results indicates that as thermal soaking time increased the mesophase content of the pitches also increased.

The fraction of mesophase of a specific pitch at a given temperature can be estimated by applying the lever rule in binary phase diagram predicted in this work (see Figure 5.2). As thermal soaking time increases , the growth of aromatic molecules takes place due to the greater extent of polymerization condensation reactions [235, 238]. Obviously, it is concluded from Figure 5.2 that the mesophase content of pitch increases as the heat treatment of the pitch progresses by the time at 380°C. This result is consistent with that obtained by Kumar et al. [12].

5.3.3 Application to ternary phase diagram prediction

The semi-quantitative treatment of phase equilibrium of mesophase pitches as the intermediate appearing in coal tar pitch carbonization process is strongly desired for improving the capabilities of the modeling of whole carbonization process. The characterization of commercial pitches shows them to be exceedingly complex materials containing from hundreds to thousands of different components, monomers, oligomers and polymers of polycyclic aromatic hydrocarbon compounds (PAHs) with a variety range of molecular weight [1, 3, 4, 21]. In order to construct a computational tool to compute and study the phase equilibrium in the pitch, such a complex system has to be simplified. the mesophase-containing pitch system can be simplified as a ternary system containing

the typical low, medium and high molecular weight compounds in the range of MW distribution analyzed and reported by Zhang et al. [21]. In this way, the phase behavior of the system can be shown and illustrated on a triangle, graphically (which is not possible for higher order systems) to help initial thermodynamic understanding of carbonization process. Consistency between estimated phase behavior of simplified system (including 2 or 3 components) and the experimental data will be a confirmation that the technique is applicable for thermodynamic behavior prediction of the higher order mesophase-containg pitches (as will be presented in section 5.3.5).

So, the phase diagram prediction of the ternary mesophase pitch systems can be considered as a research interest in the optimization of coal tar pitch carbonization process. A mesophase-containing pitch system consisting of three compounds with different molecular weights as 500, 1200 and 1600 g mol^{-1} was studied in this work at different temperatures using the approach explained in section 5.2.2.2. The criteria for the molecular weight selection has been based on the molecular weight distribution of mesophase pitch (ranging from 500 to 1800 g mol^{-1}) investigated by Greinke utilizing gel permission chromatography (GPC) [87]. Regarding to Greinke's investigation and the proposed model in Hu and Hurt's work [127], the mesophase pitch system can be defined with respect to size (MW) of the constituent compounds which appears as an important parameter, e.g. T_{cl} , in the thermodynamic model (where clearing temperature represents the property of megenic molecules).However, the model has no consideration for the existence of the hydrogen donor molecules in the mesophase pitch. The improvement can be made by taking into account other parameters, affected by the property of these molecules, in the model as future works.

All the phase diagrams in this section generated using the parameters as follows:

MW_A = 500 g mol^{-1}, MW_B = 1200 g mol^{-1}, MW_C = 1600 g mol^{-1}, $T_{cl_i}(\mathrm{K}) = 373 + (685 - 373)\frac{(MW_i - 400)}{(1000-400)}$ [127] and α = 0.0024 (cal.cc^{-1})$^{1/2}$/ (g mol^{-1}).

Figures. 5.4 and 5.5 show the phase diagrams of the ternary system at 600 K and 700 K. In these cases, three equilibrium zones can be distinguished labeled as "isotropic liquid", "mesophase" and "iso-meso" which are two one-phase and one two-phase regions, respectively.

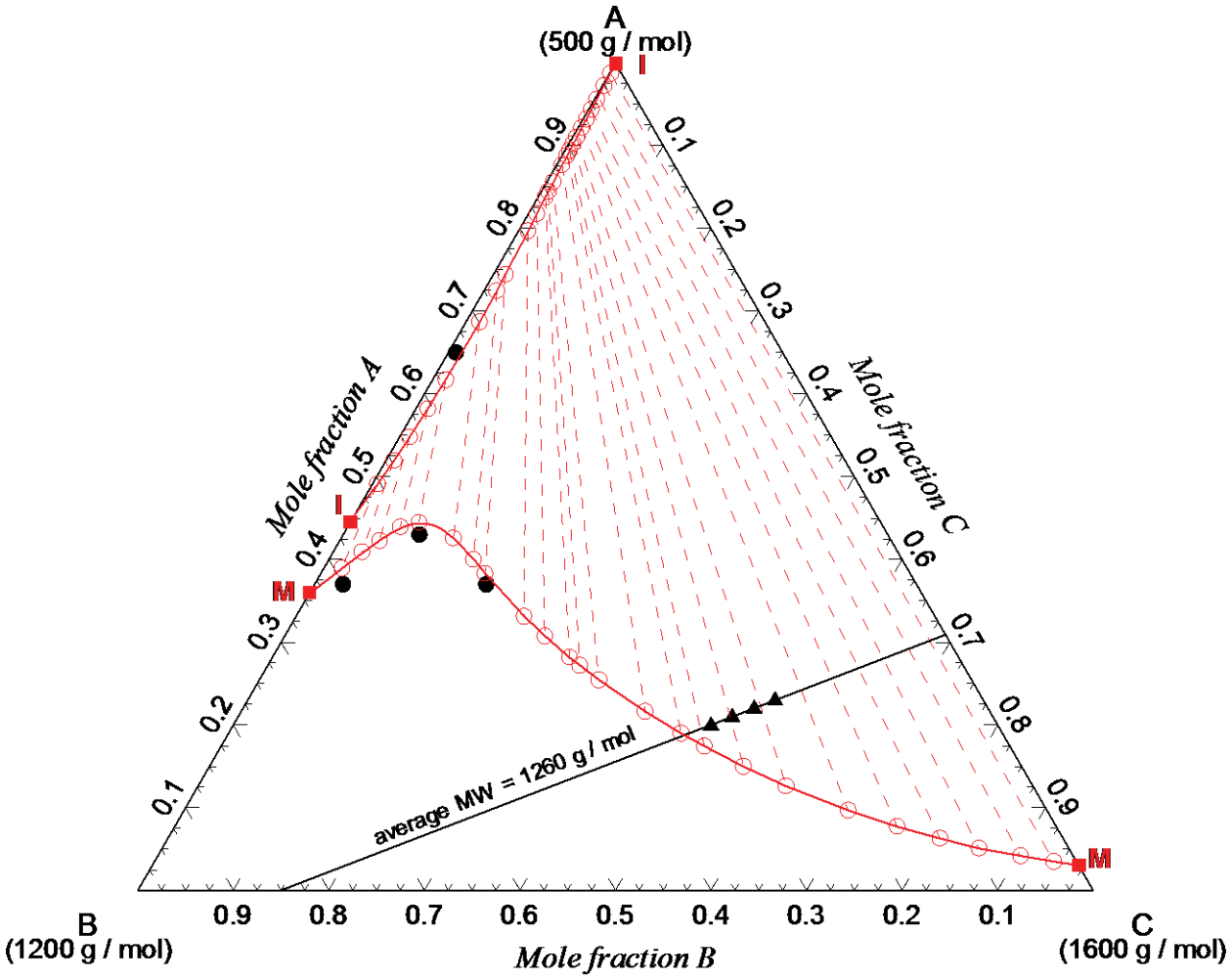

Figure 5.4 Calculated ternary phase diagram at 600 K.

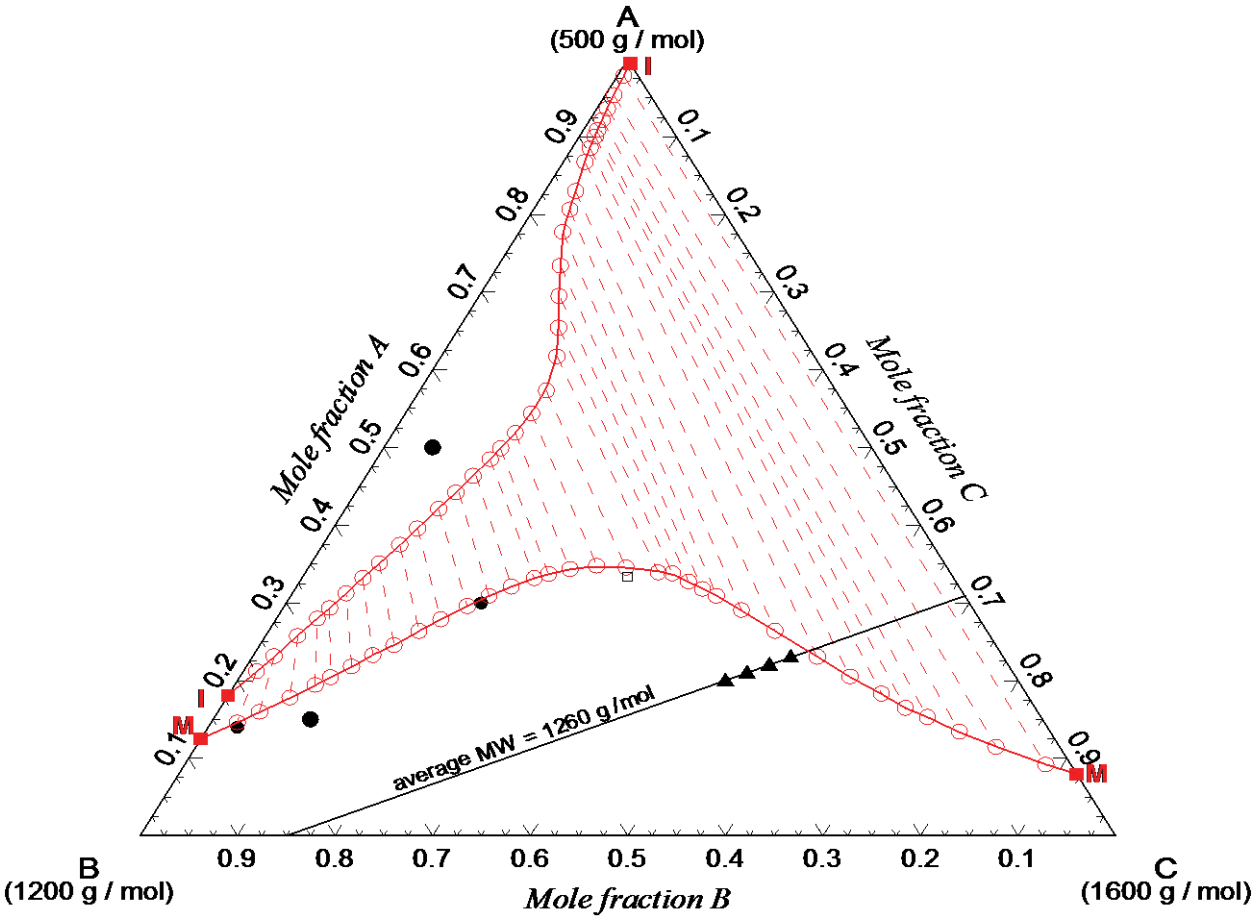

Figure 5.5 Calculated ternary phase diagram at 700 K.

In these figures, filled circles show one-phase regions. The tie –lines in two-phase regions (dotted lines in the figure) represent the composition of the phases in the equilibrium (shown as empty circles) which have been calculated following the method presented in section 5.2.2.2.

The phase diagram calculation, presented in Figure 5.6, was performed for the same ternary system at 800 K. Calculating and drawing the Gibbs free energy of three binary systems generated with two of three compounds enables us to determine the equilibrium configuration of the system when there is more than one two- phase region. Figure 5.7 shows the calculated Gibbs free energy of the binary system consists of the compounds with molecular weights 500 and 1600 versus composition

at 800 K. It is predicted that there is a miscibility gap in isotropic liquid phase which results in ternary phase diagram shown in Figure 5.6. There are four equilibrium regions named “isotropic liquid”, “mesophase”, “iso-meso” and “iso-iso” in Figure 5.6 which are two one-phase and two two-phase regions, respectively.

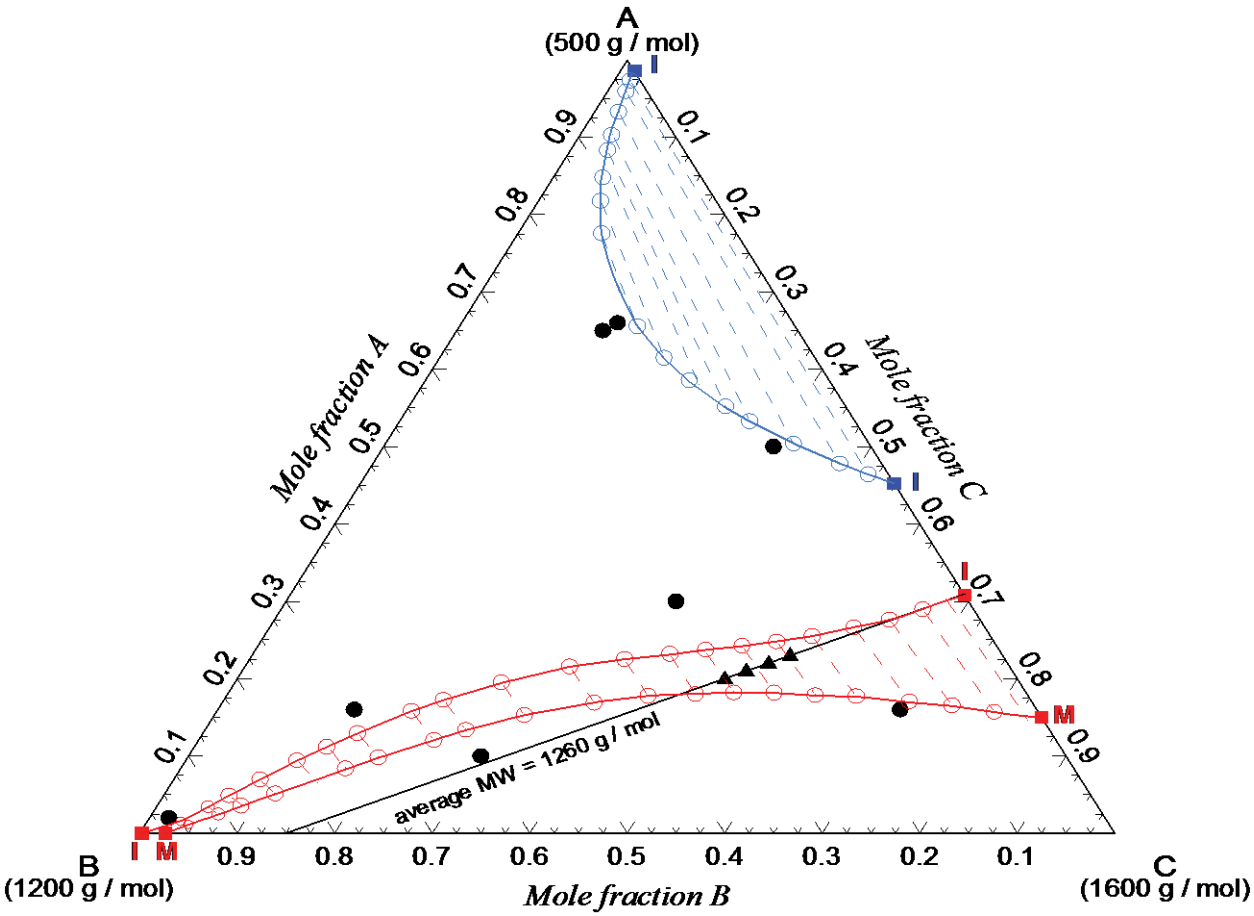

Figure 5.6 Calculated ternary phase diagram at 800 K.

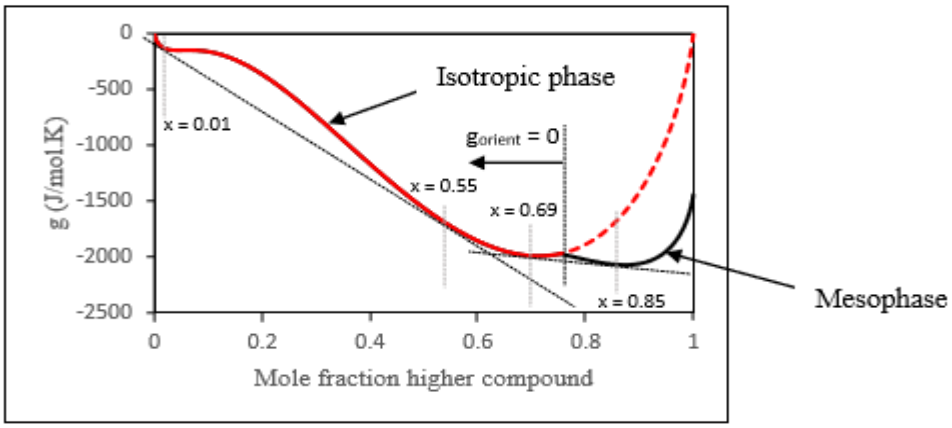

Figure 5.7 Calculated Gibbs energy of binary system (MW_1 = 500 g mol^{-1}, MW_2 = 1600 g mol^{-1}) at 800 K.

As seen in Figure 5.5, a mixture with equal amounts of A, B and C components (seen as □) at 700 K forms mesophase. So, as conclusion, a mixture containing comparable amounts of the lowest and the highest molecular weight compounds in the system (in this case, 500 and 1600 g mol^{-1}) can be appeared as mesophase, completely.

As shown in the isothermal ternary phase diagrams in Figures 5.4-5.6 and 5.8, the two-phase region is extended as the temperature of the system is decreased.

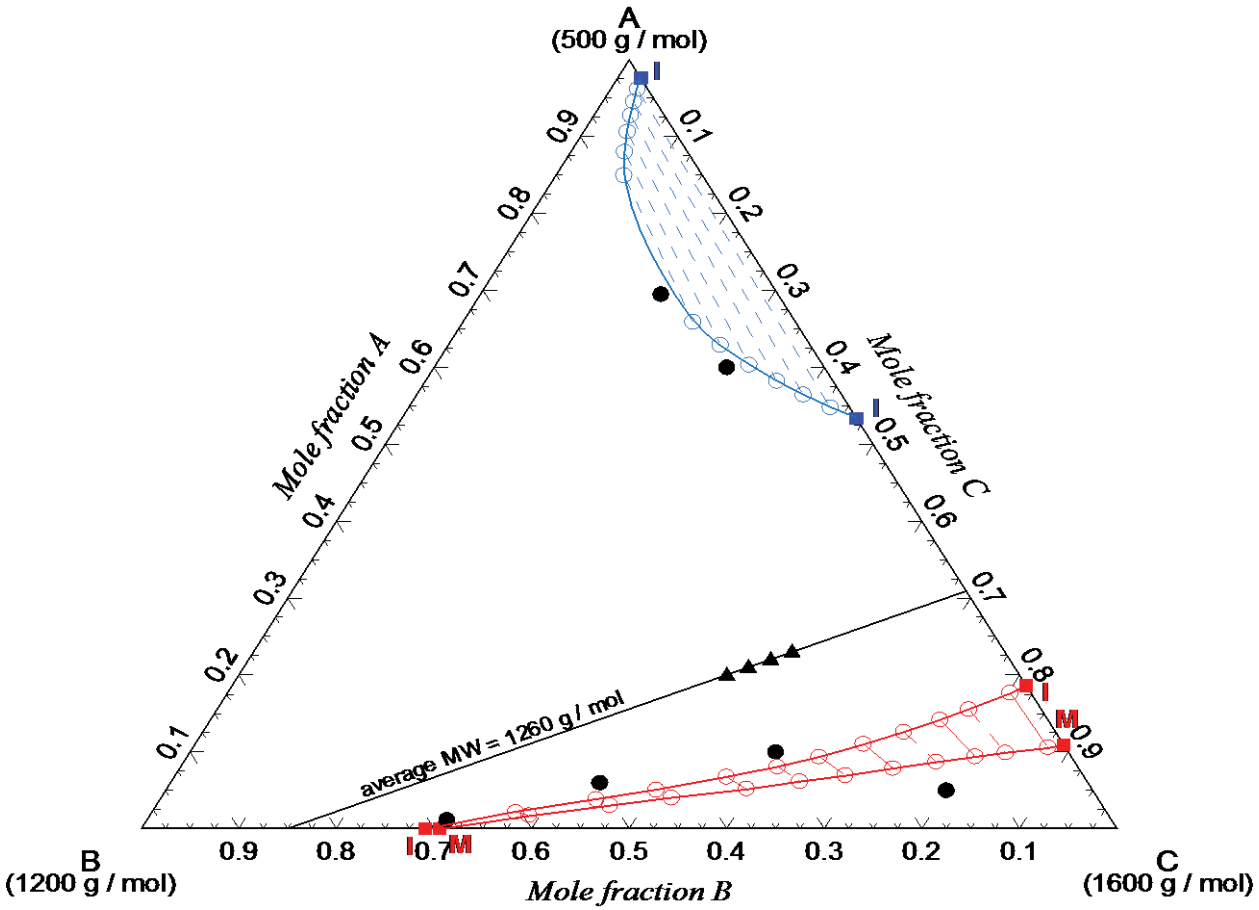

Figure 5.8 Calculated ternary phase diagram at 870 K.

5.3.4 Application of ternary phase diagram to phase behavior observation of Lewis

The phase behavior of the mixtures with different compositions including the considerable amount of the lowest molecular weight compound which have the same average molecular weight in the range of the average molecular weight of the pitches was studied by applying isothermal ternary phase diagrams predicted in section 5.3.2.

Following the mixtures with different compositions seen as filled triangles in Figures 5.5, 5.6 and 5.8 on the constant average molecular weight (1260 g mol^{-1}) line shows the conversion of the

mesophase in pitch to isotropic liquid during heating and reappearing of that upon cooling. It has agreement with the phase behavior that Lewis observed for phase transition of naphthalene pitch.

Reappearance of isotropic liquid phase in mesophase at 600 K, by following the filled triangles in Figure 5.4, is an approve of the reversible phase transition effect observed in many pitches and suggested by Lewis [236].

5.3.5 Application to petroleum pitch data of Greinke and Singer

The model is applied to predict the molecular constitutions of the coexisting anisotropic and isotropic phases of a heat treated petroleum pitch obtained by Greinke and Singer [89]. Clearing temperatures of compounds in the system are calculated based on clearing temperatures of compounds with molecular weights 400 and 1000 defined in Hu and Hurt paper: 373 K and 685 K, respectively [127].

Following the procedure defined in Section 5.2.2, number of moles of the compounds in the phases in equilibrium (i.e. mesophase and isotropic liquid) are estimated by minimization of the Gibbs energy of the system. Using the results obtained, the ratio of mass of each compound in isotropic liquid phase to that in mesophase are then calculated. Figure 5.9 shows a good agreement between the data for molecular weight distribution in the phases in equilibrium of the heat treated petroleum pitch derived by Greinke and Singer [89] and that predicted in the present work. Replacing of Eq. (17) in Hu's work by Eq. (5.7) in this work as well as utilizing precise numerical technique in Gibbs free energy minimization approach results in the phase behavior estimations with less deviations from experimental data comparing to those presented by Hu et al. [127].

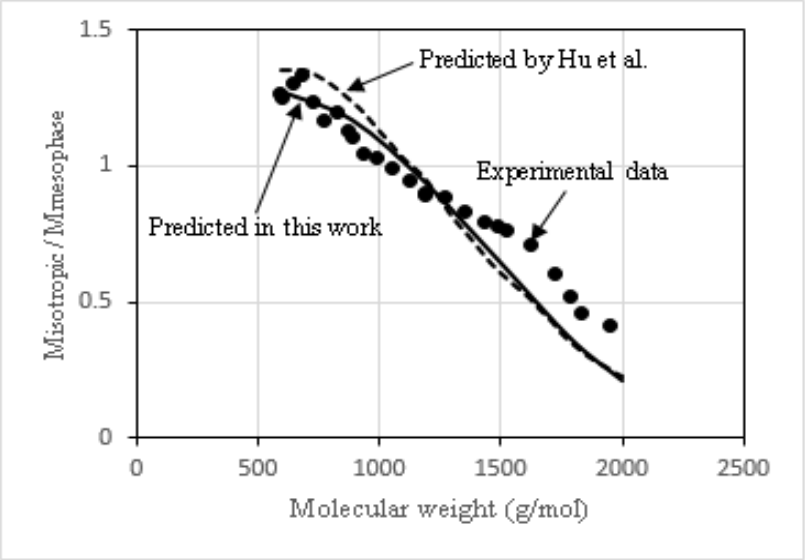

Figure 5.9 Partition ratios of molecules in the coexisting phases in a heat treated petroleum pitch. Points: experimental data obtained by Greinke and Singer [89]; dotted line: predicted by Hu [127]; solid line: predictions in this work. $T_{cl_i} = 373 + (685 - 373)\frac{(MW_i - 400)}{(1000-400)}$ (K) and α = 0.00183 $(cal.cc^{-1})^{1/2}/(g\ mol^{-1})$.

Clearly, it is interpreted from this figure that the mesophase contains significantly more of the higher molecular weight species than the isotropic phase. This result is consistence with that obtained by supercritical fractionation (experiment and prediction) by Burgess, Zhuang and Thies [222, 239, 240].

5.4 Conclusion and outlook

The phase behavior of the mesophase-containing pitch, which has an important role in optimization of coal tar pitch carbonization process, can be estimated by applying the present thermodynamic approach. The binary and ternary phase diagrams of mesophase-containing pitches reproduced the reversible phase transition observed in the hot stage microscope experiments of Lewis [28]. A

strength of the current work is that it predicted phase diagrams of mesophase pitches up to temperature very close to clearing temperature.

Estimation of mesophase content of the pitches with varying thermal soaking time is consistence with that experimentally determined by utilizing polarized light optical microscopy technique [12, 237]. The thermodynamic approach and the new proposed MADS minimization technique can be utilized easily, for the phase behavior estimation of ternary system as the simplified system of coal tar pitch containing hundreds to thousands compounds. Interpretation of theses isothermal ternary phase diagrams simplifies the phase behavior prediction of mesophase-containing pitches. Meanwhile, the miscibility gap appearing in the phase diagram of the specific systems is predictable using the proposed approach. The model is applicable to estimations of the partition ratios of molecules in the co-existing phases in equilibrium in heat treated multi-component pitch consistent with experimental data and those predicted previously.

The present thermodynamic approach as a useful calculating tool will serve for future work to predict, quantitatively, the thermal, physical and chemical evolutions of coal tar pitch occurring in carbonization process which has important effect on energy consumption, environmental emission and cost of the process.

5.5 Acknowledgements

We would like to thank Dr. Aïmen E. Gheribi for his advice in this paper. This project was supported by the Natural Sciences and Engineering Research Council of Canada - Canada, Alcoa – United States, Hydro Aluminium - Norway, Rio Tinto - Canada and Constellium - France.

CHAPTER 6 ARTICLE 3: MODELING THE COAL TAR PITCH PRIMARY CARBONIZATION PROCESS

Mahnaz Soltani Hosseini, Patrice Chartrand

Submitted to Fuel, December 15, 2020

Abstract: The properties of the carbon materials as the final product of pitch carbonization process are a consequence of the type and extent of the chemical and physical phenomena occurring under the process conditions. A new simplified approach for thermodynamic-kinetic modeling of the primary carbonization process is presented to provide the semi-quantitative knowledge about the process. The proposed approach is based on defining thermodynamic and kinetic equations for both vaporization and condensation processes simply representing numerous complicated phenomena happening during primary carbonization process. Partial pressures of the emitted volatile compound in a simple pitch system containing typical components of coal tar pitch has been studied. The model enables estimating the mass and enthalpy changes of coal tar pitch which goes under thermal treatment. Good agreement has been obtained between calculated mass losses during heat treatment (up to 550°C) of coal tar pitch and experimental data. The model has been applied to describe molecular weight distribution changes of coal tar pitch through the primary carbonization as investigated by Greinke. The effect of important parameters in carbonization of pitch, such as heating rate of pitch and carrier gas flow rate, on emission rate of volatile matters has been modeled for the first time. The present model is capable to estimate the energy requirement for thermal treatment of coal tar pitch up to 350°C.

6.1 Introduction

Pitches are of great interest as precursors for the manufacture of carbon materials (CM) having different properties and applications [241-245]. CMs are widely applied to produce graphite electrodes used in electric-arc furnaces [5-8], electric motors brushes, sealing materials, carbon bearing, current collectors [9-15], pitch-based fibers [16-19], aluminum-smelting prebaked electrodes [20, 21] and others. In the processes to prepare CM from pitches, carbonization via thermal treatment plays a fundamental role to determine the properties of the resultant CM [242, 243].

Commercial pitches are exceedingly complex materials containing from hundreds to thousands of different components, monomers, oligomers and polymers of polycyclic aromatic hydrocarbon (PAH) and heterocyclic compounds, with a variety range of molecular weight [3, 4]. During carbonization, pitch goes under physical and chemical changes and converted to infusible coke [3]. The smaller, more volatile compounds in pitch distil, raising the average molecular weight and the viscosity of the solid residue. Physical distillation is accompanied by thermal oligomerization of the more reactive residual species and the cracking of substituent side chains from aromatic rings. Further irreversible polymerization and dehydrogenation processes occur with additional heat treatment which results in a continual growth in aromatic molecular size. Release of gaseous hydrogen and methane also takes place throughout the carbonization process, being dominant gaseous products in the 500°C-1100°C range [3, 61, 246].

Precautions must be taken during industrial production of CM from pitches to maintain or improve the final product quality while minimizing the energy consumption, gas emissions and cost [32]. Current knowledge of the carbonization process is qualitative in most aspects [247]. A deeper

understanding of the vaporization and polymerization reactions occurring during carbonization process to evaluate the carbonization process, quantitatively, will improve the CM production processes and allow the development of new pitch-based materials [243].

The aim of the present work is to propose a new approach to describe and to model physical and chemical changes occurring during primary carbonization of coal tar pitch (CTP). The developed model can provide the semi-quantitative knowledge required for the estimation of mass and enthalpy changes occuring during CTP carbonization as well as the amount and composition of the released gases. Estimation of such quantities would be useful for process optimization for the above-mentioned industries. Due to complexity of the process, our proposed approach is based on using prototypes reactants and reactions that can represent the most important internal phenomena happening through the primary carbonization process and by reducing to the minimum the required time-dependent variables (such as considering only a heating rate). The important target variables studied in the present work are the mass of the residue pitch and the composition and heating value of volatile species.

The proposed model has to be calibrated using available experimental data indicating mass and molecular weight distribution changes of CTP occurring during heat treatment process. Few experimental data are available in the literature, and we took the experimental data set of Bouchard et al. [246] where mass loss of volatile maters during CTP carbonization has been presented in the thesis, coupled with molecular weight distribution changes during primary carbonization of CTP from Greinke [87] in order to perform the required calibration. So, in the present work, Bouchard's data will be utilized for calibration of the model with the expectation that the proposed approach

will be versatile enough to be applied to other set of experimental data in future works. The present work is also neglecting the role of impurities such as sulfur, nitrogen and oxygen.

6.2 Thermodynamic-kinetic modeling of coal tar pitch heat treatment process during primary carbonization

Coal tar pitches (CTP) comprise complex mixtures of polycyclic aromatic hydrocarbon (PAH) and heterocyclic compounds, which composition will be evolving during carbonization through volatilization and chemical reactions, such as polymerization and oligomerization. A number of investigations on CTP carbonization have pointed out that it can be considered as divided in two types of processes [3, 50, 248, 249]. The first process involves the removal of light PAHs from the pitch and a slight polymerization of PAH compounds and thermal cracking reactions, and the second process involves the condensation of aromatic rings giving rise to polyaromatic compounds of higher molecular mass [243] which is accompanied by evaporation of low MW PAHs. Hydrogen is removed largely in the form of H_2 and CH_4 throughout the whole process.

Considering both processes through mass balance, thermodynamic and kinetic equations can provide a semi-quantitative description useful for the simulation and optimization of primary carbonization processes to obtain CM with good properties while keeping the energy consumption, environmental emissions and costs to acceptable values. Due to the complex nature of pitches and the complicated different physical and chemical changes happening through carbonization process, the challenge is to simplify the modeling approach by a careful selection of constitutive species while keeping it representative of the major characteristics of the system.

6.2.1 Overview of general steps of primary carbonization process

Primary carbonization has been extensively reviewed starting with Franklin [54, 55] as the pioneer in these studies followed by the review works of Oberlin and Bonnamy [37, 51, 52, 56]. Primary carbonization refers to transformation of an initial precursor carbon to mesophase and ultimately a brittle solid state materials, semi-coke and reaches its penultimate stage at approximately 400 - 600°C (the exact temperature of completion depending on the precursor composition and other factors) [59]. Mesophase and semi-coke are the intermediate discotic nematic liquid crystals and solid phases, appearing after the softening and distillation of the starting CTP materials (as the initial precursor carbon) at around 350°C. They are composed of mostly fully condensed high molecular weight polycyclic aromatic hydrocarbon (PAH) molecules. The formation of mesophase permits the spatial rearrangement of the molecules favoring oligomerization and polymerization needed for semi-coke formation.

In order to develop a semi-quantitative model of internal phenomena occurring during primary carbonization, the general steps describing the major observed changes must be defined.

The numerous molecular components of CTP vary extensively in terms of their tendency to form a mesophase. Namely, it can be regarded as relatively large and disc-like molecules corresponding to mesogen molecules with tendency to liquid crystal formation and small or non-disc-like molecules to non-mesogen molecules [126, 250].

As the heat treatment temperature of CTP reaches the mesophase and semi-coke formation temperature (350 - 500°C), both distillation and thermal cracking mechanisms tends to operate in such a manner as to remove the lower molecular weight molecules of the precursor prior to mesophase formation [56, 250, 251]. The removal of these volatile components resulting in a pitch

solution rich in mesogen molecules appears to be a key factor controlling both the conversion to mesophase and subsequently semi-coke and the time required for the first appearance of mesophase nuclei [23, 250]. This nucleation and growth of the mesophase is generally thought to be a result of thermal polymerization reactions of more reactive residual species which tend to build up the higher molecular weight compounds in such a manner as to satisfy the average molecular structural requirements for liquid crystal formation [3, 252].

The kinetics of pitch polymerization during mesophase formation has been studied using gel permission chromatography (GPC) by Greinke [87]. According to Greinke's investigations, when mesophase is forming in the pitch, molecules in the MW range of 300-700 are the most reactive. Rate constant studies indicate a nearly constant reactivity of the all these molecules in this molecular weight range. The analysis of these studies shows that significant amounts of polymerized molecules with MW greater than 1000 are present in the mesophase, but that molecules with molecular weights near 2000 are not observed. This result indicates that the reactions involving of molecules with 1000 MW and larger must be extremely slow. This lack of reactivity of the larger molecules ensures that the mesophase remains highly fluid during a wide range of reaction conditions. This prolonged fluidity is critical for many industrial processes utilizing mesophase pitch.

As the temperature increases to around 450°C, higher MW PAHs become more reactive with respect to their activation energy and reaction rate constants [87]. Further irreversible polymerization accompanied by dehydrogenation process results in a continual growth in the aromatic molecular size and semi-coke formation. Greinke's investigation suggests equal molecular reactivity of the 700-1200 MW molecules in semi-coke formation step. However, a

number of experiments in his studies illustrates that the kinetics of carbonization changes significantly after mesophase has formed and when the system is transformed into a semi-coke. It is due to a physical phenomenon in which solid state reactions occur in the polymerized pitch [87].

Continuing the heat treatment of semi-coke beyond 500°C ends up in the formation of carbon materials. However, primary carbonization refers to heat treatment of pitches up to around 550°C corresponding to early stages of coke formation.

Hydrogen and methane are removed throughout the whole process due to dehydrogenation and scission of aliphatic chains from aromatic rings [61, 253].

Consequently, the proposed model to simulate simple heat treatment of an initial CTP material (containing mostly PAH compounds with different molecular weights in the range of molecular weight distribution of commercial CTPs) from room temperature to the semi-coke formation temperature will be divided in three simplified steps with respect to critical phenomena happening through the process: 1) vaporization of the low MW PAHs below 350°C (no polymerization reactions in this temperature range for simplification purpose); 2) mesophase formation between 350 - 450°C with thermal polymerization, dehydrogenation and cracking reactions taking place; and 3) semi-coke (and early steps of coke) formation occurring in the temperature range from 450 to 550°C.

6.2.2 Simplified approach for modeling of internal phenomena occurring in coal tar pitch primary carbonization

CTP is a complex material containing from hundreds to thousands of different monomers, oligomers and polymers (mostly PAHs based) with a variety range of molecular weights [21]. During primary carbonization, CTP is transformed into infusible coke via numerous complicated

physical and chemical reactions. Hence, modeling of such a complex system and reactions to simulate all the phenomena, physical and chemical changes, happening through the above-mentioned process is not possible and crude simplifications are needed, which will be discussed in the following sections.

6.2.2.1 Selection of a set of representative PAH compounds appearing during CTP primary carbonization

As shown in Fig. 6.1, coal tar pitch mostly consists of different monomers, oligomers and polymers of polycyclic and heterocyclic aromatic hydrocarbon compounds with a variety range of molecular weight typically from 200 to 2000 [3, 21]. It has been well established that the intermediate and final products of the primary carbonization, i.e. mesophase and semi-coke, are composed of polyaromatic molecules mutually cross-linked by a medium composed of carbon functions containing heteroatoms (e.g. nitrogen, sulfur, and oxygen) which enter the process through available heterocyclic compounds in the pitches [37]. These heteroatoms are important for coke-pitch interactions in anode production. For simplification purposes in our modeling approach, it is decided at this point not to consider impurities (sulfur, nitrogen and oxygen) and other non-PAH compounds (heterocyclic compounds) that can be usually found in CTP.

In order to simplify such a complex material, some criteria have been defined as follows. The criteria for selection of a set of representative PAHs are based on: either typical molecular weight distribution (MWD) or characteristic values of CTP; the information about key components which participate in vaporization and polymerization reactions occurring in the primary carbonization process (Section 6.2.1); possibility of cracking of side chains from aromatic rings; and methane and hydrogen evolutions due to polymerization reactions taking place during heat treatment of pitch.

The selected set of representative PAHs has to include molecules with MWs satisfying typical MWD of CTP (Fig. 6.1) and/or characteristic values of CTP, e.g. α-fraction and β-fraction of resin. The most frequent CTP characterization method is analysis of group composition of CTP fractions, based on partition of pitches according to solubility of their compounds in organic solvents. On this basis one can distinguish between [40]: α-fraction of resin or quinoline-insolubles (QI) and β-fraction of resin which is the difference between toluene-insolubles (TI) and quinoline-insolubles (QI) matter. Three major constituents in CTP, e.g., TS, QI and (TI-QI) are related to fractions with molecular weight less than 1000, larger than 3000 and between 1000 and 3000, respectively [22]. Another important characteristic value of CTP which is affected by MWD is the softening point (SP) of CTP. According to information reported by Radenovic [40] and Shoko et al. [254], SP of CTP is affected by QI value. Hence, it is expected that the CTP with determined PAH population which is satisfying α and β fraction, will result in a reasonable SP.

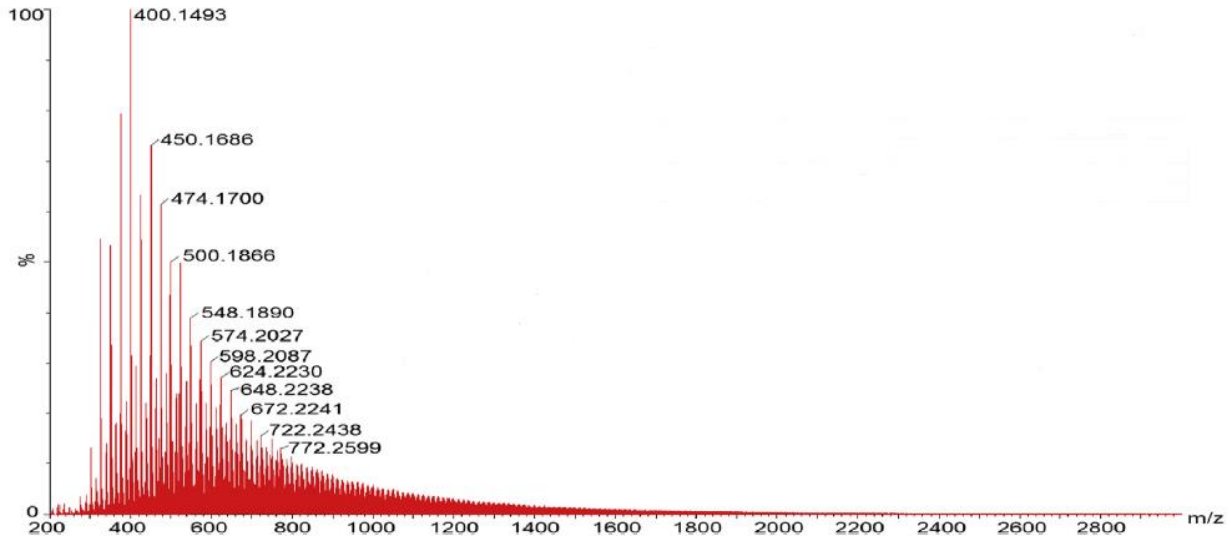

Figure 6.1 Mass spectra (MS) of a sample of coal tar pitch [21].

With respect to the first two curves of Fig. 6.2 (as the results of kinetic studies of Greinke [87]), the selected set of representative PAHs has to include at least one PAH with MW less than 400

since these volatile compounds are available in pitch and distilled out during the first steps of the heat treatment process. Meanwhile, it is well-known that carbonization of CTP has been a concern regarding health, safety and environment because of emission of low molecular weight, toxic and carcinogenic PAHs [29, 140, 255, 256]. So at least one of these PAHs must be considered in the set of representative PAHs in order to provide the prerequisite for prediction of availability of the toxic PAHs in vapor phase through the process modeling. In present work, chrysene, categorized as a highly genotoxic PAH compound [140, 256], has been selected.

Considering MW distribution changes in mesophase formation step (350 - 450°C) as discussed in Section 6.2.1 and shown in Fig. 6.2, some PAHs with MW between 300 and 700 are considered in the set of representative PAHs as reactants of oligomerization reactions.

Comparing the curves of Fig. 6.3 (which shows the molecular weight distribution in semi-coke formation step (450 -500°C) of carbonization process [87]), one can observe a very slow, but apparently equal reactivity of molecules with MW between 700 and 1200 in this step. The polymerization of pitch molecules with MW greater than 1000 results in the build-up of the 2000 MW species and larger.

These large molecular weights are considered in our model to be related to molecular weight of the initial aromatic planes of single crystallite structure which is expected to appear in this step. Ouzilleau et al. [257] presented a size-dependent thermodynamic model for coke crystallites valid for temperature range from 300K to 2500K. In their model, the Gibbs energy of coke crystallites is modulated by simple variables (as average L_a, and L_c) related to an idealized crystallite (Fig. 6.4). The large molecular weight aromatic planes at the semi-coke formation step would correspond

to an idealized crystallite structure with n≈5 (or 6) as defined in Ouzilleau's model, *n* being the number of aromatic rings on one idealized hexagonal layer as defined in Ouzilleau's model.

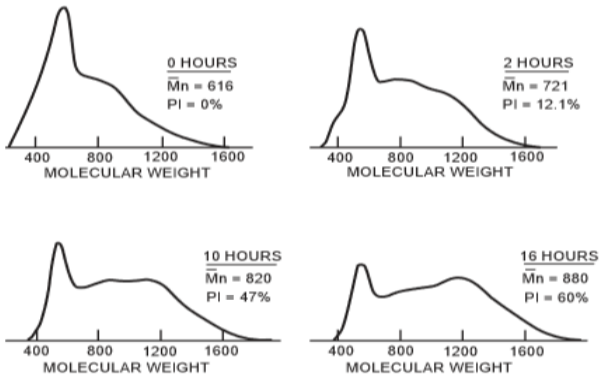

Figure 6.2 Molecular weight distribution of pitch during volatilization and mesophase formation steps [87].

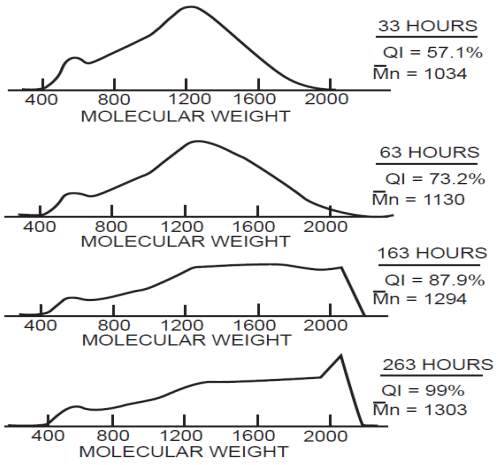

Figure 6.3 Molecular weight distribution of pitch during semi-coke formation [87].

Greinke has not studied the thermal polymerization kinetics of pitch molecules during coke formation (beyond 500°C). However, it is well known that further irreversible polymerization and dehydrogenation reactions occur with further heat treatment of CTP (up to 550°C in present work) as part of the coke formation step. It results in a continual growth in aromatic molecular size up to

4600 MW species. This is equivalent to the idealized crystallite structure with $n \approx 7$ (or 8) in Ouzilleau's model.

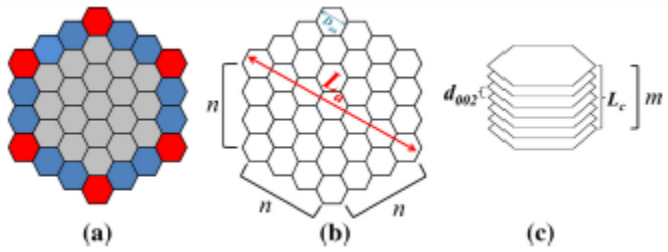

Figure 6.4 Idealized crystallite representation used in the coke model developped by Ouzileau et al. [257] : (a) idealized ''hexagonal'' plane with n = 4; (b) crystallite size L_a, D_{aa} and n parameters; (c) crystallite height L_c and d_{002} from the stacking of m planes.

It is assumed in our model that the source of methane emissions during carbonization process is the cracking of side chains in the structure of some aromatic compounds. So, the PAH compounds with side chains are considered as other key components (tetra-methyl-coronene is proposed in this work) in the set of representative PAHs. During the primary carbonization process, methane and hydrogen are evolved through complex chemical reactions in which numerous PAHs participate as reactants [3, 61, 246]. In our simplified model, these reactions are limited to a few reactions based on our choice of set of representative PAHs.

For the purpose of simplification, oligomers and polymers of PAH compounds in selected set of PAHs are limited to the oligomers of coronene and tetra-methyl-coronene monomers whose molecular weight can satisfy the typical MWD of CTP shown in Fig. 6.1.

The selected set of representative PAHs is listed in Table 6.1, together with methane and hydrogen. Its range of MW should permit to satisfy typical MWD and characteristic values of CTP. It also provides the required reactants and products for the vaporization and polymerization reactions

(either in residual pitch or in emitted gaseous mixture as low PAHs, methane and hydrogen) for modeling of the primary carbonization process.

Table 6.1 Selected set of representative PAH compounds in the present work.

Specie No.	Name	Chemical Formula	MW
1	Hydrogen	H_2	2
2	Methane	CH_4	16
3	Anthracene	$C_{14}H_{10}$	178
4	Pyrene	$C_{16}H_{10}$	200
5	Chrysene	$C_{18}H_{12}$	220
6	Coronene	$C_{24}H_{12}$	300
7	Tetra-methyl-coronene	$C_{28}H_{20}$	356
8	Bi-coronene	$C_{48}H_{20}$	596
9	Tri-coronene	$C_{72}H_{28}$	892
10	Tetra-coronene	$C_{96}H_{36}$	1188
11	Penta-coronene	$C_{120}H_{44}$	1484
12	Penta.tmc*	$C_{128}H_{52}$	1588
13	Hexa-coronene	$C_{144}H_{36}$	1764
14	Hexa-tmc*	$C_{152}H_{52}$	1876
15	Hepta-coronene	$C_{168}H_{36}$	2052
16	Hepta-tmc*	$C_{176}H_{48}$	2160
17	Octa-coronene	$C_{192}H_{40}$	2344
18	Deca-coronene	$C_{240}H_{48}$	2928
19	12-coronene	$C_{288}H_{52}$	3508
20	12-tmc*	$C_{304}H_{84}$	3732
21	14-coronene	$C_{336}H_{52}$	4084
22	14-tmc*	$C_{352}H_{76}$	4300
23	16-coronene	$C_{384}H_{60}$	4668

*tmc: tetra-methyl-coronene

6.2.2.2 **Estimation of volatile PAHs emission during CTP heat treatment**

In the first step of the primary carbonization defined above (Section 2.1), below 350°C, low MW PAHs are vaporized and removed from the condensed residue. The model simulates the primary carbonization of a fixed mass of CTP being heat treated under a fixed flow of inert gas in the equivalent of a plug-flow reactor subjected to a constant heating rate. Quantity of emitted volatile PAHs in this step at a given temperature can be estimated using the estimated partial pressure of

each compound in an ideal gas mixture based on Dalton's law and the estimated chemical activity of these compounds in the condensed mixture. Effective partial pressure of each compound in an ideal gas mixture (Eq. 6.1-b) is determined by adding a coefficient (ϕ_i) in Dalton's law (Eq. 6.1-a). This coefficient ϕ_i represents the saturation level of gas mixture by the compound *i*.

$$P_i = \frac{n_i}{n_T} \cdot P_{tot} \qquad \text{Eq. (6.1-a)}$$

$$P_{i-effective} = \phi_i \cdot \frac{n_i}{n_T} \cdot P_{tot} \qquad \text{Eq. (6.1-b)}$$

$$\alpha_i = \left[\frac{P_i}{P_i^0}\right]^{(T)} \qquad \text{Eq. (6.2)}$$

In this equations, n_i is number of mole of volatilized component *i* in the gas mixture, n_T is the total number of moles of gas, P_i is the partial pressure of component *i*, P_{tot} is the total pressure, $P_i^0(T)$ *i*s the vapor pressure of compound *i* in pure state at temperature T and α_i is the chemical activity of compounds *i* in the condensed pitch, which is assumed to be a mechanical mixture of a high viscosity isotropic+mesotropic solutions. Chemical activity of compound *i* in the pitch of a known composition at a given temperature (either isotropic liquid phase or iso-meso phases assumed in equilibrium) is determined by the chemical potentials of species *i* derived from the Gibbs free energy of the pitch system [127, 258] and using Eqs. (6.3) and (6.4):

$$\mu_i^{iso} - \mu_i^{0\,iso} = \left(\frac{\partial G}{\partial n_i}\right)_{T,P,n_{j\neq i}}^{iso} - g_i^{0\,iso} = RT\ln\alpha_i^{iso} \qquad \text{Eq. (6.3)}$$

$$\mu_i^{meso} - \mu_i^{0\,meso} = \left(\frac{\partial G}{\partial n_i}\right)_{T,P,n_{j\neq i}}^{meso} - g_i^{0\,meso} = RT\ln\alpha_i^{meso} \qquad \text{Eq. (6.4)}$$

ϕ_is in Eq. 6.1-b become the model parameters which are determined using measured values of volatiles low MW PAHs at the given temperature. They should lie in the range $0 < \phi_i \leq 1$ and will be discussed in Section 6.2.2.4.

The computation of $P_i^0(T)$, the vapor pressures of all species *i* at a given temperature T, can be performed using our critical evaluation of the thermodynamic properties of PAH compounds [Chapter 4] or from other vapor pressure functions available in the literature. In the present work, the FactSage^{TM} Thermochemical Software [259, 260] with the data base obtained in Chapter 4 is used to compute the vapor pressures.

6.2.2.3 Defining prototype chemical reactions as a reduced description of the mesophase and semi-coke formation steps

In the second step of our model, as the temperature of the CTP reaches approximately 350°C, the low molecular weight compounds have been mostly removed from the condensed system, and the nucleation of mesophase spheres starts due to numerous thermal polymerization reactions between the more reactive PAH compounds. In order to construct a model for estimating the mass and enthalpy changes of the residual pitch, some prototype reactions are defined. According to the kinetic studies of Greinke [87], polymerization reactions involving PAH species between 300-700 MW, the more reactive molecules are responsible for mesophase formation. MWD changes of pitch residue in this step (as shown in Fig. 6.2) are necessary to have an idea about range of molecular weight of products in proposed prototype reactions. For example, as seen in this figure, progressing the mesophase formation results in decreasing the population of PAHs with MW 300 and 600 and increasing of 900 MW molecules. So, with respect to selected set of PAHs in Section

6.2.2.1, one can postulate that the following reaction can be used to replace most reactions that are really taking place in CTP for this discussed change of MWD:

$$C_{24}H_{12(iso/meso)} + C_{48}H_{20(iso/meso)} = C_{72}H_{28(iso/meso)} + 2H_{2(g)} \quad \text{Eq. (6.5)}$$

The Gibbs free energy change of this prototype reaction at a given temperature in the temperature range of mesophase formation step (350°C and higher) can be calculated using our critical evaluation of the thermodynamic properties of PAH compounds [Chapter 4]. This reaction has a negative standard Gibbs energy change (ΔG°) which indicates that it occurs spontaneously under standard condition (here we can assume $P(H_2)$ is high). Eqs. (6.6) - (6.8) are other examples of the proposed prototype reactions, consuming 300MW, 592MW and 892MW PAHs to produce 892 MW, 1180 MW and 1484MW molecules:

$$3C_{24}H_{12(iso/meso)} = C_{72}H_{28(iso/meso)} + 4H_{2(g)} \quad \text{Eq. (6.6)}$$

$$C_{48}H_{20(iso/meso)} + C_{72}H_{28(iso/meso)} = C_{120}H_{32(iso/meso)} + 8H_{2(g)} \quad \text{Eq. (6.7)}$$

$$2C_{48}H_{20(iso/meso)} = C_{96}H_{28(iso/meso)} + 6H_{2(g)} \quad \text{Eq. (6.8)}$$

Table 6.2 presents reactants and products of some proposed prototype reactions of this type with negative standard Gibbs energy change occurring in mesophase formation step.

Some other reactions with negative standard Gibbs free energy change (presented in Table 6.2) are proposed in this step which are responsible for light PAHs production and methane formation due to thermally induced bond cleavage of naphthenic rings or scission of aliphatic side chains from aromatic rings, respectively. Some example of these type of reactions are as follows:

$$C_{28}H_{20(iso/meso)} + 4H_{2(g)} = C_{24}H_{12(iso/meso)} + 4CH_{4(g)} \quad \text{Eq. (6.9)}$$

$C_{48}H_{20(iso/meso)} + 2H_{2(g)} = 2C_{24}H_{12(iso/meso)}$ Eq. (6.10)

Hydrogen and methane as well as produced low MW PAHs in this step are removed from the system.

In the next step of modeling, occurring in the temperature range between 450 and 550°C, polymerization reactions involving species with MW between 700-1200 are taking place. The measured changes in MWD shown in Fig. 6.3 are used to propose prototype reactions occurring in this step, as a replacement for the myriad of all reactions really occurring. Eqs. 6.11 and 6.12 (having negative standard Gibbs energy change) can be some examples of these type of reactions regarding the decrease in population of 900 to1200 MW molecules and the increase in population of 1800 to 2000 MW molecules as seen in Fig.6.3.

Table 6.2 Proposed prototype oligomerization reactions in mesophase formation step of carbonization process.

Reaction	**Type of reaction**	**Chemical reaction**
R_1	Oligomerization/Polymerization	$2C_{24}H_{12} = C_{48}H_{20} + 2H_2$
R_2	Oligomerization/Polymerization	$3C_{24}H_{12} = C_{72}H_{28} + 4H_2$
R_3	Oligomerization/Polymerization	$2C_{48}H_{20} = C_{96}H_{36} + 2H_2$
R_4	Oligomerization/Polymerization	$C_{24}H_{12} + C_{48}H_{20} = C_{72}H_{28} + 2H_2$
R_5	Oligomerization/Polymerization	$C_{48}H_{20} + C_{72}H_{28} = C_{120}H_{44} + 2H_2$
R_6	Oligomerization/Polymerization	$2C_{28}H_{20} = C_{56}H_{36} + 2H_2$
R_7	Oligomerization/Polymerization	$C_{56}H_{36} + C_{72}H_{28} = C_{128}H_{52} + 6H_2$
R_8	Oligomerization/Polymerization	$C_{56}H_{36} + C_{72}H_{28} = C_{120}H_{52} + 6H_2$
R_9	Cracking	$C_{28}H_{20} + 4H_2 = C_{24}H_{12} + 4CH_4$
R_{10}	Cracking	$C_{56}H_{36} + 8H_2 = C_{48}H_{20} + 8CH_4$
R_{11}	Cracking	$C_{48}H_{20} + 2H_2 = 2C_{24}H_{12}$
R_{12}	Cracking	$C_{56}H_{36} + 2H_2 = 2C_{28}H_{20}$

$2\ C_{72}H_{28(iso/meso)} = C_{144}H_{36(semi\text{-}coke)} + 10H_{2(g)}$ Eq. (6.11)

$C_{72}H_{28(iso/meso)} + C_{96}H_{36(iso/meso)} = C_{168}H_{36(semi\text{-}coke)} + 14H_{2(g)}$ Eq. (6.12)

Beyond 500°C (up to 550°C in this work), some prototype polymerization reactions are defined resulting in larger molecules with MW about 4600 equivalent to n≈7 (or 8) and initiation of coke formation:

$$2C_{176}H_{48(semi\text{-}coke)} = C_{352}H_{76(coke)} + 10H_{2(g)} \quad \text{Eq. (6.13)}$$

$$2C_{192}H_{40(semi\text{-}coke)} = C_{384}H_{60(coke)} + 10H_{2(g)} \quad \text{Eq. (6.14)}$$

Defined prototype reactions in this work which are responsible for semi-coke and coke formation in CTP heat treatment has been summarized in Table 6.3. This Table includes some cracking reactions which are also taken place in this step of process producing light PAHs and small amount of methane.

Table 6.3 Proposed prototype polymerization reactions in semi-coke / coke formation step of carbonization process.

Reaction	Type of reaction	Chemical reaction
R_1	Oligomerization/Polymerization	$2C_{72}H_{28} = C_{144}H_{36} + 10H_2$
R_2	Oligomerization/Polymerization	$C_{48}H_{20} + C_{96}H_{36} = C_{144}H_{36} + 10H_2$
R_3	Oligomerization/Polymerization	$C_{72}H_{28} + C_{96}H_{36} = C_{168}H_{36} + 14H_2$
R_4	Oligomerization/Polymerization	$C_{56}H_{36} + C_{96}H_{36} = C_{152}H_{52} + 10H_2$
R_5	Oligomerization/Polymerization	$C_{56}H_{36} + C_{120}H_{44} = C_{176}H_{48} + 16H_2$
R_6	Oligomerization/Polymerization	$2C_{96}H_{36} = C_{192}H_{40} + 16H_2$
R_7	Oligomerization/Polymerization	$2C_{120}H_{44} = C_{240}H_{48} + 20H_2$
R_8	Oligomerization/Polymerization	$2C_{144}H_{36} = C_{288}H_{52} + 10H_2$
R_9	Oligomerization/Polymerization	$2C_{152}H_{52} = C_{304}H_{84} + 10H_2$
R_{10}	Oligomerization/Polymerization	$2C_{168}H_{36} = C_{336}H_{52} + 10H_2$
R_{11}	Oligomerization/Polymerization	$2C_{176}H_{48} = C_{352}H_{76} + 10H_2$
R_{12}	Oligomerization/Polymerization	$2C_{192}H_{40} = C_{384}H_{60} + 10H_2$
R_{13}	Cracking	$C_{48}H_{20} + 2H_2 = 2C_{24}H_{12}$
R_{14}	Cracking	$C_{56}H_{36} + 2H_2 = 2C_{28}H_{20}$
R_{15}	Cracking	$C_{56}H_{36} + 8H_2 = C_{48}H_{20} + 8CH_4$

Degree of advancement of all proposed prototype reactions between 350-450°C and 450-550°C becomes model parameters which can be determined using experimental values of condensable and non-condensable volatile matters and will be discussed in Section 6.2.2.4.

6.2.2.4 **Estimation of the model parameters**

ϕ_is, the empirical coefficients in Eq. (6.1-b) and the degree of advancement of the proposed prototype reactions in previous section are the model parameters which need to be fixed by fitting the experimental data (Bouchard [246] in our case). The procedure for the estimation of these model parameters is based on defining a simple system which can well describe all the internal phenomena in CTP primary carbonization process.

A small initial mass of CTP (m_0) containing PAHs with typical characterization of CTP shown in Fig. 6.1 is selected as the sample which goes under carbonization process. The model assumes this sample is heat treated at a constant heating rate ($\dot{Q}$) from room temperature to 550°C which is our final temperature for CTP primary carbonization process, in agreement with literature data. An inert gas, like Ar, with a constant flow rate ($\dot{V}_{Ar}$) is passed through the system during the heat treatment to carry the emitted gas out. We will show later the impacts of small, average or large values of this flow rate (normalized by the initial mass).

The following measurements are needed to provide the required information for the estimation of the above mentioned model parameters. Mass loss of the sample due to volatilization of light compounds has to be detected using either Thermal Gravimetric Analysis (TGA) during the heat treatment or by weighting the sample at some critical temperatures after starting the chemical reactions. These temperatures are limited to 350°C (start of mesophase formation), 450°C (semi-coke formation) and 550°C (coke formation) which are defined based on the concept of carbonization process and general steps explained in Section 6.2.1. At these temperatures, the emitted gas mixture composition has to be analyzed utilizing gas chromatography (GC) and mass spectrometry (MS) after cooling and separation into the condensable part (e.g. low MW PAHS)

and non-condensable part (mostly hydrogen and methane). Obviously, mass loss and composition of the gas mixture emitted might change depending on the type of pitch used and the heating rate during thermal treatment process of the pitch.

In the present work, ϕ_is, as the model parameters are determined using measured values of volatile PAHs emitted during pitch heat treatment previously reported by Bouchard et al. [246] . MWD of pitch residue in different steps of CTP heat treatment (either in mesophase or in semi-coke formation steps) investigated by Greinke (shown in Figs. 6.2 and 6.3) as well as measured values in Bouchard's experiments for amount of emitted condensable (e.g. low MW PAHs) and non-condensable gases (e.g. methane and hydrogen) are utilized to determine degree of advancement of the prototype reactions. However, these are limited to 350, 450 and 550°C, the important temperatures associated to the three defined steps in our model.

6.2.3 Mass and energy balance through the process

With respect to general steps occurring during heat treatment of CTP [3, 87, 250, 252] , as the temperature of the pitch reaches around 350°C, the low MW PAHs as non-mesogen molecules with no tendency to form mesophase (with respect to their clearing temperature*) have been removed from pitch and the pitch is rich in reactive mesogen molecules at this temperature to build up the higher molecular weight compounds in such a manner as to satisfy the average molecular structural requirements for mesophase formation. This temperature has been fixed at 350°C in the present work and mass and energy balances are performed in different ways, below and above this temperature. Actually, 350°C becomes like a threshold temperature.

A hypothetical reactor design, shown in Fig. 6.5, is used to compute, for a given iteration, the mass and energy balances in temperature range between 25-350°C. The border of the system under study,

mass and energy flows are shown in the figure as dashed, red solid and blue solid lines, respectively. The temperature difference between the two iterations ($\Delta T = T_{j+1} - T_j$) in the mass and energy balance calculations is fixed equal to 5°C, which is relatively low compared to the temperature difference of whole step (i.e. 325°C). The pitch at a given temperature, T_j, (from previous iteration) enters into the system and goes under carbonization process. Heat treatment on the pitch changes the temperature of the system by ΔT and vaporization of low MW PAHs is taken place (assuming neither polymerization nor thermal cracking reactions occurring in this temperature range of the process). It is assumed that all the generated gaseous species due to volatilization are removed from the system through the carrier gas to be burnt and there is not any retention of gas inside the reactor. There will be also no gas in the reactor input flow except carrier gas at 25°C and 1atm for next iteration.

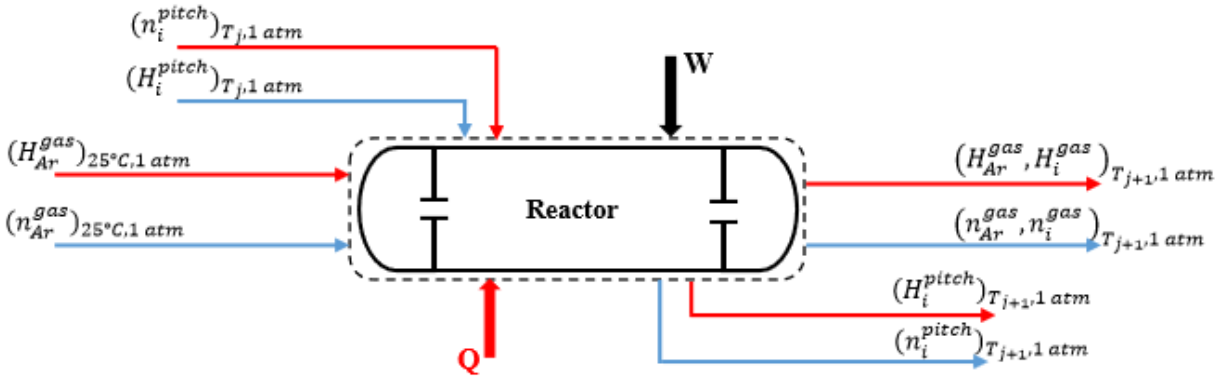

Figure 6.5 Hypothetical reactor design used to compute the mass and energy balances at every iteration in our model; dashed line: border of the system, blue lines: mass flows, and red lines: heat flows.

Applying the mass conservation law over the system between 25-350°C results in Eq. (6.15-a):

$$(n_i^{pitch})_{T_{j+1}} + (n_i^{gas})_{T_{j+1}} + (n_{Ar}^{gas})_{T_{j+1}} = (n_i^{pitch})_{T_j} + (n_{Ar}^{gas})_{25°C} \quad \text{Eq. (6.15-a)}$$

Where, $T_{j+1} = T_j + \Delta T$ is the temperature of the pitch and gas after increase, $i = 1, 2, \ldots N$ represents the species in the system excluding argon at any given temperature either in pitch or in gas (N is number of the species listed in Table 6.1), n_i^{pitch} is the number of mole of compound *i* in the pitch (either in isotropic liquid or in mesophase), and n_i^{gas} is the number of moles of volatile compound *i* in gas mixture at any given temperature which can be estimated in each iteration by following the procedure described in Section 6.2.2.2. n_{Ar}^{gas} in both sides of Eq. (15-a) will be cancel out since it is assumed that there is not any retention of gas inside the reactor for next iteration.

Above threshold temperature (350°C in this work) during mesophase and semi-coke formation, i.e. between 350-450°C and 450-550°C, polymerization and thermal cracking reactions listed in Tables 6.2 and 6.3 as well as volatilization of low MW PAHs are taken place. It is assumed that there is no gas in the reactor input flow except carrier gas at 25°C and 1atm since all the generated gaseous species due to either volatilization or polymerization and thermal cracking reactions are pushed out of the system by carrier gas. Mass conservation law is applied over the system in these steps considering one iteration of 100°C as presented in Eq. (6.15-b). The criteria for choosing 100°C step in the calculations is the lack of required experimental data for determining the degree of advancement of chemical reactions in intermediate steps.

$$(n_i^{pitch})_{450\,°C(550°C)} + (n_i^{gas})_{450°C\,(550°C)} + (n_{Ar}^{gas})_{450°C\,(550°C)} =$$

$$(n_i^{pitch})_{350°C\,(450°C)} + (n_{Ar}^{gas})_{25°C} + \nu_i^{[R_1]}\xi^{[R_1]} + \nu_i^{[R_2]}\xi^{[R_2]} + \cdots + \nu_i^{[R_n]}\xi^{[R_n]} \quad \text{Eq. (6.15-b)}$$

In this equation n_i^{gas} is the number of moles of volatile compound *i* either in condensable gas, i.e. low MW PAHs, or in non-condensable gas, i.e. methane and hydrogen at any given temperature, $\nu_i^{[R_n]}$ represents the stoichiometric number of each compounds (*i* = 1,2,…N, either PAH compound or generated gas, i.e. methane and hydrogen, due to chemical reactions, listed in Table 6.1) in each defined prototype reactions in Tables 6.2 and 6.3, and $\xi^{[R_n]}$ is the degree of advancement of those reactions between 350-450°C (or 450-550°C) as the model parameters, determined in Section 6.2.2.4.

Each term in mass balance equations either below or above 350°C are summarized in Table 6.4.

Table 6.4 Definition of different terms in Eqs. (6.15-a) and (6.15-b).

Temp. Range	$(\boldsymbol{n_i^{pitch}})_{\boldsymbol{T_j}}$	$(\boldsymbol{n_i^{pitch}})_{\boldsymbol{T_{j+1}}}$	$(\boldsymbol{n_i^{gas}})_{\boldsymbol{T_{j+1}}}$
25-350°C	0, *i* = 1,2 $(n_i^{iso})_{T_j}$, *i* = 3,4,…N	0, *i* = 1,2 $(n_i^{iso})_{T_{j+1}}$, *i* = 3,4,…N	0, *i* = 1,2, and 8, 9,…N $(n_i^{gas})_{T_{j+1}}$, *i* = 3,4,…,7
350- 450°C	0, *i* = 1,2,…5 $(n_i^{iso})_{350}$, *i* = 6,7,…N	0, *i* = 1,2,…7 $(n_i^{meso})_{450}$, *i* = 8,9,…N	0, *i* = 8,9,…N $(n_i^{gas})_{450}$, *i* = 1,2,…,7
450- 550°C	0, *i* = 1, 2,…7 $(n_i^{meso})_{450}$, *i* = 8,9,…N	0, *i* = 1,2,…7 $(n_i^{semi-coke})_{550}$, *i* = 8,9,…N	0, *i* = 8, 9,…N $(n_i^{gas})_{550}$, *i* = 1,2,…,7

The First Law of thermodynamic for an open system is formulated as follows:

$$Q + W = \Delta H + \Delta E^{kin} + \Delta E^{pot} \qquad \text{Eq. (6.16)}$$

where Q denotes the quantity of energy supplied to the system as heat, W denotes the amount of non-PV work done by the surrounding on the system, ΔH, ΔE^{kin} and ΔE^{pot} are the change in the enthalpy, kinetic energy and potential energy of the system, respectively.

The required energy for increasing the temperature of the above defined system (Fig. 6.5), from T_j to T_{j+1},can be estimated by applying Eq. (6.16) with neglecting two last terms in this equation and considering no non-PV work done on the system:

$$Q = \sum_i (H_i^{pitch})_{T_{j+1}} + \sum_i (H_i^{gas})_{T_{j+1}} + (H_{Ar}^{gas})_{T_{j+1}} - \sum_i (H_i^{pitch})_{T_j} - (H_{Ar}^{gas})_{25°C} \quad \text{Eq. (6.17)}$$

where H_i^{pitch} is the total enthalpy of compound *i* in the pitch (either in isotropic liquid or in mesophase), H_i^{gas} is the total enthalpy of volatile compound *i* either in condensable gas, i.e. low MW PAHs, or in non-condensable gas, i.e. methane and hydrogen at any given temperature and H_{Ar}^{gas} is the total enthalpy of argon at any given temperature and 1 atm. Enthalpy terms of the species in Eq. 6.17 are determined using the obtained results from mass balance calculations, below and above fixed threshold temperature, 350°C (Table 6.5). Total enthalpy of argon in Eq. (6.17) can be estimated using molar enthalpy of pure argon at any given temperature and 1 atm and number of mole of argon which is dependent on values of carrier gas flow rate ($\dot{V}_{Ar}$) and heating rate ($\dot{Q}$) fixed in Section 6.2.2.4.

Table 6.5 Definition of different terms in Eq. (6.17).

Temp. range	$\boldsymbol{H_{T_j}^{pitch}}$	$\boldsymbol{H_{T_{j+1}}^{pitch}}$	$\boldsymbol{H_{T_{j+1}}^{gas}}$
25-350°C	$\left[\sum_i (n_i h_i^0)_{T_j} + (n_T \Delta h_{mix})_{T_j}\right]^{iso}$ (i = 3,4,…N)	$\left[\sum_i (n_i h_i^0)_{T_{j+1}} + (n_T \Delta h_{mix})_{T_{j+1}}\right]^{iso}$ (i = 3,4,…N)	$\left[\sum_i (n_i h_i^0)_{T_{j+1}}\right]^{gas}$ (i = 3,4,…,7)
350- 450°C	$[\sum_i (n_i h_i^0)_{350} + (n_T \Delta h_{mix})_{350}]^{iso}$ (i = 6,7,…N)	$[\sum_i (n_i h_i^0)_{450} + (n_T \Delta h_{mix})_{450} + (n_T h_{orient})_{450}]^{meso}$ (i = 8,9,…N)	$[\sum_i (n_i h_i^0)_{450}]^{gas}$ (i = 1,2,…,7)
450-550°C	$[\sum_i (n_i h_i^0)_{450} + (n_T \Delta h_{mix})_{450} + (n_T h_{orient})_{450}]^{meso}$ (i = 8,9,…N)	$[\sum_i (n_i h_i^0)_{550}]^{semi-coke}$ (i = 8,9,…N)	$[\sum_i (n_i h_i^0)_{550}]^{gas}$ (i = 1,2,…,7)

In Table 6.5, h_i^0 are reference molar enthalpy for the pure components as isotropic liquid (either in iso or in meso phase), gas or semi-coke (coke), Δh_{mix} is the molar enthalpy of mixing of compounds in pitch as a solution and h_{orient} is the enthalpy contribution of orientational free energy of mesophase [127, 258]. The FactSage™ Thermochemical Software [259, 260] with the

data base obtained in Chapter 4, as described in Section 2.2.2, is used to compute the enthalpies of species *i* at any given temperature T, $h_i^0(T)$.

Thermodynamic theory for PAHs solutions first proposed by Hu and Hurt [127] and improved in our previous work [258] is applied to calculate enthalpy of mixing and orientation enthalpy terms for the isotropic phase and mesophase. The thermodynamic model for idealized coke crystallite developed by Ouzilleau et al. [257] can be utilized for estimation of the enthalpy of semi-coke (or coke) species.

6.2.4 Integrating equations for estimation of mass and enthalpy changes through the primary carbonization process

A small mass of pitch with known composition $\left[(n_i^{pitch})_{T_0}\right]$ at room temperature [T_0] is considered as the initial conditions of the system in the following calculations. As most CTP are obtained during a quenching procedure of liquid by-product in coke oven (see ref.[37, 38] for more detail) from 400°C to room temperature, we assume here that the state of the pitch at T_0 is a glassy isotropic liquid. This assumption is reasonable since there is no evidence for existence of crystal structure in CTP regarding to the XRD experiment results [47, 48]. Considering the above defined threshold temperature of 350°C, the calculation procedure for mass and enthalpy changes through CTP heat treatment is divided in two parts, below and above threshold temperature.

Calculations below 350°C

Starting from room temperature, the number of moles of each compounds in the pitch after increasing the temperature of the system byΔT,$\left[(n_i^{pitch})_{T_{j+1}}\right]$, is determined using Eqs. 6.1- 6.4

and 15-a. It was previously assumed that there is no chemical reaction occurring during these first steps of the process and only vaporization is taken place. The amount of the each volatile compounds in the gas mixture, $\left[(n_i^{gas})_{T_{j+1}}\right]$, is determined by applying Eq. 6.1- 6.4 to each compounds with respect to the model parameters (ϕ_is) and the way to estimate it in Section 6.2.2.4. However, combining Eqs. 6.1- 6.4 yields X equations for X unknowns, number of moles of X volatile compounds in the gas mixture. Solving these equations, numerically, results in amount of volatile PAHs at the given temperature. Summation over amount of all species in the system in the given temperature results in total mole of the pitch (n_T^{pitch}) in that temperature:

$$\left(n_T^{pitch}\right)_{T_{j+1}} = \sum_i \left(n_i^{pitch}\right)_{T_{j+1}} \qquad \text{Eq. (6.18)}$$

The result for the mass changes of system by increasing the temperature by ΔT and the energy balance on the system (Eq. 6.17 and Table 6.5) are applied to estimate the required energy for increasing the temperature of pitch from T_j to T_{j+1}.

Calculations above 350°C

Regarding to the defined prototype reactions in Section 6.2.2.3, in the temperature range between 350°C and 550°C, when the mesophase, semi-coke and coke formations start, some new high MW and low MW PAHs, hydrogen and methane are produced due to thermal polymerization and cracking reactions. The degree of advancement of these reactions which have been already determined as the model parameters in Section 6.2.2.4 controls the amount of the mass losses of either condensable (low MW PAHs) or non-condensable (hydrogen and methane) compounds through the process. However, the estimations of mass losses after 350°C are limited to interval temperatures, 350- 450°C and 450 - 550°C, since the degree of advancements of the reactions are

limited in theses ranges of temperature (Section 6.2.2.4). Degree of advancement of defined prototype reactions (Eqs. 6.5-6.14 and Tables 6.2 and 6.3) are used to determine the third term and later on right side of molar balance equation (Eq. 6.15-b) in order to estimate the mass of each species in residual pitch after increasing the temperature of the system by ΔT.

The obtained results for mass changes of residue pitch and amount of removed species from pitch in mesophase and semi-coke (initial coke) formation steps (350 – 450°C and 450 – 550°C) as well as defined energy balance in these temperature ranges (Eq. 6.17 and Table 6.5) are applied to estimate required energy for raising the temperature of pitch from 350 to 450°C and 450 to 550°C, respectively.

6.3 Results and discussion

The thermodynamic-kinetic model proposed in Section 6.2 was applied to perform quantitative analysis of physical and chemical changes occurring during CTP primary carbonization process. In order to make a general investigation of volatile matter emission rate through CTP heat treatment, a simplified system containing typical low, medium and high molecular weight PAHs available in CTP analyzed by Zhang et al. [21] was modeled. The variation of evaporation rate of low MW with temperature and composition of the system was studied. Observations of mass losses during heat treatment of CTP from Thermo-Gravimetric Analysis (TGA) of Bouchard et al. [246] was modeled. A sensitivity analysis was performed to investigate the ability of the model to estimate the effect of some important parameters in carbonization process on quantity of emitted volatile matters. The variation of mass losses of low MW PAHs occurring during the process with heating rate, carrier gas flow rate, and saturation level of emitted gaseous species as real and internal variables of the model, respectively, were evaluated. The molecular weight distribution

changes through mesophase and semi-coke formation steps of carbonization process were calculated consistent with Greinke's investigation [87]. Required energy to increase the temperature of pitch sample in Bouchard's experiment from room temperature to 350°C, which results in estimated mass losses in this temperature range, was calculated. Estimation of the enthalpy changes of pitch (with the aim of energy requirement analysis) through the carbonization process in temperature range beyond 350°C needs further research.

6.3.1 General prediction of gas emission rate during heat treatment of coal tar pitch (below 350°C)

With respect to the typical molecular weight distribution of coal tar pitch shown in Fig. 6.1, a simplified pitch system containing a low molecular weight PAH, anthracene (MW: 178 g / mole), and some medium and high molecular weight PAHs (e.g. bi-coronene, tri-coronene and Tetra-coronene) with MW 596, 892 and 1180 g / mole, respectively, is selected to be studied in this section. In order to simplify the studies, a binary phase diagram exhibiting the thermodynamic behavior of this pitch system (Fig. 6.6) is generated by applying the proposed thermodynamic approach in our previous work [258].

The partial pressure of anthracene in the pitch system in the temperature range of 25 – 350°C (either in one-phase or two-phase region) can be estimated by following the procedure explained in Sections 6.2.2.2 and 6.2.4, assuming a near-equilibrium state during a given ΔT iteration. Indeed, calculating the chemical activity of anthracene in above defined pitch solution (as a mixture of PAH compounds) using the developed approach in our previous work [258] with the aid of Eq. (6.2) permits to create the iso- partial- pressure lines of anthracene on Fig. 6.6. These lines are the indicators of the emission rate of low molecular weight compound in the system. The dashed lines

and dash-dotted lines represent the iso-partial pressure of anthracene in single isotropic liquid, two-phase and metastable single-phase regions, respectively.

As seen in the figure, the partial pressure of low MW compounds through the constant temperature process will decrease if the system under study has a single isotropic liquid phase and will be the same when the system contains two phases in the equilibrium, even though in this case the amount of the volatile compound decreases with increasing time. So, it takes more time to evaporate a same amount of this compound from the single isotropic phase system in an isothermal process, and similarly in a heating process if the high viscosity isotropic liquid is maintained rather than an equilibrated high MW mesophase with a low MW isotropic liquid. This figure can be used to study the volatile PAHs emissions aspects of CTP heat treatment from room temperature to 350°C (623 K) when the significant amount of the low MW PAHs are evolved. According to mass spectrum of typical CTP shown in Fig. 6.1, there is a few amount of low MW PAH compounds, like anthracene, in CTP containing PAHs with different molecular weight. Hence, the starting point of this study will be on the right side (anthracene-lean region) of Fig. 6.6. A zoom view of the anthracene-lean region of Fig. 6.6 is shown in Fig. 6.7.

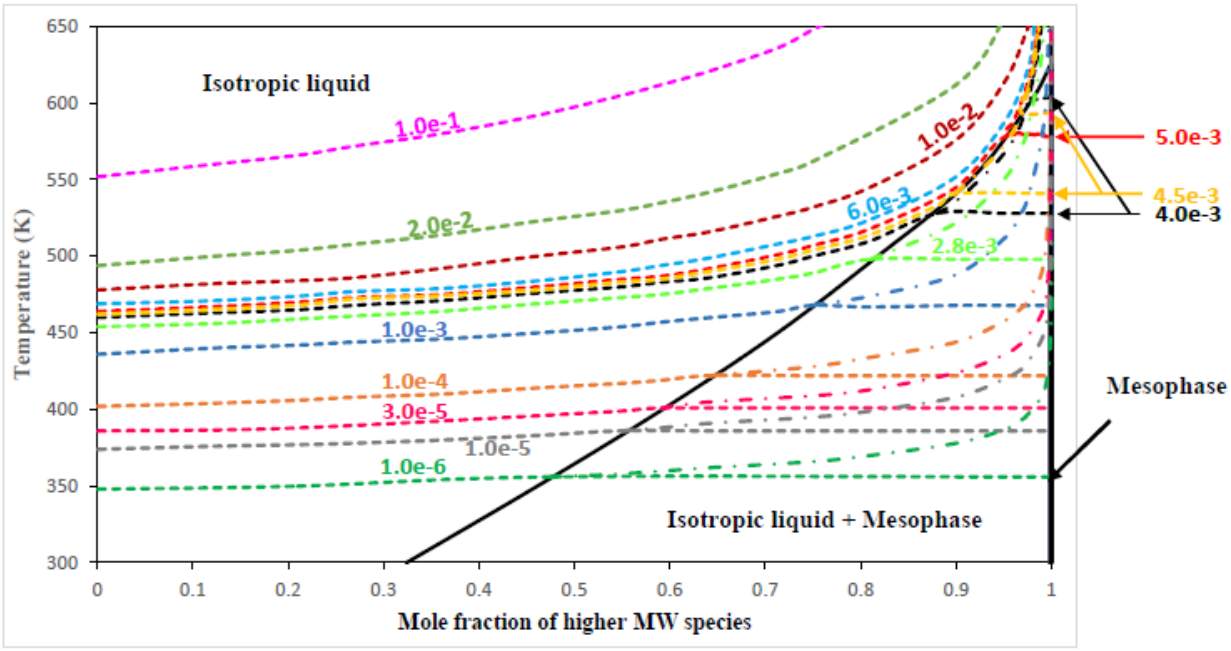

Figure 6.6 Binary phase diagram of anthracene and a mixture of representative PAHs, which do not contain anthracene indicating partial pressure of low MW compound; Dashed lines: iso-partial-pressure (bar) of anthracene and dash-dotted lines: metastable iso-partial-pressure (bar) of anthracene.

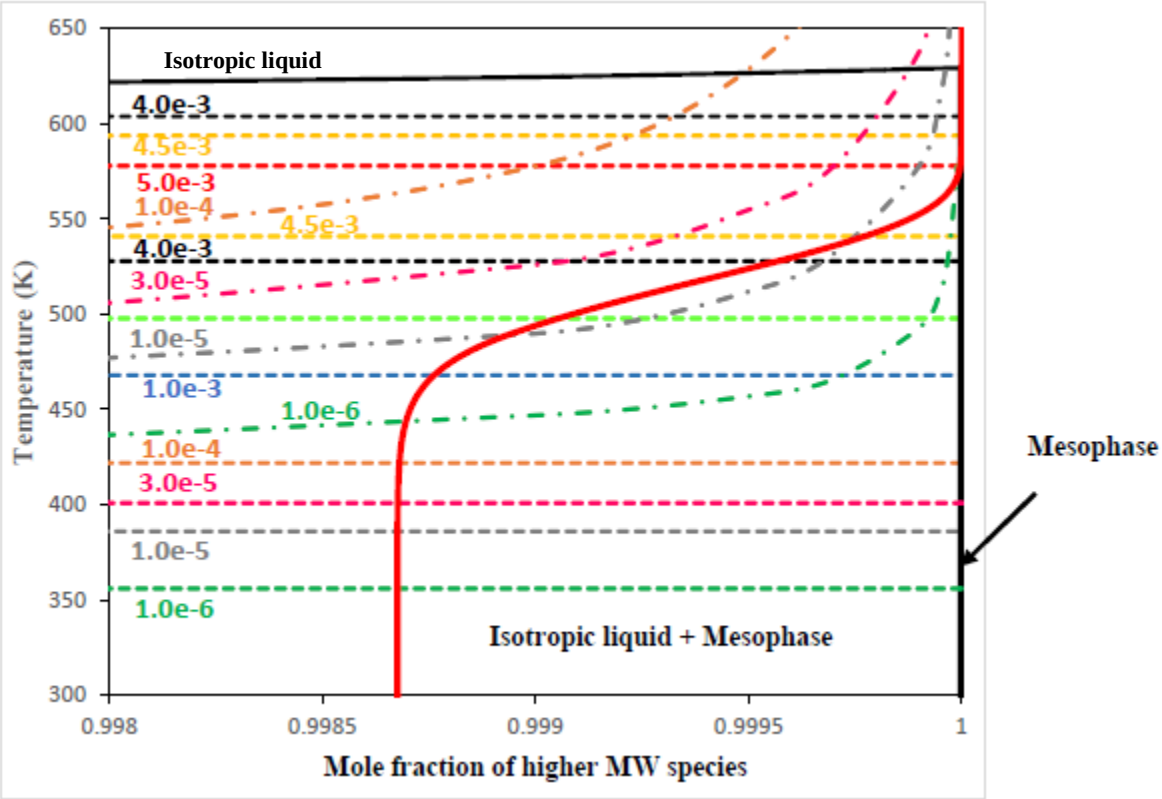

Figure 6.7 Zoom view of the anthracene-lean region of Fig. 6.6; Red solid line: evaporation path of anthracene during heat treatment of a 50 g pitch sample (heating rate: 50°C/h and carrier gas flow rate: 560 cm^3/min)

Meanwhile, it is considered that the assumed quenched structure of CTP at 25°C (discussed in Section 6.2.4) is retained until 350°C and the iso-meso equilibrium in pitch is kinetically prohibited in our model below 350°C. So, partial pressure changes of anthracene during heat treatment of CTP are evaluated by following the dash-dotted lines in Fig. 6.6 in anthracene-lean region which will be very different with partial pressure of anthracene in a two-phase system. As the temperature of CTP increases and the evaporation of anthracene is progressing, CTP becomes further diluted in anthracene. A schematic of changes in pitch composition by temperature is shown as red solid

line in Fig. 6.7. As seen in the figure, this composition changes results in a substantial changes on partial pressure of anthracene.

6.3.2 Application to Bouchard's experiments

Bouchard et al. [246] designed several experiments to study the mass loss of the pitches when they go under carbonization process. They measured and analyzed the condensable and non-condensable parts of released gaseous mixture through the CTP heat treatment.

A 50 grams mass of pitch containing PAHs from Table 6.1 is considered as the sample to be studied in this work. Type and quantity of PAHs in the sample (shown in Table 6.6) are chosen with respect to MWD of the typical CTP analyzed and reported by Zhang (Fig. 6.1). The criteria for choosing the 50 grams mass of pitch is Bouchard's experiments which have been performed for this quantity of pitch. Heating rate of CTP and flow rate of carrier gas in our calculations are fixed with respect to operating conditions of Bouchard's experiments, 50°C/h and 2300 cm^3/h (at 25°C and 1atm), respectively.

6.3.2.1 **Estimation of mass changes of CTP (during heat treatment)**

The calculations in this section are based on our choise of the threshold temperature of 350°C (fixed in this work, Section 6.2.3) for the starting point of mesophase spheres formation. However, the model has flexibility to be used with another threshold temperature (in the range of 300 - 400°C) based on own experimental data.

The total amount of emitted volatile PAHs in the first step of heat treatment (25 to 350°C) was estimated applying the proposed approach described in Sections 6.2.2.2 and 2.4 (considering ΔT = 5°C in the calculations). Experimental data for total mass loss during this step of the process

obtained by Bouchard et al. [246] is utilized to determine the model parameters ($\phi_i s$), as described in Section 6.2.2.4. A strength of the proposed model is that the emission of volatile compounds is predictable even at low temperatures. By setting the reasonable values of the saturation level coefficients for all volatile species (in this case equal to 1), the model can estimate the trend of the total amount of PAHs lost with temperature observed by Bouchard et al. in their experiments (Fig. 6.8).

Table 6.6 Mass distribution of an arbitrary 50 grams pitch sample at room temperature subjected to the calculations in the present work.

Name	Chemical Formula	MW	Mass (g)
Anthracene	$C_{14}H_{10}$	178	0.03
Pyrene	$C_{16}H_{10}$	200	0.04
Chrysene	$C_{18}H_{12}$	220	0.044
Coronene	$C_{24}H_{12}$	300	9
Tetra-methyl-coronene	$C_{28}H_{20}$	356	27
Bi-coronene	$C_{48}H_{20}$	596	10
Tri-coronene	$C_{72}H_{28}$	892	3
Tetra-coronene	$C_{96}H_{28}$	1180	0.886

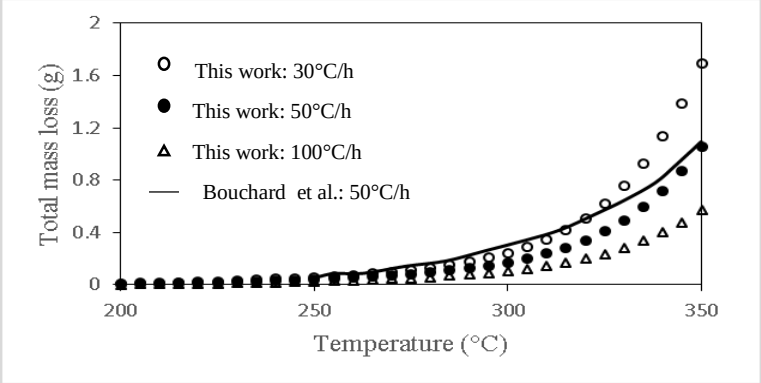

Figure 6.8 Effect of heating rate on total mass loss during heat treatment of a 50 g pitch in temperature range below 350°C, Solid line: experimental data obtained by Bouchard et al. [246] at 50°C/h; Points: predictions in this work (using ϕ_is = 1 and carrier gas flow rate : 2300cm^3/min).

As shown in Fig. 6.8, heating rate affects the residence time of pitch at each temperature and consequently on emission of volatile matter. However, a sensitivity analysis will be helpful to study (in detail) the effect of heating rate as well as flow rate of carrier gas on the mass loss of volatile matters during CTP heat treatment and will be discussed as follows.

In this section, mass losses of each volatile PAH compounds has been estimated every 5°C (between 25 and 350°C) assuming full equilibrium (by setting ϕ_is for all volatile species equal to 1 in Eq. 6.1-b) at every temperature intervals and no constrains for diffusion of volatile matter to the carrier gas.

The carrier gas flow rate affects the evaporation rate of each volatile PAHs with significant volatility. As seen in Figs. 6.9a -6.9c, in higher carrier gas flow rate, total mass losses of volatile compounds are taken place in a more narrow and lower range of temerature range. Changes of pitch composition due to evaporation of anthracene in different flow rates of carrier gas can be shown on zoom view of anthracen-lean region, Fig. 6.7. As shown in Fig. 6.10, evaporation paths of anthracene are affected by flow rate of carrier gas: more flow rate of carrier gas, more evaporation rate of anthracene.

In order to evaluate the heating rate effect on mass losses, the calculations for estimation of changes in mass loss of each volatile PAHs with temperature have been performed for two different heating rates, 50 and 100°C/h. As shown in Figs. 6.11a -6.11c, as the hating rate decreases, release of volatile matters is taking place at lower temperatures. On the other hand, when the heat treatment of CTP is performed with higher heating rate, the system is further away from the equilibrium state. It means that there is an optimum heating rate to be used in pitch carbonization process. As an

industrial case, a few researchers investigated that the heating rate in anode baking furnace in aluminum industry should not exceed 10 to 14°C/h between 200-600°C [138, 261].

However, changing the ϕ_is values for each volatile species , as the extremely simple kinetic model parameter, to less than 1(in the previous calculations) enables us to estimate the behavior of a system with conditions closer to the equilibrium state (Figs. 6.11d -6.11f). These figures show the variation of mass loss of three volatile components (e.g. anthracene, pyrene and chrysene) with temperature by setting two different values of ϕ_is (0.7 or 1) but equal for all volatile species in each calculation.

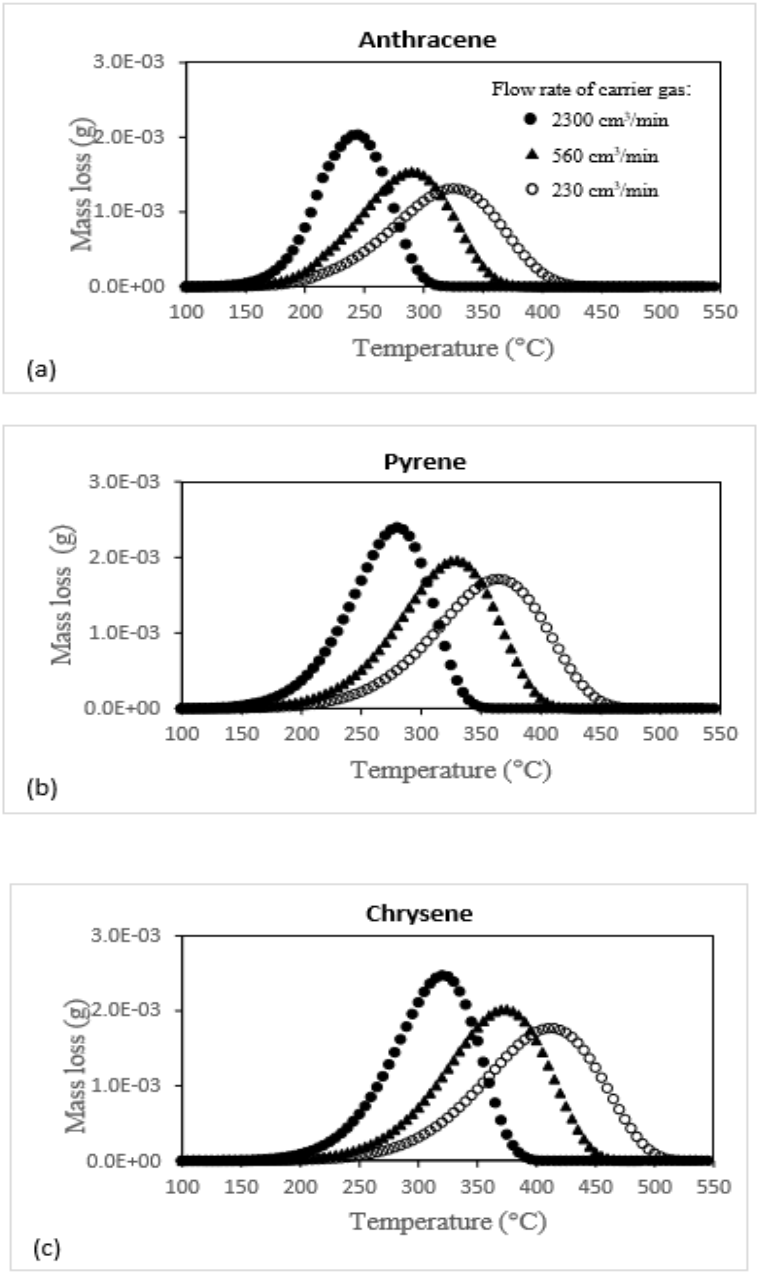

Figure 6.9 Estimated mass loss of a)antheracene, b)pyrene and c)chrysene versus temperature for different carrier gas flow rates. Solid circle: 2300 cm^3/min, solid triangle: 560 cm^3/min and empty circle: 230 cm^3/min (heating rate: 50°C/h and $\phi_i s$: 1).

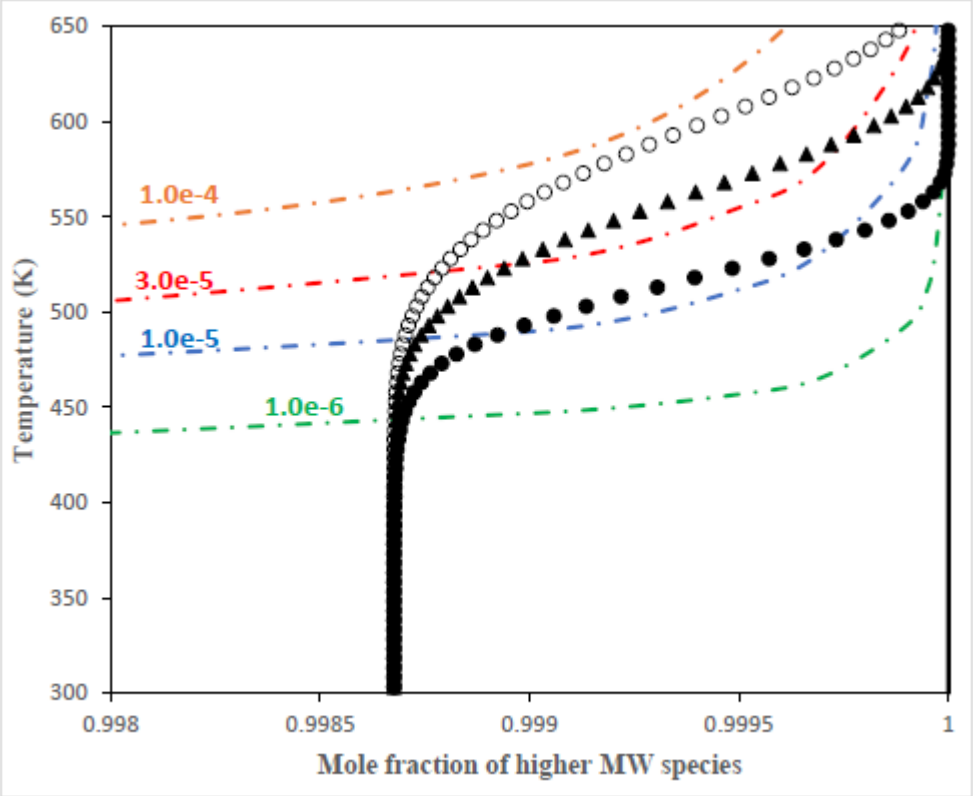

Figure 6.10 Effect of carrier gas flow rate on anthracene evaporation path during heat treatment of a 50 g pitch sample (assumed as one-phase glassy isotropic liquid); Solid circle: 2300 cm^3/min, solid triangle: 560 cm^3/min, and empty circle: 230 cm^3/min (heating rate: 50°C/h and $\phi_i s$: 1).

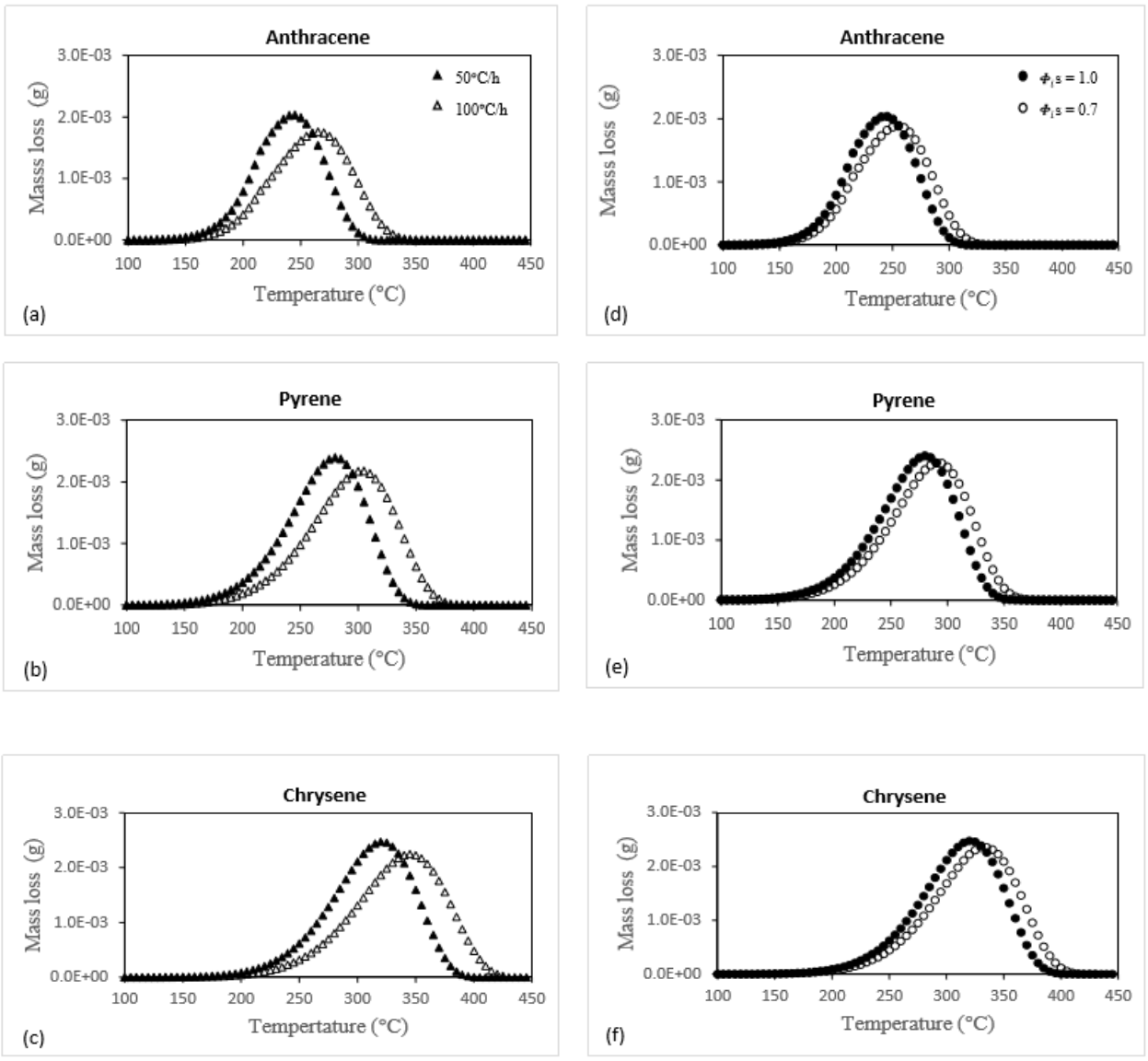

Figure 6.11 Estimated mass loss of anthracene, pyrene and chrysene versus temperature for: different heating rates at carrier gas flow rate of 2300cm^3/min and ϕ_is = 1 (a – c) and different values of ϕ_is parameters (0.7 and 1) at heating rate 50°C/h, carrier gas flow rate 2300 cm^3/min (d – f).

Next step of CTP primary carbonization (350 – 450°C), where the mesophase formation starts, has been modeled based on the defined procedure in Section 2.2.3 by arranging the prototype oligomerization reactions between available reactive PAHs and thermal cracking reactions listed in Table 6.2.

Degree of advancement of prototype reactions as model parameters are determined by following the explanations in Section 6.2.2.4 and using available experimental data (obtained by Bouchard [246]) for the amount of released condensable (volatile PAH) and non-condensable (H_2 and CH_4) matters in this range of temperature. In the present work, these model parameters has been only determined for carbonization treatment with 50°C/h heating rate since the Bouchard's experiments are limited. Calculated amount of volatile matter emitted from the 50 g coal tar pitch sample during mesophase formation step of heat treatment as well as MWD of the pitch residue, shown in Figs. 6.12 and 6.13, respectively, are comparable with experimental data of Bouchard and trend of MWD changes investigated by Greinke [87] (seen in Fig. 6.2).

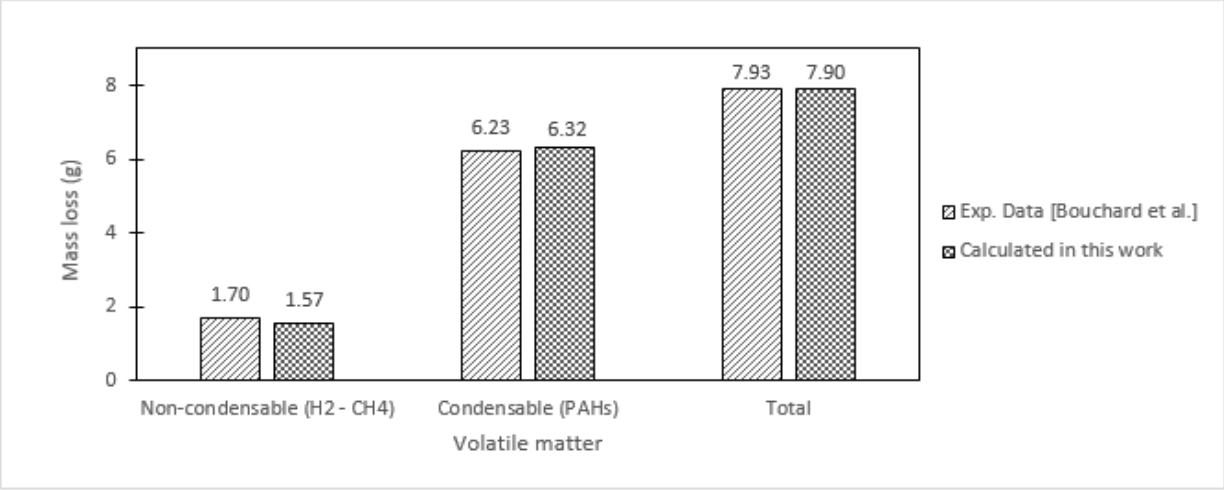

Figure 6.12 Calculated released volatile matter from a 50 g coal tar pitch heat treated from T_{amb} to 450°C with heating rate of 50°C/h.

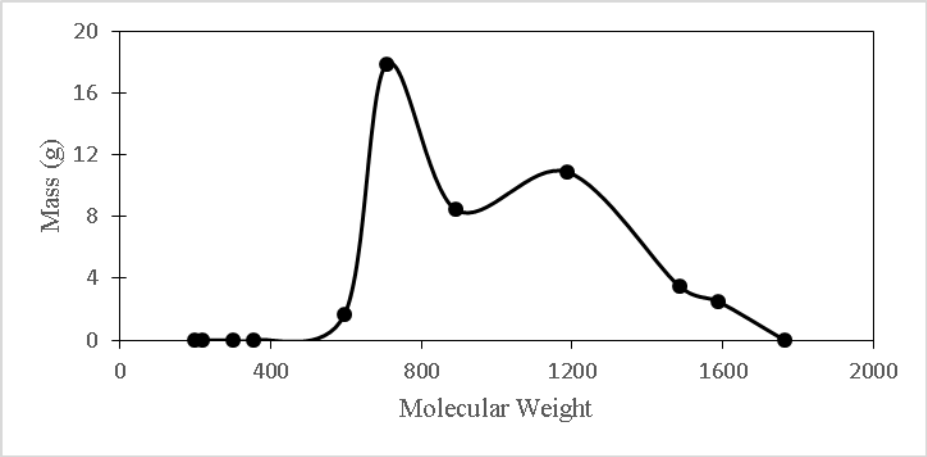

Figure 6.13 Calculated molecular weight distribution of the residue of a 50 g mass coal tar pitch at the end of mesophase formation step of carbonization process with heating rate of 50°C/h.

Modeling of semi-coke and coke formation steps (450 - 550°C) is performed by arranging the prototype polymerization reactions proposed in Table 6.3. The measured values by Bouchard [246] for the amount of released condensable (volatile PAH) and non-condensable (H_2 and CH_4) matters in this range of temperature are the criteria to fit the degree of advancement of prototype reactions as the model parameter in this step. Calculated mass loss either by volatilization of produced low MW PAHs due to thermal cracking or emission of hydrogen and methane through dehydrogenation reactions and thermal cleavage of side chains from aromatic rings are shown in Fig. 6.14. Calculated MWD of CTP at the end of semi-coke formation shown in Fig. 6.15 is consistent with that obtained by Greinke [87]. Fig. 6.16 shows MWD at 550°C when the initial plane of coke is built up.

It is important to point out that the proposed model can be applied to estimate the mass loss of CTP during the primary carbonization by using any available set of experimental data, not necessarily Bouchard's data, to calibrate the model and following the overall procedure defined above (with some changes in certain aspects of the model).

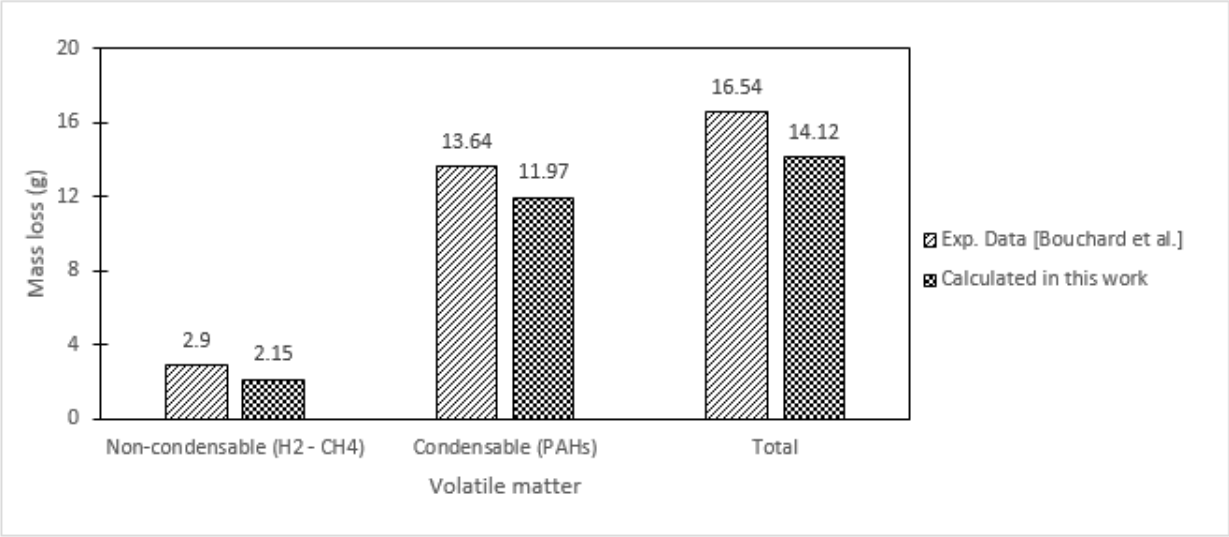

Figure 6.14 Calculated released volatile matter from a 50 g coal tar pitch in temperature range of Tamb - 550°C during carbonization process with heating rate of 50°C/h.

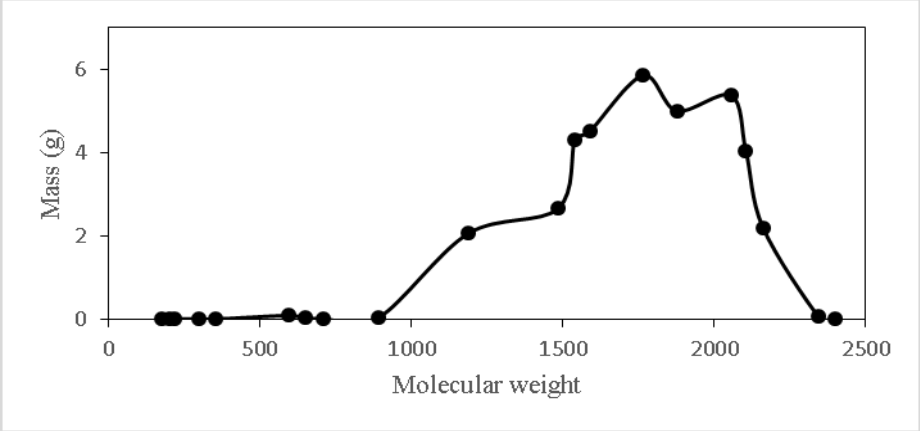

Figure 6.15 Calculated molecular weight distribution of the residue of a 50 g coal tar pitch at the end of semi-coke formation step of carbonization process with heating rate of 50°C/h.

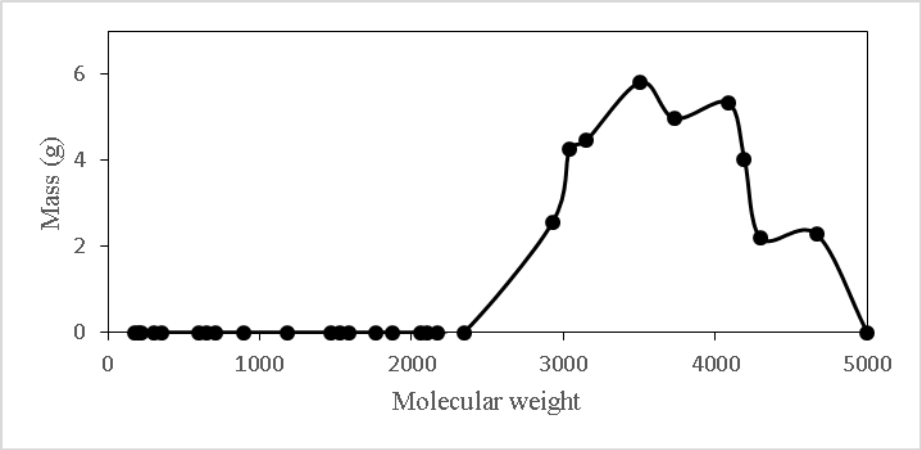

Figure 6.16 Calculated molecular weight distribution of the residue of a 50 g coal tar pitch during coke formation step (where the temperature is about 550°C) of carbonization process with heating rate of 50°C/h.

6.3.2.2 **Estimation of energy requirement of different steps of CTP primary carbonization**

Required energy in the first step of CTP heat treatment (25 to 350°C) can be calculated by following the procedure explained in Sections 6.2.3 and 6.2.4. This energy is required both to increase the temperature of pitch to any given temperature and to meet the mass changes at that temperature estimated in section 6.3.2.2. Starting with a 50 g sample of CTP (MWD shown in Table 6.6) at room temperature, calculated total required energy at any given temperature in the range of 25-350°C has been presented in Fig. 6.17. The results obtained in Section 6.3.2.1 for mass changes of CTP with temperature (every 5°C) has been used in this calculation.

Calculation of required energy in next steps of CTP heat treatment (beyond 350°C) needs the estimation of enthalpies of large PAHs oligomer species and semi-coke crystallite appearing during mesophase and semi-coke formation steps, respectively:

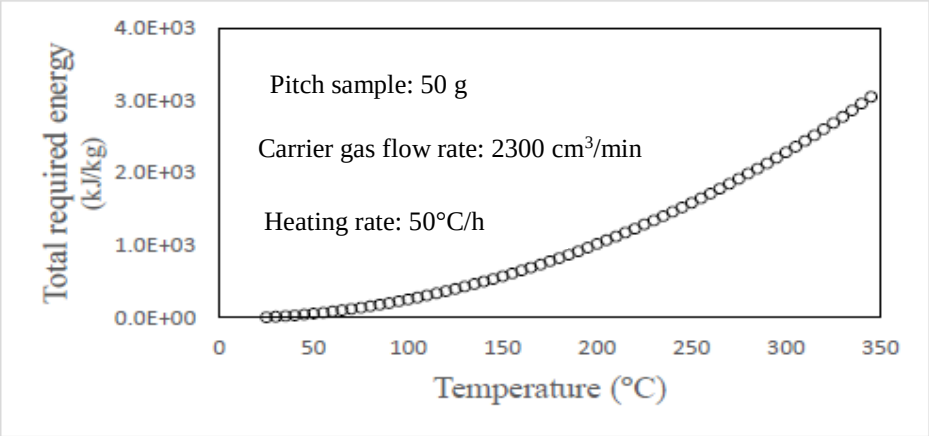

Figure 6.17 Total required energy in first step of carbonization (25-350°C) of a 50 g CTP sample (using ϕ_is = 1, heating rate: 50°C/h and carrier gas flow rate : 2300 cm^3/min).

-In the present work, estimation of enthalpies of any PAHs is based on critical assessment presented in our previous work [Chapter 4]. Due to the lack of experimental data, the application of developed model to estimate the thermodynamic properties of PAH oligomers has only been justified for a limited number of PAH oligomers.

-As it was proposed in Section 6.2.3, the enthalpy of semi-coke crystallite (with the aim of required energy calculation in semi-coke formation step in temperature range 450-550°C) can be estimated by applying developed coke model by Ouzilleau et al. [257]. In their model, the perfectly parallel plane (shown in Fig.6.4) whose enthalpy of stacking to be zero are assumed in Gibbs energy calculations. However some considerations has to be taken into account in switching from the formalism for estimation of enthalpy of the large planes of oligomer PAHs (established in Chapter

4) in mesophase formation step to Ouzilleau's formalism for enthalpy estimation of the idealized crystallite structure in semi-coke formation step. In other word, transforming such a large plane of high MW PAH oligomers to idealized semi-coke crystallite (satisfying Ouzilleau's model) requires energies to bring them to the configuration shown in Fig. 6.4 and to parallelize them.

However, in the present work, calculation of the required energy in CTP primary carbonization process above 350°C, where the above mentioned considerations are needed, has not been presented and left for future works.

6.4 Conclusion and outlook

Mass and energy changes of coal tar pitch occurring during primary carbonization process can be estimated by applying the present thermodynamic-kinetic model. Model estimations on mass losses of CTP in different steps of primary carbonization, i.e. vaporization, mesophase and semi-coke formation steps are in good agreement with corresponding experimental data. A strength of the current work is that it predicts the emission of volatile compounds even at low temperatures. The proposed model is able to evaluate the partial pressure changes of emitted low MW PAHs during heat treatment of the typical CTP. Estimation of molecular weight distribution changes of residual pitch through thermal treatment (up to 550°C) of CTP is consistent with that experimentally investigated by utilizing gel permission chromatography technique. The strength and innovation of the present work for theoretical evaluation of the effect of the important parameters during carbonization of pitch, such as the heating rate of the pitch and the flow rate of the carrier gas, on the emission rate of volatile matter was demonstrated. The present model was applied to calculate the enthalpy changes of coal tar pitch (with the aim of process energy requirement calculations) in early stage of the primary carbonization process, below 350°C. A discussion was given on

complexity in estimating the enthalpy changes of residual pitch during mesophase and semi-coke formation as part of CTP carbonization, above 350°C.

Obviously, due to the complex nature of CTP and the primary carbonization process, some hypothesis and simplifications were needed to make the modelling of the process possible, which resulted in a certain number of limitations and weaknesses in the present model as follows:

- The first limitation is related to the neglecting the role played by the impurities, such as sulfur, nitrogen, and oxygen etc., as well as non-PAHs (heterocyclic compounds) which are usually found in CTP, in carbonization process. It has been well established that the intermediate and final products of the primary carbonization, i.e. mesophase and semi-coke, are composed of polyaromatic molecules mutually cross-linked by a medium composed of carbon functions containing heteroatoms (e.g. nitrogen, sulfur, and oxygen) which enter the process through available heterocyclic compounds in the pitches [37]. These heteroatoms (N_2 and O_2) are important for coke-pitch interactions in anode production. Indeed, in the present model the effect of the ratio of cross-linking heteroatoms (e.g. sulfur, nitrogen and oxygen) to hydrogen atoms of precursor carbon materials (CTP in this work) on the efficiency of the primary carbonization and the quality of the final product was ignored by neglecting the presence of the impurities and heterocyclic compounds in coal tar pitch. Hence, one aspect that will be treated in future work is development of a more appropriate model to predict the physical and chemical evolutions occurring during primary carbonization of any source of CTP containing heteroatoms.

- In the mass and energy balance calculations, the temperature of the condensed pitch was assumed to become equal and uniform in all directions instantaneously at each iterations after increasing the temperature of the pitch by a heat treatment. This assumption is not compatible with what really

happens in industrial processes. So, it is recommended to improve the predictive capacity of the present model by considering adequate heat transfer equations for the calculation of temperature gradients in condensed pitch.

- Only one set of experimental data (Bouchard's experiments) was found in the literature to calibrate the model. Although the model developed seems to be versatile enough to reproduce the experimental data for the heat treatment of different types of CTP in different operating conditions, it is recommended to design and run a certain number of experiments reporting the changes of both the mass of residue pitch and the composition of volatile species throughout CTP primary carbonization in order to extend the application of the proposed model to predict different experimental data sets.

- The paucity of experimental data made it difficult to assess the uncertainties associated with the process energy requirement calculations in 25-350°C temperature range. Performing some CTP heat treatment experiments in order to generate a data set including energy consumption of different steps of primary carbonization process for model justification purposes is recommended.

- Following the discussion in Section 3.2.2 presented the weakness of the present model to estimate the enthalpy changes of residual pitch during mesophase and semi-coke formation steps of primary carbonization process, another important aspect as future work is to extend the present model so that it can be applied to calculate the required energy for heat treatment of CTP beyond 350°C.

In the longer term, the developed thermodynamic-kinetic model will serve as the basis for future work to simulate any industrial process (such as anode baking, cathode production, and ramming paste processes in aluminum industries) in which the primary carbonization is involved.

6.5 Acknowledgements

This project was supported by the Natural Sciences and Engineering Research Council of Canada, Alcoa, Hydro Aluminium, Rio Tinto and Constellium.

CHAPTER 7 GENERAL DISCUSSION

The main goal of the present thesis can be summarized as follows:

Predict the thermodynamic properties of the final products and the emissions of volatiles in carbon material production process, using a basic kinetic model, for different coal tar pitches used as precursors.

As a reminder and conclusion from previous chapters (Introduction and Literature Review), the capacity of thermal transformation of coal tar pitches (CTP) to carbon materials (CM) as well as their specific binding properties make CTPs an important source of precursors in CM production processes. Among these processes, the production of green anode blocks and prebaked anodes is very important in Québec due to its intensive aluminum production. Also, the calcining of carbon ramming pastes used between cathode blocks in aluminum electrolysis cells is important for the same industry.

The specifications of CTPs have a major effect on both the properties of the final product and the quality and quantity of the gaseous (hazardous) mixtures that evolve during the thermal transformation of CTPs in both CM production and ramming processes. The present thesis thus aimed to provide a semi-quantitative understanding of the CTP thermal transformation process to industries that depend on this process. In this way, estimation of volatile matter emissions (including genotoxic compopunds) and energy consumption of the CTP carbonization process as well as prediction of CMs will be possible which can be useful to develop an efficient green process.

Based on the main goal of the present thesis, the first step was to simplify the modeling approach by a careful selection of constitutive species, which represent the major characteristics of the system. The second step was to gain a better understanding of the thermodynamic properties of

polycyclic aromatic hydrocarbon (PAH) monomers and oligomers, which are the main constituents of CTP. It was found that the current knowledge of the thermodynamic properties (such as specific heat and standard entropy and enthalpy of formation) of PAHs, which first proposed by Richard and Helgeson [111], are not defined in a consistent manner. It suffers from a lack of consistency to reconcile phase transition data and the computation of the vapor pressures using the Gibbs energy functions of the condensed and gaseous phases of a given PAH compound. In addition, their model does not take into consideration structural anomalies in some solid PAH compounds, such phenanthrene and pyrene that are associated with peaks in the temperature dependence of the heat capacity curves. The development of an approach aimed at improving the Richard and Helgeson's method for predicting the thermodynamic properties of PAHs in a consistent manner thus became one of the most important goals of the present thesis and led to the writing of the first paper (Chapter 4). The two objectives of the paper were to apply the CALPHAD approach to estimate the phase transition data and vapor pressure values of PAH compounds consistently with experimental data, and to use CEF to predict heat capacity (as a function of the temperature) of PAHs exhibiting an unusual phase transition in the solid state.

A comprehensive literature review of the thermal transformation of the pitches provided information on the thermodynamics and phase behavior of the carbonaceous materials during this transformation. Brooks and Taylor first demonstrated that the mesophase is observed as an intermediate phase during the thermal transformation of the pitches and aromatic compounds to coke. The characterization of the mesophase showed that it is mainly composed of fully condensed high molecular weight PAHs, which are generated by polymerization reactions between basic compounds in CTP occurring during the transformation process. The molecular ordering in these intermediate phases lies between that of a solid and that of an isotropic liquid. Studying the phase

behavior of the mesophase in CTP is a critical step for optimizing this process. The comprehensive literature review of a large number of studies on the thermodynamics of the carbonaceous mesophase revealed the work of Hu and Hurt [127], which proved to be key to the present thesis. Hu and Hurt developed the Gibbs free energy model for mesophase-containing pitches based on non-ideal solutions and liquid crystal behaviors of the mesophase. They predicted the equilibrium configuration of pitch systems by equating the chemical potential of each compounds in the isotropic liquid and the mesophase phases in equilibrium derived from the Gibbs free energy function. The numerical (stochastic) method used by Hu and Hurt to minimize the absolute difference between both sides of these equations is difficult to implement from a technical point of view as the orientation Gibbs energy of the mesophase is defined through the second Legendre function. Due to the limitations in their formalism, they only applied it to three experimental data sets. Following the work of Hu and Hurt, the path to be taken was to propose a new thermodynamic approach to describe the phase behavior of mesophase-containing pitches while overcoming the above-mentioned limitations. This led to the writing of a second paper (Chapter 5). The new approach described in this paper proposes to estimate the equilibrium configuration of a mesophase-containing pitch system by minimization of Gibbs free energy function developed by Hu and Hurt, directly, utilizing NOMAD (Nonlinear Optimization with the MADS algorithm), a precise and robust numerical technique.

Lastly, it is important to discuss the place of the thermodynamic-kinetic model (Chapter 6) in the present thesis. Prior to the present thesis, investigations of the thermal transformation (carbonization) of pitch to coke had been qualitative in most aspects. The thermodynamic developments described in Chapters 4 and 5 focus on one aspect of the process: the impact of temperature. The combination of a thermodynamic description and kinetic studies to incorporate

the effect of time is needed to achieve the main goal of the present thesis: i.e. predicting the relationship between the properties of CTPs and the important target variables of the transformation process, i.e. the properties of the product and the compositions and heating values of volatile species. The proposed approach is based on defining thermodynamic and kinetic equations for the vaporization and the condensation processes simply representing the numerous complicated phenomena happening during the primary carbonization process and by reducing to the minimum the required time-dependent variables (such as considering only a heating rate). The work presented herein is the first to describe a semi-quantitative knowledge that can be used to simulate and optimize the primary carbonization process and reflects the highly innovation nature of the present thesis.

CHAPTER 8 CONCLUSION

In this thesis, for the first time, a thermodynamic model for the prediction of thermodynamic properties of PAH compounds, using the CALPHAD approach, was developed. The heat capacity functions and standard thermodynamic properties of PAHs in solid, liquid, and gas states initially calculated based on group additivity algorithms (first proposed by Richard and Helgeson), are optimized by applying the CALPHAD approach where all thermodynamic data are rendered consistent with phase transitions and vapor pressure data. Some PAH compounds exhibit heat capacity anomaly in the solid state. An anomalous absorption of energy is found in the vicinity of the temperature at which the anomalous behavior appears and results in a big jump in temperature-dependent heat capacity function of these PAHs in the crystalline phase. The heat capacity function of these PAHs was modeled using the Compound Energy Formalism (CEF). The proposed model offers an improvement of the predictive capacity compared to previous methods predicting thermodynamic properties of PAHs at typical temperature ranges of the primary carbonization process.

In this doctoral project, for the first time, a thermodynamic approach for phase behavior estimation of mesophase-containing pitches, by Gibbs free energy minimization (using MADS algorithms), was developed. The Gibbs energy function of mesophase pitches, first proposed by Hu and Hurt, is minimized, directly, to describe well equilibrium configuration of binary, ternary, and multi-component PAH mixtures. The models enables predicting phase diagram of the specific systems, which exhibit the miscibility gap.

In the present thesis, for the first time, a new simplified approach for thermodynamic-kinetic modelling of the primary carbonization process was presented. This model makes it possible to

estimate emission rate of volatile compounds and mass and enthalpy changes of CTP which goes under thermal treatment. The effect of important parameters in carbonization of pitch, such as heating rate of pitch and carrier gas flow rate, on emission rate of volatile matter can be theoretically evaluated by applying the proposed model. The model developed is capable to estimate the energy requirement for thermal treatment of coal tar pitch up to 350°C.

This chapter discusses the following aspects: A summary of the work and its limitations and recommendations for future research. The summary of the work emphasizes the main innovations and contributions of the work to the advancement of carbon science and the development of related technologies. The limitations discussed provide a clear understanding of the scope of the conclusions in order to avoid extrapolating them beyond their fundamental limit. The last part highlights some proposals for extending and improving the work presented herein and demonstrates the multidisciplinary and collaborative potential of the work.

8.1 Summary of the work

In the framework of the present thesis, a new thermodynamic model for predicting the thermodynamic properties of polycyclic aromatic hydrocarbon (PAH) compounds, which are major constituents of coal tar pitch (CTP), is proposed. It is based on the group additivity algorithms developed by Helgeson et al. [111] to predict the thermodynamic properties of any given PAH compound using the thermodynamic properties of groups that contribute to the compounds. As a reminder, the thermodynamic properties of the group constituents were calculated using the thermodynamic properties of low MW PAHs, with enough experimental data to use them as reference compounds. The CALPHAD approach was applied for the first time to optimize the standard thermodynamic properties of PAHs derived from the group contribution method, where

all data are rendered consistently with the phase transition and vapor pressure data. Good agreement and a major improvement were found comparing to experimental data and the results from previous predictive methods. As a specific case, the heat capacity of PAHs exhibiting an unusual phase transition in the solid state was predicted using Compound Energy Formalism (CEF) and was validated using a set of experimental data. The proposal of utilizing the CALPHAD approach and CEF to predict the thermodynamic properties of PAHs in the temperature ranges of carbonization process is the first of the major contributions of the present thesis (Paper 1 presented in Chapter 4).

With respect to the critical technological role played by the mesophase as an intermediate phase appearing during thermal treatment of CTP in CM production processes, a new approach for describing the phase behavior of mesophase-containing pitches is proposed (Paper 2 presented in Chapter 5). Based on the thermodynamic theory developed by Hu and Hurt [127] for the Gibbs energy calculation of mesophase-containing pitch systems, proposal of a new approach for minimization of the Gibbs energy is one of the key advances of the present thesis. NOMAD and MATLAB Software were utilized to apply the proposed approach for description of the equilibrium configuration of the mesophase-containing pitches. In fact, the model developed enables estimating the reversible phase transition of the mesophase upon temperature cycling, the molecular weight distribution of species in the phases in equilibrium, and phase behavior of the specific systems exhibiting miscibility gaps.

A final significant contribution of the work reported in the present thesis is the thermodynamic-kinetic model developed for predicting the physical and chemical changes occurring during the primary carbonization process (Paper 3 presented in Chapter 6). This model, which combines a set

of thermodynamics and kinetics notions, is the main result of the present thesis. The partial pressures of the volatiles emitted as well as the mass and enthalpy changes of residue pitch that undergoes thermal treatment can be estimated by applying the proposed model. For the first time the effect of the important parameters in carbonization of pitch, such as the heating rate of the pitch and the flow rate of the carrier gas, on the emission rate of volatile matters has been evaluated theoretically. There is a good agreement between results obtained and the measurements, and observations during the CTP heat treatment experiments.

8.2 Limitations of the work

Obviously, the models proposed in the present thesis, whether to predict the thermodynamic properties of PAH compounds as major constituents of CTP or to estimate the physical and chemical changes occurring during the heat treatment of CTP, have a certain number of weaknesses and limitations.

The first limitation is related to the neglecting the role played by the impurities, such as sulfur, nitrogen, and oxygen etc., as well as non-PAHs (heterocyclic compounds) which are usually found in CTP, in carbonization process. It has been well established that the intermediate and final products of the primary carbonization, i.e. mesophase and semi-coke, are composed of polyaromatic molecules mutually cross-linked by a medium composed of carbon functions containing heteroatoms (e.g. sulfur and oxygen) which enter the process through impurities and (or) heterocyclic compounds in the pitches. Indeed, in the present model the effect of the ratio of cross-linking heteroatoms (e.g. sulfur, nitrogen and oxygen) to hydrogen atoms of precursor carbon materials (CTP in this work) on the efficiency of the primary carbonization and the quality of the

final product was ignored by neglecting the presence of the impurities and heterocyclic compounds in coal tar pitch.

The approach proposed in Chapter 4 for the prediction of the thermodynamic properties of PAHs, which suffers from a lack of experimental data given that the CALPHAD approach could not be used, needs information on the resonance energy of the molecules. This information is available in the literature for a limited number of PAHs. However this is not the case for PAH oligomers, which are of great interest in the present thesis. One proposal presented in the present thesis is to estimate the resonance energy of these oligomers roughly as a factor of the resonance energy of the corresponding monomers. However, the accuracy of this approach has to be justified by comparing the estimated thermodynamic properties of these oligomers with the experimental data, which was not possible for all cases due to the lack of experimental data.

Another limitation concerns the assumed uniform temperature profile of the condensed pitch in the thermodynamic-kinetic modeling of the CTP heat treatment process (as presented in Chapter 6). In the mass and energy balance calculations, the temperature of the residue pitch is assumed to become equal and uniform in all directions instantaneously at each iterations after increasing the temperature of the pitch by a heat treatment. This assumption is not compatible with what really happens in industrial processes.

The next limitation is the approach used to calibrate the thermodynamic-kinetic model presented in Chapter 6. Although the model developed seems to be versatile enough to reproduce the experimental data for the heat treatment of different types of CTPs in different operating conditions, only one set of experimental data was available in the literature to calibrate the model

(Bouchard's experiments). As such, some new CTP heat treatment experiments for validation purposes will need to be designed and performed.

Lastly, there are a number of limitations with respect to the application of the proposed thermodynamic-kinetic model to estimate the energy requirements of the different steps of CTP primary carbonization. The paucity of experimental data makes it difficult to assess the uncertainties associated with the calculated required energy of the process in the 25-350°C temperature range. Moreover, as was discussed in Chapter 6, some considerations have to be taken into account for energy balance calculations above 350°C. Indeed, switching from the formalism proposed in the present thesis for the enthalpy calculations of PAH oligomers (available in the mesophase) to the formalism developed by Ouzilleau et al. for the enthalpy calculations of semi-coke needs further research, which was beyond the scope of the present thesis.

8.3 Recommendations for future research

This section discusses recommendations aimed at mitigating the limitations associated with the proposed models (presented in Section 8.2) and the potential of applying the research presented herein to future research and development.

- Ignoring the presence of impurities such as sulfur, oxygen and nitrogen in the CTP constituents limits the applicability of both proposed models in Chapters 4 and 6. Hence, one aspect that will be treated in future work is development of a more appropriate model to predict the physical and chemical evolutions occurring during primary carbonization of any source of CTP containing heteroatoms and impurities.

- It is recommended that the mass and energy balance calculations in heat treatment process modeling be modified by considering adequate heat transfer equations for the calculation of

temperature gradients in condensed pitch. In fact, substituting the former assumed uniform temperature with a predicted temperature profile of residue pitch at each iterations in these calculations will improve the predictive capacity of the proposed thermodynamic-kinetic model.

- In the context of Chapter 6, only reported experimental data set of Bouchard et al. was used to justify the application of the thermodynamic–kinetic model to evaluate the effect of CTP specification, the heating rate and the flow rate of the carrier gas in the CTP heat treatment process on mass losses occurring during the process. It would be interesting to extend the application of the proposed model to predict the other data set of experimental data reporting the mass of the residue pitch, the composition and heating value of volatile species as well as the energy consumption of the process that vary with time and temperature throughout the process. However, it would first be necessary to design and run a certain number of experiments to analyze the important target variables of the primary carbonization process.

- The scope of this work could be extended by attempting to estimate the enthalpy of residue pitch at heat treatment temperatures exceeding 350°C. An approach will have to be developed to estimate the enthalpy of the pseudo transition of PAH oligomers to semi-coke (that occurs at 450°C as fixed in this work). This would make it possible to predict the energy requirements of the different steps of the primary carbonization process.

- The thermodynamic-kinetic model of CTP primary carbonization will serve for future developments in carbon science-based technologies. It could be integrated in carbon material production processes (such as anode baking, cathode production or ramming paste processes contributing in electrolytic production of aluminum) for simulation and optimization purposes.

REFERENCES

[1] L. S. Singer, "The mesophase in carbonaceous pitches," *Faraday discussions of the Chemical Society,* vol. 79, pp. 265-272, 1985.

[2] G. and C. M. Co., "Webster's New Collegiate Dictionary," 1956.

[3] I. Lewis, "Chemistry of pitch carbonization," *Fuel,* vol. 66, pp. 1527-1531, 1987.

[4] I. Lewis and L. Singer, "Carbonization of aromatic hydrocarbons.[18 refs]," *Am. Chem. Soc., Div. Fuel Chem., Prepr.;(United States),* vol. 13, 1969.

[5] I. Mochida, K.-i. Fujimoto, and T. Oyama, *Chemistry in the production and utilization of needle coke* vol. 24: Marcel Dekker, Inc: New York-Basel-Hong Kong, 1994.

[6] K. Janerka, J. Jezierski, M. Stawarz, and J. Szajnar, "Method for Resistivity Measurement of Grainy Carbon and Graphite Materials," *Materials,* vol. 12, p. 648, 2019.

[7] G. Wang and S. Eser, "Molecular composition of the high-boiling components of needle coke feedstocks and mesophase development," *Energy & fuels,* vol. 21, pp. 3563-3572, 2007.

[8] J. P. Abrahamson, R. T. Wincek, and S. Eser, "Scheme for Hydrotreatment of fluid catalytic cracking decant oil with reduced hydrogen consumption and high needle coke yield upon carbonization," *Energy & Fuels,* vol. 30, pp. 8150-8155, 2016.

[9] G. Deepak Kumar and S. Singh Arora, "Evaluation of Physico-Chemical, Thermal and Mechanical Properties of Sintered Graphite and Mesophase Formulations," *J Material Sci Eng,* vol. 6, pp. 2169-0022.1000314, 2017.

[10] M. Endo, C. Kim, K. Nishimura, T. Fujino, and K. Miyashita, "Recent development of carbon materials for Li ion batteries," *Carbon,* vol. 38, pp. 183-197, 2000.

[11] S. Flandrois and B. Simon, "Carbon materials for lithium-ion rechargeable batteries," *Carbon,* vol. 37, pp. 165-180, 1999.

[12] S. Kumar and M. Srivastava, "Mesophase formation behavior in petroleum residues," *Carbon letters,* vol. 16, pp. 171-182, 2015.

[13] S. K. Martha, J. O. Kiggans, J. Nanda, and N. J. Dudney, "Advanced lithium battery cathodes using dispersed carbon fibers as the current collector," *Journal of The Electrochemical Society,* vol. 158, pp. A1060-A1066, 2011.

[14] S. Somiya, *Handbook of advanced ceramics: materials, applications, processing, and properties*: Academic press, 2013.

[15] S. Yoshimura and R. P. H. Chang, *Supercarbon: synthesis, properties and applications* vol. 33: Springer Science & Business Media, 2013.

[16] Y. Korai, S. Ishida, F. Watanabe, S.-H. Yoon, Y.-G. Wang, I. Mochida, *et al.*, "Preparation of carbon fiber from isotropic pitch containing mesophase spheres," *Carbon,* vol. 35, pp. 1733-1737, 1997.

[17] S. Otani, "Carbonaceous mesophase and carbon fibers," *Molecular Crystals and Liquid Crystals,* vol. 63, pp. 249-263, 1981.

[18] L. Wang and A. Rey, "Pattern selection mechanism in mesophase carbon fibres," *Modelling and Simulation in Materials Science and Engineering,* vol. 5, p. 67, 1997.

[19] S.-H. Yoon, Y. Korai, and I. Mochida, "Spinning characteristics of mesophase pitches derived from naphthalene and methylnaphthalene with HF/BF3," *Carbon,* vol. 31, pp. 849-856, 1993.

[20] B. Rand, S. P. Appleyard, and M. F. Yardim, *Design and control of structure of advanced carbon materials for enhanced performance* vol. 374: Springer Science & Business Media, 2012.

[21] W. Zhang, J. T. Andersson, H. J. Räder, and K. Müllen, "Molecular characterization of large polycyclic aromatic hydrocarbons in solid petroleum pitch and coal tar pitch by high resolution MALDI ToF MS and insights from ion mobility separation," *Carbon,* vol. 2015 v.95, pp. pp. 672-680, 2015-12 2015.

[22] J. Lauzon-Gauthier, "Multivariate latent variable modelling of the pre-baked anode manufacturing process used in aluminum smelting," M. Sc. Thesis, Laval University: Québec city, Canada, 2011.

[23] J. Brooks and G. Taylor, "The formation of graphitizing carbons from the liquid phase," *Carbon,* vol. 3, pp. 185-193, 1965.

[24] P. J. Wojtowicz, P. Sheng, and E. Priestley, *Introduction to liquid crystals*: Springer, 1975.

[25] F. Cataldo, O. Ursini, G. Angelini, and S. Iglesias-Groth, "On the way to graphene: the bottom-up approach to very large PAHs using the Scholl reaction," *Fullerenes, Nanotubes and Carbon Nanostructures,* vol. 19, pp. 713-725, 2011.

[26] J. D. Brooks and G. Taylor, "The formation of some graphitizing carbons," *Chemistry and physics of carbon,* vol. 4, pp. 243-286, 1968.

[27] D. Cummings and R. Diefendorf, "The chemical vapor deposition of carbon on graphite surfaces," in *16th Biennial Conference on Carbon,* 1983.

[28] I. Lewis, "Thermal polymerization of aromatic hydrocarbons," *Carbon,* vol. 18, pp. 191-196, 1980.

[29] J.-P. Farant and M. Gariépy, "Relationship between benzo [a] pyrene and individual polycyclic aromatic hydrocarbons in a Söderberg primary aluminum smelter," *American Industrial Hygiene Association Journal,* vol. 59, pp. 758-765, 1998.

[30] R. Paulus and S. Meseguer, "An ecofriendly ramming paste for the aluminum electrolysis cell," in *Proceedings of the 129th TMS Annual Meeting, Toronto, Canada*, 2001.

[31] L. Tian, F. s. Xu, G. Xie, R. x. Li, and S. y. Li, "A More Ecofriendly Cold Ramming Paste for an Aluminum Electrolysis Cell with Phenol–Formaldehyde Resin As Binder," *Industrial & Engineering Chemistry Research,* vol. 52, pp. 1750-1755, 2013.

[32] N. Oumarou, D. Kocaefe, Y. Kocaefe, and B. Morais, "Transient process model of open anode baking furnace," *Applied Thermal Engineering,* vol. 107, pp. 1253-1260, 2016.

[33] R. D. Heidenreich, W. Hess, and L. Ban, "A test object and criteria for high resolution electron microscopy," *Journal of Applied Crystallography,* vol. 1, pp. 1-19, 1968.

[34] K. Lafdi, S. Bonnamy, and A. Oberlin, "TEM studies of coal tars: crude tar and its insoluble fractions," *Carbon,* vol. 28, pp. 57-63, 1990.

[35] I. Lewis, "Chemistry and development of mesophase in pitch," *Journal de Chimie Physique,* vol. 81, pp. 751-758, 1984.

[36] S. L. Sauter, L. R. Murphy, and J. J. Hurrell, "Prevention of work-related psychological disorders: A national strategy proposed by the National Institute for Occupational Safety and Health (NIOSH)," *American Psychologist,* vol. 45, p. 1146, 1990.

[37] A. Oberlin and S. Bonnamy, "Colloidal and Supramolecular Aspects," *Chemistry & Physics of Carbon,* vol. 26, p. 1, 1999.

[38] Available: https://www.steel.org/making-steel/how-its-made/processes/processes-info/coke-production-for-blast-furnace-ironmaking

[39] *NIST Chemistry WebBook*. Available: http://webbook.nist.gov/chemistry/

[40] A. Raðenoviæ, "Properties of carbon anode components for aluminium production," *Nafta,* vol. 63, pp. 111-114, 2012.

[41] G. R. Romovacek, "Estimating the concentration of secondary quinoline insolubles," *Carbon,* vol. 24, pp. 417-421, 1986.

[42] H. Marsh, C. Latham, and E. Gray, "The structure and behaviour of QI material in pitch," *Carbon,* vol. 23, pp. 555-570, 1985.

[43] J. Barr and I. Lewis, "Characterization of pitches by differential scanning calorimetry and thermomechanical analysis," *Thermochimica Acta,* vol. 52, pp. 297-304, 1982.

[44] B. Rand and P. Shepherd, "Glass transformations in some pitch materials," *Fuel,* vol. 59, pp. 814-816, 1980.

[45] R. Wallouch, H. Murty, and E. Heintz, "Pyrolysis of coal tar pitch binders," *Carbon,* vol. 10, pp. 729-735, 1972.

[46] A. D, "Standard Test Method for Toluene-Insoluble (TI) Content of Tar and Pitch," *Annual Book of Standards*.

[47] P. N. Kuznetsov, E. S. Kamenskiy, and L. I. Kuznetsova, "Comparative study of the properties of the coal extractive and commercial pitches," *Energy & Fuels,* vol. 31, pp. 5402-5410, 2017.

[48] L. Shoko, "Effects of the chemical composition of coal tar pitch on dimensional changes during graphitization," 2014.

[49] B. Rand, "Handbook of composites; Vol I: Strong fibers,(Edited by W. Watt and BV Pirov), Chap. 13, p 495," ed: Elsevier, 1985.

[50] I. Lewis, "Chemistry of carbonization," *Carbon,* vol. 20, pp. 519-529, 1982.

[51] A. Oberlin, "Carbonization and graphitization," *Carbon,* vol. 22, pp. 521-541, 1984.

[52] A. Oberlin and S. Bonnamy, "Carbonization and graphitization," *Graphite and Precursors,* pp. 199-220, 2001.

[53] D. Cottinet, P. Couderc, J. Saint Romain, and P. Dhamelincourt, "Raman microprobe study of heat-treated pitches," *Carbon,* vol. 26, pp. 339-344, 1988.

[54] R. E. Franklin, "The structure of graphitic carbons," *Acta crystallographica,* vol. 4, pp. 253-261, 1951.

[55] R. E. Franklin, "Crystallite growth in graphitizing and non-graphitizing carbons," *Proceedings of the Royal Society of London. Series A. Mathematical and Physical Sciences,* vol. 209, pp. 196-218, 1951.

[56] K. Oshida and S. Bonnamy, "Primary carbonization of an anisotropic 'mesophase'pitch compared to conventional isotropic pitch," *Carbon,* vol. 40, pp. 2699-2711, 2002.

[57] P. Lespade, A. Marchand, M. Couzi, and F. Cruege, "Caracterisation de materiaux carbones par microspectrometrie Raman," *Carbon,* vol. 22, pp. 375-385, 1984.

[58] J. Rouzaud, A. Oberlin, and C. Beny-Bassez, "Carbon films: structure and microtexture (optical and electron microscopy, Raman spectroscopy)," *Thin Solid Films,* vol. 105, pp. 75-96, 1983.

[59] P. Ouzilleau, A. E. Gheribi, P. Chartrand, G. Soucy, and M. Monthioux, "Why some carbons may or may not graphitize? The point of view of thermodynamics," *Carbon,* vol. 149, pp. 419-435, 2019.

[60] H. Marsh, "A tribute to Philip L. Walker," *Carbon,* vol. 29, pp. 703-704, 1991.

[61] M. Dumont, M.-A. Dourges, X. Bourrat, R. Pailler, R. Naslain, O. Babot*, et al.*, "Carbonization behaviour of modified synthetic mesophase pitches," *Carbon,* vol. 43, pp. 2277-2284, 2005.

[62] I. Lewis and L. Singer, "Thermal conversion of polynuclear aromatics to carbon," *Am. Chem. Soc., Div. Pet. Chem., Gen. Pap., Prepr.;(United States),* vol. 31, 1986.

[63] S. E. Stein, "Thermochemical kinetics of anthracene pyrolysis," *Carbon,* vol. 19, pp. 421-429, 1981.

[64] R. Livingston, H. Zeldes, and M. S. Conradi, "ESR of transient radicals during pyrolysis of fluids," *Journal of the American Chemical Society,* vol. 101, pp. 4312-4319, 1979.

[65] A. Streitwieser and A. Streitwieser, *Molecular orbital theory for organic chemists*: ACS Publications, 1961.

[66] E. Vorpagel and J. Lavin, "Most stable configurations of polynuclear aromatic hydrocarbon molecules in pitches via molecular modelling," *Carbon,* vol. 30, pp. 1033-1040, 1992.

[67] S. E. Stein, "A fundamental chemical kinetics approach to coal conversion," *New Approaches in Coal Chemistry,* vol. 169, p. 97, 1981.

[68] S. Stein, L. Griffith, R. Billmers, and R. Chen, "Pyrocondensation of anthracene," *The Journal of Organic Chemistry,* vol. 52, pp. 1582-1591, 1987.

[69] T. Sasaki, R. G. Jenkins, S. Eser, and H. H. Schobert, "Carbonization of anthracene and phenanthrene. 2. Spectroscopy and mechanisms," *Energy & fuels,* vol. 7, pp. 1047-1053, 1993.

[70] J. A. Mulholland, J. Mukherjee, and A. F. Sarofim, "Statistical and steric effects on pyrene pyrolysis product distributions at high temperature," *Energy & fuels,* vol. 11, pp. 392-395, 1997.

[71] J. Mulholland, J. Mukherjee, M. Wornat, A. Sarofim, and G. Rutledge, "Semiempirical molecular orbital estimation of the relative stability of bianthryls produced by anthracene pyrolysis," *Combustion and flame,* vol. 94, pp. 233-243, 1993.

[72] R. Greinke and I. Lewis, "Carbonization of naphthalene and dimethylnaphthalene," *Carbon,* vol. 22, pp. 305-314, 1984.

[73] P. Ramdohr, "Mikroskopische Beobachtungen an Graphiten und Koksen," *Archiv für das Eisenhüttenwesen,* vol. 1, pp. 669-672, 1928.

[74] C. E. Marshall, *Petrology of natural coke*: Colliery Guardian Company, 1945.

[75] E. Stach, "Mikroskopie natürlicher Kokse," *Handbuch der Mikroskopie in der Technik,* vol. 2, pp. 411-422, 1952.

[76] C. Abramski and M.-T. Mackowsky, "Methoden und Ergebnisse der angewandten Koksmikroskopie," in *Handbuch der Mikroskopie in der Technik.* vol. 2, ed: Umschau Frankfurt, 1952, pp. 311-410.

[77] H. Honda, "Carbonaceous mesophase: history and prospects," *Carbon,* vol. 26, pp. 139-156, 1988.

[78] G. Taylor, "Development of optical properties of coke during carbonization," *Fuel,* vol. 40, pp. 465-472, 1961.

[79] S. R. Bagheri, "Mesophase Formation in Heavy Oil," University of Alberta, 2012.

[80] H. Marsh and M. Diez, "Mesophase of graphitizable carbons," in *Liquid Crystalline and Mesomorphic Polymers*, ed: Springer, 1994, pp. 231-257.

[81] P. Oswald and P. Pieranski, *Nematic and cholesteric liquid crystals: concepts and physical properties illustrated by experiments*: CRC press, 2005.

[82] T. Imamura, Y. Yamada, S. Oi, and H. Honda, "Orientation behavior of carbonaceous mesophase spherules having a new molecular arrangement in a magnetic field," *Carbon,* vol. 16, pp. 481-486, 1978.

[83] J. Zimmer and J. White, "Disclination structure in carbonaceous mesophase and graphite [Z]," *Aerospace report*, pp. 1-5, 1976.

[84] H. Marsh and R. Menendez, "Mechanisms of formation of isotropic and anisotropic carbons," in *Introduction to carbon science*, ed: Elsevier, 1989, pp. 37-73.

[85] H. Gasparoux, "Carbonaceous mesophase and disc-like nematic liquid crystals," *Molecular Crystals and Liquid Crystals,* vol. 63, pp. 231-248, 1981.

[86] G. Yuan, Z. Jin, X. Zuo, Z. Xue, F. Yan, Z. Dong, *et al.*, "Effect of carbonaceous precursors on the structure of mesophase pitches and their derived cokes," *Energy & Fuels,* vol. 32, pp. 8329-8339, 2018.

[87] R. Greinke, "Kinetics of petroleum pitch polymerization by gel permeation chromatography," *Carbon,* vol. 24, pp. 677-686, 1986.

[88] R. Greinke, "Early Stages of Petroleum Pitch Carbonization—Kinetics and Mechanisms," *Chemistry and physics of carbon,* vol. 24, p. 1, 1994.

[89] R. Greinke and L. Singer, "Constitution of coexisting phases in mesophase pitch during heat treatment: Mechanism of mesophase formation," *Carbon,* vol. 26, pp. 665-670, 1988.

[90] D. Coleman and G. Pilcher, "Heats of combustion of biphenyl, bibenzyl, naphthalene, anthracene and phenanthrene," *Transactions of the Faraday Society,* vol. 62, pp. 821-827, 1966.

[91] J. Pearce and W. Tanner, "The Heat Capacity and the Free Energy Formation of Naphthalene," in *Proceedings of the Iowa Academy of Science*, 1934, pp. 123-126.

[92] H. M. Huffman, G. S. Parks, and A. C. Daniels, "Thermal data on organic compounds. VII The heat capacities, entropies and free energies of twelve aromatic hydrocarbons," *Journal of the American Chemical Society,* vol. 52, pp. 1547-1558, 1930.

[93] M. V. Roux, M. Temprado, J. S. Chickos, and Y. Nagano, "Critically evaluated thermochemical properties of polycyclic aromatic hydrocarbons," *Journal of Physical and Chemical Reference Data,* vol. 37, pp. 1855-1996, 2008.

[94] J. Southard and F. Brickwedde, "Low Temperature Specific Heats. I. An Improved Calorimeter for Use from 14 to 300° K. The Heat Capacity and Entropy of Naphthalene1," *Journal of the American Chemical Society,* vol. 55, pp. 4378-4384, 1933.

[95] P. Goursot, H. L. Girdhar, and E. F. Westrum Jr, "Thermodynamics of polynuclear aromatic molecules. III. Heat capacities and enthalpies of fusion of anthracene," *The Journal of Physical Chemistry,* vol. 74, pp. 2538-2541, 1970.

[96] C. J. Jacobs and G. S. Parks, "Thermal data on organic compounds. XIV. Some heat capacity, entropy and free energy data for cyclic substances," *Journal of the American Chemical Society,* vol. 56, pp. 1513-1517, 1934.

[97] A. McClellan and G. C. Pimentel, "Vibrational Assignment and Thermodynamic Properties of Naphthalene," *The Journal of Chemical Physics,* vol. 23, pp. 245-248, 1955.

[98] G. M. Barrow and A. McClellan, "The thermodynamic properties of naphthalene," *Journal of the American Chemical Society,* vol. 73, pp. 573-575, 1951.

[99] O. V. Dorofeeva, L. V. Gurvich, and S. J. Cyvin, "On calculation of thermodynamic properties of polycyclic aromatic hydrocarbons," *Thermochimica acta,* vol. 102, pp. 59-66, 1986.

[100] M. Spaght, S. B. Thomas, and G. Parks, "Some heat-capacity data on organic compounds obtained with a radiation calorimeter," *The Journal of Physical Chemistry,* vol. 36, pp. 882-888, 1932.

[101] M. Radomska and R. Radomski, "Calorimetric studies of binary systems of 1, 3, 5-trinitrobenzene with naphthalene, anthracene and carbazole. I. Phase transitions and heat capacities of the pure components and charge-transfer complexes," *Thermochimica Acta,* vol. 40, pp. 405-414, 1980.

[102] P. Bender and J. Farber, "The heats of combustion of anthracene transannular peroxide and dianthracene," *Journal of the American Chemical Society,* vol. 74, pp. 1450-1452, 1952.

[103] S. A. Kudchadker, A. P. Kudchadker, and B. J. Zwolinski, "Chemical thermodynamic properties of anthracene and phenanthrene," *The Journal of Chemical Thermodynamics,* vol. 11, pp. 1051-1059, 1979.

[104] P. Robinson and H. Scott, "The anthracene-carbazole system," *Molecular Crystals and Liquid Crystals,* vol. 5, pp. 387-404, 1969.

[105] R. Chirico, S. Knipmeyer, A. Nguyen, and W. Steele, "The thermodynamic properties to the temperature 700 K of naphthalene and of 2, 7-dimethylnaphthalene," *The Journal of Chemical Thermodynamics,* vol. 25, pp. 1461-1494, 1993.

[106] R. Sabbah and L. E. Watik, "New reference materials for the calibration (temperature and energy) of differential thermal analysers and scanning calorimeters," *Journal of Thermal Analysis and Calorimetry,* vol. 38, pp. 855-863, 1992.

[107] R. H. Boyd, R. L. Christensen, and R. Pua, "The heats of combustion of acenaphthene, acenaphthylene, and fluoranthene. Strain and delocalization in bridged naphthalenes," *Journal of the American Chemical Society,* vol. 87, pp. 3554-3559, 1965.

[108] C. J. Pope and J. B. Howard, "Thermochemical properties of curved PAH and fullerenes: a group additivity method compared with MM3 (92) and MOPAC predictions," *The Journal of Physical Chemistry,* vol. 99, pp. 4306-4316, 1995.

[109] W.-K. Wong and E. F. Westrum, "Thermodynamics of polynuclear aromatic molecules I. Heat capacities and enthalpies of fusion of pyrene, fluoranthene, and triphenylene," *The Journal of Chemical Thermodynamics,* vol. 3, pp. 105-124, 1971.

[110] N. Smith, R. Stewart, A. Osborn, and D. Scott, "Pyrene: vapor pressure, enthalpy of combustion, and chemical thermodynamic properties," *The Journal of Chemical Thermodynamics,* vol. 12, pp. 919-926, 1980.

[111] L. Richard and H. C. Helgeson, "Calculation of the thermodynamic properties at elevated temperatures and pressures of saturated and aromatic high molecular weight solid and liquid hydrocarbons in kerogen, bitumen, petroleum, and other organic matter of biogeochemical interest," *Geochimica et Cosmochimica Acta,* vol. 62, pp. 3591-3636, 1998.

[112] P. Spencer, "A brief history of CALPHAD," *Calphad,* vol. 32, pp. 1-8, 2008.

[113] S. Matsumoto and T. Fukuda, "An X-ray Study on the Phase Transition of Phenanthrene Crystal," *Bulletin of the Chemical Society of Japan,* vol. 40, pp. 743-746, 1967.

[114] D. Spielberg, R. Arndt, A. Damask, and I. Lefkowitz, "Dielectric and Neutron Inelastic Scattering Measurements on Phenanthrene," *The Journal of Chemical Physics,* vol. 54, pp. 2597-2601, 1971.

[115] Y. Nagano, "Standard enthalpies of formation of phenanthrene and naphthacene," *The Journal of Chemical Thermodynamics,* vol. 34, pp. 377-383, 2002.

[116] H. Finke, J. Messerly, S. Lee, A. Osborn, and D. Douslin, "Comprehensive thermodynamic studies of seven aromatic hydrocarbons," *The Journal of Chemical Thermodynamics,* vol. 9, pp. 937-956, 1977.

[117] R. Arndt and A. Damask, "Heat-Capacity Anomaly in Phenanthrene," *The Journal of Chemical Physics,* vol. 45, pp. 755-756, 1966.

[118] F. Casellato, C. Vecchi, A. Girelli, and B. Casu, "Differential calorimetric study of polycyclic aromatic hydrocarbons," *Thermochimica Acta,* vol. 6, pp. 361-368, 1973.

[119] C. Frampton, K. Knight, N. Shankland, and K. Shankland, "Single-crystal X-ray diffraction analysis of pyrene II at 93 K," *Journal of Molecular Structure,* vol. 520, pp. 29-32, 2000.

[120] A. Hazell, F. Larsen, and M. Lehmann, "A neutron diffraction study of the crystal structure of pyrene, C16H10," *Acta Crystallographica Section B: Structural Crystallography and Crystal Chemistry,* vol. 28, pp. 2977-2984, 1972.

[121] H. Ringel, A. Damask, and R. Arndt, "Heat Capacity Anomaly in Chrysene," *Molecular Crystals and Liquid Crystals,* vol. 5, pp. 295-296, 1969.

[122] R. Zallen, C. Griffiths, M. Slade, M. Hayek, and O. Brafman, "The solid state transition in pyrene," *Chemical Physics Letters,* vol. 39, pp. 85-89, 1976.

[123] M. Kay, Y. t. Okaya, and D. Cox, "A refinement of the structure of the room-temperature phase of phenanthrene, C14H10, from X-ray and neutron diffraction data," *Acta Crystallographica Section B: Structural Crystallography and Crystal Chemistry,* vol. 27, pp. 26-33, 1971.

[124] R. Kulver and C. J. Eckhardt, "Translational-rotational modes in noncentrosymmetric lattices: A lattice-dynamical interpretation of the phenanthrene phase transition," *Physical Review B,* vol. 37, p. 5351, 1988.

[125] R. H. Hurt and Y. Hu, "Thermodynamics of carbonaceous mesophase," *Carbon,* vol. 37, pp. 281-292, 1999.

[126] I. H. Shishido M., Arai K., Saito S., "Application of liquid crystal theory to the estimation of mesophase pitch phase transition behavior," *Carbon,* vol. 35, pp. 797-799, 1997.

[127] Y. Hu and R. H. Hurt, "Thermodynamics of carbonaceous mesophase: II. General theory for nonideal solutions," *Carbon,* vol. 39, pp. 887-896, 2001.

[128] Y. Hu, "Thermodynamics and Dynamics of Carbon Nanostructure Formation," Brown University, 2001.

[129] R. Humphries, P. James, and G. Luckhurst, "Symp. Faraday Soc. 5, 107 (1971)," *Google Scholar Crossref, CAS,* 1971.

[130] R. Humphries and G. Luckhurst, "A statistical theory of liquid crystalline mixtures: phase separation," *Proceedings of the Royal Society of London. A. Mathematical and Physical Sciences,* vol. 352, pp. 41-56, 1976.

[131] I. Mochida and Y. Korai, "Chemistry of mesophase pitch for its preparation and property design," *Fuel Soc. Jpn,* vol. 64, pp. 796-808, 1985.

[132] A. Oberlin, "High-resolution TEM studies of carbonization and graphitization," *Chem. Phys. Carbon,* vol. 22, pp. 1-143, 1989.

[133] R. H. Hurt, G. P. Crawford, and H.-S. Shim, "Equilibrium nanostructure of primary soot particles," *Proc. Combust. Inst.,* vol. 28, pp. 2539-2546, 2000.

[134] G. W. Smith, J. L. White, and M. Buechler, "Mesophase/isotropic phase interfacial energy: determination from coalescence kinetics of mesophase pitch," *Carbon,* vol. 23, pp. 117-21, 1985.

[135] W. Maier and A. Saupe, "A simple molecular-statistics theory of the liquid-crystalline phase. Part II," *Z. Naturforsch., 15a,* pp. 287-292, 1960.

[136] A. Saupe, "Recent results in the field of liquid crystals," *Angewandte Chemie International Edition in English,* vol. 7, pp. 97-112, 1968.

[137] R. Humphries, P. James, and G. Luckhurst, "Molecular field treatment of nematic liquid crystals," *Journal of the Chemical Society, Faraday Transactions 2: Molecular and Chemical Physics,* vol. 68, pp. 1031-1044, 1972.

[138] W. K. Fischer, F. Keller, R. C. Perruchoud, and S. Oderbolz, "Baking parameters and the resulting anode quality," *Light Metals 1993,* pp. 683-689, 1993.

[139] H. Marsh, "Carbonization and liquid-crystal (mesophase) development: Part 1. The significance of the mesophase during carbonization of coking coals," *Fuel,* vol. 52, pp. 205-212, 1973.

[140] B. Allard, R. Paulus, and G. Billat, "A new Ramming Paste with improved potlining working conditions," in *Light Metals 2011,* ed: Springer, 2011, pp. 1091-1096.

[141] W. E. Acree, "Thermodynamic properties of organic compounds: enthalpy of fusion and melting point temperature compilation," *Thermochimica acta,* vol. 189, pp. 37-56, 1991.

[142] D. H. Andrews, G. Lynn, and J. Johnston, "The heat capacities and heat of crystallization of some isomeric aromatic compounds," *Journal of the American Chemical Society,* vol. 48, pp. 1274-1287, 1926.

[143] M. Balcan, S. Arzik, and T. Altunata, "The determination of the heats of combustion and the resonance energies of some substituted naphthalenes," *Thermochimica acta,* vol. 278, pp. 49-56, 1996.

[144] R. D. Chirico, S. Knipmeyer, and W. Steele, "Heat capacities, enthalpy increments, and derived thermodynamic functions for naphthalene between the temperatures 5K and 440K," *The Journal of Chemical Thermodynamics,* vol. 34, pp. 1873-1884, 2002.

[145] D. David, "Determination of Specific Heat and Heat of Fusion by Differential Thermal Analysis. Study of Theory and Operating Parameters," *Analytical Chemistry,* vol. 36, pp. 2162-2166, 1964.

[146] E. S. Domalski and E. D. Hearing, "Estimation of the Thermodynamic Properties of C-H-N-O-S-Halogen Compounds at 298.15 K," *Journal of Physical and Chemical Reference Data,* vol. 22, pp. 805-1159, 1993.

[147] J. L. Goldfarb and E. M. Suuberg, "Vapor pressures and thermodynamics of oxygen-containing polycyclic aromatic hydrocarbons measured using knudsen effusion," *Environmental toxicology and chemistry,* vol. 27, pp. 1244-1249, 2008.

[148] W. D. Good, "The enthalpies of formation of some bridged-ring polynuclear aromatic hydrocarbons," *The Journal of Chemical Thermodynamics,* vol. 10, pp. 553-558, 1978.

[149] J. H. Hildebrand, A. D. Duschak, A. Foster, and C. Beebe, "The specific heats and heats of fusion of triphenyllmethane, anthraquinone and anthracene" *Journal of the American Chemical Society,* vol. 39, pp. 2293-2297, 1917.

[150] V. Kestens, G. Auclair, K. Drozdzewska, A. Held, G. Roebben, and T. Linsinger, "Thermodynamic property values of selected polycyclic aromatic hydrocarbons measured by differential scanning calorimetry," *Journal of thermal analysis and calorimetry,* vol. 99, pp. 245-261, 2010.

[151] Z. Lisicki and M. E. Jamróz, "(Solid+ liquid) equilibria in (polynuclear aromatic+ tertiary amide) systems," *The Journal of Chemical Thermodynamics,* vol. 32, pp. 1335-1353, 2000.

[152] H. Mackle and P. O'Hare, "A high-precision aneroid semi-micro combustion calorimeter," *Transactions of the Faraday Society,* vol. 59, pp. 2693-2701, 1963.

[153] S. Mastrangelo, "Adiabatic Calorimeter for Determination of Cryoscopic Data," *Analytical Chemistry,* vol. 29, pp. 841-845, 1957.

[154] J. McCullough, H. Finke, J. Messerly, S. Todd, T. Kincheloe, and G. Waddington, "The low-temperature thermodynamic properties of naphthalene, l-methylnaphthalene, 2-methylnaphthalene, 1, 2, 3, 4-tetrahydronaphthalene, trans-decahydronaphthalene and cis-decahydronaphthalene," *The Journal of Physical Chemistry,* vol. 61, pp. 1105-1116, 1957.

[155] R. M. Metzger, C. Kuo, and E. Arafat, "A semi-micro rotating-bomb combustion calorimeter," *The Journal of Chemical Thermodynamics,* vol. 15, pp. 841-851, 1983.

[156] N. F. Moiseeva and O. V. Dorofeeva, "Group additivity scheme for calculating the chemical thermodynamic properties of gaseous polycyclic aromatic hydrocarbons containing five-membered rings," *Thermochimica acta,* vol. 168, pp. 179-186, 1990.

[157] Y. Nagano, "High-precision micro-combustion calorimetry of anthracene," *The Journal of Chemical Thermodynamics,* vol. 33, pp. 377-387, 2001.

[158] U. Rai, O. Singh, and N. Singh, "Some thermodynamic aspects of organic eutectics-succinonitrile-phenanthrene system", vol 26, ed: Council Scientific Industrial Resaerch Publ & Info Directorate, New Delhi 110012, INDIA, 1987, pp. 947-949.

[159] R. Rastogi and P. S. Bassi, "Mechanism of eutectic crystallization," *The Journal of Physical Chemistry,* vol. 68, pp. 2398-2406, 1964.

[160] A. Rojas and E. Orozco, "Measurement of the enthalpies of vaporization and sublimation of solids aromatic hydrocarbons by differential scanning calorimetry," *Thermochimica acta,* vol. 405, pp. 93-107, 2003.

[161] A. F. L. Santos, J. A. Oliveira, and M. J. Monte, "Experimental and computational thermodynamics of pyrene and 1-pyrenecarboxaldehyde and their photophysical properties," *The Journal of Chemical Thermodynamics,* vol. 90, pp. 282-293, 2015.

[162] D. M. Speros and F. D. Rossini, "Heats of combustion and formation of naphthalene, the two methylnaphthalene, cis and trans-decahydronaphthalene, and drelated compounds" *The Journal of Physical Chemistry,* vol. 64, pp. 1723-1727, 1960.

[163] P. Storoniak, K. Krzymiński, A. Boużyk, E. Koval'chuk, and J. Błażejowski, "Melting, volatilisation and crystal lattice enthalpies of acridin-9 (10H)-ones," *Journal of thermal analysis and calorimetry,* vol. 74, pp. 443-450, 2003.

[164] W. B. Tanner, "The heat capacity and the free energy of formation of naphthalene," Torch Press, 1934.

[165] R. D. Wauchope and F. W. Getzen, "Temperature dependence of solubilities in water and heats of fusion of solid aromatic hydrocarbons," *Journal of Chemical and Engineering Data,* vol. 17, pp. 38-41, 1972.

[166] W.-K. Wong and E. F. Westrum Jr, "Thermodynamics of polynuclear aromatic molecules: II. Low-temperature thermal properties of perylene, coronene, and naphthacene," *Molecular Crystals and Liquid Crystals,* vol. 61, pp. 207-228, 1980.

[167] J. D. Cox and G. Pilcher, "Thermochemistry of organic and organometallic compounds," 1970.

[168] M. A. R. da Silva, G. Pilcher, L. M. Santos, and L. M. S. S. Lima, "Calibration and test of an aneroid mini-bomb combustion calorimeter," *The Journal of Chemical Thermodynamics,* vol. 39, pp. 689-697, 2007.

[169] S. Hafsaoui and R. Mahmoud, "Solid-liquid equilibria of binary systems containing n-tetracosane with naphthalene or dibenzofuran," *Journal of thermal analysis and calorimetry,* vol. 88, pp. 565-570, 2007.

[170] K. Khimeche and A. Dahmani, "Solid− liquid equilibria of naphthalene+ alkanediamine mixtures," *Journal of Chemical & Engineering Data,* vol. 51, pp. 382-385, 2006.

[171] V. Laštovka, M. Fulem, M. Becerra, and J. M. Shaw, "A similarity variable for estimating the heat capacity of solid organic compounds: Part II. Application: Heat capacity calculation for ill-defined organic solids," *Fluid Phase Equilibria,* vol. 268, pp. 134-141, 2008.

[172] T. C. A. D. R. B. Jr., "NIST Special Publication 1186, Thermodynamic Properties of Polycyclic Aromatic Hydrocarbons."

[173] S. W. Benson and J. H. Buss, "Additivity rules for the estimation of molecular properties. Thermodynamic properties," *The Journal of Chemical Physics,* vol. 29, pp. 546-572, 1958.

[174] C. Joblin, C. Masselon, P. Boissel, P. de Parseval, S. Martinovic, and J. F. Muller, "Simulation of interstellar aromatic hydrocarbons using ion cyclotron resonance. preliminary results," *Rapid communications in mass spectrometry,* vol. 11, pp. 1619-1623, 1997.

[175] G. F. Voronin and I. B. Kutsenok, "Universal method for approximating the standard thermodynamic functions of solids," *Journal of Chemical & Engineering Data,* vol. 58, pp. 2083-2094, 2013.

[176] B. Sharma, S. Gupta, S. Tandon, and R. Kant, "Physico-mechanical properties of naphthalene–acenaphthene eutectic system by different modes of solidification," *Materials Chemistry and Physics,* vol. 111, pp. 423-430, 2008.

[177] E. S. Domalski and E. D. Hearing, "Heat capacities and entropies of organic compounds in the condensed phase. Volume III," *Journal of physical and chemical reference data,* vol. 25, pp. 1-525, 1996.

[178] J. L. Goldfarb and E. M. Suuberg, "Vapor pressures and enthalpies of sublimation of ten polycyclic aromatic hydrocarbons determined via the Knudsen effusion method," *Journal of Chemical & Engineering Data,* vol. 53, pp. 670-676, 2008.

[179] A. B. Macknick and J. M. Prausnitz, "Vapor pressures of high-molecular-weight hydrocarbons," *Journal of Chemical and Engineering Data,* vol. 24, pp. 175-178, 1979.

[180] D. Ambrose, M. Ewing, N. Ghiassee, and J. S. Ochoa, "The ebulliometric method of vapour-pressure measurement: vapour pressures of benzene, hexafluorobenzene, and naphthalene," *The Journal of Chemical Thermodynamics,* vol. 22, pp. 589-605, 1990.

[181] D. L. Camin and F. D. Rossini, "Physical properties of fourteen API research hydrocarbons, C9 to C15," *The Journal of Physical Chemistry,* vol. 59, pp. 1173-1179, 1955.

[182] C. De Kruif, "Enthalpies of sublimation and vapour pressures of 11 polycyclic hydrocarbons," *The Journal of Chemical Thermodynamics,* vol. 12, pp. 243-248, 1980.

[183] L. Fowler, W. N. Trump, and C. E. Vogler, "Vapor pressure of naphthalene. Measurements between 40. deg. and 180. deg," *Journal of Chemical & Engineering Data,* vol. 13, pp. 209-210, 1968.

[184] P. C. Hansen and C. A. Eckert, "An improved transpiration method for the measurement of very low vapor pressures," *Journal of Chemical and Engineering Data,* vol. 31, pp. 1-3, 1986.

[185] L. Malaspina, G. Bardi, and R. Gigli, "Simultaneous determination by knudsen-effusion microcalorimetric technique of the vapor pressure and enthalpy of vaporization of pyrene and 1, 3, 5-triphenylbenzene," *The Journal of Chemical Thermodynamics,* vol. 6, pp. 1053-1064, 1974.

[186] O. Nelson and C. Senseman, "Vapor Pressure Determinations on Naphthalene, Anthracene, Phecanthrene, and Anthraquinone between Their Melting and Boiling Points," *Industrial & Engineering Chemistry,* vol. 14, pp. 58-62, 1922.

[187] V. Oja and E. M. Suuberg, "Vapor pressures and enthalpies of sublimation of polycyclic aromatic hydrocarbons and their derivatives," *Journal of Chemical & Engineering Data,* vol. 43, pp. 486-492, 1998.

[188] K. Růžička, M. Fulem, and V. Růžička, "Recommended vapor pressure of solid naphthalene," *Journal of Chemical & Engineering Data,* vol. 50, pp. 1956-1970, 2005.

[189] K. Sasse, J. Jose, and J.-C. Merlin, "A static apparatus for measurement of low vapor pressures. Experimental results on high molecular-weight hydrocarbons," *Fluid phase equilibria,* vol. 42, pp. 287-304, 1988.

[190] M. A. Siddiqi, R. A. Siddiqui, and B. Atakan, "Thermal stability, sublimation pressures, and diffusion coefficients of anthracene, pyrene, and some metal β-diketonates," *Journal of Chemical & Engineering Data,* vol. 54, pp. 2795-2802, 2009.

[191] J.-i. Aihara, "Why aromatic compounds are stable," *Scientific American,* vol. 266, pp. 62-69, 1992.

[192] R. W. Havenith, J. H. van Lenthe, F. Dijkstra, and L. W. Jenneskens, "Aromaticity of Pyrene and Its Cyclopentafused Congeners Resonance and NICS Criteria. An Ab Initio Valence Bond Analysis in Terms of Kekulé Resonance Structures," *The Journal of Physical Chemistry A,* vol. 105, pp. 3838-3845, 2001.

[193] J. Poater i Teixidor, M. Duran i Portas, and M. Solà i Puig, "Aromaticity determines the relative stability of kinked vs. straight topologies in polycyclic aromatic hydrocarbons," *Frontiers In Chemistry, 2018, vol. 6, art. 561*, 2018.

[194] M. J. Dewar and C. De Llano, "Ground states of conjugated molecules. XI. Improved treatment of hydrocarbons," *Journal of the American Chemical Society,* vol. 91, pp. 789-795, 1969.

[195] W. C. Herndon, "Resonance energies of aromatic hydrocarbons. Quantitative test of resonance theory," *Journal of the American Chemical Society,* vol. 95, pp. 2404-2406, 1973.

[196] I. Lukovits, "Resonance energy in graphite," *Journal of chemical information and computer sciences,* vol. 44, pp. 1565-1570, 2004.

[197] T. Carnelley, "XIII. Chemical symmetry, or the influence of atomic arrangement on the physical properties of compounds," *The London, Edinburgh, and Dublin Philosophical Magazine and Journal of Science,* vol. 13, pp. 112-130, 1882.

[198] R. Brown and R. Brown, "Melting point and molecular symmetry," *Journal of Chemical Education,* vol. 77, p. 724, 2000.

[199] E. Martin, S. H. Yalkowsky, and J. E. Wells, "Fusion of disubstituted benzenes," *Journal of pharmaceutical sciences,* vol. 68, pp. 565-568, 1979.

[200] S. H. Yalkowsky, "Estimation of entropies of fusion of organic compounds," *Industrial & Engineering Chemistry Fundamentals,* vol. 18, pp. 108-111, 1979.

[201] J. Wei, "Molecular symmetry, rotational entropy, and elevated melting points," *Industrial & engineering chemistry research,* vol. 38, pp. 5019-5027, 1999.

[202] S. H. Yalkowsky, "Carnelley's rule and the prediction of melting point," *Journal of pharmaceutical sciences,* vol. 103, pp. 2629-2634, 2014.

[203] S. H. Yalkowsky, J. F. Krzyzaniak, and P. B. Myrdal, "Relationships between melting point and boiling point of organic compounds," *Industrial & engineering chemistry research,* vol. 33, pp. 1872-1877, 1994.

[204] S. Matsumoto, "A Phase Transition in Phenanthrene Crystal," *Bulletin of the Chemical Society of Japan,* vol. 39, pp. 1811-1813, 1966.

[205] B. McArdle, J. Sherwood, and A. Damask, "The growth and perfection of phenanthrene single crystals: 1. Purification and single crystal growth," *Journal of Crystal Growth,* vol. 22, pp. 193-200, 1974.

[206] G. N. Zhizhin and E. Mukhtarov, *Optical spectra and lattice dynamics of molecular crystals* vol. 21: Elsevier, 1995.

[207] M. Hillert and L. Staffansson, "Regular-solution model for stoichiometric phases and ionic melts," *Acta Chem. Scand.,* vol. 24, pp. 3618-3626, 1970.

[208] B. Sundman and J. Ågren, "A regular solution model for phases with several components and sublattices, suitable for computer applications," *Journal of physics and chemistry of solids,* vol. 42, pp. 297-301, 1981.

[209] M. Fulem, V. c. Laštovka, M. Straka, K. Ruzicka, and J. M. Shaw, "Heat capacities of tetracene and pentacene," *Journal of Chemical & Engineering Data,* vol. 53, pp. 2175-2181, 2008.

[210] H. Inokuchi, S. Shiba, T. Handa, and H. Akamatu, "Heats of sublimation of condensed polynuclear aromatic hydrocarbons," *Bulletin of the Chemical Society of Japan,* vol. 25, pp. 299-302, 1952.

[211] E. Westrum Jr and S. Wong, "Strain energies and thermal properties of globular and polynuclear aromatic molecules" Michigan Univ., Ann Arbor. Dept. of Chemistry1967.

[212] J. J. Murray, R. F. Pottie, and C. Pupp, "The vapor pressures and enthalpies of sublimation of five polycyclic aromatic hydrocarbons," *Canadian Journal of Chemistry,* vol. 52, pp. 557-563, 1974.

[213] J. Trotter, "The crystal and molecular structure of phenanthrene," *Acta Crystallographica,* vol. 16, pp. 605-608, 1963.

[214] C. Frampton, K. Knight, N. Shankland, and K. Shankland, "Single-crystal X-ray diffraction analysis of pyrene II at 93K," *Journal of Molecular Structure,* vol. 520, pp. 29-32, 2000.

[215] A. Camerman and J. Trotter, "The crystal and molecular structure of pyrene," *Acta Crystallographica,* vol. 18, pp. 636-643, 1965.

[216] S. Ding, Q. Yin, W. Du, X. Sun, B. Hou, M. Zhang, *et al.*, "Formation of Solid Solution and Ternary Phase Diagrams of Anthracene and Phenanthrene in Different Organic Solvents," *Journal of Chemical & Engineering Data,* vol. 60, pp. 1401-1407, 2015.

[217] A. Kofler, "Melting and crystallizing of solid solutions: phenanthreneanthracene," *Monatsh. Chem,* vol. 86, pp. 301-311, 1955.

[218] M. J. Joncich and D. Bailey, "Zone melting and differential thermal analysis of some organic compounds," *Analytical Chemistry,* vol. 32, pp. 1578-1581, 1960.

[219] S. Kipot, R. Myasnikova, and A. Kitaigorodskii, "Study of binary organic systems of anthracene− carbazole and anthracene− phenanthrene," *Zh. Prikl. Khim,* vol. 49, pp. 815-820, 1976.

[220] N. Couvrat, Y. Cartigny, S. Tisse, M. Petit, and G. Coquerel, "Binary phase diagram between phenanthrene and its main impurity: dibenzothiophene," in *XXXVII JEEP–37th Conference on Phase Equilibria*, 2011, p. 00006.

[221] G. Yuan and Z. Cui, "Preparation, Characterization, and Applications of Carbonaceous Mesophase: A Review," in *Nematic Liquid Crystals*, ed: IntechOpen, 2019.

[222] M. S. Zhuang and M. C. Thies, "Extraction of petroleum pitch with supercritical toluene: experiment and prediction," *Energy & fuels,* vol. 14, pp. 70-75, 2000.

[223] P. J. Van Laarhoven and E. H. Aarts, "Simulated annealing," in *Simulated annealing: Theory and applications*, ed: Springer, 1987, pp. 7-15.

[224] C. Audet and J. E. Dennis Jr, "Mesh adaptive direct search algorithms for constrained optimization," *SIAM Journal on optimization,* vol. 17, pp. 188-217, 2006.

[225] E. Fermi, "Numerical solution of a minimum problem," Los Alamos Scientific Lab., Los Alamos, NM1952.

[226] V. Torczon, "On the convergence of pattern search algorithms," *SIAM Journal on optimization*, vol. 7, pp. 1-25, 1997.

[227] F. Clark, "Optimization and Nonsmooth Analysis. 1983," ed: Wiley, New York.

[228] C. Audet, V. Béchard, and S. Le Digabel, "Nonsmooth optimization through mesh adaptive direct search and variable neighborhood search," *Journal of Global Optimization*, vol. 41, pp. 299-318, 2008.

[229] A. Gheribi, C. Audet, S. Le Digabel, E. Bélisle, C. Bale, and A. Pelton, "Calculating optimal conditions for alloy and process design using thermodynamic and property databases, the FactSage software and the Mesh Adaptive Direct Search algorithm," *Calphad*, vol. 36, pp. 135-143, 2012.

[230] A. E. Gheribi, S. Le Digabel, C. Audet, and P. Chartrand, "Identifying optimal conditions for magnesium based alloy design using the Mesh Adaptive Direct Search algorithm," *Thermochimica Acta*, vol. 559, pp. 107-110, 2013.

[231] S. Le Digabel, "Algorithm 909: NOMAD: Nonlinear optimization with the MADS algorithm," *ACM Transactions on Mathematical Software (TOMS)*, vol. 37, p. 44, 2011.

[232] "MATLAB and Statistic Toolbox Release R2015a, The MathWorks, Inc., Natick, Massachusette, United States."

[233] S. R. Bagheri, M. R. Gray, and W. C. McCaffrey, "Depolarized light scattering for study of heavy oil and mesophase formation mechanisms," *Energy & fuels*, vol. 26, pp. 5408-5420, 2012.

[234] I. Lewis, "Thermotropic mesophase pitch," 1978.

[235] H. Marsh, M. Martínez-Escandell, and F. Rodríguez-Reinoso, "Semicokes from pitch pyrolysis: mechanisms and kinetics," *Carbon*, vol. 37, pp. 363-390, 1999.

[236] R. Lewis and R. Greinke, "12th Biennial Conf. on Carbon," *Extended Abs*, p. 215, 1975.

[237] F. R. Vieira, C. H. M. de Castro Dutra, and L. D. De Castro, "Determining the anisotropic content in a petroleum pitch–Comparison of centrifugation and optical microscopy techniques," *Fuel*, vol. 90, pp. 908-911, 2011.

[238] P. Torregrosa-Rodrıguez, M. Martınez-Escandell, F. Rodrıguez-Reinoso, H. Marsh, C. G. de Salazar, and E. R. Palazón, "Pyrolysis of petroleum residues: II. Chemistry of pyrolysis," *Carbon*, vol. 38, pp. 535-546, 2000.

[239] W. Burgess, "Prediction of liquid crystalline content and molecular structures present in carbonaceous pitches," 2010.

[240] S. Zhuang, "Supercritical fractionation of petroleum pitches: Experiment and prediction," 2001.

[241] E. Fitzer, "The future of carbon-carbon composites," *Carbon*, vol. 25, pp. 163-190, 1987.

[242] R. García, J. L. Crespo, S. C. Martin, C. E. Snape, and S. R. Moinelo, "Development of mesophase from a low-temperature coal tar pitch," *Energy & fuels*, vol. 17, pp. 291-301, 2003.

[243] Y. Martín, R. García, P. Keating, C. E. Snape, and S. R. Moinelo, "A study of the polymerization and condensation reactions during the heat treatment of pitches under gas-blowing conditions," *Energy & fuels,* vol. 14, pp. 380-392, 2000.

[244] C. Song and H. H. Schobert, "Opportunities for developing specialty chemicals and advanced materials from coals," *Fuel processing technology,* vol. 34, pp. 157-196, 1993.

[245] O. Vohler, "Carbon and graphite in future markets," *Erdöl, Kohle, Erdgas, Petrochem,* vol. 39, p. 561, 1986.

[246] N. Bouchard, *Pyrolyse de divers brais utilisés dans la technologie söderberg et analyse des matières volatiles*: Université du Québec à Chicoutimi, 1998.

[247] M. Zander, "Relation between dewar localization energies and rates of thermally induced carbonization of polycyclic aromatic hydrocarbons," *Fuel,* vol. 65, pp. 1019-1020, 1986.

[248] I. Lewis and L. Singer, "Thermal conversion of polynuclear aromatic compounds to carbon," ed: ACS Publications, 1988.

[249] H. Tillmanns, "Carbonization and coke characterization," in *ACS symposium series*, 1986, pp. 215-233.

[250] D. Riggs and R. Diefendorf, "A phase diagram for pitches," *Carbon,* vol. 80, pp. 326-329, 1980.

[251] R. Diefendorf, "14th Biennial Conf. on Carbon," *Extended Abstract, USA,* vol. 407, 1979.

[252] G. W. Gray and P. A. Winsor, *Liquid crystals & plastic crystals. Editors*, 1974.

[253] I. Lewis and L. Singer, "Carbonization of Aromatic Hydrocarbons," in Abstracts of papers of the American Chemical Society, 1969, pp. FU33-&.

[254] L. Shoko, J. Beukes, C. Strydom, B. Larsen, and L. Lindstad, "Predicting the toluene-and quinoline insoluble contents of coal tar pitches used as binders in Söderberg electrodes," *International Journal of Mineral Processing,* vol. 144, pp. 46-49, 2015.

[255] U. D. o. Health and H. Services, "NIOSH recommendations for occupational safety and health standards," *Morbidity and Mortality Weekly Report Supplement,* vol. 34, 1985.

[256] Y. M. Zhou, L. Tian, G. Xie, R. X. Li, and X. H. Yu, "A New Ecofriendly Cold Ramming Paste for the Aluminum Electrolysis Cell," in *Advanced Materials Research*, 2012, pp. 1208-1213.

[257] P. Ouzilleau, A. E. Gheribi, G. Eriksson, D. K. Lindberg, and P. Chartrand, "A size-dependent thermodynamic model for coke crystallites: The carbon–hydrogen system up to 2500 K," *Carbon,* vol. 85, pp. 99-118, 2015.

[258] M. S. Hosseini and P. Chartrand, "Thermodynamics and phase relationship of carbonaceous mesophase appearing during coal tar pitch carbonization," *Fuel,* vol. 275, p. 117899, 2020.

[259] C. Bale, E. Bélisle, P. Chartrand, S. Decterov, G. Eriksson, K. Hack, *et al.*, "FactSage thermochemical software and databases—recent developments," *Calphad,* vol. 33, pp. 295-311, 2009.

[260] C. Bale, P. Chartrand, S. Degterov, G. Eriksson, K. Hack, R. B. Mahfoud, *et al.*, "FactSage thermochemical software and databases," *Calphad,* vol. 26, pp. 189-228, 2002.

[261] Y. Chamam, D. Kocaefe, Y. Kocaefe, D. Bhattacharyay, and B. Morais, "Effect of heating rate during baking on the properties of carbon anodes used in aluminum industry," in *Light Metals 2016*, ed: Springer, 2016, pp. 947-951.

APPENDIX A HEAT CAPACITY FUNCTION COEFFICIENTS AND THERMODYNAMIC PROPERTIES OF PAHS

Table A.1 Summary of coefficients for Eq. (4.5) of solid reference compounds.

Compound	Formula	Temperature (K)	Heat capacity coefficients			
			a^1	b^2	c^3	d^4
Naphthalene [92, 116, 154]	$C_{10}H_8$	50-250	4.789582E+01	5.260242E-02	-4.747476E+04	1.226948E-03
		250-500	-4.692328E+01	9.124217E-01	-3.908098E+05	-6.182930E-04
		500-1000	1.481289E+02	3.015227E-01	-6.153400E+06	-8.325301E-05
		1000-1200	1.239281E+02	3.266520E-01	-1.975335E-03	-9.033912E-05
Anthracene [92, 95]	$C_{14}H_{10}$	50-250	3.392659E+01	3.629566E-01	-3.759303E+04	7.624590E-04
		250-500	-1.529827E+02	1.458852E+00	1.288759E+06	-9.563297E-04
		500-1000	2.107971E+02	4.525379E-01	-1.365638E+07	-1.595327E-04
		1000-1200	1.968459E+02	4.230661E-01	-5.611546E-03	-1.295599E-04
Phenanthrene [92, 116, 154, 171]	$C_{14}H_{10}$	50-200	6.242438E+01	-1.131418E-03	-6.315749E+04	1.915390E-03
		200-400	-1.119287E+02	1.396477E+00	5.794539E+05	-1.115927E-03
		400-1000	1.052610E+02	5.366475E-01	-3.226375E+06	-1.724426E-04
		1000-1200	1.553805E+02	4.291547E-01	-1.914677E-02	-1.180640E-04
Pyrene [96, 109]	$C_{16}H_{10}$	50-250	3.702457E+01	3.023675E-01	-3.781335E+04	1.217449E-03
		250-500	-1.337287E+02	1.529698E+00	3.845164E+05	-1.067601E-03
		500-1000	2.606328E+02	3.722991E-01	-1.360757E+07	-1.050310E-04
		1000-1200	2.056891E+02	4.286711E-01	-3.141964E-03	-1.200230E-04
Triphenylene [109]	$C_{18}H_{12}$	50-200	1.719275E+01	7.536159E-01	-1.667881E+04	-2.926266E-05
		200-500	-1.748541E+02	1.744192E+00	1.584001E+06	-1.154687E-03
		500-1000	2.133311E+02	6.141157E-01	-1.299914E+07	-2.123189E-04
		1000-1200	2.156219E+02	5.545603E-01	-6.819850E-03	-1.678233E-04
Perylene [166]	$C_{20}H_{12}$	50-200	3.562509E+01	4.260449E-01	-2.442449E+04	1.492123E-03
		200-600	-1.769402E+02	1.734660E+00	1.995003E+06	-9.983409E-04
		600-1000	4.009765E+02	4.312657E-01	-3.282141E+07	-1.628867E-04
		1000-1200	3.020082E+02	4.974842E-01	-9.390413E-03	-1.627771E-04

Compound	Formula	Temperature (K)	Heat capacity coefficients			
			a[1]	b[2]	c[3]	d[4]
Coronene [166]	$C_{24}H_{12}$	50-200	4.073861E+01	2.076734E-01	-2.289082E+04	3.150419E-03
		200-500	2.223779E+01	1.131111E+00	-1.154316E+06	-3.576729E-04
		500-1000	-5.711782E+00	1.262698E+00	-4.098349E-02	-5.219392E-04
		1000-1200	2.486622E+02	7.154911E-01	-1.774394E-02	-2.271054E-04
1-Methylnaphthalene [154]	$C_{11}H_{10}$	50-300	-1.631462E+01	8.852082E-01	5.108956E+04	-8.425365E-04
		300-500	-7.743780E+01	8.756533E-01	2.423388E+06	-4.094545E-04
		500-1000	1.085148E+02	4.882533E-01	-9.356061E+06	-1.918050E-04
		1000-1200	1.474176E+02	3.663063E-01	-6.453756E-03	-1.177652E-04

[1] J mol^{-1} K^{-1}; [2] J mol^{-1} K^{-2}; [3] J mol^{-1} K^{-3}; [4] J mol^{-1} K

Table A.2 Summary of coefficients for Eq. (4.6) of liquid and gas reference compounds.

Compound	Formula	state	Heat capacity coefficients				
			a[1]	b[2]	c[3]	d[4]	e[5]
Naphthalene [97, 98, 105]	$C_{10}H_8$	Liq.	2.7130E+01	6.5932E-01	-3.6860E-04	7.1225E-08	0.0
		Gas	-6.9550E+01	8.8646E-01	-7.8084E-04	3.6240E-07	-6.962E-11
Anthracene [95, 156]	$C_{14}H_{10}$	Liq.	1.3464E+01	9.7811E-01	-6.0720E-04	1.3563E-07	0.0
		Gas	-9.6402E+01	1.2189E+00	-1.0497E-03	4.5313E-07	-7.7378E-11
Phenathrene [116, 156]	$C_{14}H_{10}$	Liq.	-3.3270E+00	1.0505E+00	-7.0990E-04	1.7751E-07	0.0
		Gas	-9.7607E+01	1.2353E+00	-1.0909E-03	4.9059E-07	-8.871E-11
Pyrene [109, 156]	$C_{16}H_{10}$	Liq.	-9.6011E-01	1.0904E+00	-6.9297E-04	1.5890E-07	0.0
		Gas	-1.0975E+02	1.3732E+00	-1.22724E-03	5.5601E-07	-1.0108E-10
Triphenylene [109, 156]	$C_{18}H_{12}$	Liq.	-7.8254E+00	1.3170E+00	-8.8888E-04	2.2165E-07	0.0
		Gas	-1.1827E+02	1.5448E+00	-1.3557E-03	6.0359E-07	-1.0790E-10
1-Methylnaphthalene [154]	$C_{11}H_{10}$	Liq.	2.60447E+01	8.42077E-01	-5.47808E-04	1.33512E-07	0.0
		Gas	-7.11865E+01	9.96575E-01	-8.59433E-04	3.85794E-07	-7.07358E-11

[1] J mol^{-1} K^{-1}; [2] J mol^{-1} K^{-2}; [3] J mol^{-1} K^{-3}; [4] J mol^{-1} K^{-4}; [5] J mol^{-1} K^{-5}

Table A.3 Prediction of heat capacity coefficients for Eq. (4.5) of solid PAHs.

Compound	Formula	Temp. (K)	Heat capacity coefficients			
			a[1]	b[2]	c[3]	d[4]
Naphthacene	$C_{18}H_{12}$	50-250	1.995737E+01	6.733108E-01	-2.771129E+04	2.979702E-04
		250-400	-2.590421E+02	2.005283E+00	2.968327E+06	-1.294366E-03
		400-500	-2.590421E+02	2.005283E+00	2.968327E+06	-1.294366E-03
		500-1000	2.734653E+02	6.035530E-01	-2.115936E+07	-2.358124E-04
		1000-1200	2.697637E+02	5.194802E-01	-9.247756E-03	-1.687806E-04
Pentacene	$C_{22}H_{14}$	50-200	5.988141E+00	9.836649E-01	-1.782956E+04	-1.665187E-04
		200-250	-6.155798E+00	1.009002E+00	3.402372E+04	4.262108E-05
		250-400	-3.651015E+02	2.551714E+00	4.647896E+06	-1.632403E-03
		400-500	-2.501148E+02	1.836391E+00	5.174311E+06	-7.021610E-04
		500-1000	3.361335E+02	7.545682E-01	-2.866234E+07	-3.120921E-04
		1000-1200	2.697637E+02	5.194802E-01	-9.247756E-03	-1.687806E-04
Perylene	$C_{20}H_{12}$	50-200	-8.207050E+00	1.057115E+00	8.665330E+03	-7.272038E-04
		200-250	-2.590085E+01	6.500822E-01	9.667334E+05	1.178689E-03
		250-400	-1.966541E+02	1.877413E+00	1.389063E+06	-1.106362E-03
		400-500	-4.138438E+02	2.737243E+00	5.194892E+06	-2.049846E-03
		500-1000	3.687029E+02	4.497673E-01	-2.338033E+07	-1.449073E-04
		1000-1200	2.659305E+02	5.540766E-01	9.184918E-03	-1.697824E-04
Coronene	$C_{24}H_{12}$	50-200	-5.900666E+01	1.664113E+00	5.935361E+04	-2.123086E-03
		200-250	2.720057E+02	-1.538138E+00	-2.678011E+05	5.845444E-03
		250-400	-2.402542E+02	2.143855E+00	9.991880E+05	-1.009711E-03
		400-500	-8.918231E+02	4.723344E+00	1.241667E+07	-3.840164E-03
		500-1000	6.794466E+02	1.210705E-01	-4.414273E+07	-1.008414E-05
		1000-1200	3.665477E+02	5.531094E-01	4.119445E-02	-1.737004E-04

[1] J mol^{-1} K^{-1}; [2] J mol^{-1} K^{-2}; [3] J mol^{-1} K^{-3}; [4] J mol^{-1} K

Table A.4 Prediction of heat capacity coefficients for Eq. (4.6) of liquid and gas PAHs.

Compound	Formula	state	Heat capacity coefficients				
			a[1]	b[2]	c[3]	d[4]	e[5]
Naphthacene	$C_{18}H_{12}$	Liquid	-2.030040E-01	1.296900E+00	-8.458040E-04	2.000330E-07	0.000000E+00
		Gas	-1.232540E+02	1.551290E+00	-1.318570E-03	5.438740E-07	-8.513870E-11
pentacene	$C_{22}H_{14}$	Liquid	-1.386970E+01	1.615680E+00	-1.084410E-03	2.644370E-07	0.000000E+00
		Gas	-1.501060E+02	1.883700E+00	-1.587430E-03	6.346100E-07	-9.289910E-11
perylene	$C_{20}H_{12}$	Liquid	-5.457510E+00	1.356900E+00	-8.719490E-04	2.030470E-07	0.000000E+00
		Gas	-1.304110E+02	1.682780E+00	-1.491960E-03	6.690170E-07	-1.202780E-10
coronene	$C_{24}H_{12}$	Liquid	-7.218320E-01	1.436720E+00	-8.380880E-04	1.658300E-07	0.000000E+00
		Gas	-1.546870E+02	1.958740E+00	-1.764530E-03	7.998560E-07	-1.450300E-10

[1] J mol^{-1} K^{-1}; [2] J mol^{-1} K^{-2}; [3] J mol^{-1} K^{-3}; [4] J mol^{-1} K^{-4}; [5] J mol^{-1} K^{-5}

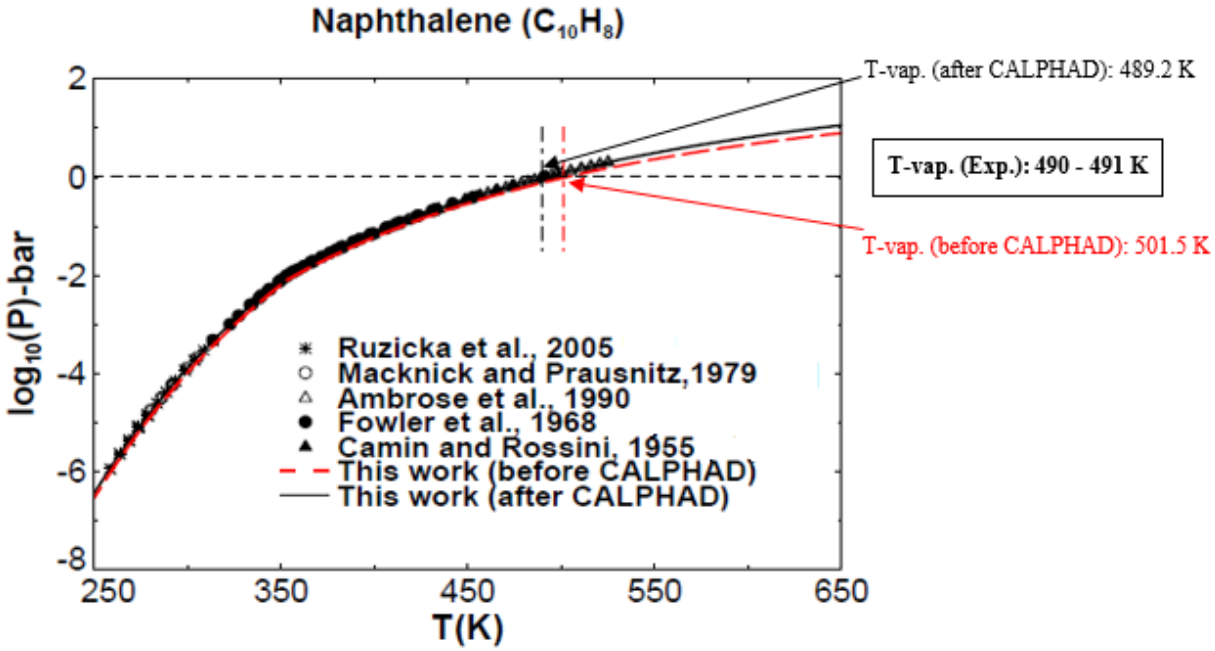

Figure A.1 Vapor pressure of naphthalene as a function of temperature [179-181, 183, 188].

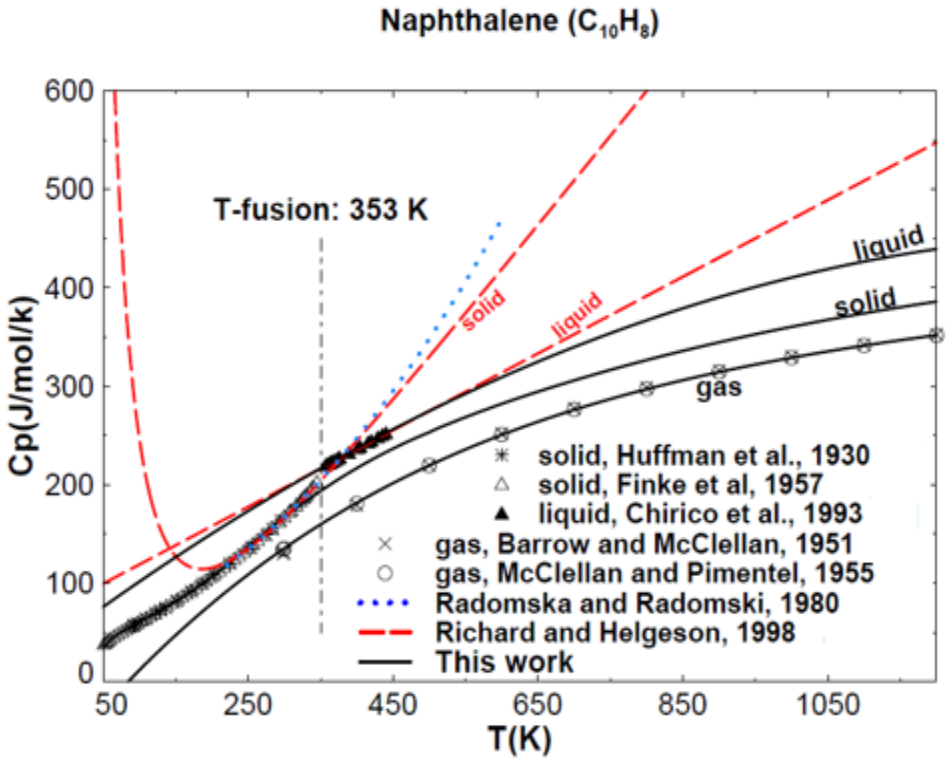

Figure A.2 Heat capacity of naphthalene (solid, liquid and gas) as a function of temperature [92, 97, 98, 101, 105, 111, 154].

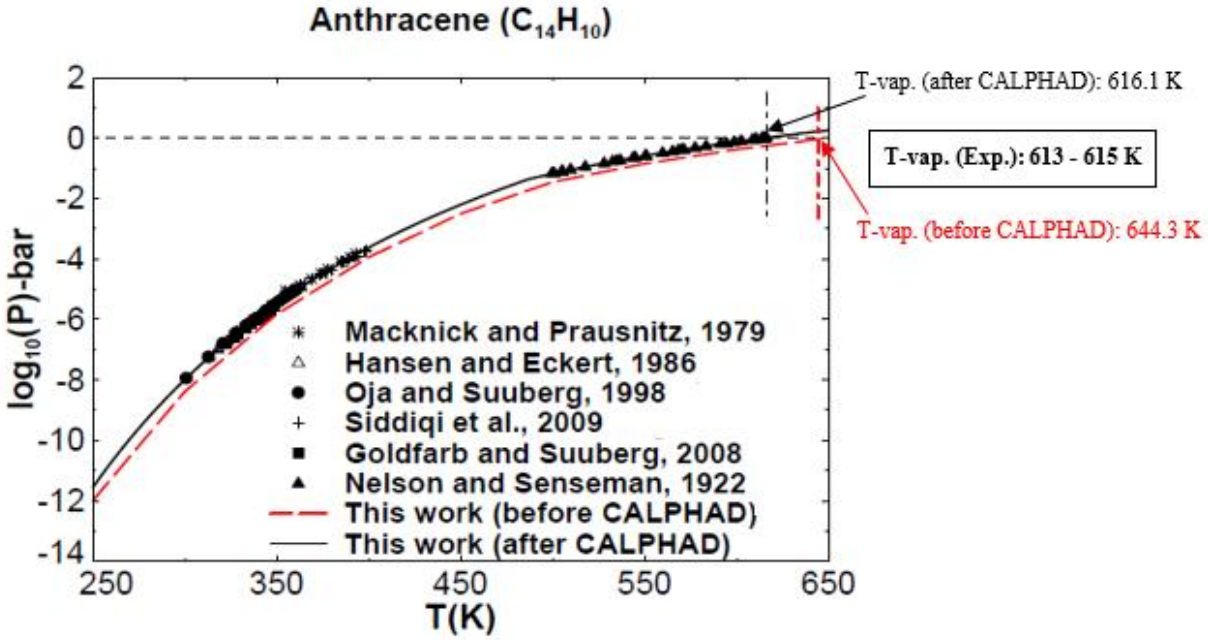

Figure A.3 Vapor pressure of anthracene as a function of temperature [178, 179, 184, 186, 187, 190].

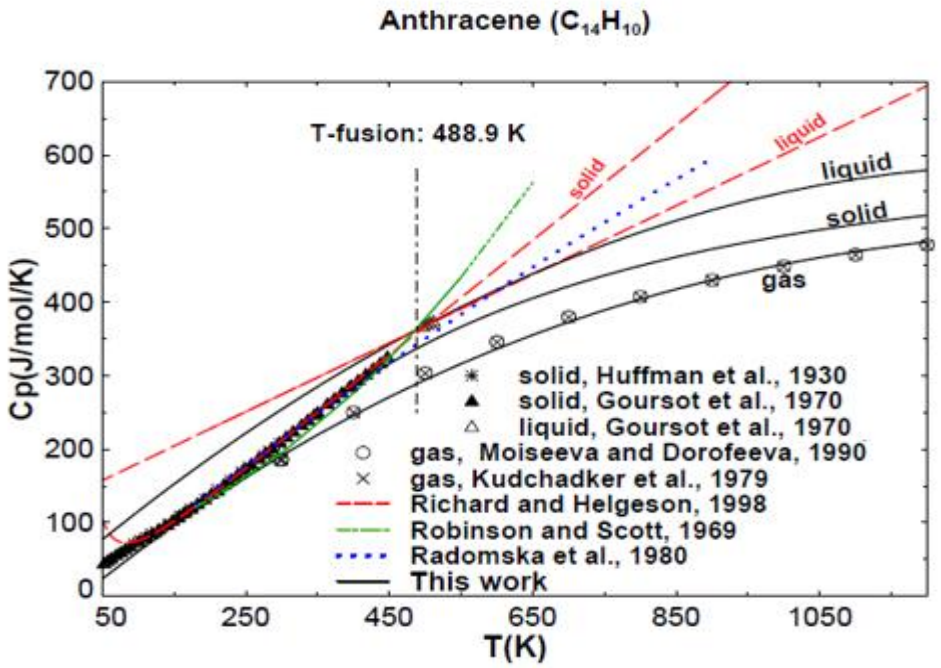

Figure A.4 Heat capacity of anthracene (solid, liquid and gas) as a function of temperature [92, 95, 101, 103, 104, 111, 156].

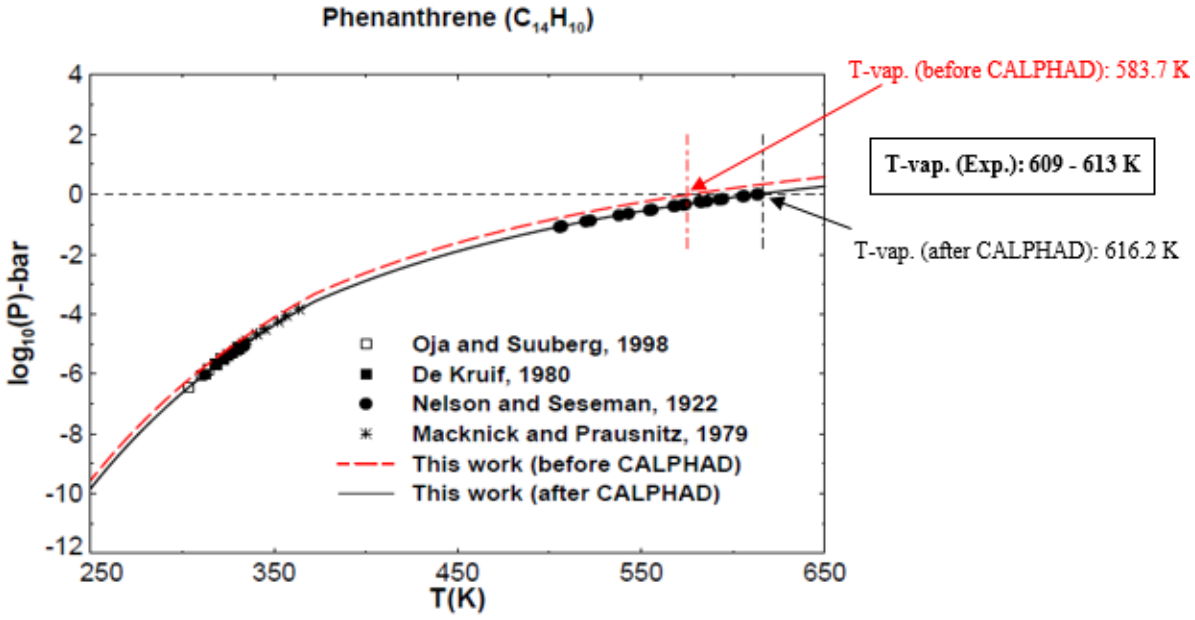

Figure A.5 Vapor pressure of phenantrene as a function of temperature [179, 182, 186, 187].

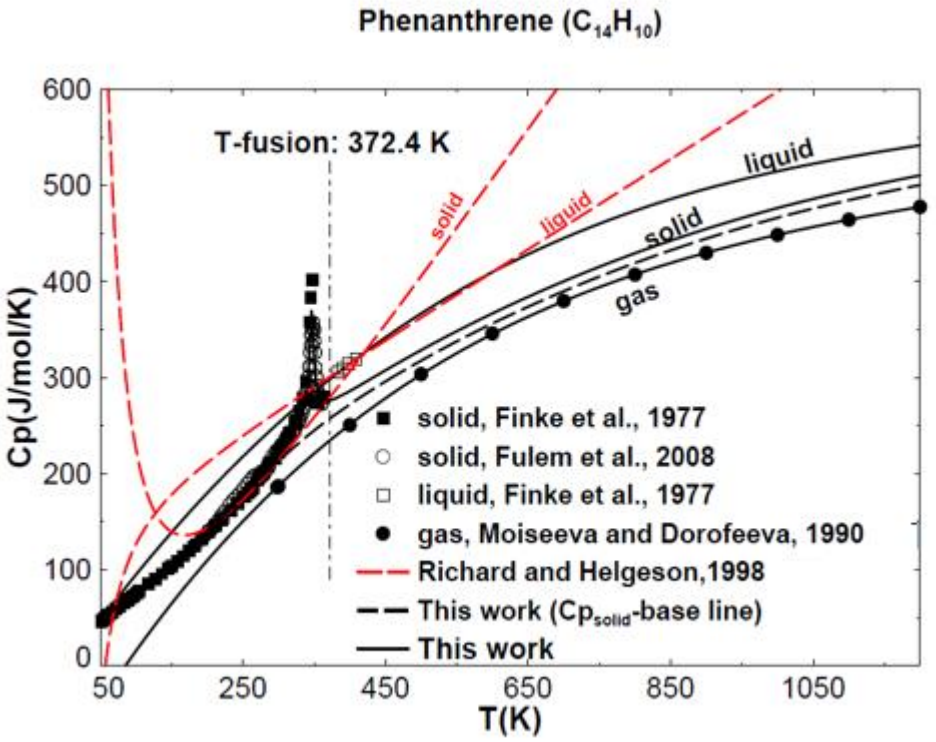

Figure A.6 Heat capacity of phenanthrene (solid, liquid and gas) as a function of temperature [111, 116, 156, 171] (for anomaly, see Section 4.4.4).

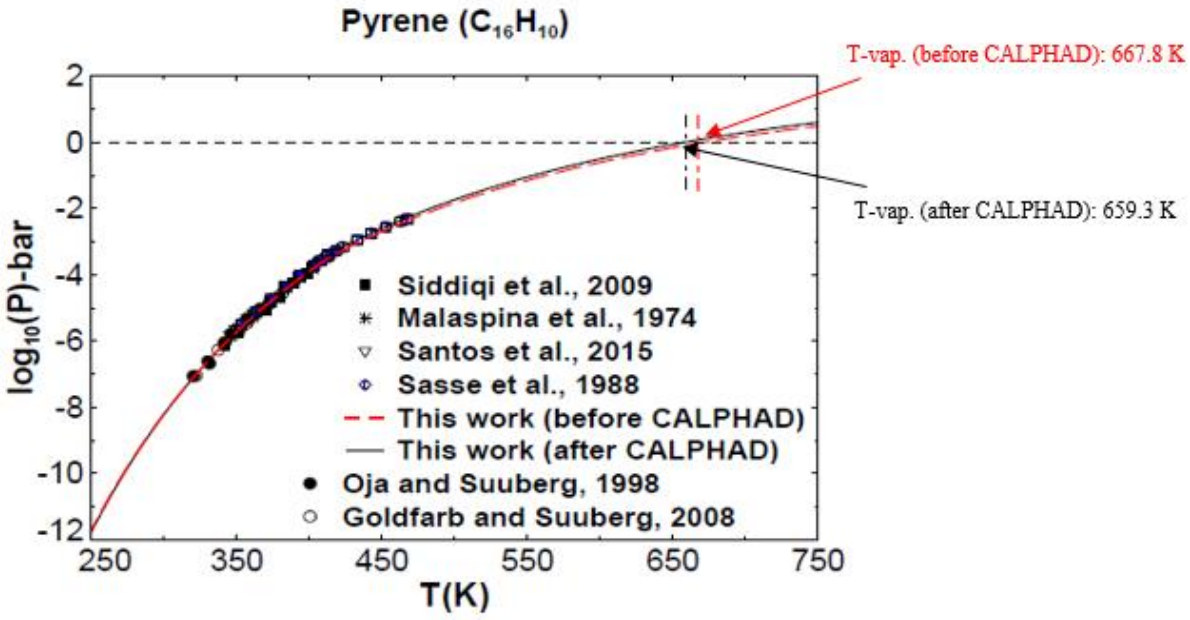

Figure A.7 Vapor pressure of pyrene as a function of temperature [147, 161, 185, 187, 189, 190].

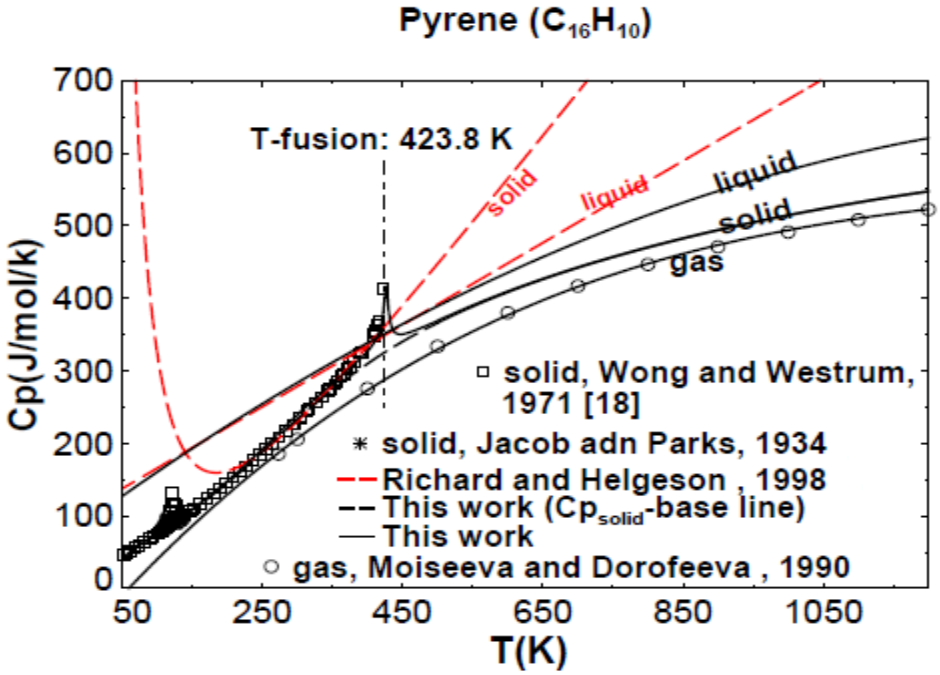

Figure A.8 Heat capacity of pyrene (solid, liquid and gas state) as a function of temperature [96, 109, 111, 156] (for anomaly, see Section 4.4.4).

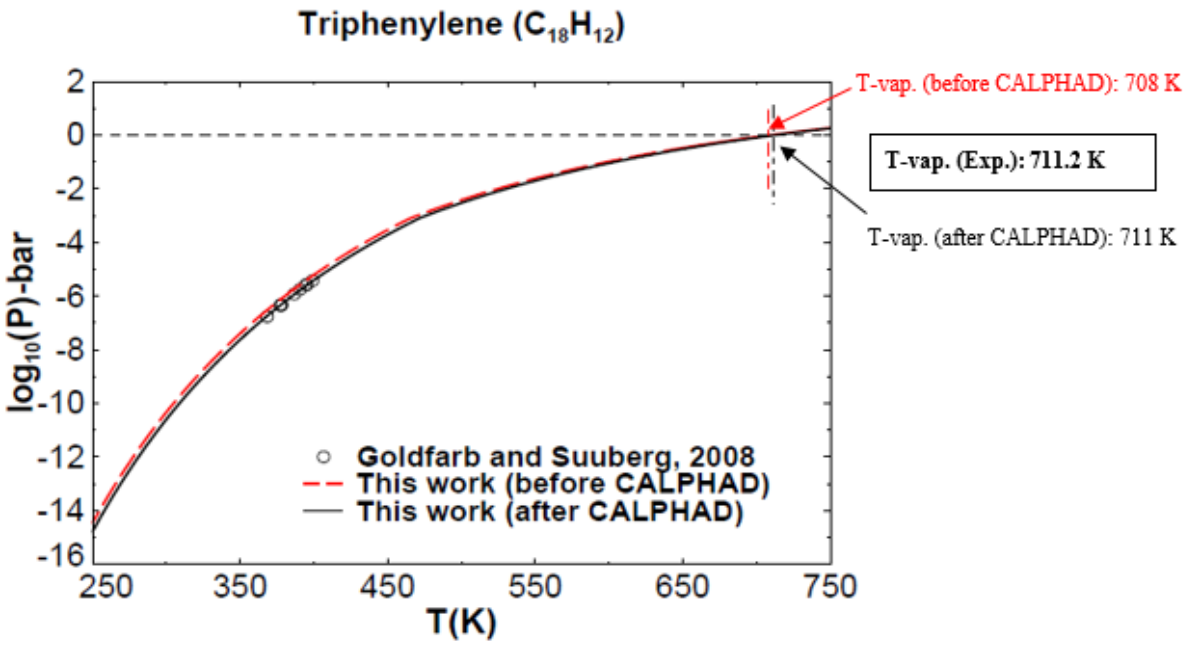

Figure A.9 Vapor pressure of triphenylene as a function of temperature [178].

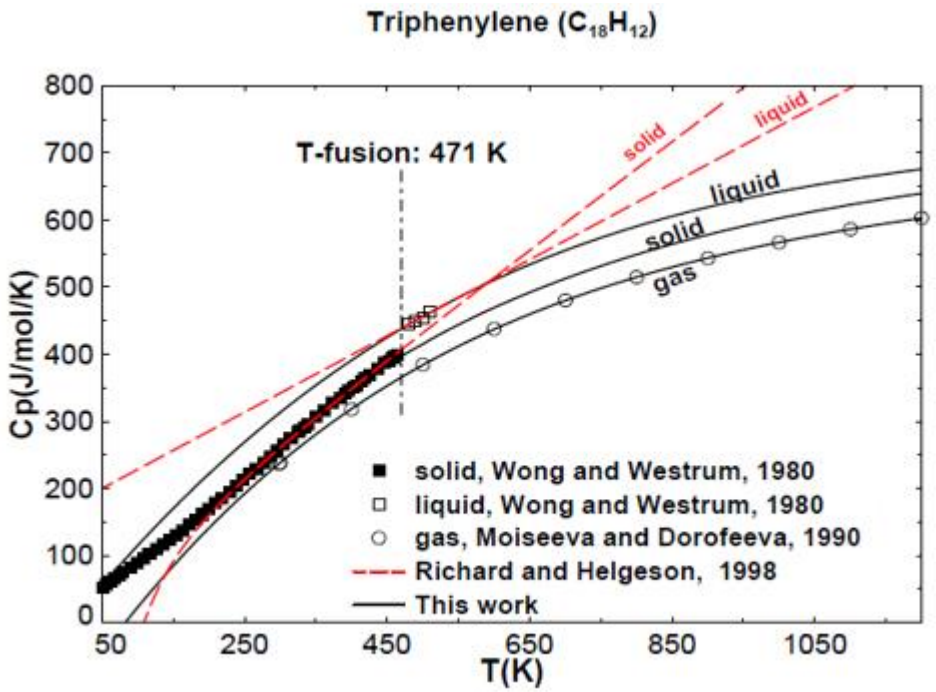

Figure A.10 Heat capacity of triphenylene (solid, liquid and gas state) as a function of temperature [111, 156, 166].

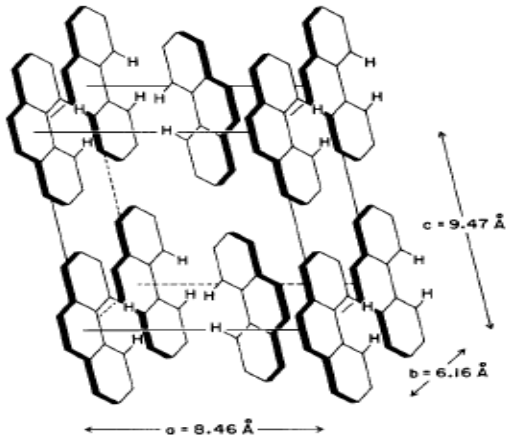

Figure A.11 Position of the phenanthrene molecule in the unit cell [124]

Table A.5 Experimental data and optimized values of entropy and enthalpy of formation at 298.15K and 1 bar of solid, liquid and gas reference PAH compounds.

Compound	Formula	ΔH°_{298} (kJ mole^{-1})					S°_{298} (J mole^{-1} K^{1})				
		solid		gas			solid		gas		
		Exp. value	Opt. val.	Exp. value	FPC value	Opt. val.	Exp. value	Opt. val.	Exp. value	FPC value	Opt. value
Naphthalene [39, 90, 92-98, 102, 103, 105, 116, 143, 152, 154, 156, 162, 164, 172]	$C_{10}H_8$	64.9-81.6	77.8	146.0-155.0	150.6	150.8	162.8-167.4	167.1	333.9-336.5	334.2	335.8
Anthracene [39, 90, 92, 93, 95, 102, 103, 155-157, 167, 168, 172]	$C_{14}H_{10}$	116.2-128.9	124.9	227.0-233.0	230.9	226.7	207.2-207.5	207.0	391.4-392.6	389.5	393.2
Phenanthrene [39, 90, 92, 93, 95, 96, 102, 103, 116, 156, 172]	$C_{14}H_{10}$	109.6-116.2	110.1	201.2-207.1	201.4	201.5	211.7-215.1	215.4	394.6-396.7	395.9	393.1
Pyrene [93, 96, 109] [39, 110, 172]	$C_{16}H_{10}$	114.5-125.2	120.0	214.9-225.7	225.5	221.4	215.1-234.9	220.1	402.0	399.5	400.5
Triphenylene [39, 93, 109, 148, 172]	$C_{18}H_{12}$	141.0-151.8	147.6	265.7-274.5	270.1	267.4	254.6	254.7	-	450.4	451.5
Perylene [39, 93, 172, 211]	$C_{20}H_{12}$	180.0-184.4	183.1	315.0-321.3	319.4	315.1	264.4	261.1	-	461.6	469.1
Coronene [93, 166, 172]	$C_{24}H_{12}$	145.4-159.2	152.3	284.0-306.0	294.9	293.3	280.9	281.0	-	468.8	467.4
1-Methylnaphthalene [39, 162]	$C_{11}H_{10}$	-	47.1	114.2-119.6	-	120.1	-	218.2	-	-	386.3

Table A.6 Experimental data and optimized values of phase transition thermodynamic data of reference PAH compounds.

Compound	**Formula**	**T^{o}_{fusion}**		**$\Delta H°_{fusion}$ (kJ mole^{-1})**		**$\Delta S°_{fusion}$ (J mole^{-1} K^{-1})**	
		Exp. value	Opt. value	Exp. value	Opt. value	Exp. value	Opt. value
Naphthalene[39, 93, 100, 141, 142, 144, 145, 153, 154, 159, 169, 170, 176]	$C_{10}H_8$	350.0-353.4	351.0	16.4-19.3	18.8	51.6-54.4	53.6
Anthracene [39, 93, 95, 146, 149, 151, 160, 163]	$C_{14}H_{10}$	488.9-491.0	487.1	28.8-31.5	29.9	59.2-61.0	61.3
Phenanthrene [39, 93, 106, 151, 158-160, 173]	$C_{14}H_{10}$	371.4-373.8	371.9	15.7-18.6	18.2	46.1-49.9	48.9
Pyrene [39, 93, 109, 118, 147, 161, 165, 173, 178]	$C_{16}H_{10}$	422.3-424.0	423.8	15.3-17.4	19.7	36.3-42.5	46.5
Triphenylene[39, 93, 106, 109, 150, 173]	$C_{18}H_{12}$	471.0-471.2	470.8	23.0-24.7	24.0	49.1-52.1	51.0
Perylene [39, 106, 177]	$C_{20}H_{12}$	542.0-544.0	543.0	31.9-32.6	31.4	58.8-60.0	57.8
Coronene [39, 141]	$C_{24}H_{12}$	709.0-710.5	710.5	19.2-21.2	18.09	-	25.46
1-Methylnaphthalene [39, 177]	$C_{11}H_{10}$	240.7-242.7	241.2	6.95	6.87	20.7 and 28.6	27.17

APPENDIX B CONVERGENCE TESTS FOR MIN G AND VARIABLES IN EQ. (5.6)

For binary system:

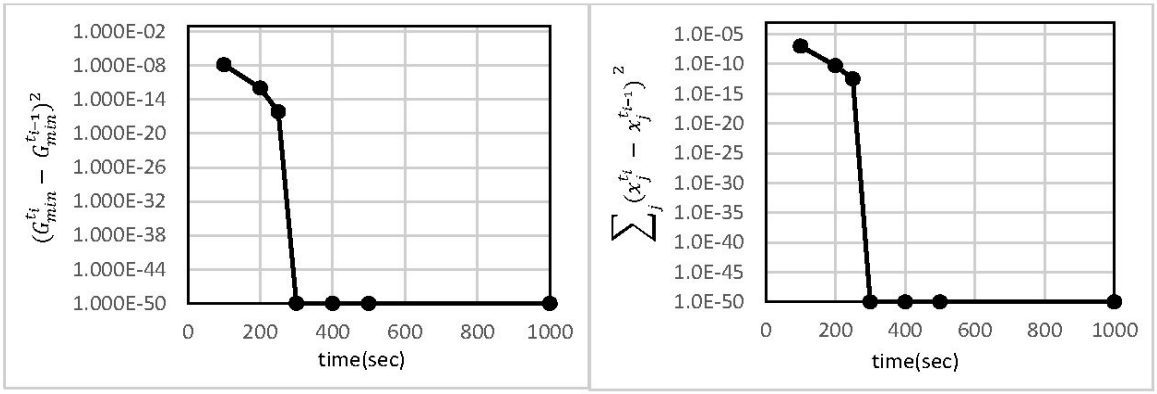

For ternary system:

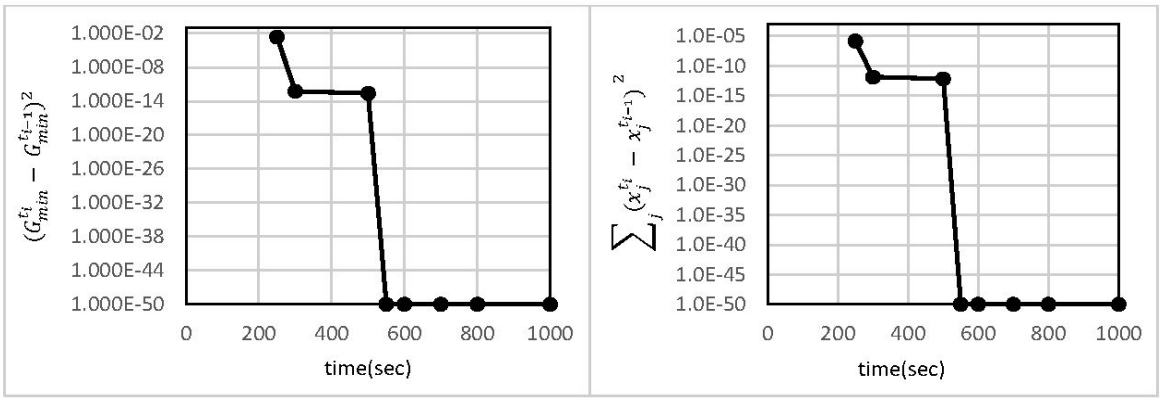

For 6-component system:

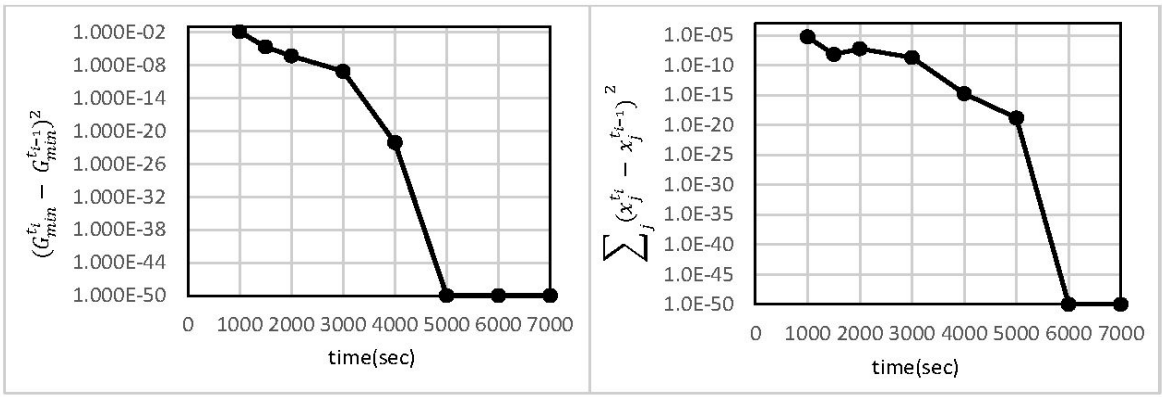

APPENDIX C CHEMICAL POTENTIAL FORMULATION OF THE SPECIES IN ISOTROPIC LIQUID AND NEMATIC PHASES

$$G^{iso} = \left[\sum_i n_i g_i^0 + RT\sum_i n_i \ln x_i + \sum_i n_i V_i \left(\delta_i - \bar{\delta}\right)^2 + RT\sum_i n_i \ln\left(\frac{\Phi_i}{x_i}\right)\right]^{iso} \quad (1)$$

$$G^{meso} = \left[\sum_i n_i g_i^0 + RT\sum_i n_i \ln x_i + \sum_i n_i V_i \left(\delta_i - \bar{\delta}\right)^2 + RT\sum_i n_i \ln\left(\frac{\Phi_i}{x_i}\right)\right]^{meso} - \left[\frac{N_{av}}{2}\sum_{i,j} n_i x_j \varepsilon_{ij} \bar{P}_{2(i)} \bar{P}_{2(j)} + RT\sum_i n_i \ln Z_i\right]^{meso} \quad (2)$$

where,

$$\varepsilon_{ij} = \tilde{\varepsilon}_{ij}\sqrt{V_i V_j} / \sum x_k V_k \quad (3)$$

$$\tilde{\varepsilon}_{ij} = -\sqrt{\tilde{\varepsilon}_{ii}\,\tilde{\varepsilon}_{jj}} \quad (4)$$

$$\tilde{\varepsilon}_{ii} = -4.54.k.T_{cl_i} \quad (5)$$

$$\bar{\delta} = \frac{\sum_i n_i \delta_i V_i}{\sum_i n_i V_i} \quad (6)$$

$$\Phi_i = \frac{x_i V_i}{\sum_k x_k V_k} \quad (7)$$

$$\ln\left(\frac{\Phi_i}{x_i}\right) = \ln\left(\frac{V_i}{\sum_k x_k V_k}\right) \quad (8)$$

$$Z_i = \int_0^{\pi/2} \exp\left\{-\frac{1}{kT}\sum_j \varepsilon_{ij} x_j \bar{P}_{2(j)} P_{2(i)}(\cos\theta)\right\} \sin(\theta)\, d\theta \quad (9)$$

$$\bar{P}_{2(i)} = \int_0^{\pi/2} P_{2(i)}(\cos\theta)\, .\, exp\left\{-\frac{1}{kT}\sum_j \varepsilon_{ij} x_j \bar{P}_{2(j)} P_{2(i)}(\cos\theta)\right\} \sin(\theta)\, d\theta \;/Z_i \quad (10)$$

Based on chemical potential definition:

$$\mu_i^{iso} = \left(\frac{\partial G}{\partial n_i}\right)_{T,P}^{iso} \quad (11)$$

$$\mu_i^{meso} = \left(\frac{\partial G}{\partial n_i}\right)_{T,P}^{meso} \quad (12)$$

Some additional relations:

$$\frac{\partial \varepsilon_{jk}}{\partial n_i^N} = \varepsilon_{jk} \frac{1}{\sum_m n_m^N} \left(1 - \frac{V_i}{\sum_m x_m^N V_m^N}\right) \quad ; j \neq k \tag{13}$$

$$\frac{\partial \varepsilon_{jk}}{\partial n_i^N} = 0 \; ; j = K \tag{14}$$

$$\frac{\partial \left(\sum_j n_j^N \ln Z_j\right)}{\partial n_i^N} = \ln (Z_i) + \sum_j n_j^N \frac{1}{Z_j} \frac{\partial Z_j}{\partial n_i^N} \tag{15}$$

$$\frac{\partial Z_j}{\partial n_i^N} = \frac{1}{KT} \sum_{j,m \neq j} x_j^N x_m^N \varepsilon_{jm} \overline{P}_{2(j)} \overline{P}_{2(m)} \frac{V_i}{\sum_k x_k^N V_k} - \frac{1}{KT} \sum_j \left(x_j^N \varepsilon_{ij} \overline{P}_{2(i)} \overline{P}_{2(j)} - x_j^N x_j^N \varepsilon_{jj} \overline{P}_{2(j)} \overline{P}_{2(j)}\right) - \frac{1}{KT} \sum_{j,m} n_j^N x_m^N \varepsilon_{jm} \overline{P}_{2(j)} \overline{P}'_{2(m)} \tag{16}$$

$$\frac{\partial \left(\sum_{j,k} n_j^N x_k^N \varepsilon_{jk} \overline{P}_{2(j)} \overline{P}_{2(k)}\right)}{\partial n_i^N} = 2 \sum_{j=i} x_j^N \varepsilon_{jj} \overline{P}_{2(j)} \overline{P}_{2(j)} - \sum_j \left(x_j^N x_j^N \varepsilon_{jj} \overline{P}_{2(j)} \overline{P}_{2(j)} - 2 n_j^N x_j^N \varepsilon_{jj} \overline{P}_{2(j)} \overline{P}'_{2(j)}\right) + 2 \sum_{j \neq i} x_j^N \varepsilon_{ij} \overline{P}_{2(i)} \overline{P}_{2(j)} - \sum_{j,m \neq j} x_j^N x_m^N \varepsilon_{jm} \overline{P}_{2(j)} \overline{P}_{2(m)} \frac{V_i}{\sum_k x_k^N V_k} + \sum_{j,m \neq j} n_j^N x_m^N \varepsilon_{jm} \overline{P}_{2(j)} \overline{P}'_{2(m)} + \sum_{j,m \neq j} n_j^N x_m^N \varepsilon_{jm} \overline{P}'_{2(j)} \overline{P}_{2(m)} \tag{17}$$

$$\frac{\partial \left(\sum_j n_j \ln x_j\right)}{\partial n_i} = \ln x_i \tag{18}$$

$$\frac{\partial \left(\sum_j n_j \ln\left(\frac{V_j}{\sum_k x_k V_k}\right)\right)}{\partial n_i} = \ln \left(\frac{V_i}{\sum_k x_k V_k}\right) + 1 - \frac{V_i}{V} \tag{19}$$

$$\frac{\partial \left(\sum_j n_j V_j \left(\delta_j - \overline{\delta}\right)^2\right)}{\partial n_i} = V_i \left(\delta_i - \overline{\delta}\right)^2 \tag{20}$$

Substituting Eqs. (13) – (20) into Eqs. (11) and (12) and equating the chemical potential of each species in the isotropic liquid and nematic phases result in:

$$\left[\ln x_i + \ln\left(\frac{V_i}{V}\right) - \frac{V_i}{V} + \frac{V_i}{RT}\left(\delta_i - \overline{\delta}\right)^2\right]^{iso} = \left[\ln x_i + \ln\left(\frac{V_i}{V}\right) - \frac{V_i}{V} + \frac{V_i}{RT}\left(\delta_i - \overline{\delta}\right)^2\right]^{meso} - \left[\ln(Z_i) + \frac{1}{2kT}\left(\sum_{j,m \neq j} x_j x_m \varepsilon_{jm} \overline{P}_j \overline{P}_m \frac{V_i}{V} + \sum_j x_j x_j \varepsilon_{jj} \overline{P}_j \overline{P}_j\right)\right]^{meso} \tag{21}$$